UNIVERSITY OF SOUTHAMPTON

FACULTY OF PHYSICAL SCIENCES AND ENGINEERING

Electronics and Computer Science

Microfluidic Electrophysiological Device for Genetic and Chemical Biology Screening of Nematodes

by

Chunxiao Hu

A thesis submitted in partial fulfilment for the degree of Doctor of Philosophy

Octorber_2013

UNIVERSITY OF SOUTHAMPTON

ABSTRACT

FACULTY OF PHYSICAL SCIENCES AND ENGINEERING

Doctor of Philosophy

Thesis for the degree of Doctor of Philosophy

MICROFLUIDIC ELECTROPHYSIOLOGICAL DEVICE FOR GENETIC AND CHEMICAL BIOLOGY SCREENING OF NEMATODES

Chunxiao Hu

Genetic and chemical biology screens of *C. elegans* have been of enormous benefit in providing fundamental insight into neural function and neuroactive drugs. Recently the exploitation of microfluidic devices has added greater power to this experimental approach providing more discrete and higher throughput phenotypic analysis of neural systems. This repertoire is extended through the design of a semi-automated microfluidic device, NeuroChip, which has been optimised for selecting worms based on the electrophysiological features of the pharyngeal neural network. This device has the capability to sort mutant from wild-type worms based on high definition extracellular electrophysiological recordings. NeuroChip resolves discrete differences in excitatory, inhibitory and neuromodulatory components of the neural network from individual animals. Worms may be fed into the device consecutively from a reservoir and recovered unharmed. It combines microfluidics with integrated electrode recording for sequential trapping, restraining, recording, releasing and recovering of *C. elegans*. Thus mutant worms may be selected, recovered and propagated enabling mutagenesis screens based on an electrophysiological phenotype. Drugs may be rapidly applied during the recording thus permitting compound screening. For toxicology, this analysis can provide a precise description of sub-lethal effects on neural function. The chamber has been modified to accommodate L2 larval stages *C. elegans* and J2 stage *G. pallida* showing applicability for small size nematodes including parasitic species which otherwise are not tractable to this experimental approach. NeuroChip may be combined with optogenetics for targeted interrogation of the function of the neural circuit. NeuroChip thus adds a new

tool for exploitation of *C. elegans* and *G. pallida* and has applications in neurogenetics, drug discovery and neurotoxicology.

Contents

ABSTRACT i

Contents i

List of tables v

List of figures vii

DECLARATION OF AUTHORSHIP xvii

Acknowledgements 1

Definitions and Abbreviations 3

Chapter 1: Introduction 1

1.1 Motivation 1
1.2 Objective 2
1.3 Thesis organization 3

Chapter 2: Literature Review 5

2.1 Introduction to *C. elegans* 5
2.2 Development of microfluidic approaches for research of nematodes 5
2.2.1 Microfluidic devices for *C. elegans* 6
2.2.1.1 Immobilization of *C. elegans* on-chip 6
2.2.1.2 Observation and imaging of *C. elegans* on-chip 8
2.2.1.3 Rapid sorting and screening on-chip 19
2.2.1.4 Laser surgery of *C. elegans* on-chip 27
2.2.1.5 Droplet-based application of *C. elegans* on-chip 31
2.2.2 Microfluidic devices for parasitic nematodes 36
2.3 Electrophysiological investigation of *C. elegans* 38
2.3.1 Experimental method 39
2.3.2 Neurobiological researches of *C. elegans* with EPGs 41
2.3.2.1 Defining drug effects 41
2.3.2.2 Defining gene functions 44

Chapter 3: Microfluidic Channels for Acquiring EPGs 47

3.1 Channel design for trapping single adult *C. elegans* 48
3.2 Device fabrication and experimental procedure 50
3.2.1 Device fabrication 50
3.2.1.1 Mask design 50
3.2.1.2 SU-8 master fabrication 51

3.2.1.3 PDMS casting 58
3.2.2 Experimental procedure for acquiring EPGs on-chip 60
3.3 Result 62
Chapter 4: Integrated Microfluidic Platform for EPGs - NeuroChip ...79
4.1 Improvement on design of NeuroChip 81
4.1.1 Orientation structure 83
4.1.2 Micro-valve system 86
4.1.3 Side perforated chamber 91
4.1.4 Integrated electrode 95
4.2 Device fabrication 98
4.2.1 Method for improving the valves' performance 101
4.2.2 Bonding PDMS onto glass with platinum electrode 109
4.3 Device Operation 112
4.3.1 External control system 112
4.3.2 Operation of NeuroChip 114
4.4 Conclusions 116
Chapter 5: Experiments with NeuroChip for Genetic and Chemical Biology Screening of *C. elegans* 119
5.1 Preparation 119
5.1.1 Worm culture and sample preparation 119
5.1.2 Data acquisition and signal analysis setup 119
5.2 Validation of the performance of NeuroChip 120
5.3 Rapid application of compounds 127
5.4 Mutant sorting 133
5.5 Interrogating neural network properties with optogenetics 137
5.6 Comparison with another 'EPG chip' 141
5.7 Conclusions 145
Chapter 6: Modified NeuroChip for Smaller Nematodes 147
6.1 EPGs from second stage larvae (L2) *C. elegans* 147
6.1.1 Two-photon polymerization 148
6.1.2 Fabrication of modified chip for L2 stage *C. elegans* 150
6.1.2.1 3D lithography with Nanoscribe 150
6.1.2.2 Results of 3D lithography 156
6.1.3 EPGs from L2 stage *C. elegans* 162
6.2 EPGs from plant parasitic nematode *Globodera pallida* 165
6.2.1 The plant parasitic nematode *Globodera pallida* 166
6.2.2 Electrophysiological recordings from the nematode *G. pallida* 168

6.2.2.1 Reported EPGs research on *Globodera* 168
6.2.2.2 EPGs collected from *G. pallida* with modified NeuroChip 170
6.3 Conclusions 181
Chapter 7: Conclusion and Future Work 183
Appendices 187
Appendix 1: Mask for microfluidic channel 187
Appendix 2: SU-8 5 recipe (12 μm) 188
Appendix 3: SU-8 50 recipe (60 μm) 189
Appendix 4: SU-8 master for microfluidic channel 190
Appendix 5: Mask for NeuroChip 191
Appendix 6: Masters for NeuroChip 192
Appendix 7: External Control System 193
Appendix 8: Java programme for controlling the microfluidic valves 194
Appendix 9: Microfluidic platform for NeuroChip 200
Appendix 10: *peat-4::ChR2;mRFP* integration for *eat-4* mutant 201
Appendix 11: Method for expression of ChR2 in cholinergic neurones 202
Bibliography 205

List of tables

Table 1: Attempts to trap & record worms with diverse trapping channel designs. 70

Table 2: A summary of EPG parameters compared for NeuroChip and conventional recordings. 124

Table 3: *eat-4* mutants recorded with NeuroChip or conventional recordings have the same phenotype. 127

Table 4: Differences between Shawn Lockery's device and the NeuroChip. 144

Table 5: J2 *G. pallida* recorded with the modified NeuroChip or conventional recordings have the same phenotype. 176

List of figures

Figure 2.1: Three different methods for immobilizing *C. elegans.* 7

Figure 2.2: Design of the microfluidic device for lifelong observation of *C. elegans.* 9

Figure 2.3: Microfluidic chip for high-throughput study of synaptic transmission. 11

Figure 2.4: Microfluidic chamber arrays for whole-organism behaviour-based chemical screening. 12

Figure 2.5: C.L.I.P (continuous live imaging platform) for direct observation of *C. elegans* physiological processes. 14

Figure 2.6: Microfluidic platform for calcium imaging of chemosensory neurons in *C. elegans*. 16

Figure 2.7: The glycerol-evoked response from the ASH neuron. 18

Figure 2.8: Schematic and image of the microfluidic system for high-throughput whole-animal sorting and screening at subcellular resolution. 19

Figure 2.9: Structure and operating steps of the high-throughput sorter and cross-section view of the valve. 20

Figure 2.10: Incubation chamber for large-scale screening 22

Figure 2.11: Schematics of the microfluidic device for rapid microscopy, phenotyping and sorting of *C. elegans*. 23

Figure 2.12: Phenotyping and sorting are based on synaptic features in this microfluidic system. (A) Schematic shows the process of a mixed population of worms is injected, imaged, phenotyped and then sorted in the device. Representative images of punc-25-YFP–RAB-5 reporter expression in wild-type (B) and unc-16–/– mutant (C) worms provide the means for sorting. Pictures are adapted from [50]. 25

Figure 2.13: Schematics of the microfluidic device for rapid screening of chemotaxis-defective *C. elegans* mutants. 26

Figure 2.14: The nanoaxotomy lab-on-a-chip for in vivo nerve regeneration studies. 28

Figure 2.15: Overview of the experimental design for single-synapse ablation and long-term imaging in live *C. elegans*. 29

Figure 2.16: The results of the ablation of a mature synapse made by the HSNL neuron ablation experiments are shown by a sequence of images (60s intervals).....30

Figure 2.17: Schematic diagram of the droplet-based microfluidic device for individual *C. elegans* assays.....32

Figure 2.18: Schematic of the droplet-based microfluidic device for characterizing the neurotoxin-induced responses in individual *C. elegans*.....34

Figure 2.19: Fluorescence images and corresponding stroke frequencies of individual UA57 worms in response to 6-OHDA at the third day.35

Figure 2.20: Microfluidic device for drug screening tests on *O. dentatum*. 37

Figure 2.21: Model organism *Caenorhabditis elegans*. 38

Figure 2.22: Schematic of the instrumentation for conventional EPG experiment and equivalent circuit of the EPG arrangement.....39

Figure 2.23: The schematic of the pharynx of the nematode *C. elegans* and a typical EPG signal. 40

Figure 2.24: Serotonin regulates repolarisation of the *C. elegans* pharyngeal muscle by observation of EPG signals. 42

Figure 2.25: The effects of ethanol on *C. elegans*.....43

Figure 2.26: Example of single electropharyngeogram (EPG) recording trace from the wild-type worm and *eat-4* mutant. 45

Figure 2.27: Mutations that cause slow pumping and starvation. 46

Figure 3.1: Microfluidic channel for acquiring EPG signals.....47

Figure 3.2: Suction tube and pseudo-3D model of trapping channel, and schematic image of the microfluidic channel. 49

Figure 3.3: Mask design of the microfluidic channel for acquiring EPGs. 51

Figure 3.4: Schematic diagram showing the steps of standard photolithography. 52

Figure 3.5: The cross linking reaction that turns liquid SU-8 into solid resist..53

Figure 3.6: Schematic of the process for fabricating an SU-8 master, and an enlarged view of the trapping channel.....54

Figure 3.7: Schematic illustration showing the procedure of aligning the second layer onto the first layer of negative photoresist.....55

Figure 3.8: Two approaches to make the 57

Figure 3.9: Examples of aligned and misaligned SU-8 masters used to make the microfluidic channel.....58

Figure 3.10: PDMS microfluidic channel fabrication process.....59

Figure 3.11: PDMS microfluidic channel. 60

Figure 3.12: Simplified diagram of the setup for acquiring EPG signals on chip.61

Figure 3.13: Young adult (L4+1) *C. elegans* trapped in the microfluidic channel.62

Figure 3.14: Comparison of EPG waveforms obtained from the conventional method and the microfluidic channel. 63

Figure 3.15: A comparison of different preliminary designs of microfluidic trapping channel and the resulting electropharyngeogram (EPG) signal.....64

Figure 3.16: The exposure dose or time affects the final geometry of the pattern of interest in negative photoresist.....65

Figure 3.17: Three approaches to further optimise the geometry of the trap using PDMS fabrication.....67

Figure 3.18: SEM of the PDMS microfluidic channel. 68

Figure 3.19: Bubbles are generated when the nematode is sucked into the trap of the microfluidic channel, because PDMS is air-permeable. ...68

Figure 3.20: Four basic designs of trapping channel. 69

Figure 3.21: Two different age wild type worms in two different sized channels. Red arrows point to the position of corpus and terminal bulb in the trap respectively. 71

Figure 3.22: Two different age wild type worms in two different size channels.72

Figure 3.23: An EPG signal trace recorded from a trapped wild type N2 *C. elegans* in microfluidic channel processed by the software AutoEPG. 74

Figure 3.24: Six specific useful parameters (Pump Rate, Pump Duration, P Peaks, Group of Pumps, R/E Ratios, and R-E Intervals) extracted from the EPG trace shown in Figure 3.23. 75

Figure 3.25: Worms can be recovered from the microfluidic chip following recording and show normal fecundity and viability. 77

Figure 3.26: Schematic of one possible design to increase the throughput of electrophysiological analysis of *C. elegans* with the microfluidic device. Eight microfluidic channels can be incorporated on a single chip in parallel. Black squares indicate the postions to place the external Ag/AgCl electrode. (Picture is not drawn to scale.).....78

Figure 4.1: Problems encountered in the microfluidic channel. (i) Unexpected bits of material in the inlet channel that block the trap; (ii) Worm enter the trapping channel in the wrong orientation (tail first); (iii) Worms try to escape from the trap by bending; (iv) Worm is being sucked out of the channel through the inlet port. Black arrow indicates the direction of flow. Scale bar: 200 μm. 80

Figure 4.2: Evolution of the improved microfluidic chip.....81

Figure 4.3: Diagram of the NeuroChip.....82

Figure 4.4: Worm is captured by the tail in a microfluidic chip and the EPG signals. 84

Figure 4.5: Micro-pillars adjacent to the worm port control worm orientation. 85

Figure 4.6: Probability of worms entering the trapping channel with head-to-tail orientation in the absence and presence of post structure (n=55). 86

Figure 4.7: Schematic diagram of two micro-valve geometries: push-down and push-up..... 87

Figure 4.8: Schematic of fabrication procedures for making a multi-layer pneumatic control system. 88

Figure 4.9: Actuation pressure is symmetric with width of both flow and control channels..... 89

Figure 4.10: Cross-over area is enlarged to optimize the performance of the push-up microfluidic valve..... 91

Figure 4.11: Schematic showing the straight channel with a side perforated wide chamber (Flow channel in blue and control in white). 92

Figure 4.12: Flow velocity simulations for the straight channel and a side perforated wide chamber (0.3 mBar positive pressure is applied on the inlet port in both designs). 93

Figure 4.13: Food dye in both designs (with trapped nematodes) showing that the side perforated wide chamber provides a better access for drugs. 94

Figure 4.14: I/V characteristic of a polarized and non-polarized electrode and the correlated equivalent circuit. 96

Figure 4.15: Model of an electrical double-layer. 98

Figure 4.16: Procedures for fabricating masters for casting PDMS channels. .. 99

Figure 4.17: The procedure for combining the PDMS channels to the NeuroChip100

Figure 4.18: The flow channel with a square shape. 102

Figure 4.19: Flow channel with a square shape. 103

Figure 4.20: A young adult *C. elegans* in the square flow channel. 104

Figure 4.21: Reaction of sensitizer when a positive photoresist is exposed by the UV light. 105

Figure 4.22: Shape change during reflow of resist at different baking temperature and for different times. Images are of 50-μm thick positive photoresist AZ40XT posts.....106

Figure 4.23: Attempts were made to find the best baking temperature and time for different width channels.....107

Figure 4.24: Comparison of the trapping channel before and after reflow at 130 ˚C for 30 seconds. 107

Figure 4.25: Images of flow channel with semi-circular shape moulded from a reflowed AZ40XT master. 108

Figure 4.26: Flow channel with semi-circular shape. 109

Figure 4.27: After surface treatment with oxygen plasma, hydrophilic oxide surfaces with H_2O/OH groups are produced on both PDMS and glass. 110

Figure 4.28: A NeuroChip that was not bonded properly over the electrode region. 110

Figure 4.29: Chemical bonding of PDMS to platinum electrodes with APTES and GPTMS. 111

Figure 4.30: Electrical circuit diagram of the external control system. 112

Figure 4.31: Diagram of the solenoid valve and schematic of the pneumatic connections. 113

Figure 4.32: Interface of the custom-made computer program written in Java, to control each port of the NeuroChip. 114

Figure 4.33: Micrograph of the NeuroChip. 115

Figure 4.34: Comparison of the examples of single EPG traces obtained from the microfluidic device with.....116

Figure 5.1: A comparison of basal EPG recordings with conventional method and the microfluidic device. 121

Figure 5.2: 5-HT (serotonin) stimulated worms: comparison of conventional method and the microfluidic device. Wild-type worms were incubated in 10 mM 5-HT for at least 10 minutes before, and throughout the entire experiment. 123

Figure 5.3: A comparison of basal EPG recordings with conventional method and the microfluidic device. Recordings were made from *eat-4 (n2474)* mutant worms in the absence of 5-HT. 126

Figure 5.4: Three different designs of microfluidic chips for rapid application of compounds. Dye labelling of the perfusate was used to track the time-course of application. 128

Figure 5.5: EPG recordings taken from three different designs of microfluidic chips for rapid application of compounds.....129

Figure 5.6: Response time to 5-HT for three different designs. 131

Figure 5.7: Detecting modulatory drug effects with NeuroChip. 132

Figure 5.8: Criteria of NeuroChip detection and selection of *C. elegans* mutants. 134

Figure 5.10: (A) Confocal image of an adult worm (L4 + 1 day; *peat-4::ChR-2;mRFP*).....137

Figure 5.11: Interrogation of neural network properties with optogenetics. .139

Figure 5.12: Shawn Lockery's microfluidic design for recording EPGs.....142

Figure 5.13: Ivermectin (IVM) effects on wild-type *C. elegans* and changes in EPG waveform and frequency. 143

Figure 6.1: Comparison of the size between the young adult (L4+1) and L2 stage *C. elegans*. 148

Figure 6.2: Two approaches for polymerization of photoresist. 149

Figure 6.3: The procedure (three steps) for fabricating a 3D structure with Nanoscibe. 150

Figure 6.4: Schematic of the two-photon polymerization with Nanoscribe. ...151

Figure 6.5: Designs a microfluidic device for smaller *C. elegans*. 152

Figure 6.6: Application main window of the Nanoslicer. 153

Figure 6.7: Application main window of the DeScribe. 154

Figure 6.8: Application main window of the Nanowrite with loaded structure for L2 stage *C. elegans*.....155

Figure 6.9: The structure visualized in graph view of NanoWrite.....155

Figure 6.10: Comparison of resolution after reducing the hatch distance by half. 156

Figure 6.11: Isolated complete voxel, the 3D image of the two photon excitation focal spot. 157

Figure 6.12: SEM image of the trapping channel written with 100× objective.158

Figure 6.13: The interface for focusing is found before writing. 159

Figure 6.14: Different initial writing interfaces gives different trap thickness.159

Figure 6.15: SEM images of the trapping channel master with an interface 8 μm below the glass-resist interface.....160

Figure 6.16: Top view of 6 trapping channels written by Nanoscribe with different interfaces, showing that Interface 0 has the best surface roughness while Interface 10 has the worst. 161

Figure 6.17: SU8 master fabricated by two-photon polymerization combined with standard photolithography. 162

Figure 6.18: Comparison of the trapped images and EPG waveforms collected from young adult (L4+1) and L2 *C. elegans* on-chip. 163

Figure 6.19: Video frames reveal the correlation between the pharyngeal pumping and the EPG waveform. 164

Figure 6.20: Comparison of the pump frequency collected from L4+1(3.43±0.15) and L2 (2.84±0.05) *C. elegans* on-chip. 165

Figure 6.21: Micrographic image shows the difference of the dimensions of the young adult *C. elegans*, L4 *C. elegans* and J2 *G. pallida*. 166

Figure 6.22: Geographical Distribution of the Potato Cyst Nematodes (PCN) distribute over the globe. 166

Figure 6.23: The process of J2 *G. pallida* invading the potato root. 167

Figure 6.24: Previously reported EPG recording obtained with conventional method. 169

Figure 6.25: Several trap shapes were tested to find the best shape for capturing the anterior of J2 *G. pallida*. 171

Figure 6.26: Different trapping position of J2 *G. pallida* generate EPG signal with different amplitude (in the presence of 2 mM 5-HT). 172

Figure 6.27: Comparison of EPG waveforms from L4+1 *C. elegans*, J2 *G. rostochiensis* 173

Figure 6.28: Comparison of EPG signals from J2 *G. pallida*, taken with the conventional method and the modified NeuroChip. 174

Figure 6.29: Time courses of EPG pump frequency, pump duration, and amplitude, comparing the stability of recording with conventional method (n=5) and the NeuroChip (n=9). 175

Figure 6.30: Video frames (80ms per frame) reveal the correlation between the stylet motion of J2 *G. pallida* and the EPG waveform. 177

Figure 6.31: Three different EPG waveforms observed during recording with the modified NeuroChip on J2 *G. pallida*. 178

Figure 6.32: Drug diffusion experiment to validate the performance of the modified NeuroChip on J2 *G. pallida*. 180

DECLARATION OF AUTHORSHIP

I, Chunxiao Hu

declare that the thesis entitled

Microfluidic Electrophysiological Device for Genetic and Chemical Biology Screening of Nematodes

and the work presented in the thesis are both my own, and have been generated by me as the result of my own original research. I confirm that:

- this work was done wholly or mainly while in candidature for a research degree at this University;
- where any part of this thesis has previously been submitted for a degree or any other qualification at this University or any other institution, this has been clearly stated;
- where I have consulted the published work of others, this is always clearly attributed;
- where I have quoted from the work of others, the source is always given. With the exception of such quotations, this thesis is entirely my own work;
- I have acknowledged all main sources of help;
- where the thesis is based on work done by myself jointly with others, I have made clear exactly what was done by others and what I have contributed myself;
- parts of this work have been published as: [[1, 2]]

Signed: ……

Date:……

Acknowledgements

I would like to thank Professor Hywel Morgan and Professor Lindy Holden-Dye for introducing me to the fascinating world of Lab-on-a-chip. I am grateful for their advice, feedback and patience. I would like to thank Professor Vincent O'Connor for generously giving me so much useful advice.

A special thank you is extended to the following people without whom this project would never have been accomplished: Caitriona Murray for showing me the operation of *C. elegans*; James Dillon for teaching me how to use the conventional electrophysiological equipments and the AutoEPG software for analyzing EPG recordings; James Kearn for doing all the conventional measurements involved in the validation experiments of the chip; Gareth Jones for advice on microfluidic valve design and continually loaning equipment; Sumit Kalse for advice on operating Nanoscribe; and Ben Mulcahy and Hans Schuppe for the assistance with confocal imaging.

I would like to thank my wife Zifang Zhang for tolerating my late nights and long working hours. I would like to thank my parents, Xueshi Hu and Xinmei Shen, my parents in law, Yuejin Zhang and Weiqun Zhuang and my family for all of their support throughout my University studies. I would like to thank my friends at home and in the Hybrid Biodevices Group for their encouragement.

Definitions and Abbreviations

3-D	Three-dimensional
6-OHDA	6-hydroxydopamine
AOM	Acousto-Optic Modulator
APTES	3-aminopropyltrimethoxysilane
ATW	Artificial Tap Water
BSA	Bovine Serum Albumin
CAD	Computer-aided design
CCD	Charge-Coupled Device
C. elegans	*Caenorhabditis elegans*
CFP	Cyan Fluorescent Protein
ChR2	Channelrhodopsin2
CO_2	Carbon Dioxide
DC	Direct Current
DIC	Differential Interference Contrast
DNA	Deoxyribonucleic Acid
DNQ	diazonaphthoquinone
EPG	Electropharyngeogram
EPSPs	Excitatory Postsynaptic Potentials
FRET	Förster Resonance Energy Transfer
G. pallida	*Globodera pallida*
GPTMS	3-glycidoxypropyltrimethoxysilane
G. rostochiensis	*Globodera rostochiensis*

GWL	General Writing Language
IBM	Ion Beam Milling
IPSPs	Inhibitory Postsynaptic Potentials
IR	Infrared
IVM	Ivermectin
J2	Second-stage Juveniles
L1, L2, L3, L4	Larvae 1, 2, 3, 4 stage
LED	Light-Emitting Diode
LEVR	Levamisole-Resistant
MC	Marginal Cell Neurone
MI	Moto-Interneurone
mRFP	monomeric Red Fluorescent Protein
ms	millisecond
mV	millivolt
N_2	Nitrogen
NA	Numerical Aperture
NGM	Nematode growth media
NP	Normal Pump
NSM	Neurosecretory Motoneurone
O_2	Oxygen
O. dentatum	*Oesophagotomum dentatum*
PCN	Potato Cyst Nematodes
PCR	Polymerase Chain Reaction
PD	Parkinson's disease

PDMS	Poly-Dimethyl-Siloxane
PEB	Post Exposure Bake
PSI	Pound per Square Inch
RFP	Red Fluorescent Protein
RNA	Ribonucleic Acid
RNAi	Ribonucleic Acid interference
RP	Rapid Pump
rpm	round per minute
s.d.	standard deviation
s.e.m	standard error of the mean
SEM	Scanning Electron Microscope
SNR	Signal to Noise Ratio
SP	Short Pump
STL	Standard Tessellation Language
TB	Terminal bulb
UV	Ultraviolet
YFP	Yellow Fluorescent Protein

5-HT	Serotonin
N2	Wild Type
M1, M2, M3, M4, M5	5 *C. elegans* Motoneurones
I1, I2, I3, I4, I5, I6	6 *C. elegans* Interneurones
SENS	Levamisole-Sensitive
e spike	The first positive spike of the EPG signal

E spike	The second positive spike of the EPG signal
P spike	The small negative spike following E spike
R spike	The first negative spike after P spikes
r spike	The second negative spike after P spikes

Chapter 1: Introduction

1.1 Motivation

The nematode *Caenorhabditis elegans* (*C. elegans*) is a small (1mm long and 959 somatic cells), free living and transparent roundworm. It is the first multicellular organism to have its genome completely sequenced and neurons mapped [3-6]. Genetic and chemical biology screens on the nematode *Caenorhabditis elegans* have provided fundamental insight into neural function encompassing key aspects of neurosecretion, synapse formation and regeneration [7-9]. These approaches are based on visual observation to delineate phenotypes. The ability to screen for *C. elegans* synaptic phenotypes based on an electrophysiological signature would add a new level of refinement to probing synaptic function. Indeed mutations that alter synaptic transmission are not always associated with an obvious morphological or behavioural phenotype [10]. Typically, electrophysiological recordings, particularly in *C. elegans*, are technically challenging and time-consuming and thus not suited to screening approaches. However, the *C. elegans* pharyngeal neural network provides an opportunity to circumvent this. Its activity, the electropharyngeogram (EPG), can be captured by a suction electrode placed over the mouth of the intact worm [11]. This records the electrical signal of the rhythmically pumping pharynx to monitor frequency and duration of the contraction-relaxation cycle. Moreover, fine features of the EPG are synaptically driven events from excitatory and inhibitory neurones and can report on modulatory components of the circuit [11-15]. However, with a small, flexible, and continuously moving body, the manipulation of *C. elegans* becomes a challenging task [16]. For many years, it has been hard to exploit some of the unique properties of *C. elegans* because of this limitation.

Other parasitic species of nematode, such as the plant parasitic nematodes [17], are a global menace to agriculture and have a severe economic impact as most major food crops are susceptible to infestation. These nematodes possess a stylet, a hollow protrusible spear that is integral in the invasion of the host plant as a juvenile and in feeding once immotile within the host plant.

When invading the host, the movements of the stylet back and forth are believed to allow mechanical piercing of the root epidermis to allow entry [18, 19]. It is clear that the behaviour of the stylet is utterly essential for plant parasitism and yet relatively little is known about the molecular and neural mechanisms that underpin these behaviours. Moreover, inhibition or interference of stylet activity presents a potentially effective means of reducing root penetration by PPNs by preventing feeding and hence development beyond the juvenile stages. However, the second juvenile *G. pallida* has a size even smaller than *C. elegans*, making it more difficult to be studied.

1.2 Objective

Recently microfluidic devices have been designed that facilitate *C. elegans* screens by allowing controlled immobilization [20-23], high resolution imaging [21, 22, 24-26], and behavioural or developmental observation [27-35]. Not only has this enabled high-throughput studies [36-40] but it has also delineated new phenotypes by virtue of refined analysis [41]. The objective of this project was the development of a microfluidic device to replace the need for manual trapping and conventional suction tube and to progress towards resolving synaptically driven events in the EPG. Moreover, the objective was to design a device that would be optimised for trapping worms in the correct orientation, mimicking the shape of a conventional suction tube aperture and for rapid drug or chemical application. The project also sought to establish capability for selection of mutant from wild-type worms on the basis of their distinctive electrophysiological signature.

Finally, the project aimed to use the *C. elegans* design to develop a device that could accommodate second larval (L2) stage *C. elegans* and second juvenile (J2) stage *G. pallida*, showing applicability for small nematodes which otherwise are not tractable to this experimental approach.

Compared to the existing approach, this device is easier to operate and especially for intact worm, has a higher throughput, is cable of doing some novel experiments such as mutant sorting, imaging, and optogenetics, and is

easy to be modified for other organisms. It has the potential to undertake various applications related to electrophysiological analysis.

1.3 Thesis organization

Chapter 2 is the literature review, including the conventional electrophysiological method on *C. elegans* and recent microfluidic approaches for the research on both *C. elegans* and *G. pallida*.

Chapter 3 demonstrates a microfluidic channel that has successfully acquired EPG signals from *C. elegans*. Standard photolithography [42] and soft lithography [43] had been employed for the fabrication. It has a simple structure with one single channel, containing an inlet port for loading the *C. elegans*, an outlet port for disposing liquid, and a trapping channel for capturing the worm's head. Compared to the conventional method, this microfluidic channel is able to deliver the worm to the trap, restrict the movement of the nematode and collect the EPG recording with easier and more precise control. High quality EPG signals have been obtained with this device.

In Chapter 4, an integrated microfluidic platform for electrophysiological analysis of *C. elegans* is introduced, called NeuroChip. Compared to the microfluidic channel introduced in last chapter, NeuroChip has additional bypass flow channels, enabling transportation of the worm and application of drug under precise control. Another layer of control channel was designed to actuate individual pneumatic microfluidic valves for opening and closing these bypass flow channels separately. In addition a series of micro-pillars were placed near the worm port for directing the orientation of the nematode, facilitating the movement of the worm into the trap with head-to-tail orientation. Platinum electrodes were embedded to replace the external silver/silver chloride electrodes, making this device an integrated microfluidic platform for electrophysiological analysis on *C. elegans*. High quality EPG signals, which are comparable to that collected from the conventional EPG experiment, have been obtained with this integrated microfluidic chip.

Chapter 5 describes the experiments with NeuroChip for genetic and chemical biology screening of *C. elegans*, such as detection of effects on synaptic cholinergic signalling, rapid application of compounds and simultaneous electrophysiological recording, detection of effects on inhibitory

neurotransmission and mutant sorting, and interrogating neural network properties with optogenetics.

Modified NeuroChip for smaller nematodes is demonstrated in Chapter 6. So far, no microfluidic chip has been published for electrophysiological studies on smaller species of nematodes but this would be of great utility in analysis of feeding in this economically and medically important phylum and furthermore have potential applications in antiparasitic drug discovery. Technology called two-photon polymerization was adopted for fabricating the smaller trapping channel. EPG signals have been successfully acquired from both the L2 stage *C. elegans* and J2 stage *G. pallida*. This microfluidic device could also be modified to trap other parasitic species for broader applications.

Chapter 7 provides the conclusions from this study and discusses the future prospects it underpins.

Chapter 2: Literature Review

2.1 Introduction to *C. elegans*

C. elegans is a nematode worm that lives on bacteria in the soil and rotting fruit which was introduced for biological investigations in the 1960s by Sydney Brenner. It has proven to have many advantages for investigations of developmental biology, neurobiology and behavioral biology [44]. First, *C. elegans* is a eukaryote and it shares cellular and molecular structures and control pathways with higher organisms. It is a multicellular organism, which goes through a complex developmental process, including embryogenesis, morphogenesis, and growth to an adult. Thus, biological information learnt from *C. elegans* may be directly applicable to more complex organisms, such as humans. About 35% of *C. elegans* genes have human homologs. Second, *C. elegans* is very genetically tractable. Its genome size is relatively small (9.7×10^7 base pairs), when compared to the human genome which is estimated to consist of 3 billion base pairs (3×10^9 base pairs). The entire *C. elegans* genome has been sequenced. In addition, it is one of the simplest organisms with a nervous system. In the hermaphrodite, this comprises 302 neurons [45] whose pattern of connectivity has been completely mapped. Third, the nematode is easy to maintain in the laboratory and has a fast and convenient life cycle (~ 3 days). Embryogenesis occurs in about 12 hours, development to the adult stage occurs in 2.5 days including four larval stages (L1 to L4), and the life span is 2-3 weeks.

2.2 Development of microfluidic approaches for research of nematodes

In recent years, microfluidics has been used as a new tool for neurobiological studies [16]. It has several distinct advantages. First microchannels can be fabricated with small dimensions ranging from several microns to hundreds of microns, providing an excellent microenvironment for the manipulation of worms and economical usage of chemicals or drugs. Second, the material used in the fabrication of microfluidic devices is usually poly-dimethyl-siloxane (PDMS). It is a transparent, air-permeable, elastic and cheap material, which is

ideal for observing or imaging worms, and fabricating disposable devices. Third, microfluidic devices are capable of handling large populations of nematodes in a high-throughput fashion with automatic control. In addition, different sizes of channels can be easily and quickly designed and fabricated for accommodating different species of nematode.

2.2.1 Microfluidic devices for *C. elegans*

C. elegans is the model nematode used in research involving microfluidic devices. Five applications of microfluidic chips will be described in this section: Immobilization of *C. elegans* on-chip; observation and imaging of *C. elegans* on-chip; rapid sorting and screening on-chip; laser surgery of *C. elegans* on-chip; droplet-based application of *C. elegans* on-chip.

2.2.1.1 Immobilization of *C. elegans* on-chip

As previously introduced, *C. elegans* has a small, flexible, and continuously moving body, thus immobilizing the worm on a chip is challenging. Conventional experiment requires the worm to be fixed: glue [46, 47] or anaesthetic compounds [48] are used to achieve this. Although these methods have good performance, some limitations occur with increased requirement for precise analysis. The emergence of microfluidic technology makes it possible to immobilize the roundworm in different ways as shown by the examples of Figure 2.1.

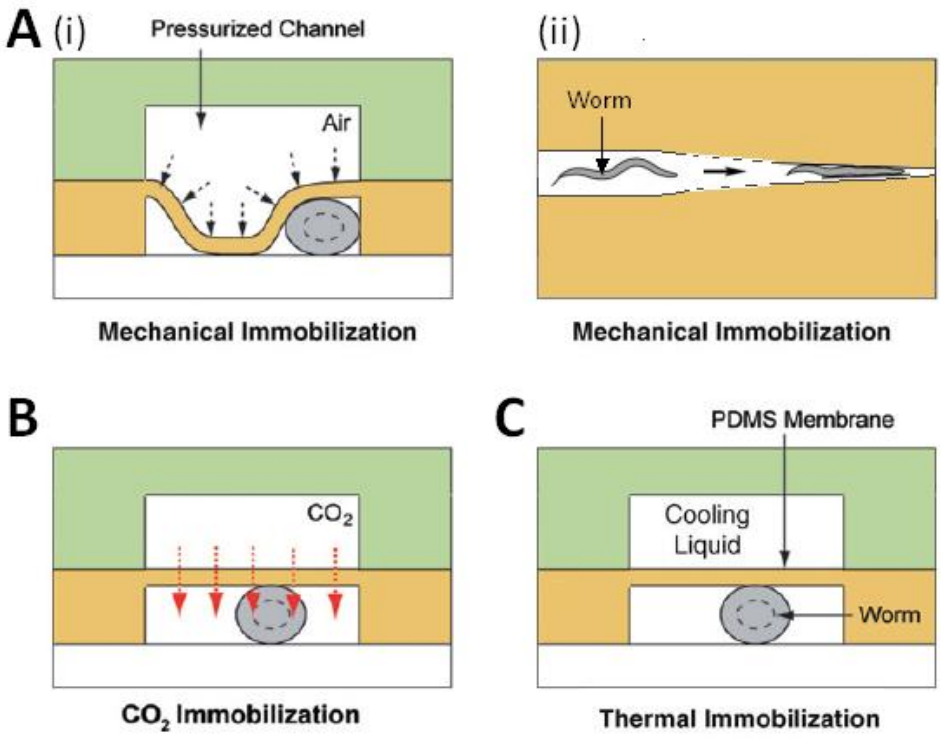

Figure 2.1: Three different methods for immobilizing *C. elegans.* (A) Mechanical method: (i) Pressurize a thin layer of PDMS membrane to compress the worm, (ii) Use a tapering channel to clamp the animal. (B) Carbon dioxide (CO_2) approach. (C) Thermal method. Picture A(ii) is the top view; all others are cross-sections. Green colour channel is for control and yellow for flow. Pictures are adapted from [20].

At present, three different microfluidic approaches are used to immobilize *C. elegans* on-chip: mechanical immobilization [20, 21], carbon dioxide (CO_2) immobilization [20], and thermal immobilization [49, 50]. There are two ways to immobilize the worm mechanically. The first one utilizes the elastic and deformable properties of PDMS (Figure 2.1A(i)). When a high pressure (about 172 kPa) is applied to the control channel, the membrane collapses onto the worm and squeezes it onto the side of the micro channel [20]. It is important to neither squeeze the nematode too much which would damage it, nor leave too much space around the worm which would allow it to escape. *C. elegans* can be immobilized for a period of a few minutes using this method. Tapering structures are another good way to restrict the movement of worm (Figure 2.1A(ii)). More than 100 tapering channels were paralleled into an array, enabling the device to investigate natural variations in the physiology and

behaviour of large populations of *C. elegans* [21]. The carbon dioxide immobilization (Figure 2.1B) uses the same structure as the first mechanical method developed by Chokshi in 2008 [20]. When *C. elegans* is loaded in the correct position in the flow channel, a CO_2 microenvironment is created by pumping pure CO_2 through the control layer. Since PDMS is highly permeable to nonpolar gases [51], CO_2 diffuses rapidly through the thin PDMS membrane into the flow layer and stops the movement of the worm. Chokshi, et al. [20] found that CO_2 at 69kPa would cause minimum deflection of the membrane, providing long-term worm immobilization of up to 2 hours. Chung, et al. [50] developed an approach to immobilise *C. elegans* by reducing the temperature. A two-layer architecture, including one control layer and one flow layer was also adopted in this approach (Figure 2.1C). Cooling liquid was added into the control channel to decrease the temperature of the flow channel where the worm resides. The PDMS membrane is thin and highly permeable, thus the temperature of the microenvironment reaches around 4 °C rapidly, 'freezing' the animal. This immobilization process provides a means of performing further research on the nematode, such as imaging, screening, and laser surgery.

2.2.1.2 Observation and imaging of *C. elegans* on-chip

C. elegans is an excellent model organism for studying the neuronal basis of behaviour [25]. However, its tiny size and continuously moving body make it challenging to do real time observation, for example continuous live imaging, delivery of any stimuli to its nose and to perform calcium imaging in a controlled environment.

In 2009, Hulme et al, [33] demonstrated a microfluidic chip for performing lifelong observation of the nematode *C. elegans*. Typically to perform long term studies, individual worms are maintained and observed on separate agar-filled culture Petri dishes. Each worm is transferred to a fresh Petri dish every day during the period of reproduction in order to distinguish the worm from its progeny, a method which is experimentally challenging [33]. Certain processes can be simplified using a microfluidic device which comprises an array of chambers to confine individual worms, an array of channels with a tapering shape for immobilizing the nematodes, and a network of microfluidic channels

for delivering bacterial food or chemicals (Figure 2.2). Two modes of observation can be undertaken with this device. One worm is confined in the round chamber and another is immobilised in the tapering microfluidic channel. Since bacterial food can be delivered into the chamber, the lifespan and any lifespan related behaviour can be observed, such as survival rate, features of the growth phase, and loss of swimming, making it possible to track behavioural and physiological phenotypes in individual worms over a period of time.

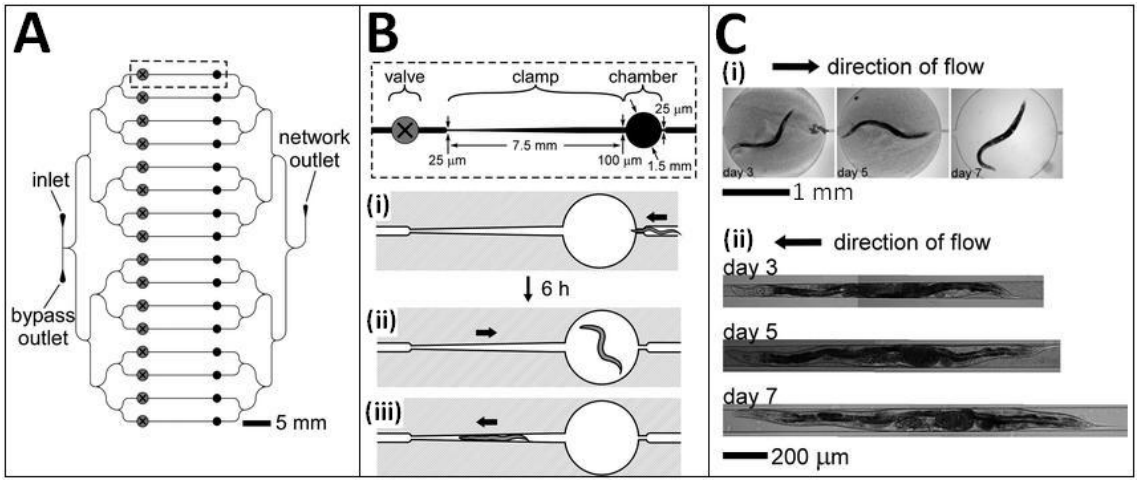

Figure 2.2: Design of the microfluidic device for lifelong observation of *C. elegans*. (A) Design of an array of 16 chambers. A network of branching distribution channels delivers a suspension of E. coli from the inlet, through the chambers, and to the outlet. The bypass outlet enables the removal of sedimented bacteria from the inlet. The presence of a screw valve in each branch of the network enables each chamber and clamp to be fluidically isolated. (B) The dashed rectangle indicates the location of the features described in (A). (i) Loading the worm into the chamber. The width of the microchannel directly to the right of the chamber is just wide enough to allow the passage of a worm in the early stage of L4 into the chamber. The arrow indicates the direction of flow. (ii) After approximately 6 hours at 24 ˚C, the worm becomes too large to fit within the microfluidic channels, and thus continuous flow of liquid through the chamber may commence. Continuous flow of a suspension of bacteria from left to right provides food to the worm and prevents the worm from entering the clamp. (iii) By reversing the direction of flow from right to left, the worm is

directed into the clamp for temporary immobilization. (C) Images of *C. elegans* inside the device. (i) Images of a single wild-type worm (N2) within the microfluidic chamber. The worm hatched on day 0, and was loaded into the microfluidic device on day 2 (during the L4 larval stage). (ii) Composite images of the worm from panel (i) immobilized within the microfluidic worm clamp. The worm was periodically loaded from the chamber into the clamp to enable detailed observation of the body of the worm. Pictures are adapted from [33].

From 2010, several microfluidic devices for real time observation and live imaging have been developed by Hang Lu's group [38, 52, 53]. The first platform was designed and fabricated in 2010 for high-throughput study of synaptic transmission [38] and contains two PDMS layers: a layer of eight imaging channels connected with a loading and an unloading chamber, and a layer of two pneumatic valves for isolating the imaging channels (Figure 2.3A). Light sensitive mutants of *C. elegans* with *channelrhodopsin-2* (ChR2) were used to examine synaptic transmission with this device. Initially worms are pushed into the imaging channels by opening Valve 2 and closing Valve 1. *Channelrhodopsins* are a subfamily of retinylidene proteins (rhodopsins) that function as light-gated ion channels [54], in which, *channelrhodopsin-1* (ChR1) is a light-gated proton channel, and *channelrhodopsin-2* is a directly light-gated cation-selective membrane channel [55]. When eight channels have been filled with the nematodes, Valve 2 is closed (Figure 2.3C), and blue light (0.3 mW/mm^2) is illuminated onto the entire chip. The changes of body length can be observed, imaged, and further analyzed by custom-written software (Figure 2.3D).

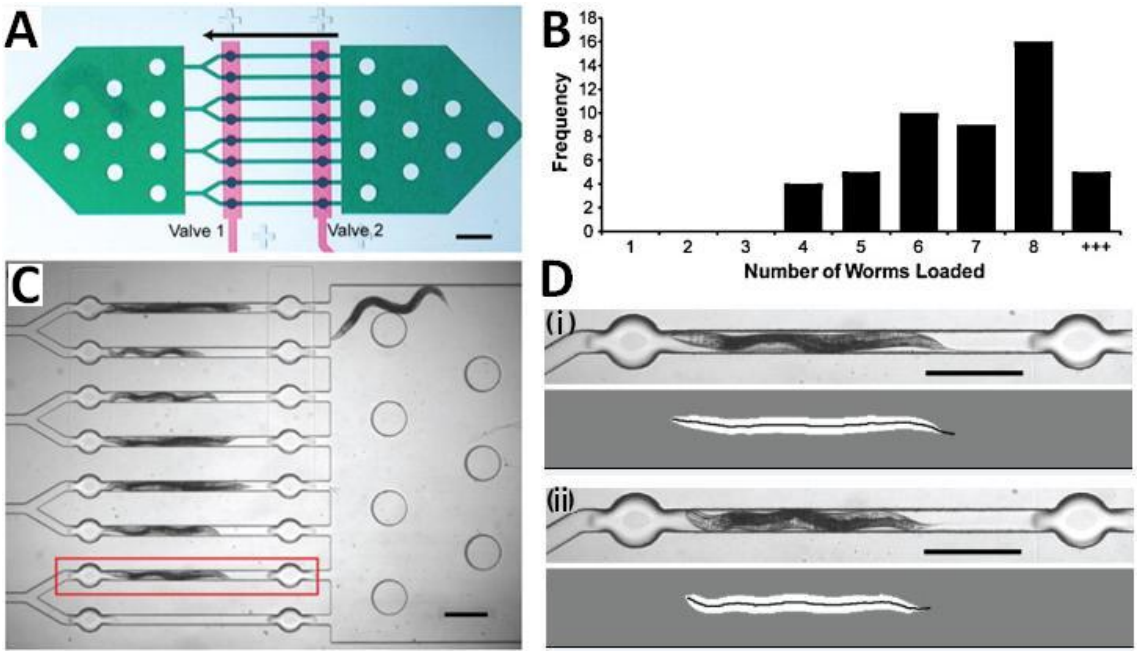

Figure 2.3: Microfluidic chip for high-throughput study of synaptic transmission. (A) Layout of the device. Green channels are in the flow layer (where *C. elegans* are located) and the red channels are the valve control layer. Arrow indicates direction of worm loading. Scale bar is 500 μm. (B) Histogram of the worm loading efficiency. Channels with zero or multiple worms (column +++) were not analyzed. An average of ~6.6 worms could be analyzed per loading cycle. (C) Bright field image of a microfluidic device with loaded worms prior to blue light illumination. (D) Zoom-in view of the areas selected by the red boxes. An example of body length (i) before and (ii) after applying the blue light illumination is shown. Custom-made software was written to measure the body length. Pictures are adapted from [38].

Around one year later in 2011, another microfluidic platform with chamber arrays was designed by Lu's group to study whole-organism behaviour-based chemical screening [52]. This single-layer PDMS device consists of a serpentine channel and an array of circular chambers that connect each row of the serpentine channel to the next (Figure 2.4A). Worm loading areas (Figure 2.4B) are separated from the main worm housing chamber by a narrow "stopper" region, permitting single worms to be trapped in the loading areas awaiting entry into the main chamber [52]. Figure 2.4C shows the operating process.

Worms are loaded from the first inlet (I1) from a liquid suspension of worms. The outlet is then opened to locate worms into the loading areas by gravity. A plug is then rapidly inserted into I1 to extend the size of the "stopper", allowing the worm to enter the chambers. Chemical stimuli are easily delivered via the second inlet (I2) by unplugging the small plug. The device reaches a steady state drug concentration in all 48 chambers in about 13 seconds [52]. The behavioural response to stimulus can be imaged and further analyzed by custom-made software through the housing chambers.

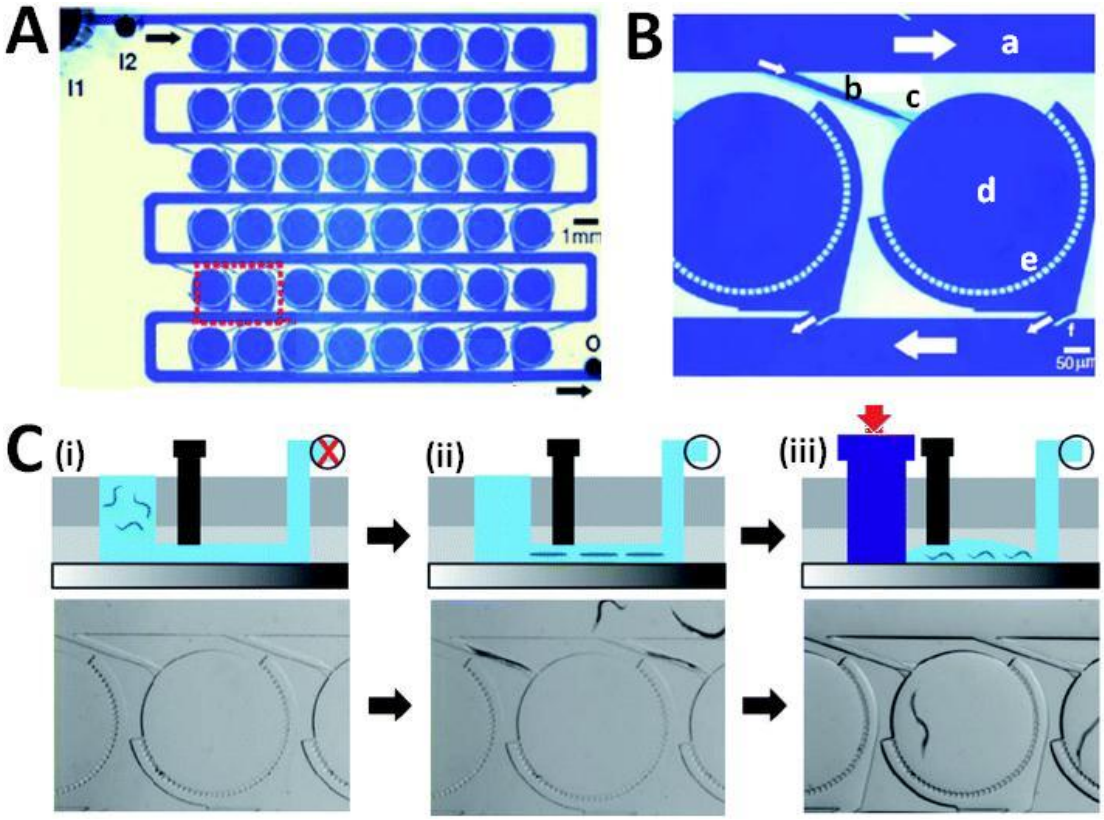

Figure 2.4: Microfluidic chamber arrays for whole-organism behaviour-based chemical screening. (A) Dye -filled image of the device showing array of 48 circular chambers connected to the serpentine channel. Black arrows represent flow direction. I1, I2 and O indicate the worm inlet, chemical inlet and outlet respectively. (B) Zoomed in image of the boxed region in (A) showing microfluidic components to enable high-throughput single worm loading and chemical delivery. (a), serpentine channel; (b), single worm loading channel; (c), stopper; (d), circular chamber; (e), diverging channels; (f), chamber outlet. White arrows represent flow direction. (C) Device operation process with schematic cross-section and optical top view of the device. (i) After

filling the device with buffer, outlet valve is closed, and worm suspension is pipetted in the worm inlet. (ii) The outlet valve is open to load the worm into the single worm loading channels by gravity. (iii) Once the worms are in the single loading channels, the large plug is rapidly inserted into the worm inlet, applying pressure to expand the stopper and push the worms through the stopper and into the chambers. Pictures are adopted from [52].

In 2013, Lu's group demonstrated a novel microfluidic device [53] for direct observation of *C. elegans* physiological processes, called C.L.I.P (continuous live imaging platform). Figure 2.5A presents the layout of this single-layer PDMS chip, which contains five inlets and outlets and an array of trapping channels. Worms are loaded into the device via the worm loading inlet, followed by application of a negative pressure from the outlet to suck the nematodes into the trapping channels. Next a solution with 10 μm microbeads is loaded from the worm loading inlet to physically prevent backward motion and tail swinging of the trapped nematode. After that, the immobilizing solution of Pluronic F127 is applied at a temperature of 0 ºC. As it warms to room temperature, it becomes a gel, which immobilizes the body of the worm firmly. Food or drug is then delivered to the head of the trapped worm through the muzzle (Figure 2.5B) via the media inlets. Long-term imaging can be undertaken under both bright field and the fluorescent microscopy (Figure 2.5C). This platform has applications in furthering the understanding of the effect of learning on synaptic physiology and mapping of functional network connections of the nervous system.

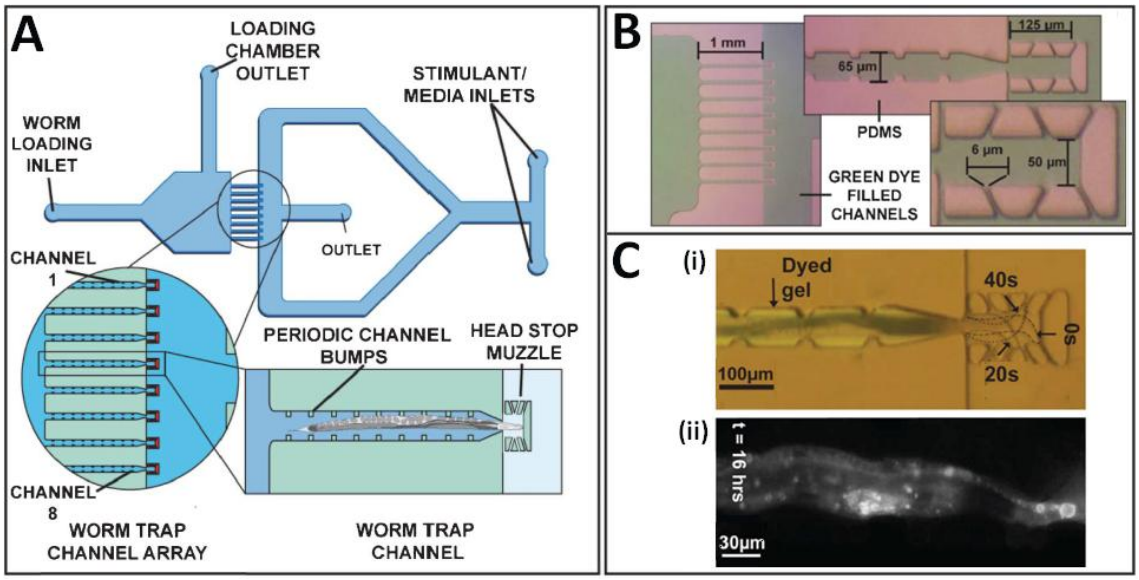

Figure 2.5: C.L.I.P (continuous live imaging platform) for direct observation of *C. elegans* physiological processes. (A) Schematic of the design of the device, which is a simple array of trapping channels. Animals and solutions are loaded through the worm loading inlet, where animals are moved to the 8-channel array. Individual worms are immobilized inside the channels just on the bodies with the immobilizing agent, Pluronic F127 solution and microbeads. The animals' heads are free to move and feed inside the head stop muzzle. Nutrients are delivered to the muzzle through media inlets via symmetric bifurcated flow. (B) PDMS channels with filled green dye. The muzzle is designed to only allow the head of an animal to enter. Narrowed channels are built for the access of chemicals. Bumps in the trapping channel help prevent sinusoidal body movement of the animals. (C) Bright field and fluorescent image of an immobilized worm. (i) Bright field images from three time points are overlaid on top of each other. The animal's head is in a different position at each time point. Meanwhile, the body is immobilized by the gel. (ii) A fluorescence image of an animal trapped on the device for 16 hours. The presence of fluorescent markers suggests that basic physiology was maintained. Pictures are adopted from [53].

Typical calcium imaging experiments are based on a so-called "glued worm preparation" procedure [56]. A problem with this approach is possible toxicity

of the glue. In order to address this problem, Chronis, et al. [25] demonstrated a microfluidic device which circumvents the requirement for glue and in turn permits high resolution calcium imaging. Three years later, they improved the design as well as the methodology, enabling automatic calcium imaging of chemosensory neurons in single *C. elegans* [26]. Similar to previous designs, the modified microfluidic biochip mainly comprises a trapping channel (used for loading and immobilizing single worms), and a 4-flow architecture for precise delivery of the stimulus of interest to the worm's nose (Figure 2.6). An additional three structures were implemented to achieve automatic operation: arrays of micropillars near the inlet port prior to the trapping channel, a 'flush' channel connected to the trapping channel, and a 'step' architecture inside the flow channel (Figure 2.6A). Seven micropillars were arranged in an array to allow the worm to enter the trap nose first, also known as 'head-to-tail' orientation. The pillars act as obstacles to the worm's passage towards the trap. Under a positive pressure from the inlet, the nematode tends to escape through the micropillar array with its head first [26]. Around 70% of the worms enter the trapping channel with head-to-tail orientation in the presence of micropillars, compared to less than 5% without this structure. The 'flush' channel was added at the side of the trapping channel for either unloading the worm, or to prevent other worms from entering the trap by generating a bi-directional flow in the trapping channel. To keep the worm in position, the size of the trapping channel is similar to the size of the young adult *C. elegans*. To quickly load and unload the worm, a channel size larger than the worm is required. Thus, a 'step' architecture was adopted. Although it is a platform operating on single worm, it is possible to capture stimulus-evoked neural responses from tens of worms per hour without any manual intervention so as to reveal the effect of age on the ASH chemosensory neuron [26].

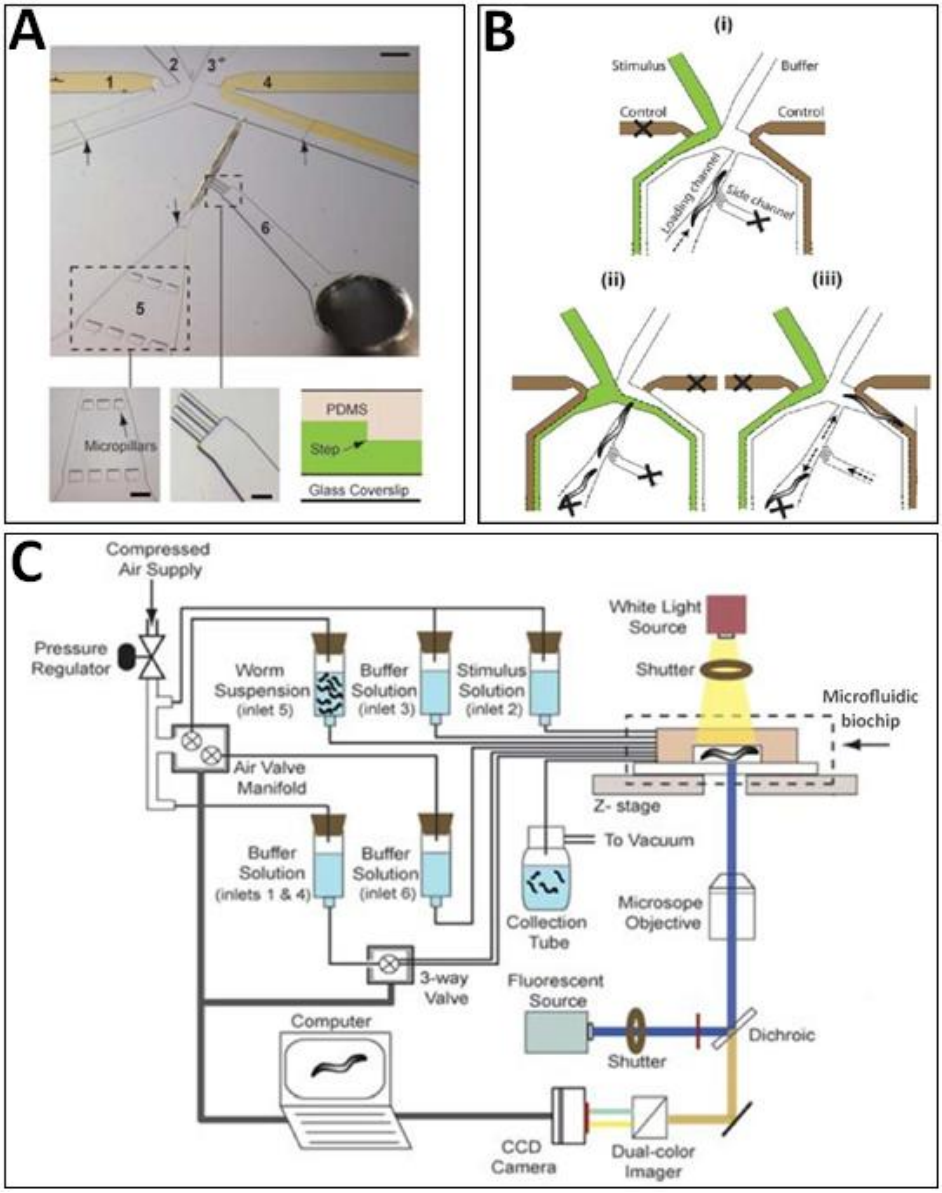

Figure 2.6: Microfluidic platform for calcium imaging of chemosensory neurons in *C. elegans*. (A) The microfluidic biochip consists of a worm-trapping channel, a 4-flow microfluidic network (labelled as 1, 2, 3 and 4) for stimulus delivery and a flush micro-channel for unloading (Scale bar, 200 μm). Two arrays of PDMS micro-pillar are labelled as 5 (Scale bars, 50 μm), a flush channel to unload the worm is labeled as 6 (Scale bars, 50 μm), and the step architecture as illustrated in the cross-sectional view are marked with 'arrows' in above image. (B) The working principle of the biochip: (i) A single worm is loaded into the trapping channel by adding a positive pressure to the inlet. The left control channel is closed to keep the stimulus away from the worm (X denotes a closed micro-channel). (ii) The worm is captured inside the

trapping channel. Open the left control channel, close the right one, and release the inlet pressure at the same time to allow the stimulus to flow through the nose of the worm. The ASH cell body is then located, brought into focus and its response to the applied stimulus is recorded. (iii) The worm is unloaded by applying a positive pressure to the flush channel. (C) The automated functional imaging platform. It integrates a microfluidic biochip, a pressure-control system connecting to the worm suspension, buffer and stimulus solutions, an epifluorescent microscope equipped with a z-moving stage, a dual-colour imager (for Förster resonance energy transfer (abbreviated FRET) imaging) attached to a back- illuminated CCD camera, and a computer with graphical LabVIEW interface. Pictures are adapted from [26].

A custom-made graphical *LabVIEW* interface was utilized to automatically control the platform (Figure 2.6C). Once individual worms are trapped in the trapping channel, an image recognition algorithm identifies the worm's orientation, and the worm is discarded by activating the flush channel if it comes in tail first. When the worm is trapped in the correct orientation, the neuronal cell body is detected and brought into focus by controlling the z-stage. After that, the stimulus of interest is delivered to the worm's nose and the corresponding response recorded. After data from one worm is recorded, it is flushed away by activating the flush channel before loading another worm to repeat the assay.

The compound TN-XL, genetically encoded FRET indicator [57, 58], is fast and stable in calcium imaging experiments, and shows a significantly enhanced fluorescence change. It was used to record glycerol-evoked response from the ASH neuron. An age-synchronous population of 212 *C. elegans* with different ages (from L4+1 day to L4+5 days) were exposed to a 70 second stimulus (1 M glycerol) pulse, and a total of 80 recordings were made from L4+1 day worms, and 60, 60, 12 from L4+3, +4, +5 days worms respectively. The stimulus-evoked calcium transients were quantified by analyzing the corresponding FRET ratio change (Figure 2.7). The average slope and peak FRET ratio change increased for Day1, Day 3, and Day 4 worms while there was an obvious

decrease for Day 5 nematode (Figure 2.7C). To quantify the stimulus-evoked calcium transients, the author obtained the corresponding FRET ratio changes, and assumed that the ASH chemosensory neuron is age-dependent.

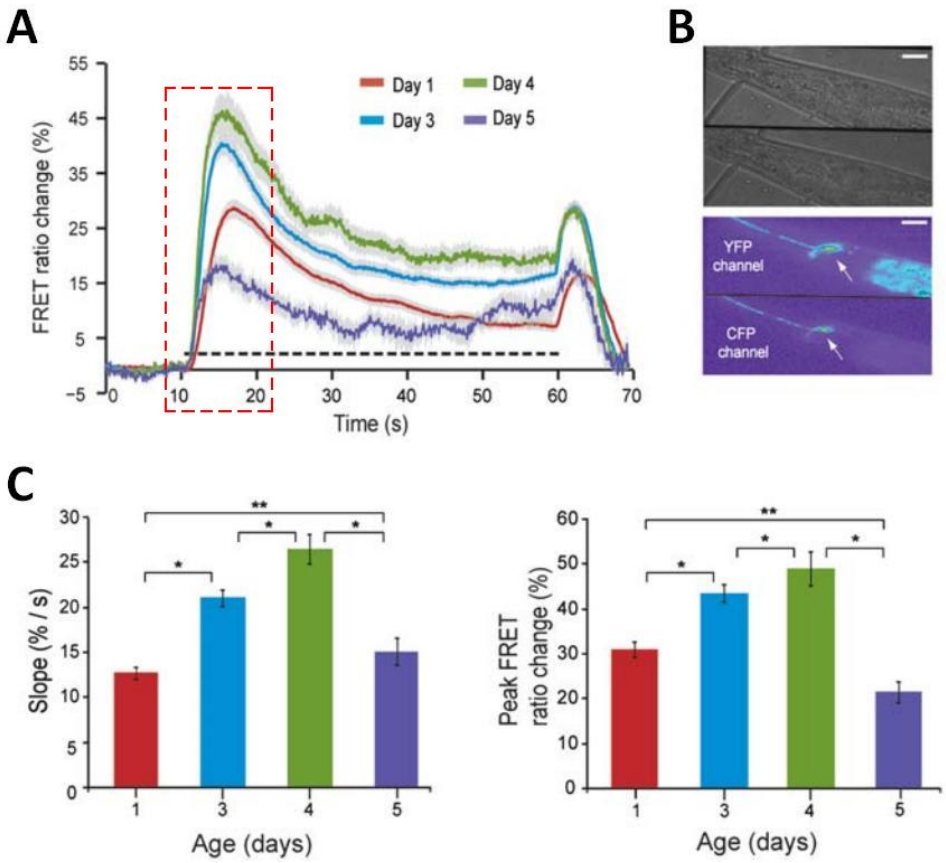

Figure 2.7: The glycerol-evoked response from the ASH neuron. (A) The FRET ratio changes with the increase of time. The individual curves represent an average of 80, 60, 60 and 12 recordings from Day 1, Day 3, Day 4 and Day 5 worms (L4+1 day worms are taken as Day 1 worms) respectively. The dashed line indicates the time of stimulus presence. (B) Bright-field (top) and pseudo colour fluorescence (bottom) image of a trapped worm. The ASH neuron is marked with white arrow. In the pseudo colour image, the top and bottom half represent the Yellow Fluorescent Protein (YFP) and Cyan Fluorescent Protein (CFP) channels respectively. Scale bars, 5 μm. (C) The slope and peak FRET ratio change from red dashed squared area in A for different age worms. Error bars indicate standard error of mean (**P<0.001, *P<0.01, student's t-test). Pictures are adapted from [26].

The automated platform enables calcium imaging from a large population of *C. elegans* at a relatively high speed (60 worms in 2 hours), revealing the physiological properties of the ASH neuron. It has the potential to be used in neurobiological research, including high-throughput functional imaging and drug screening.

2.2.1.3 Rapid sorting and screening on-chip

For many years, picking, sorting, and transferring individual *C. elegans* has been a challenge for neurobiological scientists. Large-scale assays such as mutagenesis, drug, and RNAi screens [8, 59] may take months or even years to complete [36]. The emergence of microfluidic technology offers a way to break through this barrier.

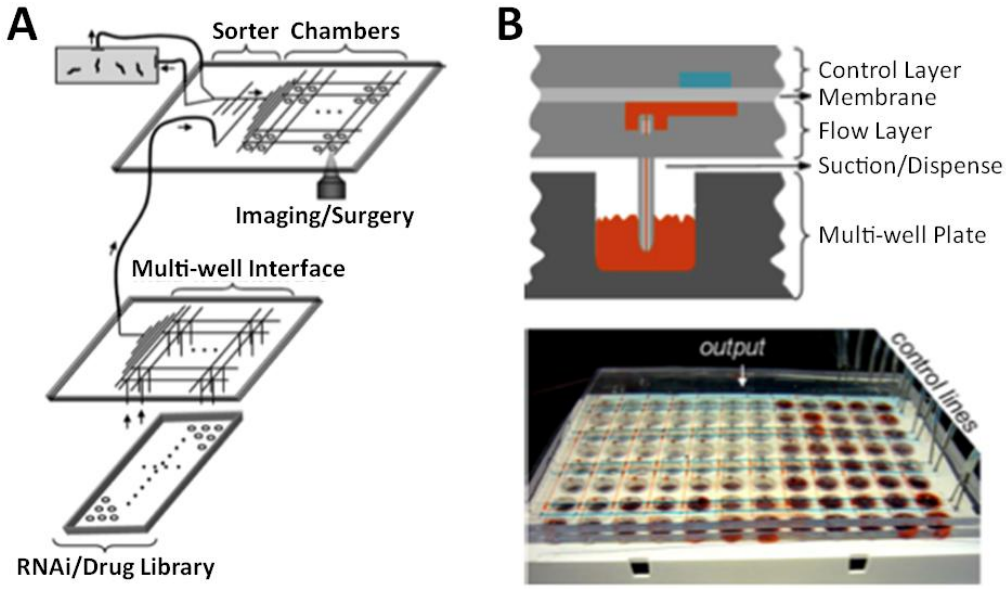

Figure 2.8: Schematic and image of the microfluidic system for high-throughput whole-animal sorting and screening at subcellular resolution. (A) Schematic of the platform. High-throughput phenotype sorting can be performed at cellular or subcellular resolution by cascading the microfluidic sorter with a multiwell dispenser. Large-scale RNAi/drug screens can be achieved by delivering standard multiwell plate libraries to the microfluidic screening chambers via the multiwell interface chips. (B) Schematic of the cross-section of the device and real look of the multi-well plate. Pictures are adapted from [36].

In 2007, Rohde, et al. [36] developed an integrated microfluidic platform which is capable of whole-worm, high-throughput sorting and large-scale drug screening with subcellular resolution. In general, this platform is divided into two functional parts: High-throughput worm-sorter and large-scale screening chamber (Figure 2.8). The sorter enables rapid selection of organisms with phenotypes of interest and multi-well chambers provide an interface for large-scale genetic and drug screens.

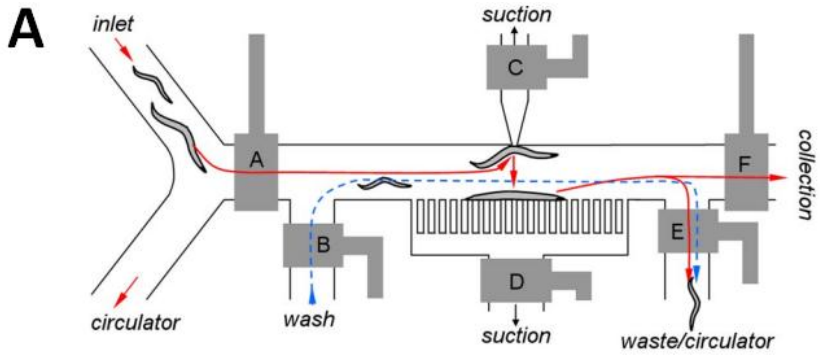

B

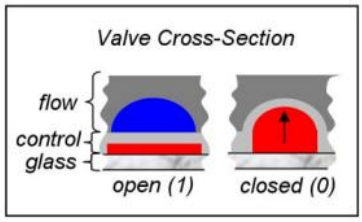

C

Steps	A	B	C	D	E	F
1 (clean)	0	1	0	0	1	0
2 (capture)	1	0	1	0	1	0
3 (wash)	0	1	1	0	1	0
4 (isolate)	0	1	1	1	0	0
5 (immobilize)	0	1	0	1	0	0
6 (collect)	0	1	0	0	1/0	0/1

Figure 2.9: Structure and operating steps of the high-throughput sorter and cross-section view of the valve. (A) In total six valves (labelled with letters A to F) are used in the sorter to control the flow of worms in the flow channel layer. (B) Schematic of the valve cross-section. The flow channel is filled with blue colour while the control channel is red. The thin membrane in between can be pressurised up to close the flow channel. (C) The operating steps are listed in the table. These six steps (clean, capture, wash, isolate, immobilize, and collect) are achieved by actuating different valves under order. A value of 1 represents an open valve, and a value of 0 represents a closed valve, as illustrated in B. The actuating power to push up the membrane of control layer is nitrogen gas. Picture is adapted from [36].

The layout and operation of the high-throughput worm-sorter are shown in Figure 2.9. It consists of two layers: a flow channel layer and control channel layer made from PDMS [60]. The flow channel layer contains micro-channels for manipulating and micro-chambers for incubating *C. elegans*. The control channel layer has micro-valves that when pressurized, push up the membrane into the flow channels to block or redirect the flow [61]. By selectively opening and closing micro-valves, one can sequentially clean the immobilization chamber, capture the worm through a suction hole from the top, flush any other worms toward the waste or circulator, isolate the chamber from all other channels, immobilize the worm by activating the suction channel from the bottom, and collect or discard the worm depending on its phenotype after imaging and processing. High speed (<100 ms) can be achieved to immobilize and release one single worm.

Conventional large-scale drug screening assays were done on worms using an automated fluorescence micro-plate reader and multi-well plates [62]. This has three main disadvantages. First, cellular and subcellular details of the worm cannot be imaged. Second, only average fluorescence is obtained from worms from each well. Third, the worms risk being flushed away during media exchange. Anaesthesia is used to immobilize the animals in this system, which is also not the best option. *C. elegans* cannot be kept anesthetised for more than a few hours, and the effect of anaesthesia on many biological processes remains uncharacterized [36]. To address these problems, Rohde, et al. [36] designed a microfluidic multi-well chamber suitable for large-scale drug/RNAi screening assay, as shown in Figure 2.10. Sorted worms from the high-throughput sorter were delivered to the chambers by opening valves via multiplexed control lines [63]. One single incubation chamber is small (~1 mm in diameter), thus hundreds of chambers could be integrated onto one single chip. Each chamber contains a structure of circular posts (Figure 2.10C) used to immobilize the worm for imaging. To start a process, a flow is actuated through the control line, by which the worm is pushed towards the posts. The movement of the worm is restrained by the constant flow, enabling subcellular imaging. The authors described that posts arranged in a near circle allow the worm to be positioned in a bent geometry, so as to reduce the complexity and processing time of image recognition algorithms. Drug/RNAi screening was achieved by exchanging the medium in the chamber. With precise control of

valves, complex screening (e.g., multiple drug targets) can be performed in this device. Furthermore, during medium exchange, the worm can be kept well and safe in the chamber without risk of being disposed. The low consumption of chemicals or drugs also reduces the cost of assays. The combination of worm-sorter, integrated micro-chambers, and multi-well plate interface chips has the potential not only for large-scale RNAi and drug screens with time-lapse imaging, but also for new types of experiments at subcellular resolution [36].

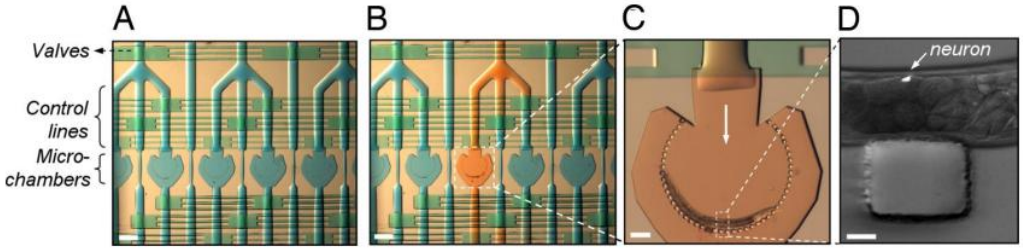

Figure 2.10: Incubation chamber for large-scale screening. (A) The chip consists of valves, control lines, and chambers. A valve network controls all the control lines to direct the flow in or out of individual chamber. (Scale bar: 500 μm.) (B) One chamber is loaded with compounds in yellow colour. After detection, the chamber can be flushed with a wash buffer through individually to prevent cross-contamination. (Scale bar: 500 μm.) (C) Close-up view of a single micro-chamber. Worms can be delivered into the chamber through the same flow line. The nematode is pushed towards the circular posts geometry by flowing compound. Instead of using anaesthetics, this unique structure can restrain the worm in a well-defined position for further assays. (Scale bar: 100 μm.) (D) A high-resolution GFP-labelled fluorescent touch-neuron image was taken with a white-light background. (Scale bar: 25 μm.) Pictures are adopted from [36].

One year later in 2008, Chung et al [50], demonstrated another microfluidic platform for rapid microscopy, phenotyping and automated sorting of *C. elegans*. Figure 2.11 illustrates the design of the device as well as the working principle. This microfluidic device is fabricated using modified multilayer soft lithography [61], and contains one flow layer for sample-loading, and one

control layer for temperature and valve control (Fig. 2.11A, B). The operation process is demonstrated in Figure 2.11C. To load a worm into the detection zone, both outlet channels are closed while the side positioning channel remains open, and a constant positive pressure is applied to drive flow into the chip. A partially closed positioning valve is actuated at the same time to reduce mechanical stress on the animal. Once the nematode is positioned, the temperature control channel is cooled to ~ 4 ºC to freeze the movement of the worm for high-magnification imaging. When a worm is present in the detection zone, the flow resistance is increased due to the small geometry of the loading channel, which prevents the second worm from entering the imaging chamber at the same time. After phenotyping and sorting, images are stored for analysis, and the worm is released by opening either of the outlet channels. Automation of the system is achieved by integrated closed-loop control software as well as engineered hardware design of the chip.

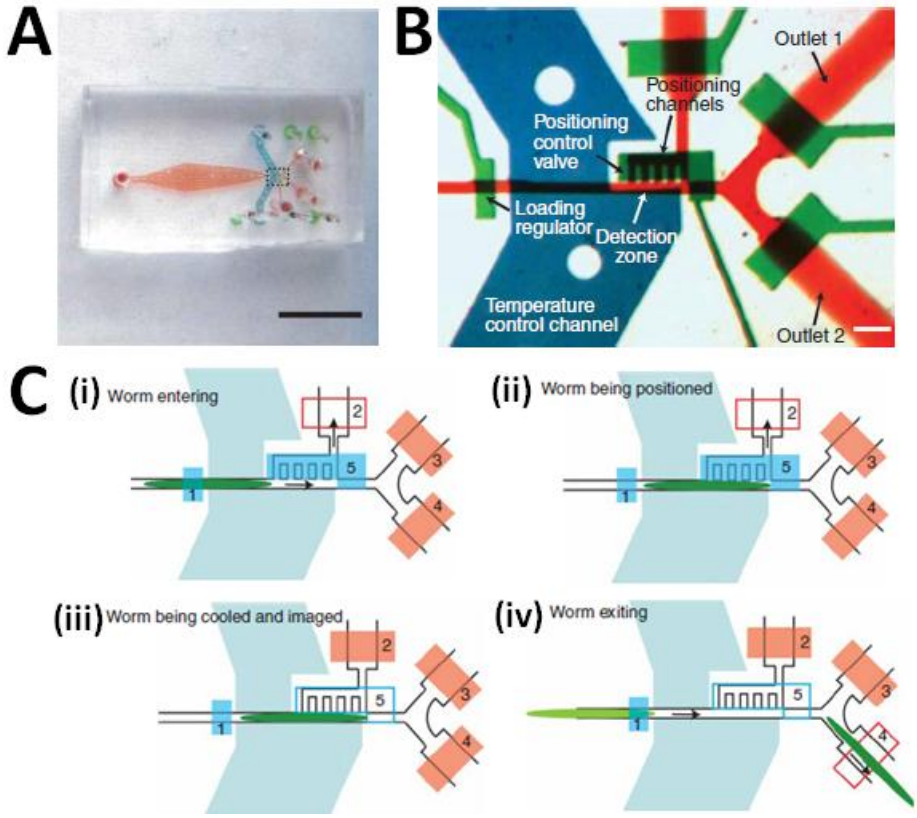

Figure 2.11: Schematics of the microfluidic device for rapid microscopy, phenotyping and sorting of *C. elegans*. (A) Photograph of the microdevice. Scale bar, 5 mm. (B) Optical micrograph of the microchip active region (boxed region in A). The channels were filled with dye to show specific features: blue, temperature control channel;

green, valves; and red, sample-loading channel. Scale bar, 100 μm. (C) operation process of the microfluidic device. Valve 1 is always partially closed to prevent multiple worms from entering. Valve 2 on the positioning channel is opened to generate a pressure gradient to guide a worm into the observation zone (i, ii). Once the worm is positioned in the observation chamber, all the valves are closed to eliminate flow fluctuation (iii). One of the outlet valves (3 or 4) is opened to allow the imaged worm to leave (iv). Once the worm leaves the flow resistance drops to allow another worm to entry. (dark blue, partially closable and tunable valves; red, fully closable valves; open boxes, valves in closed position; coloured boxes, valves in open position). Pictures are adapted from [50].

Phenotyping and sorting are based on synaptic features in this microfluidic system (Fig. 2.12A). To test the ability to screen based on subcellular changes, strains carrying an integrated reporter transgene juIs198 (punc-25-YFP–rab-5), were sorted. This strain carries expresses the fluorescent marker YFP in an endosomal subcompartment in GABAergic motorneurons[50]. This experimental platform was capable of distinguishing the pattern of fluorescence in wild-type *C. elegans*, from that in a mutant unc-16 –/– consistent with the latter having abnormal subcellular localisation of this endosome (Fig. 2.12C). Loss of worms through this microfluidic system were around 3%, and the viability of the sorted worms was nearly 100% [50].

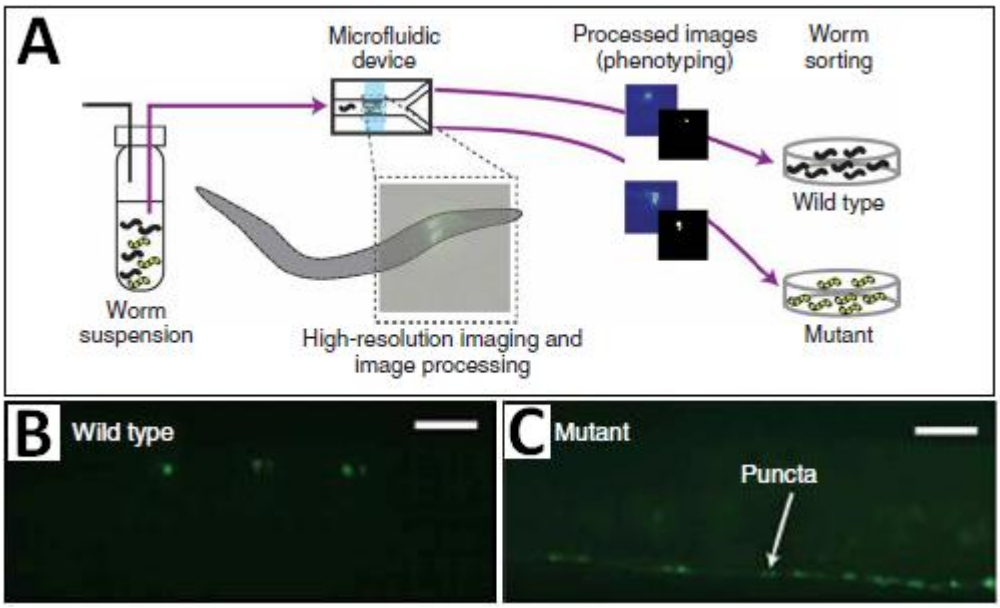

Figure 2.12: Phenotyping and sorting are based on synaptic features in this microfluidic system. (A) Schematic shows the process of a mixed population of worms is injected, imaged, phenotyped and then sorted in the device. Representative images of punc-25-YFP–RAB-5 reporter expression in wild-type (B) and unc-16–/– mutant (C) worms provide the means for sorting. Pictures are adapted from [50].

Yang et al [64], developed a microfluidic device with simple geometry for rapid screening of chemotaxis-defective *C. elegans* mutants. It consists of six "T" shaped channels with the same geometry connected to a central worm pool (Fig. 2.13A). Each "T" shape channel has one culture chamber, two inlets, one assay channel, one connecting channel, and three metal pin control valves (Fig. 2.13B). The sorting process is simple and illustrated in Figure 2.13C. A population of mixed worms is first transported to the culture chambers through the connecting channels by pressurizing the central worm pool, followed by injection of attractant and control solutions simultaneously into the two inlets. The concentration gradient of attractant is then established in the assay channel. Wild-type *C. elegans* get attracted by the chemical and accumulate in the attractive region, while mutants are not. By controlling the pin valves, N2 worms are extracted first and the mutants are sorted via another port later. Verification experiments were independently performed

giving an average accuracy rating of 91 % while screening 10 *che-1* worms from 104 wild-type N2 animals.

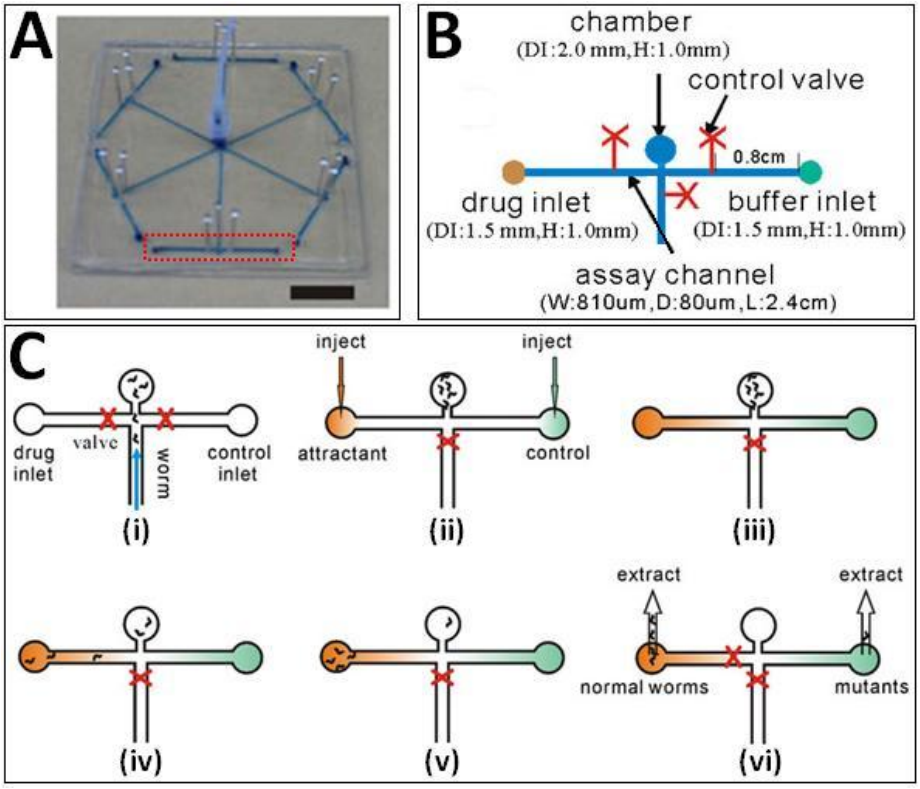

Figure 2.13: Schematics of the microfluidic device for rapid screening of chemotaxis-defective *C. elegans* mutants. (A) Photograph of the microfluidic chip (6.34 cm×6.34 cm×0.40 cm) with filled blue dye. Scale bar, 1 cm. (B) The magnified view of one operation unit as marked in A, including a culture chamber, two inlets, an assay channel, a connecting channel, and three metal pin valves. (C) The working principle of one operation unit (X denotes a closed microchannel): (i) Worms are transported to the culture chamber by pressurizing the central worm pool. (ii) Drug and control solutions were simultaneously injected into the two inlets by a slender needle by using a syringe pump. (iii) The concentration gradient of attractant was established in the assay channel. (iv) Worms sensed chemicals and responded to the attractive chemical. (v) Wild-type N2 worms swam and accumulated in the attractive region. (vi) The animals were recorded and sorted through both inlets. Pictures are modified from [64].

2.2.1.4 Laser surgery of *C. elegans* on-chip

The advantage of using ultrashort (picosecond or femtosecond) laser pulses in tissue ablation provides a method to destroy an extremely small volume of tissue with minimal heating or damage to surrounding cells [65]. When considering the use of various light manipulation techniques, such as laser surgery and light stimulation, microfluidic devices can provide the ideal laboratory environment for small multicellular model organisms, like *C. elegans* [66].

Two approaches have been developed for undertaking laser surgery on a chip [49, 67]. The first approach demonstrates a microfluidic device which is able to perform femtosecond laser nano-axotomy for *in vivo* nerve regeneration studies [49]. This device contains two main modules connected by a single channel: the trapping system for immobilization, laser surgery, and time-lapse imaging of *C. elegans*, and recovery chambers for collecting the operated worms (Figure 2.14A). Both modules are controlled by separate microfluidic pneumatic valves. In the trapping system (Figure 2.14B), four valves are used for either transporting or positioning the animals. The trapping region is formed from a two layer structure separated by a thin PDMS membrane of ~ 40 μm (Figure 2.14C). The flow channel is at the bottom with a depth of 50 μm and width of 110 μm. With the worm positioned in the trapping region, a positive pressure is applied from the top layer to pressurize the thin membrane to immobilize the worm mechanically. Imaging of injured axons and their regeneration is performed in the same trapping module. Except for regrowth observation, the whole cycle of loading, trapping, and operating takes only about 1 minute per worm. Nanosurgery of neuronal processes was performed by highly focused 220-fs laser pulses of 7.2 nJ at 1 kHz repetition rate and 780-nm wavelength [49]. Axotomies were performed at one-third of the process length from cell body to axon branching, and fluorescence images at approximately 10-min intervals were collected for time-lapse imaging. Axons reconnected to their distal end within approximately 70 min after surgery (Figure 2.14D). The design of the chip can be easily modified for other organisms or other kinds of experiments, including ablation, irradiation, stimulation or simply observation. The simple operating process of this microfluidic system enables high-throughput biological investigations.

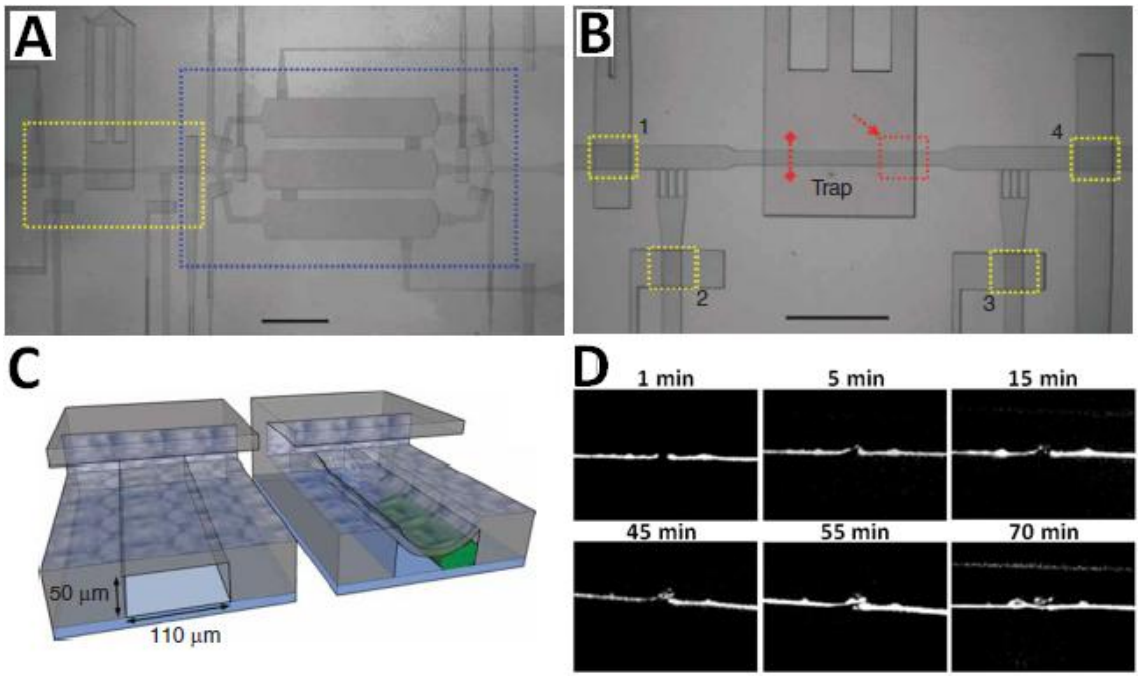

Figure 2.14: The nanoaxotomy lab-on-a-chip for in vivo nerve regeneration studies. (A) Layout of the microfluidic chip with the trapping system (yellow rectangle) and three recovery chambers (blue rectangle). Scale bar, 2 mm. (B) Zoom-in view of the trapping system as marked with yellow rectangle in A. Valves 1–4 (yellow rectangles) respectively control inlet regulation, fine positioning of the worm (2 and 3) and gating to the recovery chambers. Red rectangle indicates the position for trapping. Scale bar, 1 mm. (C) 3-D renderings of the trapping channels without and with an immobilized worm (Green objective). (D) Fluorescence images of an ALM neuron regeneration at the indicated times after the axotomy. The neuron is labbeled with green fluorescent protein (GFP). Distal ends are on the left side of the pictures and proximal ends, on the right. After 5 min, the distal end displays a growth cone that is visible above the proximal stump. At 15 min, the growth cone branches off into two. At 45 min, a third branch sprouts close to the distal stump. The other two growth cones are out of focus. At 55 min, the third branch recesses, and the first two branches develop into a broad growth cone. The proximal end starts regrowing. At 70 min, the proximal end regrew and reconnected to the distal end a bit further past the distal stump [49]. Pictures are adapted from [49].

A different microfluidic platform was developed by Allen et al [67], for single-synapse ablation and long-term imaging of live *C. elegans*. Figure 2.15A shows the arrangement of the experimental setup. Two laser sources, a blue (488 nm) and ultraviolet (355 nm), are reflected from a dichroic mirror into the back aperture of a microscope objective lens and directed into the sample for fluorescence excitation and ablation, respectively. Fluorescence is collected and imaged with a CCD camera [67]. Mechanical immobilization was also used in this microfluidic system, achieved with parallel fluidic channels with tapered structure (Figure 2.15B). Worms can be restricted in the tapered region (Figure 2.15C), which is the position of laser ablation and long-term imaging.

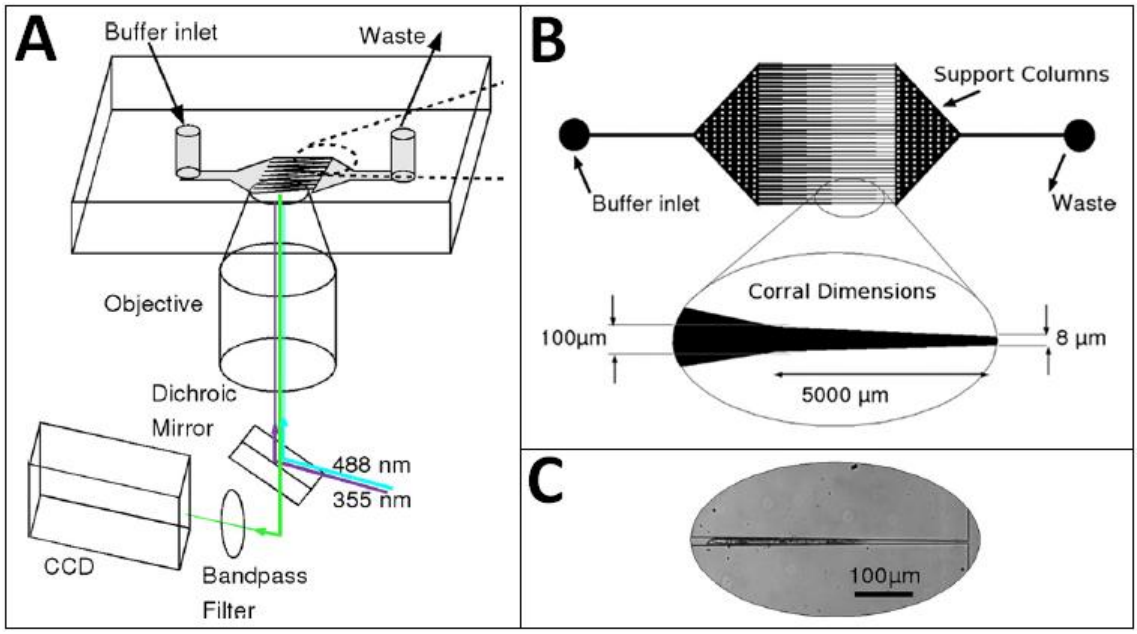

Figure 2.15: Overview of the experimental design for single-synapse ablation and long-term imaging in live *C. elegans*. (A) Schematic illustrating the arrangement of the optical setup and microfluidic chip. Two laser sources, a blue (488 nm) and an ultraviolet (355 nm), are reflected from a dichroic mirror into the back aperture of a microscope objective lens and directed into the sample for fluorescence excitation and ablation, respectively. Fluorescence is collected and imaged with a CCD camera [67]. (B) Layout of the microfluidic chip. Corrals with tapered structure are placed in parallel for constricting the nematode. (C) A bright-field image showing a worm trapped in the tapered region. Pictures are adopted from [67].

The effects of synapse ablation on the development of the HSNL neuron were examined with this microfluidic system. The HSNL motor neuron is used as a model to understand synaptogenesis in *C. elegans* [7]. Figure 2.16 shows a typical morphology of a young adult animal prior to ablation. The bright field, bright field with fluorescence, and fluorescence images of the synapse region are presented in Frame 1, 2, and 3 respectively. Ten laser pulses were used to ablate the entire synapse because the size of this synapse was much larger than the focal spot of the UV laser. The ablation process is shown in frames 3–13. Frame 14 shows the cell body, which is at a different focal plane from the synapses after ablation, and frame 15 is the bright-field image after ablation. The last frame (Frame 16) shows the re-appearance of the synapses. Small arrows indicate the normal synaptic location several hours after ablation, and big arrow points at the location ectopic synapses may appear which is not observed in this case. This approach enables direct study of the cause-and-effect relationship between the structure and function of the neuronal network of *C. elegans* [67].

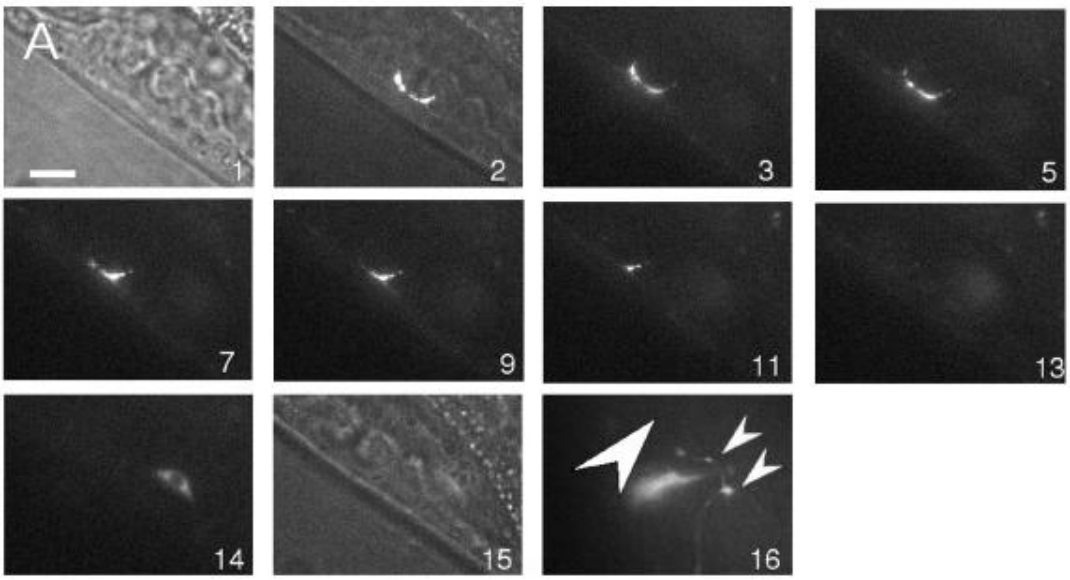

Figure 2.16: The results of the ablation of a mature synapse made by the HSNL neuron ablation experiments are shown by a sequence of images (60s intervals). The motor neuron expresses GFP::RAB-3 in a young adult worm. Ten laser pulses were used to ablate the entire synapse, because the size of this synapse was much larger than the focal spot of the UV laser. Frame 1 is a bright-field image and frame 2

is a merged bright field and fluorescence image prior to the ablation of the synapse. Frames 3-13 show the synapse during ablation. Frame 14 shows the cell body, which was out of focus in frames 3–13. Frame 15 is a bright-field image of the region where the ablated synapse was, which showed no overt damage to the specimen. Frame 16 shows the same specimen as in frame 13 and 15, but after development for 2 to 3 hours, during which the synapses reappeared as indicated with small arrows. No ectopic synapses was observed (Big arrow) [67]. Pictures are adapted from [67].

2.2.1.5 Droplet-based application of *C. elegans* on-chip

Droplet-based microfluidic systems have been shown to be compatible with many chemical and biological reagents, which have dimensional scaling benefits that enable well controlled and rapid mixing of fluids in the droplet reactors, resulting in decreased reaction times. Together with the precise generation and repeatability of droplet operations, droplet-based microfluidic system are a powerful high throughput platform for biomedical research [68]. The first droplet-based microfluidic system for individual *C. elegans* assay was demonstrated by Shi et al [31], enabling the characterization of the behaviour of *C. elegans* within an array of droplets at single-animal resolution. This is a single layer PDMS microfluidic device made with standard soft lithography, and its layout and working principle is shown in Figure 2.17. It consists of two functional segments: a T-junction droplet generator and a droplet trap array. Droplets are generated by shearing a dispersed aqueous phase with a constant oil phase at the T-junction (Figure 2.17A). The density of the worm suspension was adjusted to 5–10 worms μL^{-1} to ensure that individual worms were encapsulated into the micro-droplets. The flow rates of the two phases are controlled by syringe pumps. The droplets were captured by the droplet trap array which is a series of circular traps connected by square-wave micro-channels. The principle of single droplet capture is due to the change of flow resistance along the micro-channels, which results from the movement of the constricted droplets (Figure 2.17B). The device enables the encapsulation of individual worms into an array of droplets with more than 60% probability [31]. Large populations of worms can be handled and observed at single-animal

resolution without mechanical injury, enabling whole animal high-throughput assay or drug screening experiment.

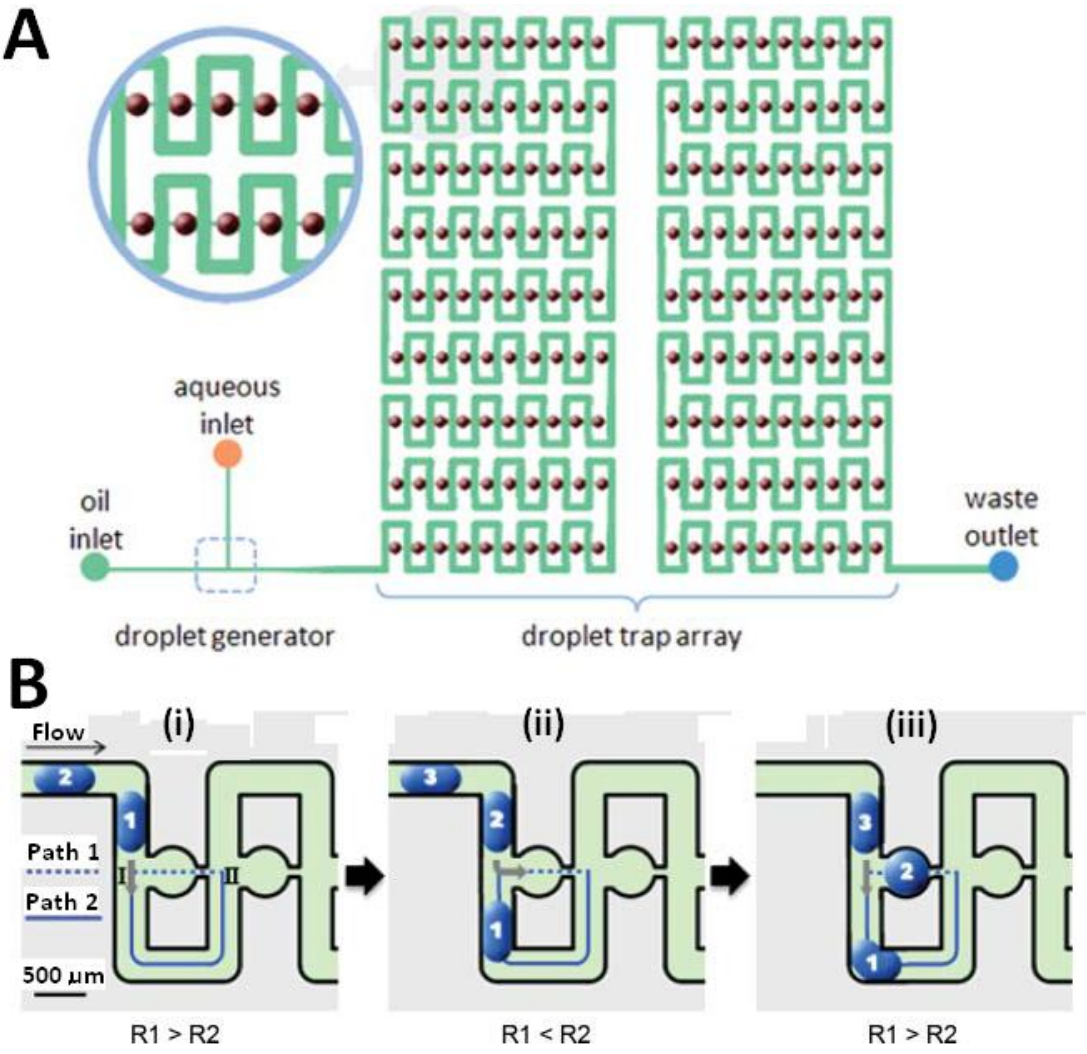

Figure 2.17: Schematic diagram of the droplet-based microfluidic device for individual *C. elegans* assays. (A) The layout of the device which consists of two functional segments: a T-junction droplet generator and a droplet trap array. Droplets are continuously generated at the T-junction and captured in the droplet trap array sequentially. The inset is a magnified view of ten traps with droplets in series. (B) Principle of the droplets to be captured in the trap array. The successive generated droplets are numbered sequentially. The two paths from junction I to II are named as Path 1 and Path 2, and the flow resistances along them are defined as R1 and R2, respectively. The process for trapping droplets is described as follows: (i) R1 > R2, droplet 1 at junction I flows into Path 2; (ii) R2 > R1, droplet 2 at

junction I flows into Path 1 and gets trapped; (iii) R1 > R2, droplet 3 at junction I flows into Path 2 and enter the next trapping process [31]. Pictures are adapted from [31].

Shi et al [69], developed another droplet-based microfluidic device with novel structures for characterizing neurotoxin-induced response in individual *C. elegans*. A schematic illustration of the chip is shown in Figure 2.18A. It is composed of two layers: The top layer contains a droplet trap array and a tapered worm immobilization channel for imaging. The worm immobilization channel (Figure 2.18B) has a gradually narrowing width from 100 μm to 20 μm. The joint part of the droplet trap and immobilization channel descends like a step-stair (Figure 2.18C), directing the worm to the immobilization channel. The 80 immobilization channels are all linked to the central waste reservoir through a 20-μm high channel. The working principle is shown in Figure 2.18D. The density of the water is lower than the fluorinated oil FC-40, so that when a droplet moves underneath an empty trap at the correct flow rate, buoyancy will move the droplet into a trap. The bottom layer includes a T-junction droplet generator and a flexural droplet transporting channel. This device enables encapsulation of individual adult worms into arrays of droplets with 30–40% probability [69]. After worm trapping, waste 1 reservoir is connected to a syringe filled with 1% agarose solution, with other ports unplugged. The agarose solution is gently injected into the chip at a flow rate of ~ 0.5 μL s, pushing worms in droplets into the adjacent tapered channels where they are immobilized (Figure 2.18E).

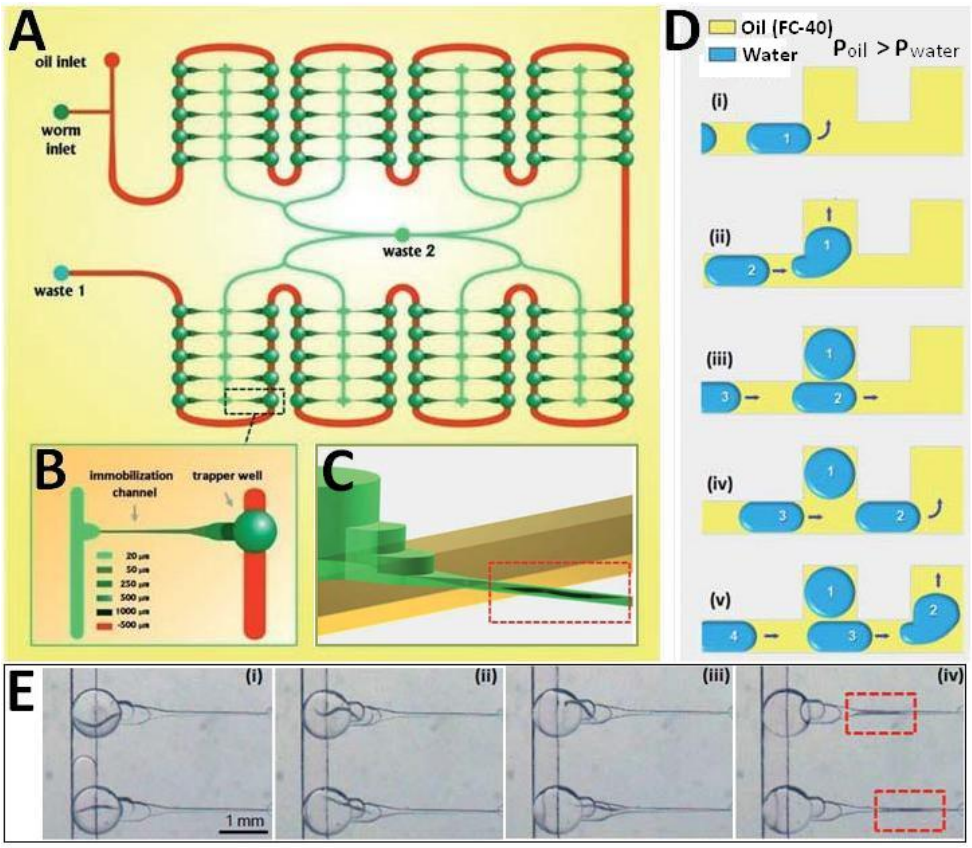

Figure 2.18: Schematic of the droplet-based microfluidic device for characterizing the neurotoxin-induced responses in individual *C. elegans*. (A) Layout of the chip which consists of two layers: the bottom layer for droplet generation and transportation in red, and the top layer for droplet trapping and worm immobilization in green. (B) The magnified view of one operation unit as squared in A, including a droplet trap and a worm immobilization channel. The depths of different parts of the operation unit are marked with different colours. (C) Illustration of a worm immobilized in the tapered channel. (D) Principle of the generated droplets to be captured in the trap array by density difference. (i) Droplet 1 moves towards an empty trap at a proper flow rate; (ii) When droplet 1 moves along the microchannel and locates right beneath the trap, the floatage drags it into the trap due to the density difference ($\rho_{oil} > \rho_{water}$); (iii) Droplet 2 passes through the below of the filled trap with droplet 1; (iv) droplet 2 moves toward the next trap; (v) Droplet 2 flows upward into the next trap, and the following droplets get trapped in the same way. (E) Micrographs showing the immobilization process. Pictures are modified from [69].

The neurotoxin 6-hydroxydopamine (6-OHDA) has been reported to cause Parkinson's disease (PD)-like symptoms in vertebrates by destroying dopamine neurons [69] in vivo. To determine whether *C. elegans* DAergic neurons are sensitive to this drug, the worm strain *UA57*, which expresses strong and specific green fluorescence in all eight DAergic neurons, was used (only the six neurons in the head were analyzed). The worms were pre-exposed to 6-OHDA at different concentrations (0mM, 5 mM, 10 mM) and then loaded into the microfluidic device at day 1, day 3, and day 5. Fluorescence images of GFP expression in 12 individual *UA57* worms and the associated stroke frequencies (a measure of mobility) for the three different 6-OHDA concentrations on the third day are shown in Figure 2.19. The untreated worms expressed intact and strong GFP in all six DAergic neurons in the head, but worms treated with 5 mM 6-OHDA showed a significant reduction. Treatment with 10 mM 6-OHDA led to a complete loss of GFP expression in most DAergic neurons. The stroke frequency dropped with increasing concentration of 6-OHDA, suggesting the obvious effects of DAergic degeneration triggered by neurotoxin [69].

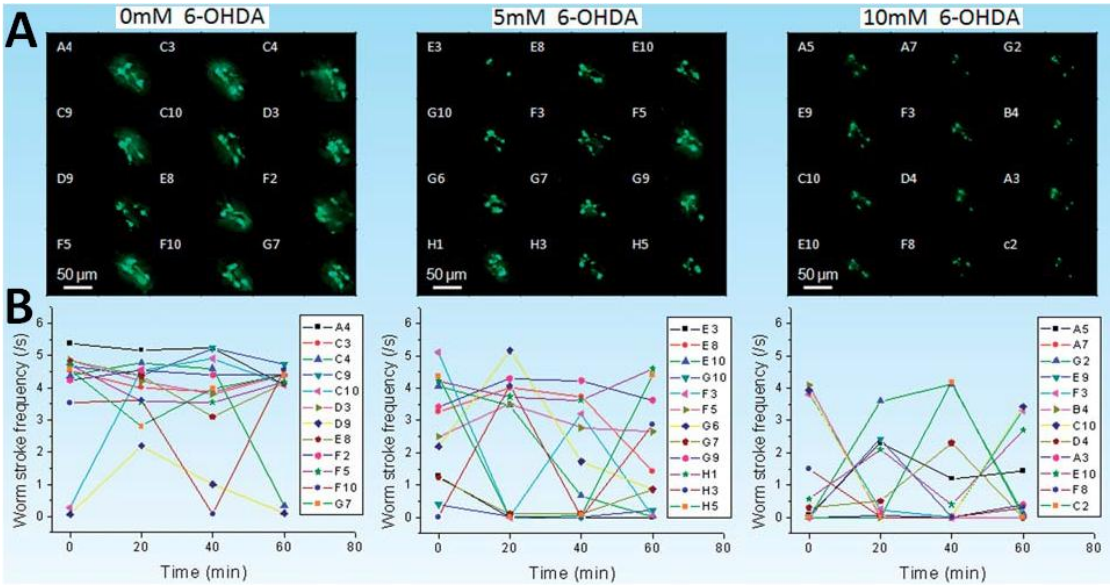

Figure 2.19: Fluorescence images and corresponding stroke frequencies of individual UA57 worms in response to 6-OHDA at the third day. (A) DAergic neurons fluorescence images of individual UA57 worms treated with different concentrations of 6-OHDA at the 3rd day. The untreated worms expressed intact and strong GFP in all six DAergic neurons in the heads; the worms treated with 5 mM 6-OHDA

showed a significant reduction of GFP expression; the worms treated with 10 mM 6-OHDA exhibited a complete loss of GFP in most DAergic neurons. (B) Stroke frequency of individual UA57 worms treated with different concentrations of 6-OHDA at the 3rd day. The stroke frequencies declined to a low level at 10 mM concentration. Pictures are modified from [69].

2.2.2 Microfluidic devices for parasitic nematodes

Most of the microfluidic devices described so far have been designed for *C. elegans*. But nematode parasites cause massive economic loss and welfare issues through infection of plants, animals, and humans [70]. Therefore, tools to facilitate their investigation are worthy of attention. Moreover early detection of strains of nematode that are resistant to chemical control and anthelmintic drugs is necessary to limit the spread of parasitic infections [71]. One aspect of this is that drug resistance may be associated with changes in the phenotype of the worm, for example its locomotion, because signalling-muscle-contraction pathways are affected [72]. Microfluidic technology provides a new tool for quantitative measurements of phenotype changes.

Carr, et al. [73] developed a microfluidic device for high-speed real-time (HSRT) drug screening of the parasitic nematode *Oesophagotomum dentatum* (*O. dentatum*). This device has an inlet port, two behaviour micro-channels with built-in scale, a drug port, a drug well, and an electrode port (Figure 2.20A). The worms were first inserted into the microchannels through the inlet port and pre-exposure locomotion characterized. They were then guided into the drug well with the drug port pre-filled. The effect of the drug on locomotion was characterized in real-time. Afterwards, the worms were sent back into the microchannels to characterize the post-exposure locomotion [73]. A uniform electric field was established by placing an anode (hollow metal) in the inlet port and a cathode in the electrode port. By changing the direction of the electric field, the worms were guided into the channels or wells of interest (Figure 2.20B). Two parasitic *O. dentatum* strains were used: levamisole-sensitive (SENS), and levamisole-resistant (LEVR). To define the responsiveness

of these two strains to different concentrations of levamisole, the author defined a circle, with a radius equal to the worm's body length around the worm. The worm is considered to be inhibited once its movement is completely covered by the circle. At low levamisole concentrations (0.1 μM for SENS, 10μM for LEVR), nearly all worms are responsive, and at higher concentrations, the percentage of worms inhibited increased. Eventually, at a concentration of ~100 μM for SENS and ~150 μM for LEVR, all worms are unresponsive (Figure 2.20C).

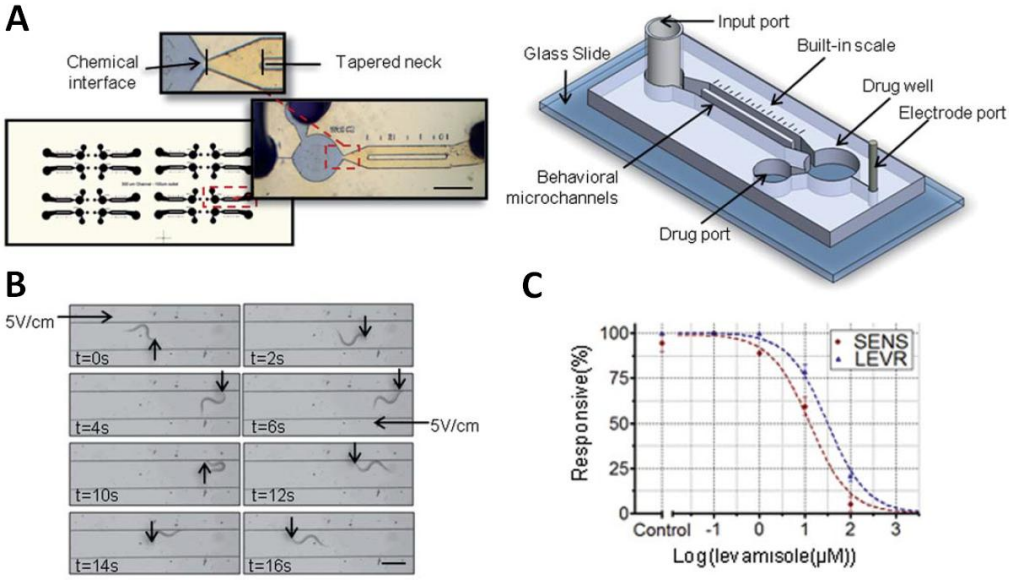

Figure 2.20: Microfluidic device for drug screening tests on *O. dentatum*. (A) Snapshot, mask design and 3-D structure of the microfluidic device. (Scale bar: 1.5 mm) (B) Time-lapsed images of a LEVR *O. dentatum* nematode in the microchannel under electric field. The worm always moves along with the direction of the electric field. Black arrows indicate the position of the head. (Scale bar: 300 μm) (C) The percentage of worms (SENS and LEVR) responsive to levamisole with different concentrations. Pictures are adapted from [73].

Increasing the dimension of the microchannels allows this microfluidic device to be applied to screening anthelmintic drugs on both *C. elegans* and *O. dentatum,* exhibiting the ability for more accurate, sensitive studies on rapid drug screening.

2.3 Electrophysiological investigation of *C. elegans*

Most *C. elegans* electrophysiology so far has been done on the pharynx [11], which has a very simple structure (only 20 neurons and 37 muscle cells) and consists of two obvious motions, pumps and isthmus peristalses, which make it suitable for cellular and molecular studies of behaviour[12]. Extracellular, intracellular, whole-cell and single-channel patch clamp recordings may all be made from the pharyngeal muscle[74]. As in other excitable polarized cells, contraction in pharyngeal muscle is controlled by changes in membrane electrical potential. These activities can be recorded extracellularly by placing a recording electrode over the nose of the worm. This technique is called the electropharyngeogram, or EPG. The EPG provides an experimental platform for defining gene function, the impact of genetic mutations, and the effects of drugs and toxins in the nematode neural network.

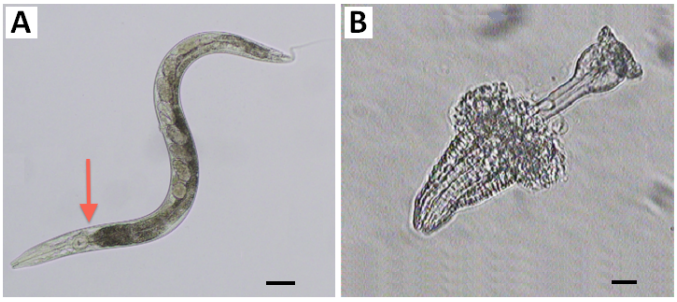

Figure 2.21: Model organism *Caenorhabditis elegans*. (A) Microscope image of an intact adult *C. elegans*. Scale bar, 50 μm. Red arrow indicates the position to cut the head off. (B) A dissected worm head. Scale bar, 5 μm.

The physiological basis of the EPG signal has been discussed by Avery et al [11] in 1995. He proposed that the pharyngeal muscle contraction was controlled by the active voltage change of the basal membrane which faces the pseudocoelom, and the apical membrane is a passive follower that faces the pharyngeal lumen. Any voltage difference between the two faces of membrane is accompanied by a proportional difference in charge [11]. It has been demonstrated by laser ablation studies and analysis of mutants that MC and M3 are the only neurons whose functions are observed in the EPGs [75]. M3 motorneurones synapse onto pm4 muscle cells and the cholingergic MC neurones act as pacemakers and synapse onto the marginal cells [76]. In 2006

Franks et al [77] pointed out that the pharynx may be arranged in a similar manner to the vertebrate heart with the marginal cells acting like Purkinje fibres to rapidly conduct the electrical excitation throughout the pharyngeal muscle.

2.3.1 Experimental method

In conventional electrophysiology experiments, recordings can be collected either from the intact worm (Fig. 2.21A) or just dissected pharynx (Fig. 2.21B). It is difficult to capture a free living *C. elegans* in the liquid, and dissected pharynxes are useful for drug and ion substitution studies, as the solution has direct access to the muscle basal membrane [11]. Therefore most studies have been undertaken on dissected pharynx. The procedure [11, 74] of getting EPG signals from the pharynx is: (1) Pick nematodes into a petri dish filled with Dent's saline (composition in mM; D-glucose 10, HEPES 10, NaCl 140, KCl 6, $CaCl_2$ 3, $MgCl_2$ 1, pH 7.4 with NaOH); (2) Cut the head away at the position of pharyngeal-intestinal valve (Fig. 2.21A); (3) Transfer the dissected head to the recording chamber which filled with Dent's saline using a pipette; (4) Attach the suction tube which was pulled from borosilicate glass capillaries to the pipette holder. The holder contains a sliver/silver chloride wire to act as an electrode and a tubing port on the side to apply suction (Fig 2.22A); (5) Move the tip of the suction tube close to the nose of the worm; (6) Apply a gentle suction on the nose to keep it in the tip; (7) Collect EPG signals.

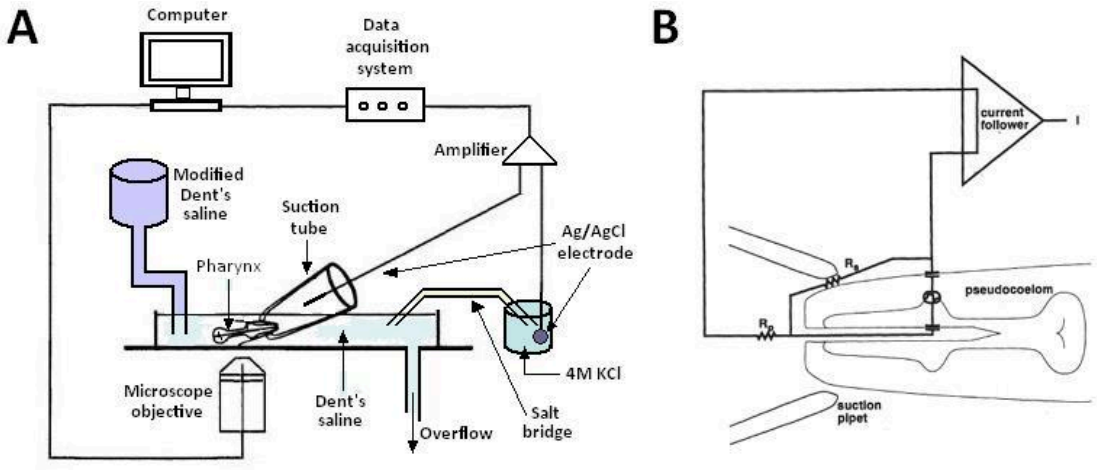

Figure 2.22: Schematic of the instrumentation for conventional EPG experiment and equivalent circuit of the EPG arrangement. (A) Diagram of the instrumentation for conventional EPG experiment. (B)

Equivalent circuit of the EPG arrangement. Pictures are modified from [11, 14].

Two electrical compartments are created by the seal between the capillary and the cuticle of the worm's head. When the pharynx is pumping, an ion flux flows out of the worm's mouth and across the resistance formed (5-20 MΩ) at the junction between the worm and the capillary. Voltage or current transients are recorded by an amplifier (Figure 2.22B) [11]. The electrical signals represent underlying electrical events in the pharyngeal muscle membranes [12]. Depolarization of pharyngeal muscles results in positive transients and repolarization results in negative transients.

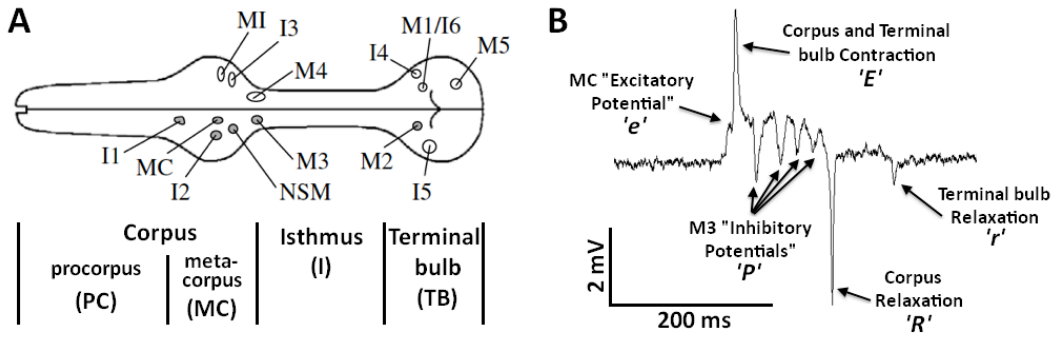

Figure 2.23: The schematic of the pharynx of the nematode *C. elegans* and a typical EPG signal. (A) The pharynx of the nematode *C. elegans*. 14 types of neurons are indicated in the picture. 8 of them are single neurons (hollow circle), and 6 of them are bilaterally symmetric pairs (filled circle)[75]. (B) A typical EPG signal recorded from a wild type (N2) *C. elegans* pharynx. It comprises three phases, E (e, E), P, and R (R, r) phases, corresponding to different neurons or muscles.

The pharynx can be subdivided into three functional sections, the corpus near the mouth of the nematode for ingesting bacteria, the isthmus (I) in the middle for passing the food to the terminal bulb by peristaltic pump, and the terminal bulb (TB) for grinding the food (Figure 2.23A). The pharyngeal behaviour consists of two motions: pumping and peristalsis. Pumping is combined by a contraction of the corpus, anterior isthmus, and terminal bulb, followed by a relaxation of these parts. Peristalsis is a posteriorly directed wave of contraction of posterior isthmus to transport the food from the anterior

isthmus to the terminal bulb [12]. An EPG signal corresponds to a single pumping action of these three parts (usually a contraction followed by a relaxation). The nervous system of the pharynx comprises 20 neurons: 7 motoneurones (M1, M2, M3, M4, M5), 8 interneurones (I1, I2, I3, I4, I5, I6), 2 neurosecretory motoneurones (NSM), 2 marginal cell neurones (MC), and 1 moto-interneurone (MI) (Figure 2.23A) [77, 78]. M4 is required for the peristalsis motion, which does not generate EPG signals. MC and M3 are the only neurons whose functions are observed in the EPGs [75]. A typical EPG signal comprises three major phases, called E, P, and R (Figure 2.23B) [12]. MC is an excitatory cholinergic motor neuron necessary for rapid pumping [79]. It triggers pharyngeal muscle action potential via the release of acetylcholine, and causes small positive spikes (e) which is also known as excitatory postsynaptic potentials (EPSPs) on EPGs, followed by a large positive (E), a large negative (R), and a small negative (r) spikes representing full muscle depolarizations and repolarizations (Figure 2.23B). M3 is an inhibitory glutamatergic motor neuron. During the action potential, the firing of M3 releases glutamate, which causes inhibitory postsynaptic potentials (IPSPs) to end the muscle action potential [14, 80, 81]. It is visible as serial small negative spikes (p) in between the 'E' and 'R' spikes (Figure 2.23B). 'E', 'R' and 'r' spikes are useful for studying muscle excitability, while 'e' and 'p' spikes are important for revealing aspects of synaptic function [12, 14]. Additionally, EPG recordings are very stable [74] and can be maintained for one hour or more even if the head is dissected away from the rest of the nematode.

2.3.2 Neurobiological researches of *C. elegans* with EPGs

The EPG provides an experimental platform for defining gene function, the impact of genetic mutations, and the effects of drugs and toxins on the nematode neural network.

2.3.2.1 Defining drug effects

5-hydroxytryptamine (5-HT; serotonin) is a neurotransmitter and neuromodulator which has important roles throughout the animal kingdom. In *C. elegans* one role of 5-HT is to regulate feeding behaviour and Niacaris and Avery revealed that serotonin regulates repolarisation of the *C. elegans*

pharyngeal muscle by observation of EPG signals [82]. They examined the electrophysiological properties of pharyngeal muscle to determine if the pharyngeal action potential is affected by serotonin. The EPG provides a good means to observe the start and end of the pharyngeal action potential as well as the MC, M3 activity. *eat-18* mutant worms, in which MC neurons are decoupled from pharyngeal muscle and is functionally defective, were used to examine the effect of serotonin.

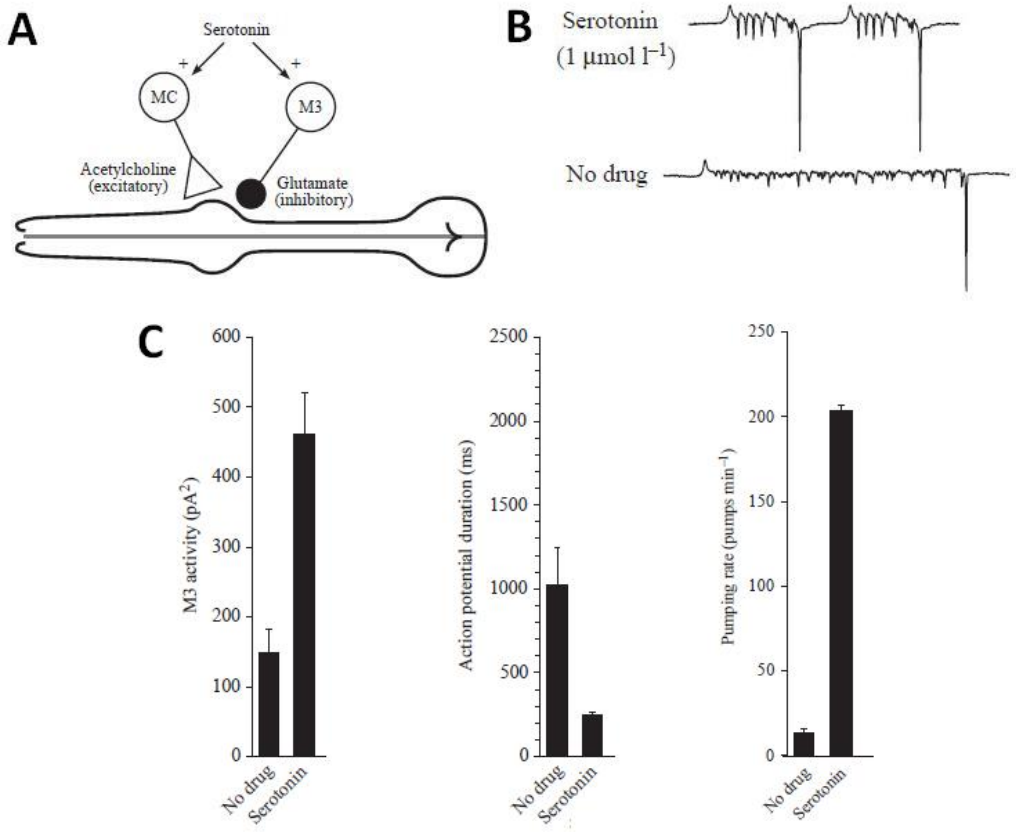

Figure 2.24: Serotonin regulates repolarisation of the *C. elegans* pharyngeal muscle by observation of EPG signals. (A) MC is an excitatory cholinergic motor neuron, and M3 is an inhibitory glutamatergic motor neuron, which control the timing of the pharyngeal muscle action potentials. Serotonin acts to increase the activity of both neurons. (B) Example of EPG traces shows that Serotonin (1 μmol^{-1}) increases the pumping frequency, M3 activity and decreases the action potential duration of *eat-18* mutants. (C) Quantitative analysis of the serotonin effects on M3 activities, pumping duration and pumping rate. Pictures are adopted from [82].

Figure 2.24 shows how EPGs of *eat-18* mutants change when the worm is exposed to serotonin. The activity of the M3 motor neurons is enhanced, the pharyngeal EPG duration is decreased to approximately one-third of the one without drug, and the pumping frequency increased from ~ 20 to ~ 200 pumps per minute. Serotonin also suppresses locomotion and enhances egg laying, mimicking the behaviours of worms in the presence of abundant food [82].

The effects of neuroactive compounds can also be discovered on *C. elegans* pharynx. For example, ethanol modulates pharyngeal activity. The effects of ethanol on neural function are dose-dependent. In the low dose range, ethanol is intoxicating and often associated with a transient excitability. But at a high concentration (greater than 100 mM), it has an anaesthetic action and elicits muscle paralysis [83]. A number of studies have investigated the behavioural response to ethanol in intact *C. elegans*, which has many genes and proteins conserved with humans. They revealed that low doses (below 0.3%, 52.3 mM) elicit hyperactivity, while higher doses (above 0.5%, 87.0 mM) decrease motility [84-86]. The cuticle of *C. elegans* represents a barrier to the entry of many drugs [87], and wild-type *C. elegans* appear remarkable resistant to ethanol. Therefore it has been assumed that the internal concentration of ethanol in *C. elegans* is much less than the external concentration [88].

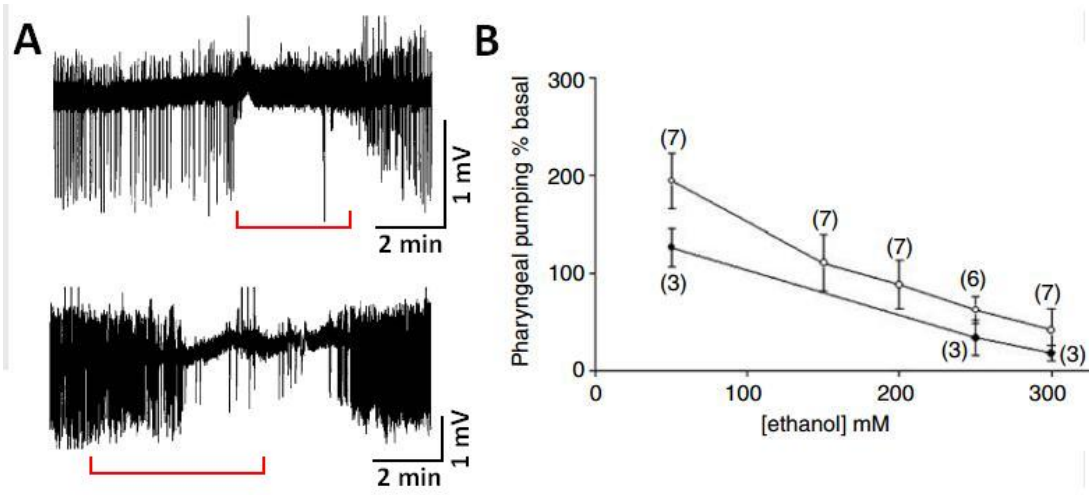

Figure 2.25: The effects of ethanol on *C. elegans*. (A) Recordings of pharyngeal activity (EPG) in exposed (above) and intact (below) worms. The duration of application of 250 mM ethanol is indicated by the red bar. 5-HT was used in both experiments to stimulate the basal

pumping rate against which inhibition could be observed. (B) A comparison of dose-dependent effect of ethanol on pharyngeal pumping rate in exposed (hollow circles) and intact (filled circles) worms. Y axis indicates the percentage of pumping rate after the presence of ethanol compared to that before the addition of ethanol. Each point is the mean ± s.e.m. of n as indicated in the figure. Pictures are adapted from [83].

In 2007, Mitchell, et al. [83] investigated the role of the C. elegans cuticle as a diffusion barrier for ethanol with the help of EPG recordings, since the EPG signal may be captured either from exposed (the body is dissected away) or intact *C. elegans*. 250 mM ethanol was added and removed from the recording chamber by replacing the solution with a pipette. Ethanol induced an inhibition that was rapid in onset and offset in both experiments (Figure 2.25A). The response time for intact animal is slightly slower (~ 3 minutes) than that for exposed pharynx, but the effect of inhibition is similar at concentrations of ethanol from below 100 mM to 300 mM (Figure 2.25). Accordingly, ethanol is likely to reach concentrations internally that are equivalent to the external concentration [83]. This study highlights the need to consider how drugs and chemicals enter the worm when investigating their effects on the pharynx.

2.3.2.2 Defining gene functions

One use of the EPG is the identification of new genes that affect synaptic function and a good exemplar of this comes from EPG analysis of M3 function [12]. Raizen and Avery [12] discovered two pharyngeal phenotypes of *eat-4* mutant worms are similar to that found in the worms have their M3 neurons killed: defective trapping of bacteria in the corpus and prolonged pumping duration. The gene *eat-4* affects multiple glutamatergic neurotransmission pathways, and is expressed predominantly in a specific subset of neurons [13]. The EPG of *eat-4* worms have shown that P spikes are absent and pharyngeal pumping durations are longer than wild-type worms (Figure 2.26). Therefore they assumed that *eat-4* may be necessary for the function of M3.

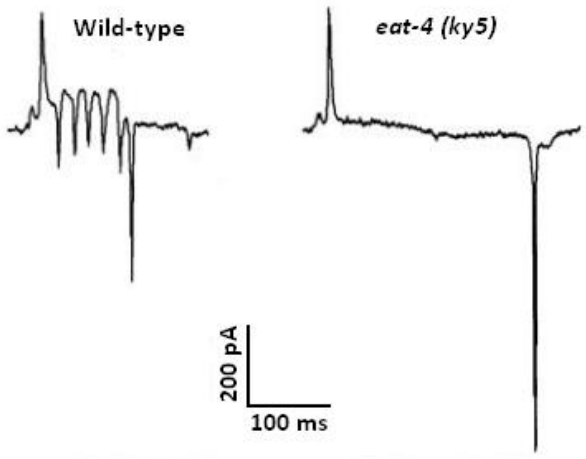

Figure 2.26: Example of single electropharyngeogram (EPG) recording trace from the wild-type worm and *eat-4* mutant. In EPG trace of mutant *eat-4 (ky5)*, which is a deletion mutant, all P phase transients are missing, and the pump duration is longer than the wild-type worm. Pictures are adapted from [13].

Lee, et al. [13] confirmed the gene *eat-4* affects multiple glutamatergic neurotransmission pathways in *C. elegans*. The expression of *eat-4* in M3 neurons suggests that *eat-4* functions in the M3 neurons to affect their glutamatergic transmission. Unlike *avr-15* mutant worms, if glutamate was applied exogenously to *eat-4* animals, their pharyngeal muscle had normal sensitivities to it, indicating that *eat-4* acts presynaptically in M3 neurons [13].

To identify genes required for MC function and neurotransmission, Raizen, et al. [79] screened for mutations that cause slow pumping and starvation. EPG was also used in this experiment to help define gene functions. Mutations in *eat-2* and *eat-18* cause the same defect in *C. elegans* feeding behaviour as well as the EPG signal, which is similar to that observed from MC^- (MC neurons were killed) worms. The pharynx is unable to pump rapidly in the presence of food, and the signal nearly misses all 'e' spikes (Figure 2.27). Therefore, they believed that *eat-2* and *eat-18* are required for processes in addition to MC function and the MC neurotransmitter may be acetylcholine.

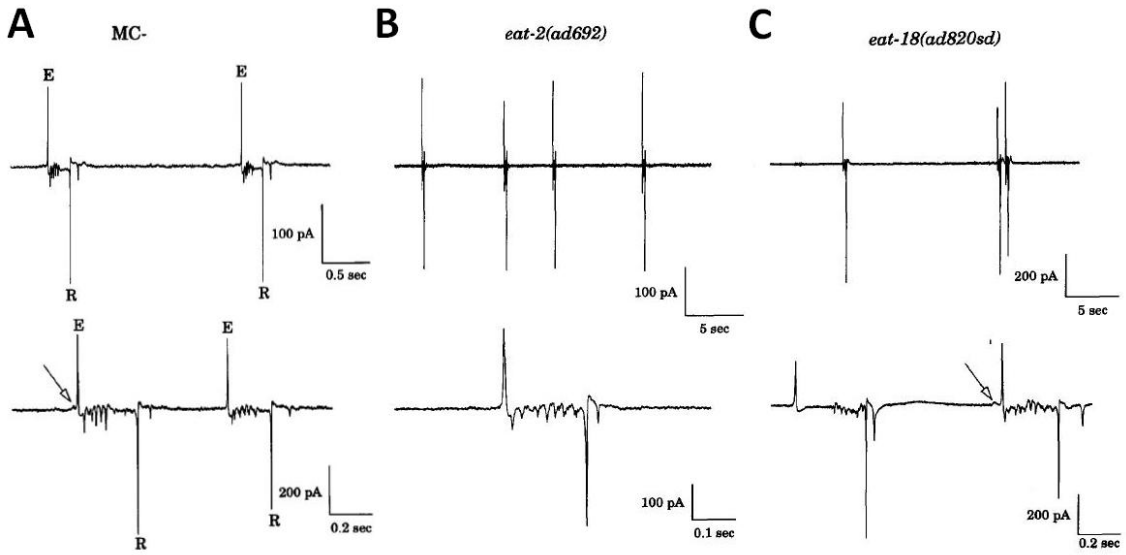

Figure 2.27: Mutations that cause slow pumping and starvation. (A) EPG signals recorded from an unc-29(e1072am) mutant after ablation of the MC neurons. The pump frequency decreases and nearly all 'e' spikes are missing. (B) *eat-2* (C) *eat-18* mutant EPGs. The waveforms of both strains are similar to that obtained from MC removed mutant shown in panel A. Pictures are adapted from [79].

Subsequently, the gene *eat-2* and *eat-18* were confirmed to be required for nicotinic neurotransmission in the pharynx of *C. elegans* [89]. *Eat-2* encodes a nicotinic acetylcholine receptor subunit specifically localized to the MC-corpus neuromuscular junction, and *eat-18* is required for the surface expression of nicotinic receptors throughout the pharynx [75, 89].

At the outset of this project no microfluidic device had been reported that permitted electrophysiological analysis of *C. elegans*.

Chapter 3: Microfluidic Channels for Acquiring EPGs

As described in the previous section, the electropharyngeogram provides an experimental platform for defining gene function, the impact of genetic mutations, and the effects of drugs and toxins on the nematode neural network and muscle function. Acquiring an EPG is a complex operation. Recordings may be made from intact worms in which case the challenge is to capture the vigorously moving worm on the tip of the suction tube. Alternatively, recordings may be made from cut heads but in this case the technical challenge involves cutting the head, pulling the suction tube and finding head manipulation. Thus these conventional methods are not easy to use, especially for a new researcher. The emergence of microfluidic technologies provides a means to address these problems. In this chapter, a single microfluidic channel is demonstrated as a means of acquiring EPG signals with simple manipulation of the worm.

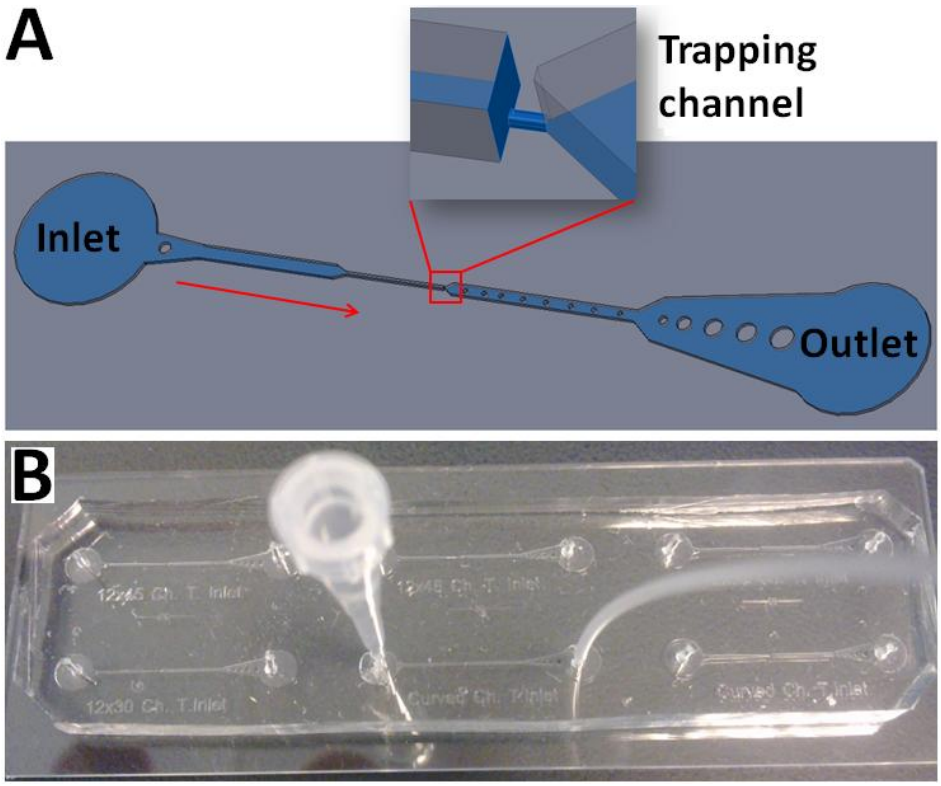

Figure 3.1: Microfluidic channel for acquiring EPG signals. (A) Layout of the microfluidic channel, with an inlet for loading the *C. elegans*, an outlet for liquid waste, and a trapping channel to capture the worm's

head. Red arrow indicates the direction of flow. (B) 6 microfluidic channels of different designs. Tests were performed to find the best geometry.

The device has a simple structure with a single channel (Figure 3.1A), containing an inlet port for the *C. elegans*, an outlet port for disposing of liquids, and a trapping channel for capturing the worm's head. To find the best size for trapping the pharynx of the nematode several different designs were examined (Figure 3.1B). Standard photolithography and soft lithography were adopted to produce a microfluidic channel. The manufacture follows several steps: design a mask with pattern of interest; fabricate master with photoresist by standard photolithography; mould PDMS replica from the master with soft lithography; bond the PDMS microfluidic channel onto a glass substrate. Compared to conventional methods, this microfluidic channel is able to deliver the worm to the trap, restrict the movement of the nematode and collect EPG recordings with precise control.

3.1 Channel design for trapping single adult *C. elegans*

The suction tube in the conventional experiment (Figure 3.2A) plays a significant role in ensuring detectable EPG signals. Obtaining a good signal to noise ratio during EPG recordings requires a robust seal around the worm's head. Thus, the geometry of the glass capillary tip needs to be mimicked in the trapping channel as shown in Figure 3.2B.

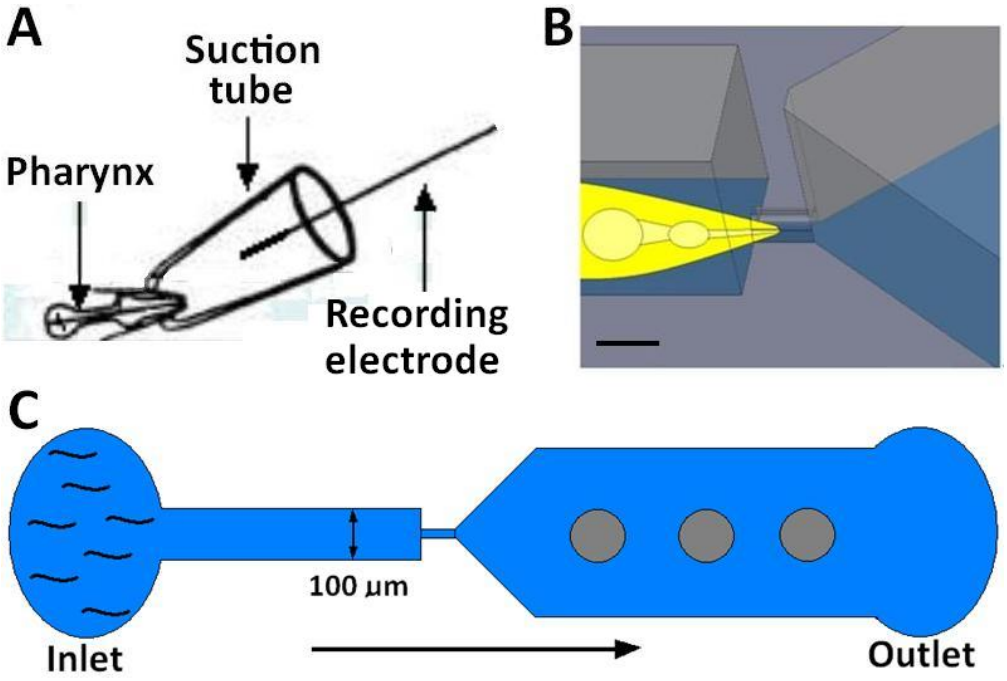

Figure 3.2: Suction tube and pseudo-3D model of trapping channel, and schematic image of the microfluidic channel. (A) The suction tube used in the conventional EPG experiment. (B) Pseudo-3D model of trapping channel. Left part is connected to the inlet channel and the right is connected to the outlet channel. A trapped *C. elegans* is drawn in yellow to demonstrate the position when captured. Scale bar, 30 µm. (C) Schematic imaging showing the design of the microfluidic channel. The size of the inlet channel is restricted to 100 µm to reduce the movement of the trapped worm. Grey posts are designed to prevent the channel from collapsing onto the substrate when suction is applied from the outlet port. Arrow indicates the direction of the flow.

In an experiment, suction is applied to the outlet port to suck the worm into the inlet channel through the inlet port. Two further structures are also incorporated in this design to facilitate trapping (Figure 3.3C). One is a straight narrow channel located just prior to the small trapping channel, called inlet channel. It is used to restrict the movement of trapped worms, since the worm may struggle once it is trapped. The other structure is a combination of several micro-pillars placed on the right hand side of the trapping channel (in the outlet channel), which is designed to prevent the channel from collapsing onto

the substrate when a negative pressure is applied form the outlet port. Worms are pre-loaded into the inlet port. Each time when negative pressure is applied on the outlet, a worm is sucked into the trap with the flow.

3.2 Device fabrication and experimental procedure

3.2.1 Device fabrication

Three steps were usually undertaken for the fabrication of the microfluidic device: designing the mask, fabrication of the SU-8 master and manufacture of the PDMS channel.

3.2.1.1 Mask design

The primary task in making a microfluidic device is to design a mask. In order to determine the best size and architecture for the *C. elegans* head, 15 channels with different shapes were designed (Appendix 1). To mimic the design of the conventional suction tube, two masks are required to make a double-layer structure. A thin layer of polymer is used to trap the worm's head and a thick layer provides enough space for movement of the worm's body (Figure 3.3). An example of microfluidic channel for acquiring EPG signals is shown in Figure 3.3.

It contains three sections: Inlet, Trapping channel (30 μm long and 12 μm wide with square edges) (Figure 3.3B), and Outlet. Mask 1 (Orange) is used to fabricate the thin layer (12μm) and Mask 2 (red channel in the middle) is for the thick layer (~ 60μm). These two masks have almost the same architecture except for the trapping channel. The difference is shown in Figure 3.3B with the areas marked by the small black squares in Figure 3.3A. Mask 1 has a small rectangular channel in the middle and Mask 2 is empty. With these two masks, the trapping channel could be made small (about 12 μm wide, 30 μm long and 12 μm high) for capturing the worm's head as well as providing enough space (~ 60μm) for worms swimming in the microfluidic channel (Figure 3.3C).

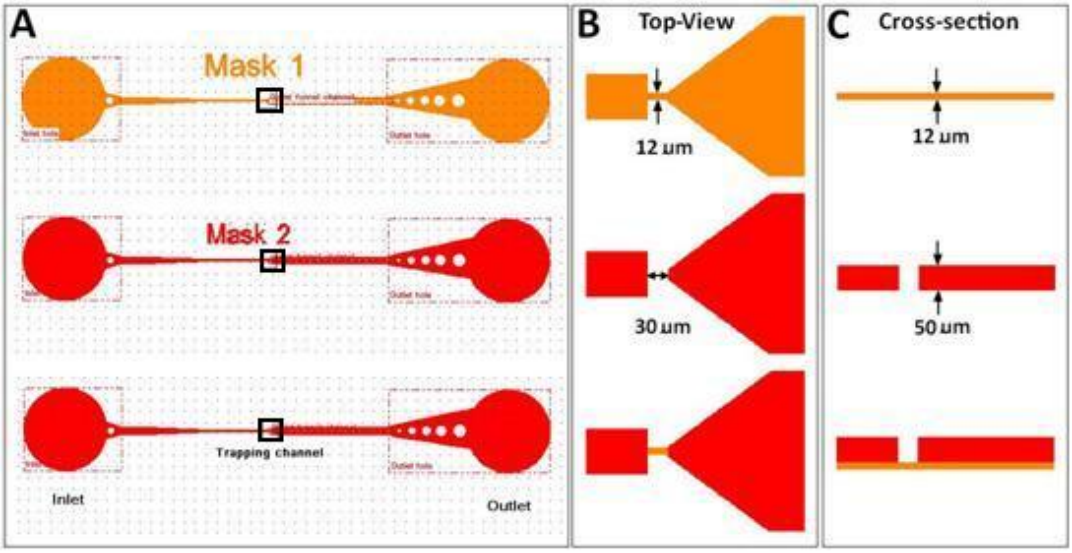

Figure 3.3: Mask design of the microfluidic channel for acquiring EPGs. (A) Double-layer structure and the two masks. Mask 1 (orange) is for the thin layer for trapping the worm's head. Mask 2 (red) is for the thick layer for transporting the worms. (B) Top view of the trapping channel, identified with black square in (A). (C) Cross-section of the trapping channel.

3.2.1.2 SU-8 master fabrication

Standard photolithography [42, 90] is used to make the SU-8 master. In photolithography, a pattern is transferred into a photoresist by exposing the photoresist to light through the mask [91]. The photolithographic procedure includes the steps illustrated in Figure 3.4: (i) prepare an acid cleaned glass or silicon substrate; (ii) spin coat photoresist onto the substrate; (iii) expose the photoresist through a mask with UV light; (iv) develop the photoresist to obtain the pattern of interest.

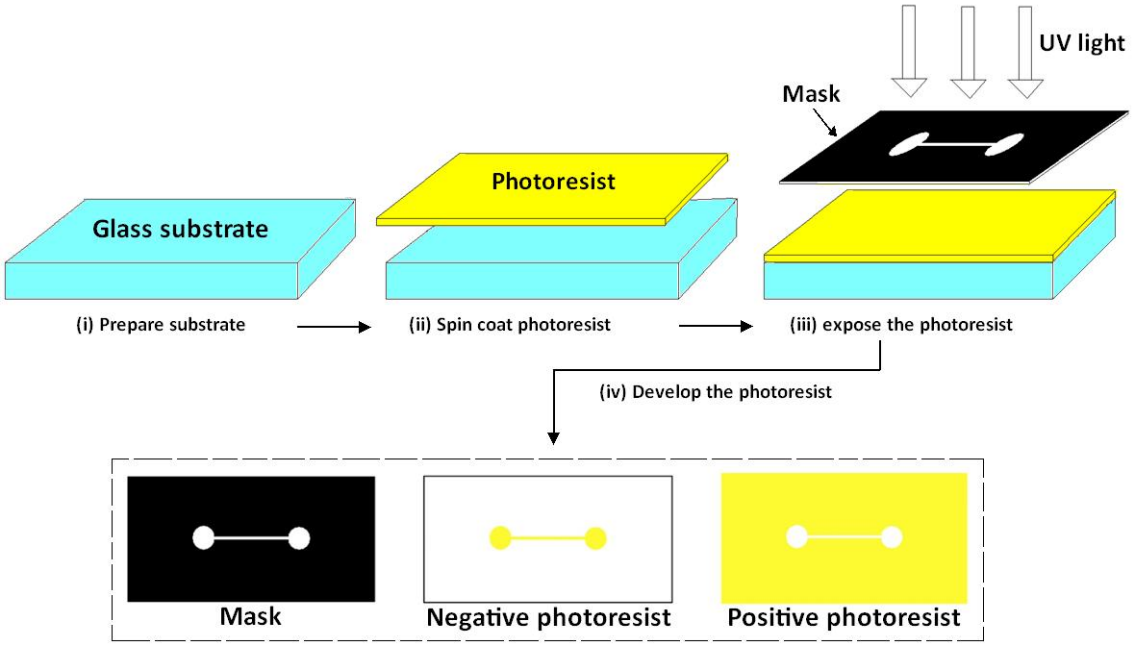

Figure 3.4: Schematic diagram showing the steps of standard photolithography.

Upon exposure to UV light, the photoresist becomes more or less soluble depending on the chemical properties of the particular resist material. The photochemical reactions include chain scission, cross-linking, and the rearrangement of molecules [91]. There are two types of photoresist: positive and negative. If the exposed areas of the photoresist become more soluble, then it is a positive resist; if the exposed resist becomes less soluble, then it is a negative resist. In developing the photoresist, the soluble material is removed leaving a positive or a negative image of the mask pattern (Figure 3.4).

Photoresist is made of four basic components: polymer, solvent, sensitizers, and other additives. The polymer will either polymerize or photosolubilize when exposed to UV light. Solvents are required to make the photoresist a liquid, allowing it to be applied by spin-coating. The sensitizers control the photochemical reactions and additives may be used to facilitate processing or to enhance material properties [91].

The negative photoresist SU-8 (MicroChem, Newton, USA) was used to fabricate the master. SU-8 consists of chemically amplified epoxy based negative resists

that are highly functional, optically transparent and photo imageable at near UV (365nm) radiation. Cured films or microstructures are very resistant to solvents, acids and bases and have excellent thermal and mechanical stability, making them well suited for fabricating permanent structures such as pixel walls, fluidic channels and nozzles, micro arrays and spacers [92]. SU-8 is formed of three basic components: a polymeric epoxy resin that dissolves in an organic solvent and a photo-acid [93]. Figure 3.5 illustrates the process of cross linking, turning SU-8 from liquid to solid state. On average a single SU-8 molecule contains 8 epoxy groups (Figure 3.5A) hence it is called SU-8. Once the photoresist is exposed to the UV light (365 nm), the photo-acid is photochemically produced and this cross-links the epoxy molecules (Figure 3.5B). Following exposure, a Post-Exposure-Bake (PEB) is performed to fully cross-link the SU-8 (Figure 3.5C). The photoresist is heated above 55˚C which turns the viscous fluid to a solid glass [93]. During this process, the photo-acid acts as a catalyst.

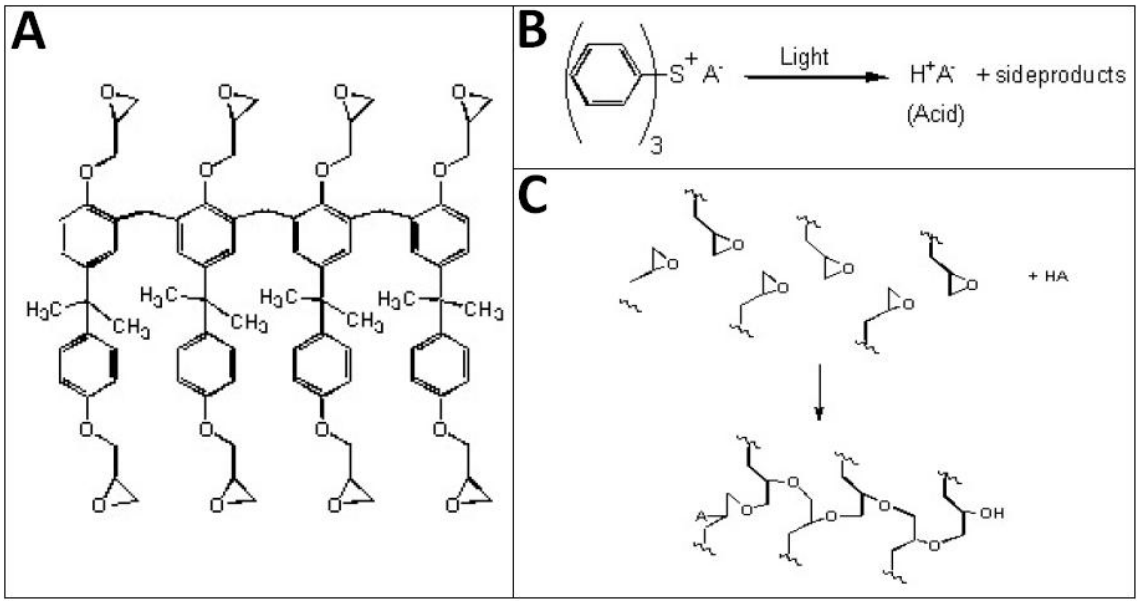

Figure 3.5: The cross linking reaction that turns liquid SU-8 into solid resist. (A) Ideal model of SU-8 molecule with epoxy groups. (B) Mechanism of photoacid generation during exposure. (C) The cross linking reaction that occurs during post exposure bake (PEB). Each epoxy group can react with another epoxy group. Pictures are copied from [93].

In order to fabricate a microfluidic channel with a trap height of 12 μm (to capture the worm's head) and channel height of 60 μm (to flow the worm), SU-8 5 was used. This is suitable for thicknesses from 5 μm to 15 μm. SU-8 50 (40 μm to 100 μm) was used to make the layer for the flow channel (Figure 3.6).

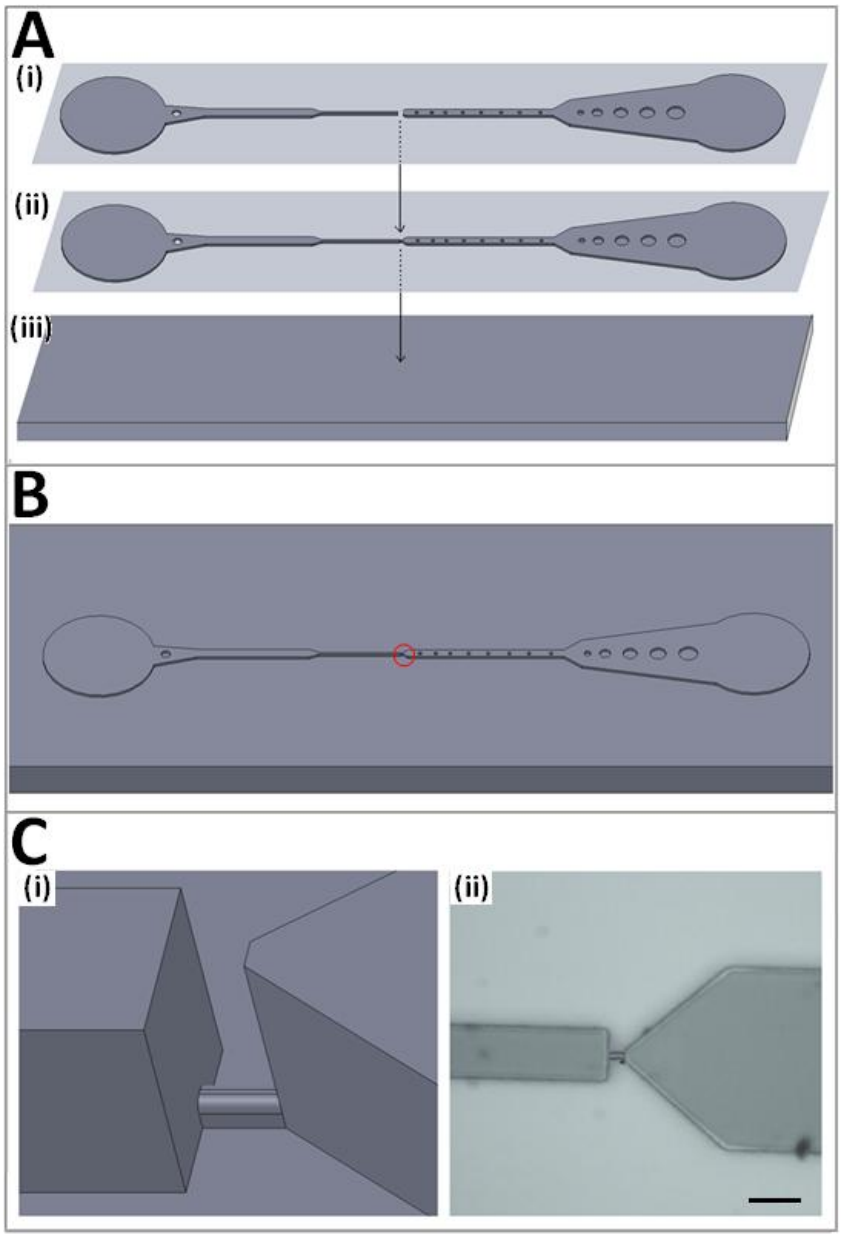

Figure 3.6: Schematic of the process for fabricating an SU-8 master, and an enlarged view of the trapping channel. (A) The process of making an SU-8 master. Take a piece of acid cleaned silicon wafer (iii) as a substrate. Spin coat a layer of SU8-5 (ii) to a thickness of 12 μm. Expose, bake and develop. Spin another layer of SU8-50 (i) with a thickness of 60 μm. Expose with precise alignment; bake and develop. (B) SU-8 master after photolithography. (C) Enlarged view of the

trapping channel, marked with red circle in B. (i) shows a pseudo 3-D structure of the trap, and (ii) is a micrographic top view of the master. Scale bar, 100 μm.

The photolithographic procedure for fabricating these two layers is similar and is illustrated in Figure 3.4. The recipes are detailed in Appendix 2 and 3. Because it is a double layer structure, the second layer must be aligned to the first with a mask aligner. Alignment marks are essential for positioning the second layer precisely over the first layer. Figure 3.7 shows how the alignment is done with the "+" alignment mark. Mask 1 and Mask 2 are both designed with transparent "+" alignment mark in the same position on either side. The first layer is fabricated with SU-8 5, then SU-8 50 spin coated to form the second layer. Cross-linking make the first layer pattern visible even when covered by a second layer of photoresist.

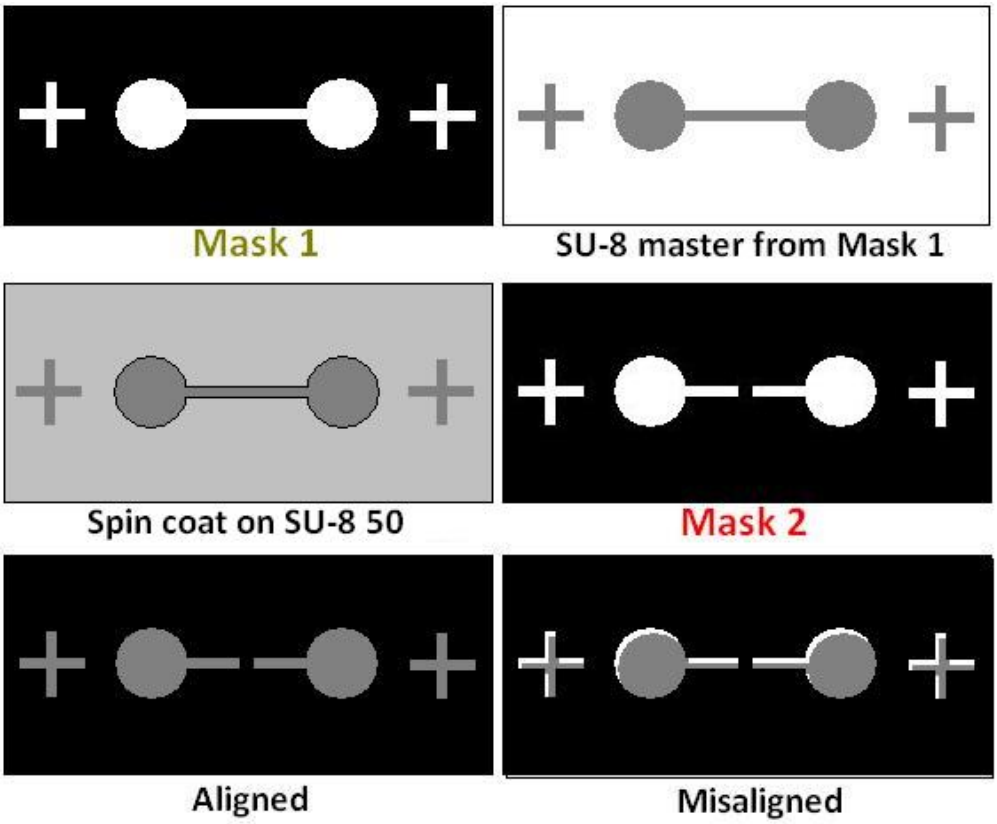

Figure 3.7: Schematic illustration showing the procedure of aligning the second layer onto the first layer of negative photoresist. Clear "+" alignment marks are placed symmetrically on the left and right sides of both masks in the same position. After producing the fist layer with

Mask 1, the second layer of SU-8 50 is spin coated. The first layer pattern is visible through the second layer photoresist since it is cross linked. Mask 2 is aligned onto the substrate by adjusting the position of the alignment marks on both sides. Only when two alignment marks on the first layer exactly fit into the clear "+"alignment marks on Mask 2, is the mask correctly aligned.

Cross linked SU-8 is darker in colour compared to unexposed resist, making it visible after coating a second layer of SU-8. The second layer of SU-8 50 has a thickness of 60 µm, much thicker than the first layer of 12 µm. This increases the difficulty of making an accurate alignment. Two aligning marks written on the first layer are visible with a conventional microscope, but not with the mask aligner. Two approaches (Figure 3.8) were utilized to solve the problem. One is called "Tape Trick" (Figure 3.8A). After producing the first layer, instead of directly coating the second layer photoresist, two pieces of tape were stuck over the alignment mark on this layer. Thick SU-8 50 is then spun coated onto the wafer with the tape attached. Before pre-baking, the tape is removed, revealing the alignment marks without resist.

A second method is to colour the marks making them darker (Figure 3.8B). UV light at a wavelength of 365 nm is used to polymerize the SU8 photoresist, achieved with an I-line filter in the mask aligner. Ultraviolet (UV) light has a wavelength range from 10 nm to 400 nm. Removing the I-line filter results in higher photon energies absorbed by the photoresist, increasing the cross linking process. Highly cross linked SU-8 exhibits a very dark colour, which helps with alignment. After producing the first layer and before spinning the second layer, the wafer is exposed to broad spectrum UV light without the I-line filter to make it darker.

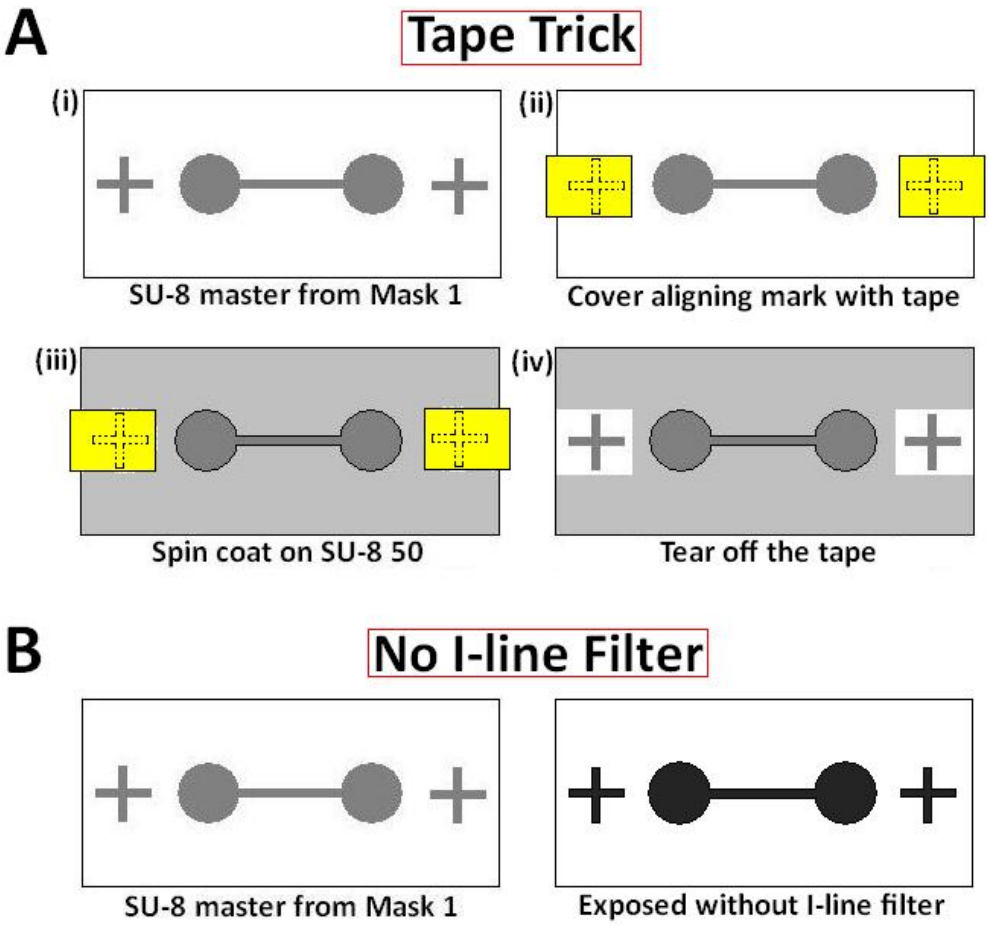

Figure 3.8: Two approaches to make the alignment marks visible after coating a second layer of photoresist. (A) The "Tape Trick". (i) Produce the first layer from Mask1; (ii) Cover two alignment marks with tape separately; (iii) Spin coat the second layer of SU-8 50; (iv) Tear off the tape to reveal the uncovered alignment mark area and bake. (B) Method without I-line filter. After producing the first layer, take out the I-line filter, and flood expose the master with high power UV light, turning the alignment marks darker. The marks remain visible in the mask aligner even when covered by 60 μm SU-8 50.

Both methods have been used and give precise alignment (Figure 3.9A). The SU-8 master used for moulding the microfluidic channel is shown in appendix 4.

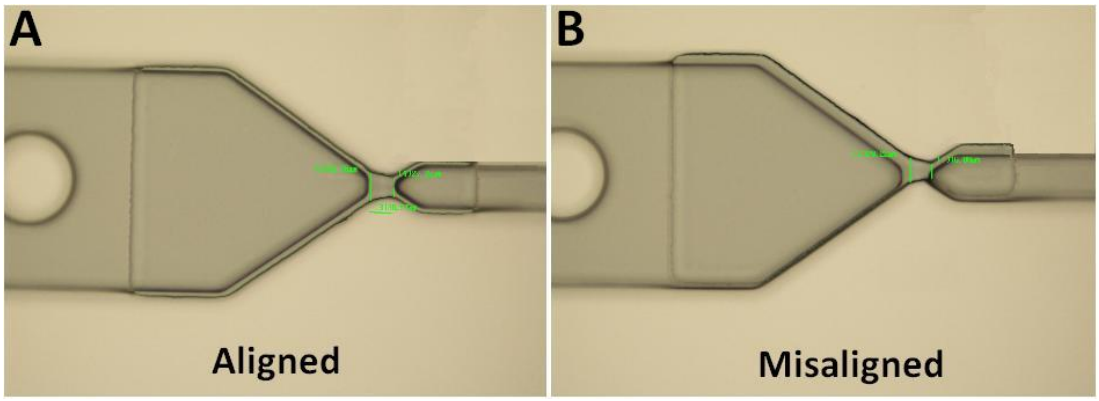

Figure 3.9: Examples of aligned and misaligned SU-8 masters used to make the microfluidic channel. (A) Micrograph of aligned SU-8 master using "Tape trick". (B) Micrograph of misaligned SU-8 master.

3.2.1.3 PDMS casting

Once the SU-8 master has been made, the next steps involve PDMS replication and bonding. Standard soft lithography [43] is used for this process. Figure 3.10 illustrates the process of PDMS casting and microfluidic channel assembly [94]. PDMS (Sylgard 184 Silicone Elastomer Kit) consists of two parts: pre-polymer and curing agent. Different mixing ratios lead to different stiffness of PDMS. First the SU-8 master is treated with trichloro (1H, 1H, 2H, 2H-perfluorooctyl) silane making the surface hydrophobic (not sticky) to the PDMS. Liquid PDMS mixed in a ratio of 10:1 (10 pre-polymer and 1 curing agent by weight), is made and degassed in a vacuum desiccator. After sitting the treated SU-8 master into a custom-made foil container, the degassed PDMS is poured over it and degassed again in a vacuum desiccator to get rid of all the air bubbles. The foil container is then put in an oven and allowed to cure at 50 ˚C overnight. After curing, the PDMS replica (Figure 3.11A) is carefully peeled from the mould, and holes are punched using a PDMS puncher, creating fluidic inlets and outlets in the PDMS channel. Prior to bonding the surfaces of the PDMS replica and glass substrate are treated with oxygen plasma ashing (50 w, 30 s) [95] to make them hydrophilic. Bonding is performed immediately after surface treatment, followed by baking at 100 ºC for at least one hour. A flat piece of PDMS is inserted between the channel and the substrate (Figure 3.10), which provides an elastic base so as a better seal.

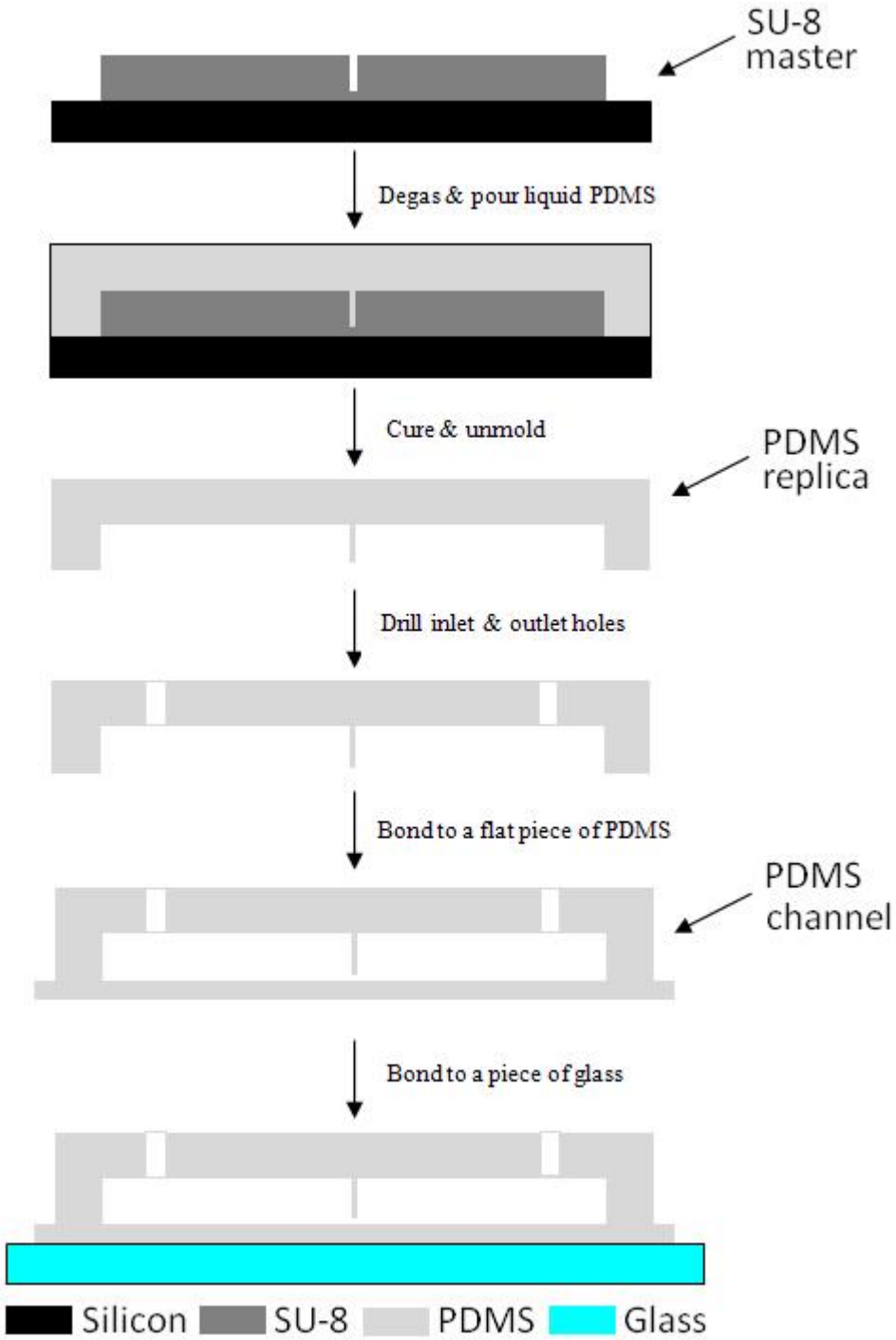

Figure 3.10: PDMS microfluidic channel fabrication process: (i) Silanize the surface of SU-8 master with trichloro silane. (ii) Degas liquid PDMS and pour over the master. Degas again and bake overnight at 50 ˚C. (iii) Peel off the PDMS replica from the master after curing. (iv) Drill inlet and outlet holes on the replica and wash thoroughly. (v) Bond onto a flat piece of PDMS using oxygen plasma (50w, 30s). (vi) Bond the structure onto a piece of glass, and bake at 100 ˚C for at least one hour.

A single microfluidic chip is smaller than a one pound coin (Figure 3.11B). The inlet and outlet holes have a diameter of around 1 mm, compatible with equipment used in conventional EPG experiment.

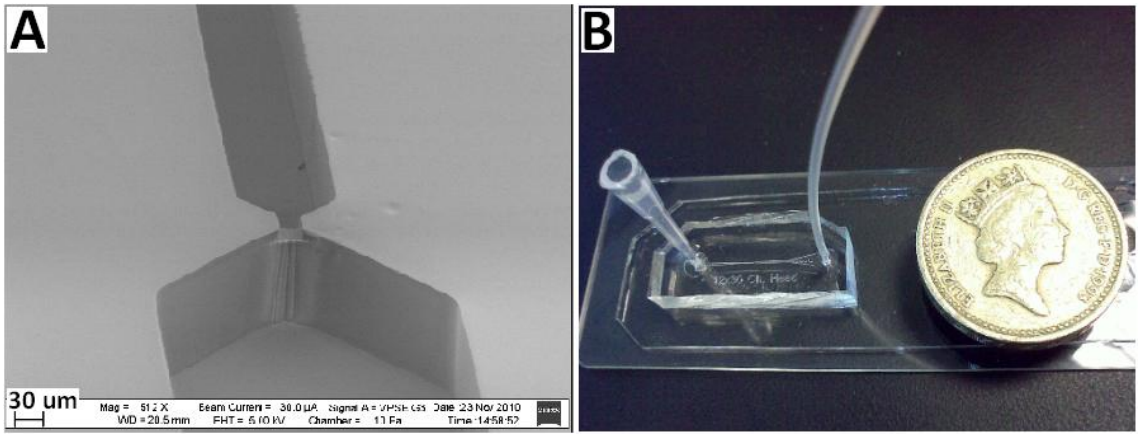

Figure 3.11: PDMS microfluidic channel. (A) Close view of the PDMS trapping channel imaged with Scanning Electron Microscope (SEM). (B) Microfluidic channel after bonding with a pipette tip and a section of polythene tubing attached. The size of the chip is slightly smaller than a one pound coin.

3.2.2 Experimental procedure for acquiring EPGs on-chip

The microfluidic channel can be used within a conventional EPG setup (Figure 2.2A) replacing the petri dish (Figure 3.12). Young adult wild type *C. elegans* (Day 1 worm) were used because their feeding behaviour is robust and stable for around 1 to 2 days [96]. A solution of 0.1% bovine serum albumin (BSA) was added to Dent's saline to release the worm from the bottom of the Petri dish and prevent the worms from sticking in the pipette as well as in the PDMS channel. Dent's saline was filtered with a 0.2 µm syringe filter to eliminate any debris that may block the trapping channel.

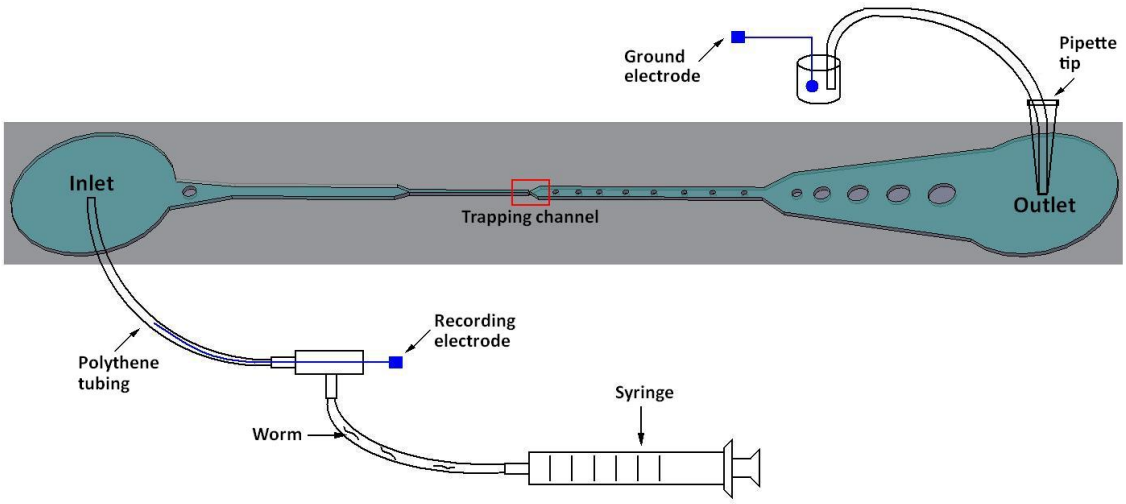

Figure 3.12: Simplified diagram of the setup for acquiring EPG signals on chip. The microfluidic chip can be placed in a conventional EPG setup by replacing the petri dish. The position of trapping channel is indicated by a red square.

The experimental procedure for acquiring EPGs in the microfluidic channel is simple. Dent's saline is first of all injected into the chip to get rid of all air bubbles, providing a liquid environment. A single worm is then picked out from a worm culture dish and transported in a Petri dish containing Dent's saline. The next step is to load the worm into the microfluidic channel. In doing this, the worm is gently sucked out of the petri dish with a syringe with recording electrode attached (Figure 3.12). Pressing on the syringe pushes the worm into the channel towards the trapping channel with flow. At the same time, the ground electrode is connected to the outlet of the chip through a salt bridge, which is made of a length of polythene tubing filled with KCl Agar (4% Agar dissolved in 3M potassium chloride). Once *C. elegans* is captured in the trap and pumping, EPG signals are recorded by connecting the two electrodes to an Axoclamp amplifier, as used in the conventional method.

3.3 Result

After several attempts, the *C. elegans* was successfully captured in the microfluidic channel (Figure 3.13A). Figure 3.13B is a close-up view of the trapped head showing the young adult *C. elegans* trapped just prior to the corpus, which is the appropriate position for collecting EPG signals. The constant geometry of the trap guarantees individual worms are trapped in the same position every time, which is required for rigorous statistical analysis of the EPG recordings.

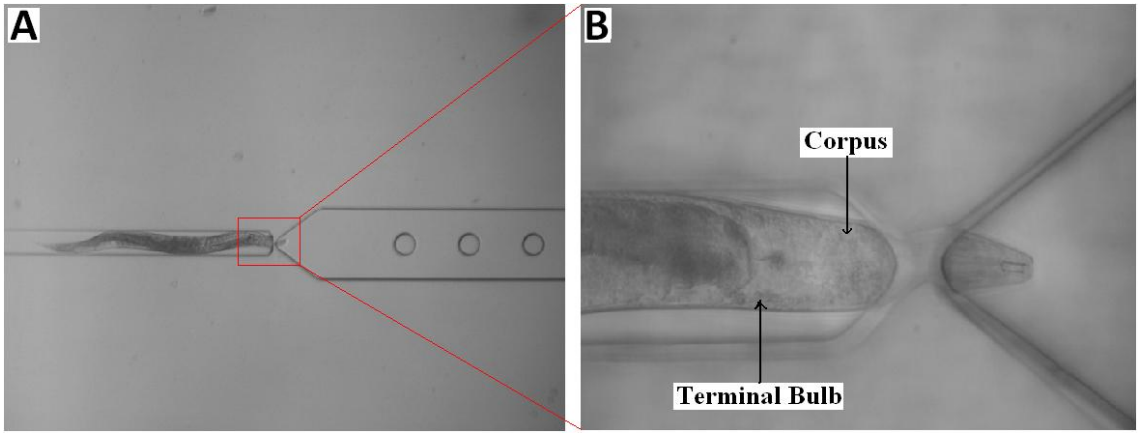

Figure 3.13: Young adult (L4+1) *C. elegans* trapped in the microfluidic channel. (A) Micrograph of a trapped *C. elegans* in the microfluidic channel. (B) Close-up view of the trapped head of the worm (zoom of the red square in A). The pharynx, including the corpus, terminal bulb and grinder can be observed. The worm is captured in the right place, just prior to the corpus.

High quality EPG signals were obtained from trapped worms with the microfluidic channel (Figure 3.14B). These signals are similar to those observed with the conventional method (Figure 3.14A) in terms of both amplitude and waveform.

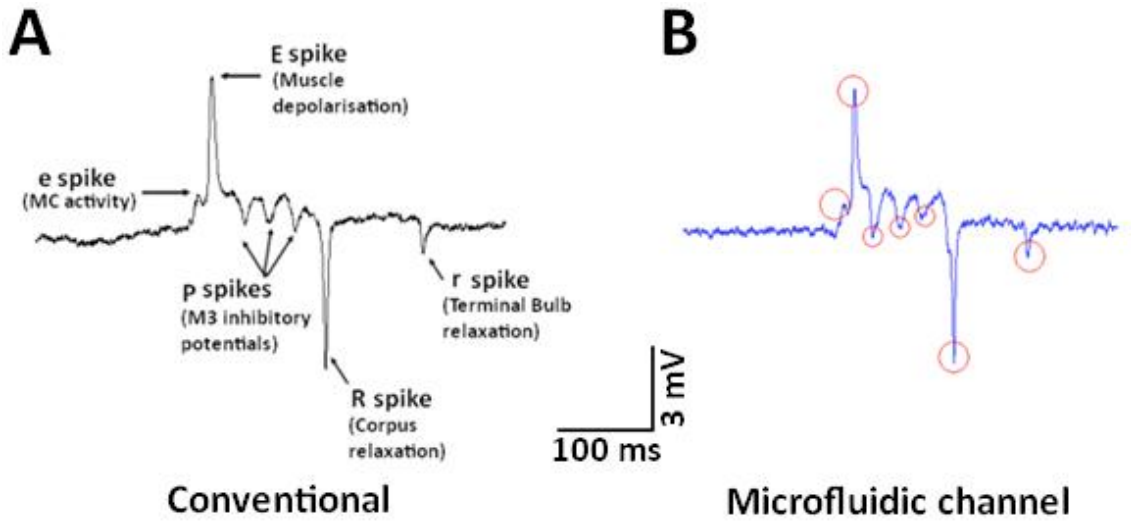

Figure 3.14: Comparison of EPG waveforms obtained from the conventional method and the microfluidic channel. (A) An example of a single pharyngeal pump recording, EPG, obtained using a conventional suction tube placed over the mouth of the worm using a cut head preparation. This waveform depicts three phases: E (e, E), P, and R (R, r) phase, which report on the activity of the neural circuit that regulates the worm's feeding behaviour. (B) An example of a single pharyngeal pump recording, EPG, obtained using a microfluidic channel. All phases and functional spikes are clearly observed - marked with red circles.

To achieve a high quality EPG signal, a robust and electrically tight seal is required around the worm's head. In order to make a trapping channel that mimicked the capability of the conventional electrode to extract discrete neural components of the waveform, fabrication of the microfluidic device was optimised over several iterations (Figure 3.15). The key steps are indicated in Figure 3.15A. The incorporation of a soft under-layer and an additional procedure to form semi-cylindrical channels so that the microfluidic chamber has a rounded 'ceiling' ultimately permitted the robust capture of EPG signals that were indistinguishable from those obtained using conventional glass suction tube (Figure 3.14A; Figure 3.15B). Before this optimisation the amplitude and waveform were quite weak (Figure 3.15B, first recording).

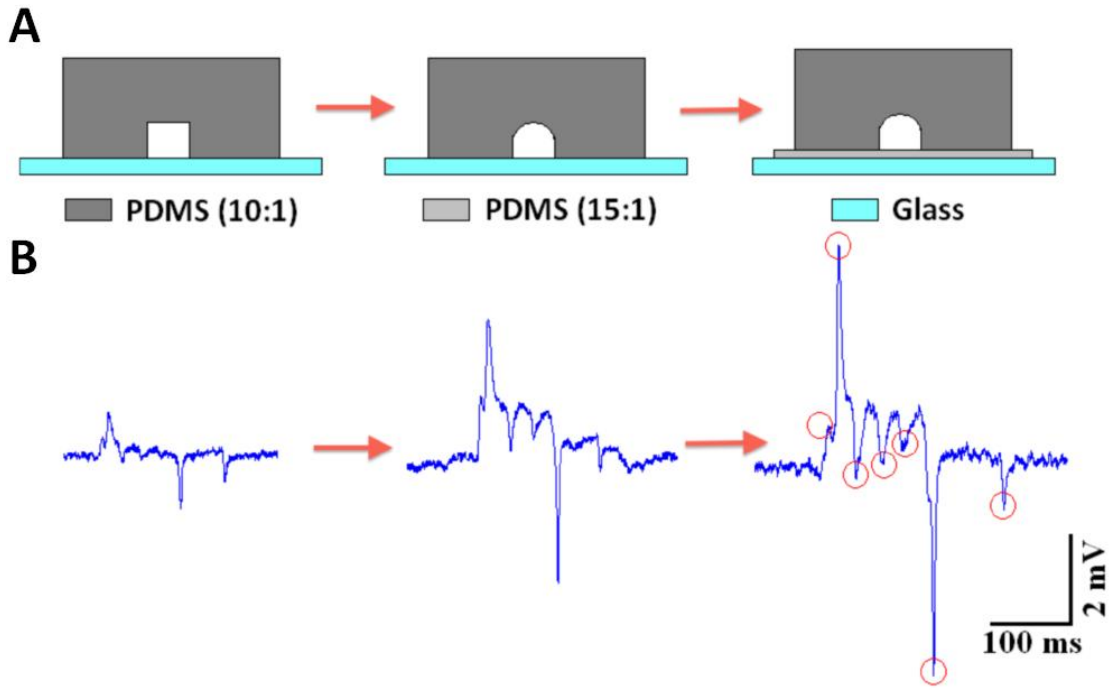

Figure 3.15: A comparison of different preliminary designs of microfluidic trapping channel and the resulting electropharyngeogram (EPG) signal. (A) Evolution of the shape of the aperture and (B) the corresponding EPG signals. The first signal is obtained from a single layer chip and the aperture which traps the worm's anterior is square. The signal in the middle is taken from a single layer chip with semi-circular aperture, which is similar to the shape of the worm. The last example of an EPG signal is recorded from a two-layer chip with semi-circular shaped aperture. The softer base provides a better seal and thus generates a larger amplitude EPG and improved resolution of subcomponents of the waveform reporting neural activity. Each phase and feature of the EPG is of greater magnitude in this last waveform. All the features are marked with red circles.

Semi-cylindrical channels were produced by optimising the fabricating process of the SU-8 master. Two factors affect the final shape of the SU-8. The main factor is exposure energy. The exposure parameters required to achieve accurate pattern transfer from the mask to the photosensitive layer depends primarily on the wavelength of the radiation source and the dose (time) required to achieve the desired properties change of the photoresist [97]. The wavelength is kept constant as 365 nm for negative photoresist in this work.

By only increasing or reducing the exposure dose or time, the size and shape of the pattern could be controlled.

At the edges of the pattern, light is scattered and diffracted, so that the dose received by the photoresist at the edge may become significant [97]. Figure 3.16 demonstrates how the exposure dose or time affects the final geometry of the pattern when using negative photoresist. If the pattern is over-exposed, the photoresist image is dilated, causing the features to be larger than desired. This is accompanied by a loss of sharpness of corners. If it is under-exposed, the photoresist image becomes eroded along the edges, resulting in a decrease in feature size and again a loss of sharpness or corners.

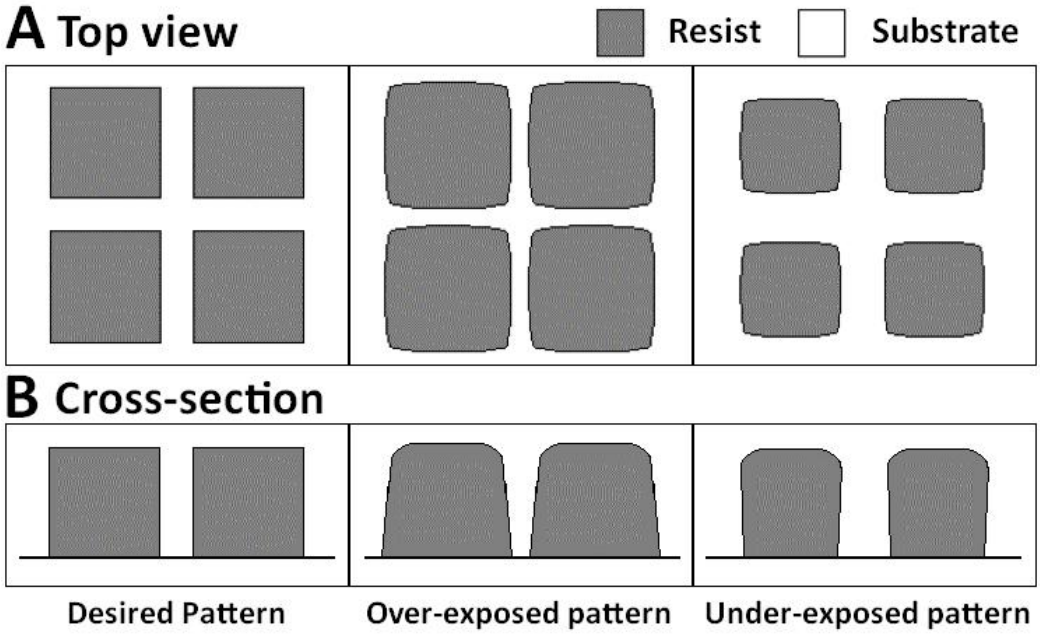

Figure 3.16: The exposure dose or time affects the final geometry of the pattern of interest in negative photoresist. Top view (A) together with cross-section (B) show that the photoresist image may be either dilated or eroded along the edges by over or under exposure. Both result in a loss of sharpness or corners.

To achieve a near semi-cylindrical SU-8 trapping channel, not only does the pattern need be over-exposed to remove the corners, but it is also over-developed to further polish the edges.

The ideal shape required for a perfect seal around the worm's head is a circle. After obtaining a near semi-cylindrical SU-8 trapping channel on the master, three additional approaches were examined to further optimise the PDMS fabrication method to give the best geometry of trap (Figure 3.17). Moulding the treated SU-8 master gives a near semi-cylindrical PDMS trapping channel (Figure 3.18). The first idea is based on a simple principle that one circle can be made from two semi-circles (Figure 3.17A). Two symmetric semi-cylindrical PDMS trapping channel are placed face-to-face and bonded with manual alignment after surface treatment with O_2 plasma. Precise alignment leads to a round hole. The second method uses liquid PDMS. A very thin layer of PDMS (4 μm) is spin coated onto the glass substrate with a spin speed of 6000 rpm. The PDMS channel is gently placed on top of this layer. The square edges that contact with the liquid PDMS can fill with liquid PDMS, forming a near semi-circular surface. A near circular hole is formed after baking the chip to harden the liquid PDMS base (Figure 3.17B). The third method uses a PDMS sheet bonded onto the glass substrate to provide a soft base (Figure 3.17C). In general, the higher the mixing ratio the softer the PDMS. To achieve a soft and elastic base a mixing ratio of 15:1 was chosen. A ratio of 20:1 is too loose and does not keep the worm in trap. The first two methods work fine but only on large channels (> 50 μm). In terms of the first approach the trapping channel has a diameter of 12 μm, which makes alignment difficult. In the second method, very small holes can be entirely filled by liquid PDMS, depending on the thickness of the liquid and the pressure applied. Unlike the first two methods, the last one does not generate a perfect circular trap. However, compared to the many uncertainties in the first two approaches, the addition of a layer of soft sheet PDMS provides a tight seal and generates good signals, as shown in Figure 3.15. It was chosen as the optimum method for fabricating the near circular trapping channels and trapping the *C. elegans* head.

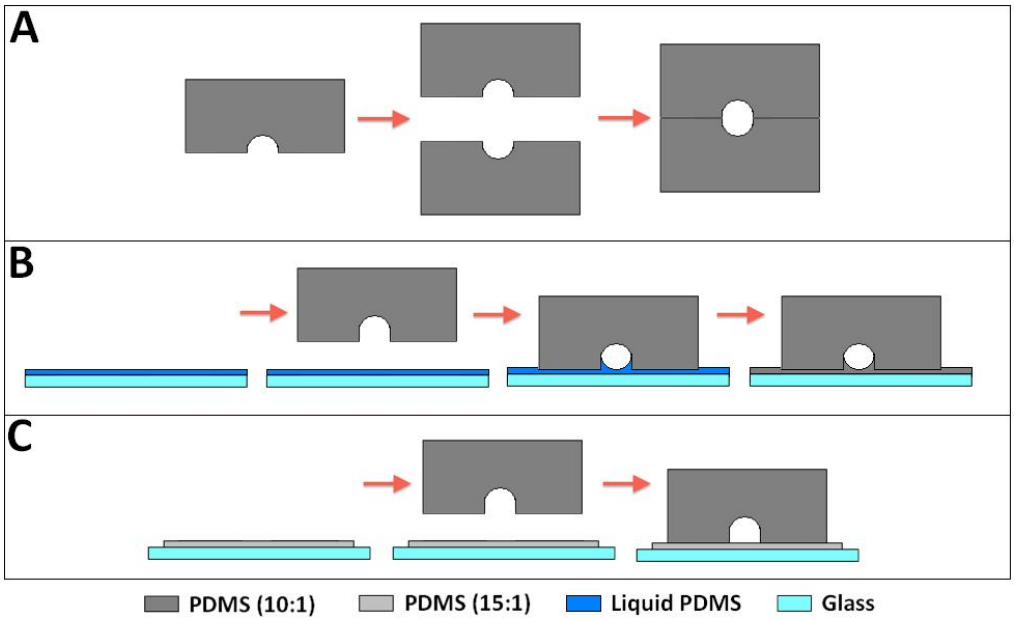

Figure 3.17: Three approaches to further optimise the geometry of the trap using PDMS fabrication. (A) Two symmetric semi-cylindrical PDMS trapping channel are placed face-to-face and bonded with manual alignment after surface treatment with O_2 plasma to achieve a round hole. (B) A very thin layer of liquid PDMS is spin coated onto the glass substrate before bonding the PDMS channel onto the glass substrate. The square edges contacted with the liquid PDMS are filled with the liquid, forming a near semi-circular surface under surface tension. (C) Before bonding the final feature onto the glass substrate, a layer of PDMS sheet is first bonded to the glass. Mixing ratio of 15:1 gives a softer PDMS sheet, providing a more elastic trap and generating a better seal.

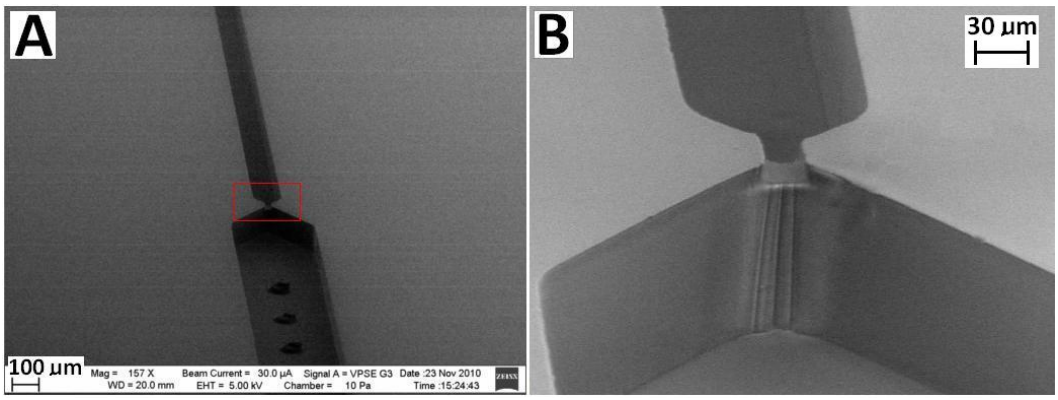

Figure 3.18: SEM of the PDMS microfluidic channel. (A) Bottom view of the PDMS microfluidic channel. (B) Zoomed in area (marked by red square in A), showing the trapping region.

As in the conventional EPG experiment, the nematode was sucked into the trapping channel by applying negative pressure to the outlet. However, unlike the glass tube, PDMS is air-permeable which means that air gets sucked into the channel from outside. In other words, bubbles are generated when system is driven by suction (Figure 3.19). The microfluidic channel may get blocked by these air bubbles, leading to an "open circuit" in the electrical recording system. In order to eliminate the air bubbles, instead of sucking the worm into the trap with a negative pressure on the outlet, a positive pressure is applied to the inlet to push the worm into the trapping hole. Positive pressure provides a bubble-free environment (Figure 3.13).

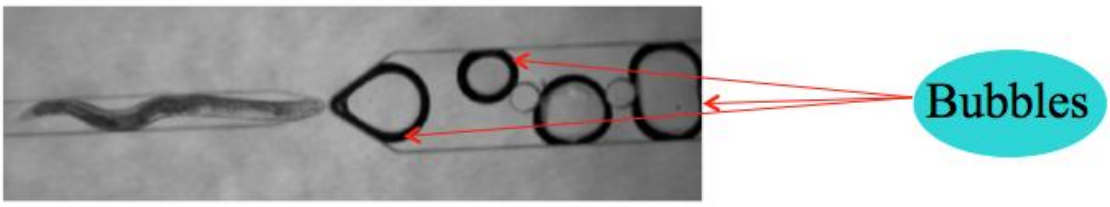

Figure 3.19: Bubbles are generated when the nematode is sucked into the trap of the microfluidic channel, because PDMS is air-permeable.

Reproducible placement of the worm in the trap is necessary for reproducible EPG waveforms. The optimum size for trapping a one day old adult hermaphrodite was determined by fabricating a range of different channel dimensions ranging from 9 μm x 5 μm x 15 μm to 40 μm x 12 μm x 30 μm (width x height x length). 12 μm was finally chosen as the best height for capturing the worm's head, thus it is the default size.

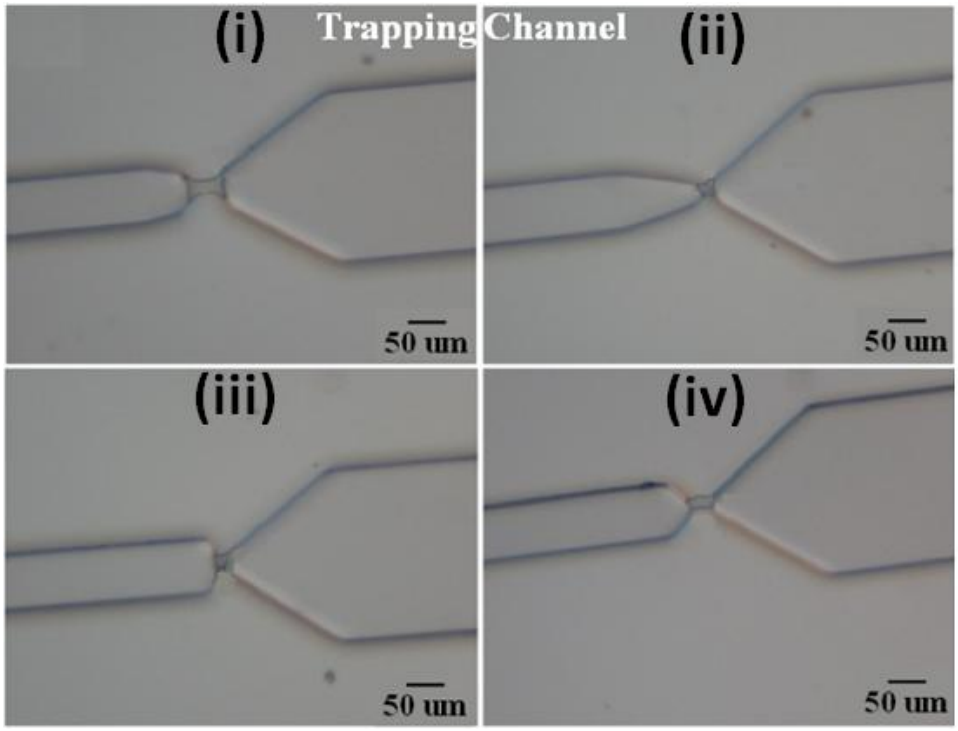

Figure 3.20: Four basic designs of trapping channel. (i) Curved, 40μm-17μm-40μmx12μm (width (left-middle-right) x length); (ii) Tapered, 20μm-30μm x25μm (width (left-right) x length); (iii) Straight square, 18μmx25μm square (width x length); (iv) Straight, 17μmx40μm (width x length).

Microfluidic channels with eleven different designs of trapping channel (Figure 3.20) were validated, with the aiming of finding the best size for trapping L4+1 *C. elegans* (Table 1). Each design was examined with at least 20 worms. At the beginning of the experiment, these microfluidic channels were only tested for the ability to trap worms, not for EPG signals. This is why the number of trapped worms is larger than the number of EPG recording in Table 1. Survival observation was undertaken after collecting the EPG recording with 6 released nematodes that were randomly selected. All six worms were healthy and propagated as normal *C. elegans*.

Table 1: Attempts to trap & record worms with diverse trapping channel designs. The first column lists the sizes (Width (left-right) x Length) of the trapping channels that have been examined; the second column describes the quantity of worms used in each channel; the third column shows how many worms were trapped in the channel; the fourth column indicates the numbers of trapped worms that generate EPG signals; the last column provides survival results (Survivals/Released). The reason that not every trapped worm gives an EPG signal is at the beginning of this project, these channels were tested in the absence of an EPG setup. Once the chip is connected to the EPG equipment, EPG signals are collected from nearly every trapped C .elegans. Six released worms were randomly picked out for survival tests and all of them were healthy. In total 5 different size channels provide effective electrophysiological recordings from trapped worms. The first two size channels have better performance. And survival tests were only undertaken on some of the released worms which were randomly picked.

Sizes (μm)	Worms	Trapped	EPG Signal	Survive
15-23×22	~30	10	5	2/2
20-30×25	~30	8	3	2/2
18×25	~30	4	1	1/1
18×25 square	~30	3	2	1/1
25×20	~30	3	1	--
25×10	~30	0	--	--
17×40	~30	0	--	--
Curved (40-17-40)×30	~30	0	--	--
10-20×30	~20	2	0	--
12×30	~20	0	--	--
9×30	~20	0	--	--

Electrophysiological signals of good quality were recorded from the worms trapped in two channel sizes: 15-23×22 μm and 20-30×25 μm. The trapping position of the worm determines the quality of the EPG signal (Figure 3.21). The primary trapping position is just prior to the corpus. If the worm goes further into the trap, it may get damaged. Figure 3.21 shows two different age wild type worms in two different size microfluidic channels. Day 1 worm stands for young adult (L4+1) *C. elegans*, and Day 2 is one day older. Day 1 worm is trapped on the corpus in a channel of size 15-23×22 μm while a Day 2 worm is trapped on the corpus in a channel of size 20-30×25 μm. The latter is slightly bigger than required for trapping Day 1 worm, thus when Day 1 *C. elegans* was pushed into the trap, it got trapped at the position between the corpus and terminal bulb (Figure 3.21).

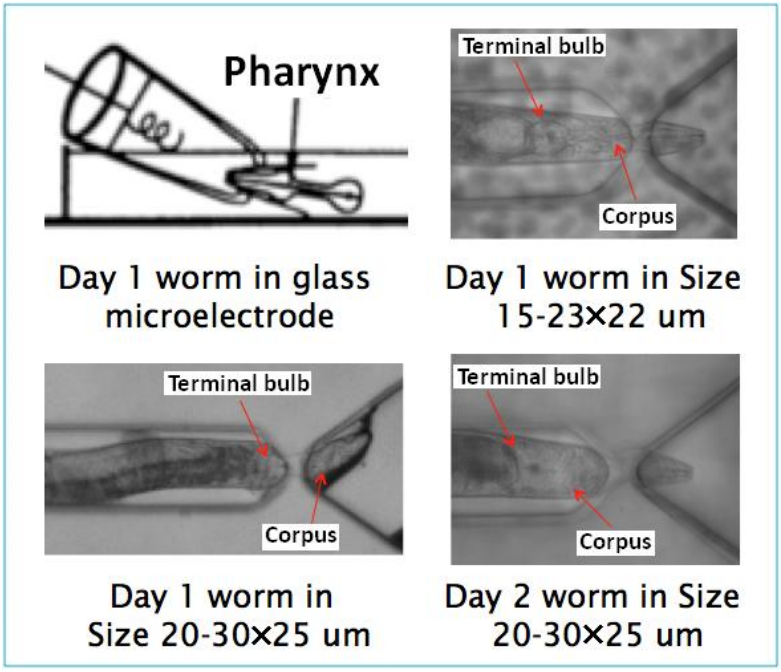

Figure 3.21: Two different age wild type worms in two different sized channels. Red arrows point to the position of corpus and terminal bulb in the trap respectively. Day 1 worm is trapped on the right position in channel of size 15-23×22 μm while Day 2 worm in channel of size 20-30×25 μm. Size 20-30×25 μm is slightly bigger than is required for Day 1 worm.

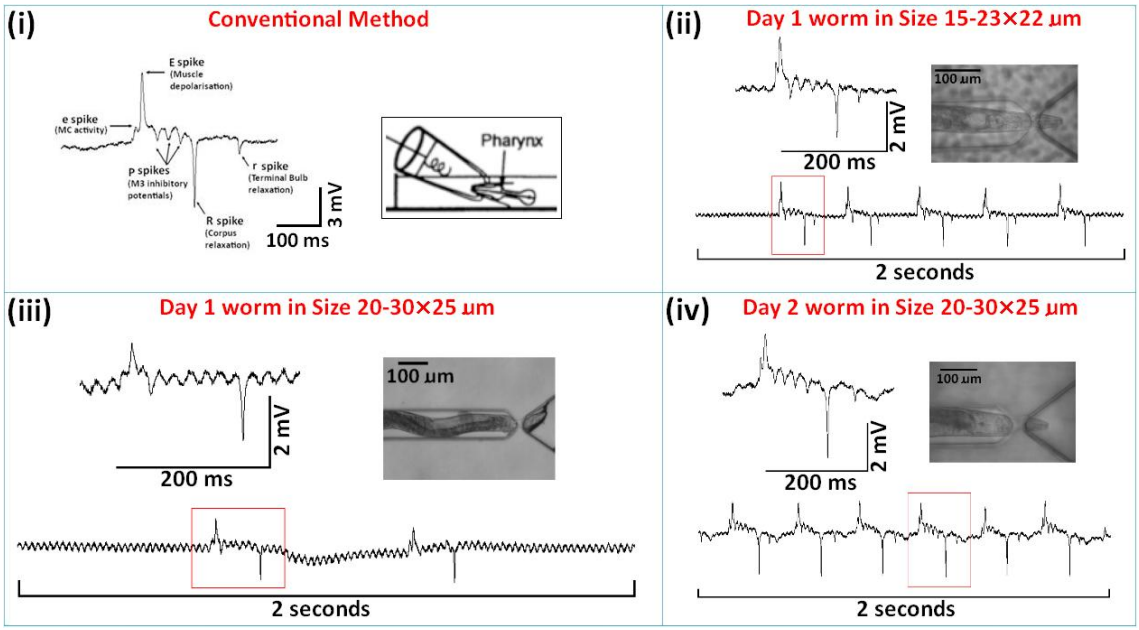

Figure 3.22: Two different age wild type worms in two different size channels. Red arrows indicate the position of corpus and terminal bulb in the trap respectively. Day 1 worm is trapped in the correct position in channel of size 15-23×22 µm while Day 2 worm in size 20-30×25 µm. Channel of size 20-30×25 µm is slightly bigger than required for a Day 1 worm.

Figure 3.22 shows electrical activities obtained from two different age worms in two different size channels, correlated with Figure 3.21. From worms trapped on the front of corpus (Day 1 worm in size 15-23×22 µm and Day 2 worm in size 20-30×25 µm), high quality electropharyngeogram waveforms, showing all functional spikes were obtained. The EPG signal collected from worms trapped between the corpus and terminal bulb is less good. The amplitude is small (~2 mV) and the P spikes are difficult to identify due to the large background noise (~0.5 mV). There are two possible reasons for this. Firstly, the size of the trapping channel is bigger than desired for a Day 1 worm, leading to an ion leakage around the worm's head, which may reduce the electrical signals. Secondly, in order to achieve a good seal, a higher pressure is applied, which may increase the background noise. After comparing these three EPG traces, channel with dimension of 15-23×22 µm was chosen to be the optimum for trapping young adult *C. elegans*. After analysing all the EPG signals collected from the diverse microfluidic channels,

the bigger worm gives the larger signal. This is because the pharyngeal muscle cells are capable of myogenic activity and therefore can pump in the absence of the pharyngeal nervous system [76]. Raizen et al [12] found that if all pharyngeal neurons are killed except M4 which is essential for survival, EPG signals can still be recorded without P spikes. Thus EPG is basically generated by muscle events. Bigger worm has stronger muscles (larger cell membrane area) so as to produce larger signals. The average peak-to-peak amplitude of the EPG signals obtained from Day 2 worm in 20-30×25 μm channel is ~7 mV, while that from Day 1 worm in 15-23×22 μm channel is ~5 mV.

In order to examine the performance of the microfluidic channels the worms were exposed to 10 mM serotonin (5-HT). This enhances the activity of the M3 motor neurons and the pharyngeal action potential duration is decreased to approximately one-third of the one without drug. The pumping frequency is also increased from ~ 20 to ~ 200 pumps per minute. 5-HTalso suppresses locomotion of the worm, making it easy to load and capture the nematode [82].

As introduced in the last chapter, a complete EPG signal includes three phases: the E or excitation phase (E & e); the P or plateau phase; and the R or relaxation phase (R & r). These electrical 'landmarks' of the EPG waveform have been used to extract and quantify discrete aspects of pharyngeal behaviour, such as pump rate and pump duration. Software called AutoEPG [15] was utilized for the rapid identification of these pharyngeal phenotypes in the conventional method, permitting rapid extraction of specific parameters from the EPG traces. It uses a special signal processing algorithm that detects different features of the EPG signal automatically. EPG recordings obtained with the microfluidic channels were easily recognized and processed with AutoEPG (Figure 3.23), providing evidence that high quality EPG signals can be collected with the microfluidic chip.

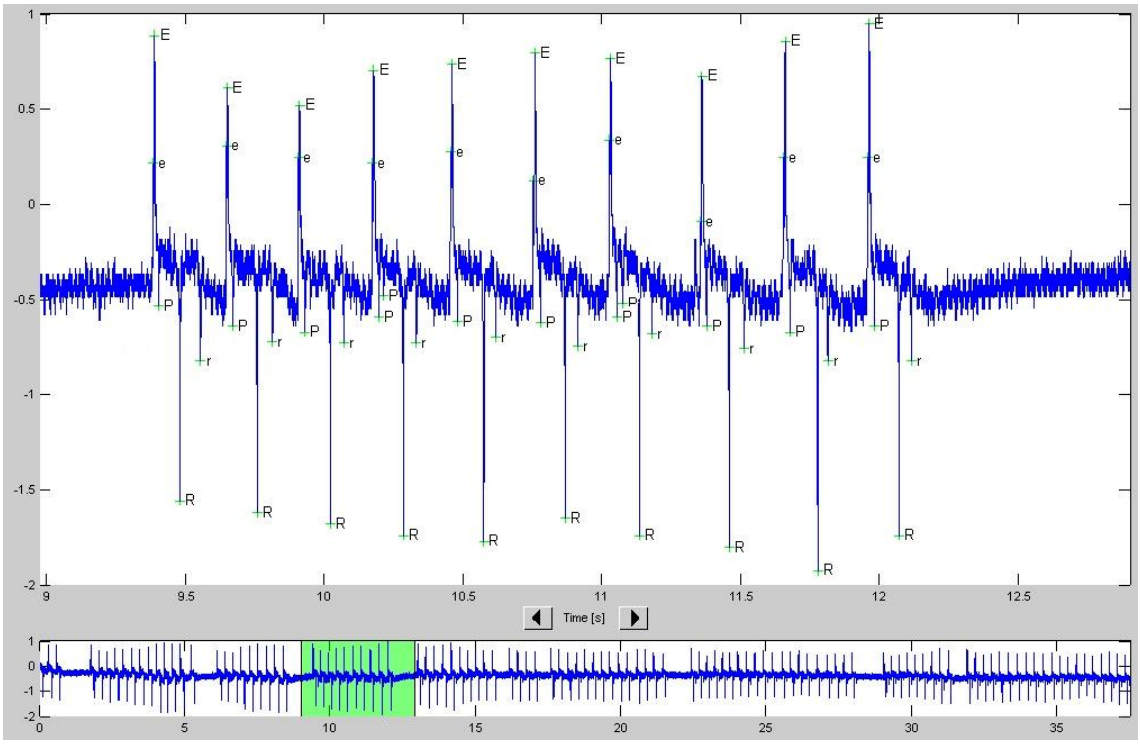

Figure 3.23: An EPG signal trace recorded from a trapped wild type N2 *C. elegans* in microfluidic channel processed by the software AutoEPG. All functional spikes of the EPG waveform were recognised and annotated by the software, indicating the EPG recordings obtained with the microfluidic chip are of good quality.

As well as performing automated annotation, the software is also capable of statistical analysis of whole EPG traces enabling the quantification of subtle pharyngeal phenotypes. Figure 3.24 demonstrates six specific parameters (Pump Rate, Pump Duration, P Peaks, Group of Pumps, R/E Ratios, and R-E Intervals) extracted from a processed EPG signal trace with AutoEPG that is shown in Figure 3.23. These six parameters provide nearly all the basic information about a pharyngeal pump in terms of extracellular recording, which is necessary for research on drug screening and mutant sorting. Pump Rate indicates the number of single pharyngeal pumps in a certain time; Pump Duration shows how long a single pump lasts; P peaks represents the number of p spikes during one single pump. In the case of groups of pumps, as in this example, the time interval has been set to 0.3 seconds (i.e. consecutive pumps that occur within 300 seconds of each other will be classified by AutoEPG as belonging to the same group). R/E Ratio is the ratio of R spike amplitude to E

spike amplitude in the same single pump; R-E Intervals is the time interval between two different pumps (the time from one r spike to next e spike). AutoEPG enables fast and accurate analysis of EPG traces, which facilitates the efficient statistical analysis of large EPG data sets. Combined with this software, the microfluidic channel provides a new way for electrophysiological analysis of *C. elegans* in a high throughput fashion.

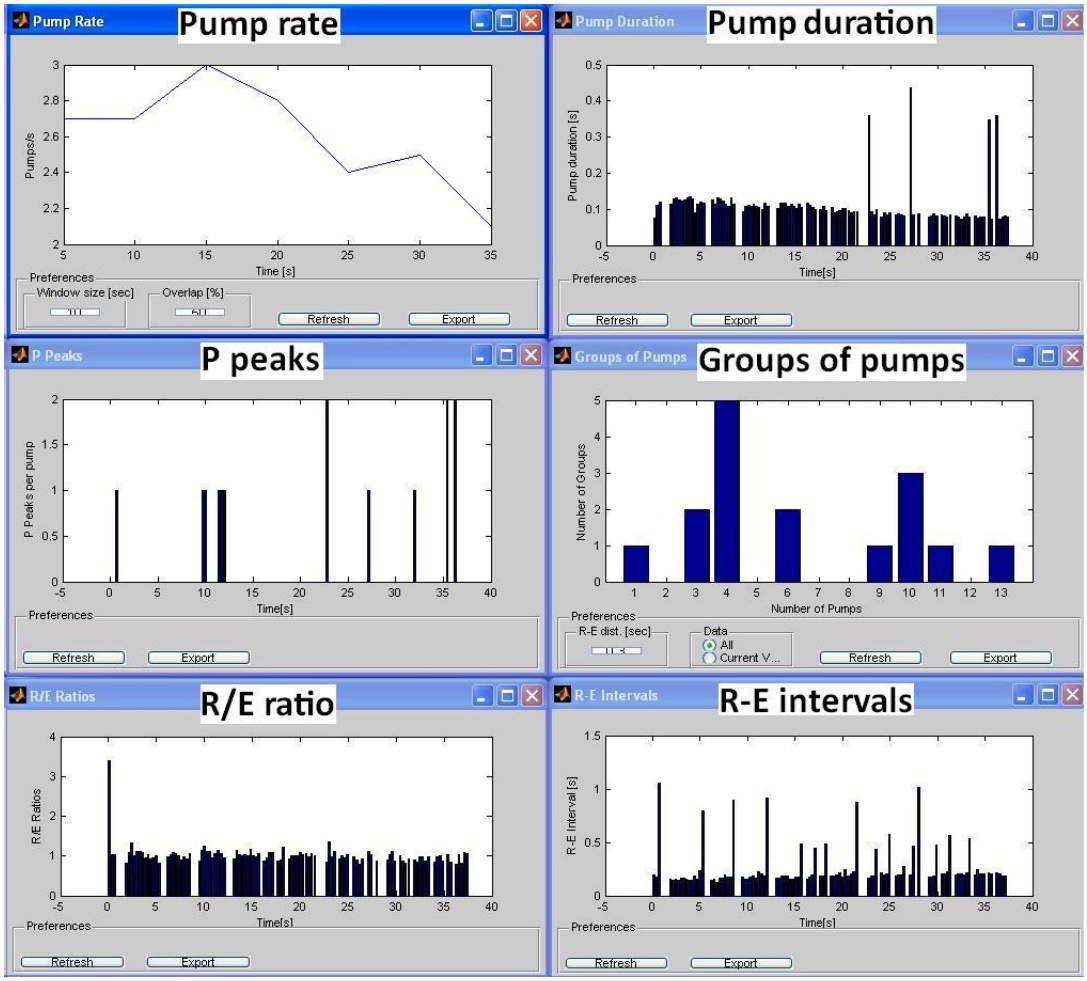

Figure 3.24: Six specific useful parameters (Pump Rate, Pump Duration, P Peaks, Group of Pumps, R/E Ratios, and R-E Intervals) extracted from the EPG trace shown in Figure 3.23. Pump Rate gives a graphical view of the pharyngeal pumping frequency, with time on the x-axis and number of pumps on the y-axis; Pump Duration indicates how long each pump lasts for; P peaks shows number of p spikes during one pump; In the case of groups of pumps in this example the time interval has been set to 0.3 seconds (i.e. consecutive pumps that occur within 300 seconds of each other will be classified by AutoEPG as belonging to the same group; R/E Ratios shows the ratio of R spike

amplitude to E spike amplitude in the same pump; R-E Intervals tells the time intervals between two different pumps (the time from one r spike to next e spike). In the case of pump duration, P- peaks and R/E-ratios, each bar in the graphical output represents a single pump, with time on the x-axis.

To evaluate whether or not the trapping of worms in the microfluidic device causes damage recovery experiments were conducted in which worms were captured in the channel, EPGs recorded for five minutes, and the worms then retrieved and placed back on culture plates. The impact of trapping on motility was measured by transferring individual worms onto an agar plate without food and after one hour counting the number of body bends made in 3 minutes. Control worms were treated in the same way except they were not trapped in the device prior to transfer to the agar plate. Trapped and released worms moved with a frequency of 21.3 ± 6.4 body bends per minute whilst controls moved at a frequency of 26.0 ± 7.2 body bends per minute (n=3; mean ± s.d.). Thus no significant difference was observed in motility. To test whether trapping impacted on a worm's ability to grow and reproduce trapped worms were released onto individual culture plates with food and counted the number of progeny from each worm. Worms that had been released from the device were still alive and had a similar growth rate and propagation compared to un-trapped ('normal') worms (Figure 3.25). (Two days following release from the trap the average brood size for six worms was 104 ± 4; mean ± s.d. This is similar to the expected brood size for 2 day old worms [98]. Therefore, despite a slight reduction in motility, the trapped and released worms were able to grow and produce viable progeny.

Thus individual worms may be recovered and propagated following electrophysiological analysis with the microfluidic chip, an important consideration for applying this approach for mutant screens.

Figure 3.25: Worms can be recovered from the microfluidic chip following recording and show normal fecundity and viability. Wild-type (N2) worms that were not trapped in the device (top row, 'normal'), or trapped and released (bottom two rows) were followed for development and survival over the course of six days. The worms that had been released from the device were alive, moved in a similar manner and produced the same number of progeny as untreated worms.

In order to increase the throughput of electrophysiological analysis of *C. elegans* with the microfluidic device, eight microfluidic channels can be easily incorporated in parallel, forming a single chip with the ability to record from 8 worms at one time (Figure 3.26). Eight microfluidic channels are connected to one inlet port where one joint recording electrode is placed. Another eight ground electrodes are located in the outlet channels, connected to eight amplifiers respectively. To start an experiment, a large population of worms are firstly loaded into the chip thought the inlet port. After each trap has been occupied by one single nematode, electrophysiological signals are to be recorded by eight amplifiers at the same time.

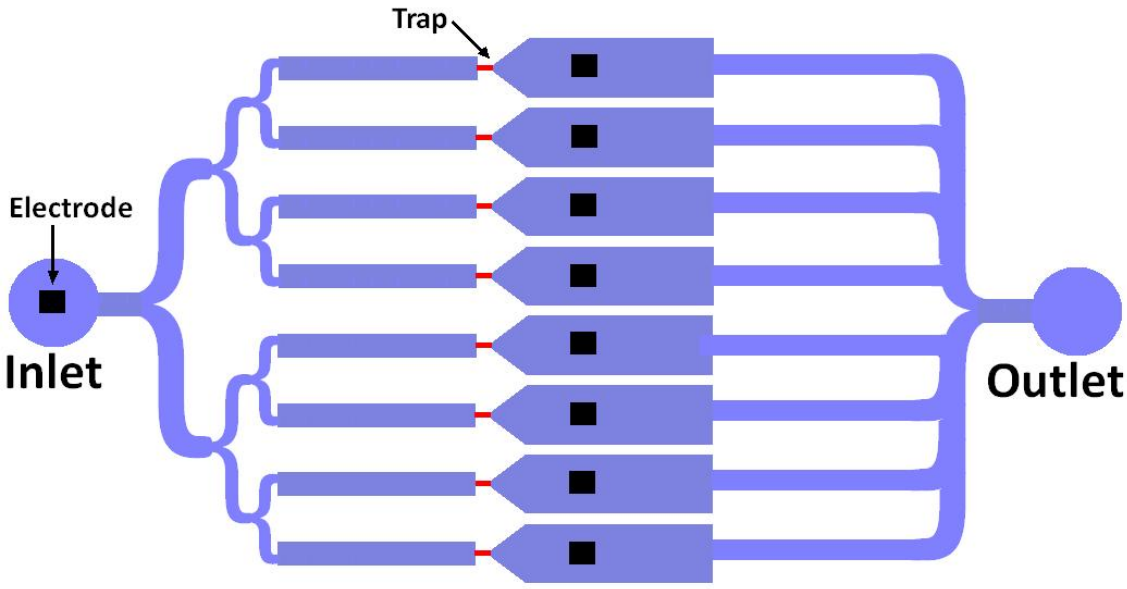

Figure 3.26: Schematic of one possible design to increase the throughput of electrophysiological analysis of *C. elegans* with the microfluidic device. Eight microfluidic channels can be incorporated on a single chip in parallel. Black squares indicate the postions to place the external Ag/AgCl electrode. (Picture is not drawn to scale.)

In summary, a microfluidic device that allows trapping of single worms with precise control and recording of EPG signals has been described in this chapter. This microfluidic channel is able to trap and analyze the electrophysiological response of individual intact worms exposed to different drugs. Compared to conventional EPG experiment, this device provides a better microenvironment for immobilization and transportation of worms and a consistent trapping channel for reproducible applications. The quality of the EPG signals obtained from this device is as good as that collected from a conventional set-up. In addition, released worms remain unharmed and can propagate normally after the electrophysiological analysis with the microfluidic chip.

Chapter 4: Integrated Microfluidic Platform for EPGs - NeuroChip

The overall aim of this thesis is to design an integrated microfluidic platform that can trap worms and capture EPG activity in a system that has the capability to apply drug solutions sequentially in a high-throughput fashion. The microfluidic channel introduced in chapter 3 is only capable of trapping worms and collecting EPG signals with a low probability of success. Some problems were exposed during the assay (Figure 4.1). The first issue is that bits of debris may enter the chip and block the trapping channel. The liquid was filtered with 0.22 μm pore size syringe filter (Sigma-Aldrich, Dorset, UK) and the PDMS channel washed thoroughly to improve the channel environment. However the debris appears from everywhere and is hard to get rid of completely. Secondly the worm has a 58% chance of entering the trapping channel tail first. Third, it seems that *C. elegans* does not like to be trapped. It keeps moving and bending its body in order to escape from the trap. The last problem concerns the whole channel architecture. With only one inlet and one outlet, it is difficult to apply drugs to the worm as well as to unload one worm and reload another worm in a high throughput fashion. Therefore an improved design was developed that attempts to resolve all these problems.

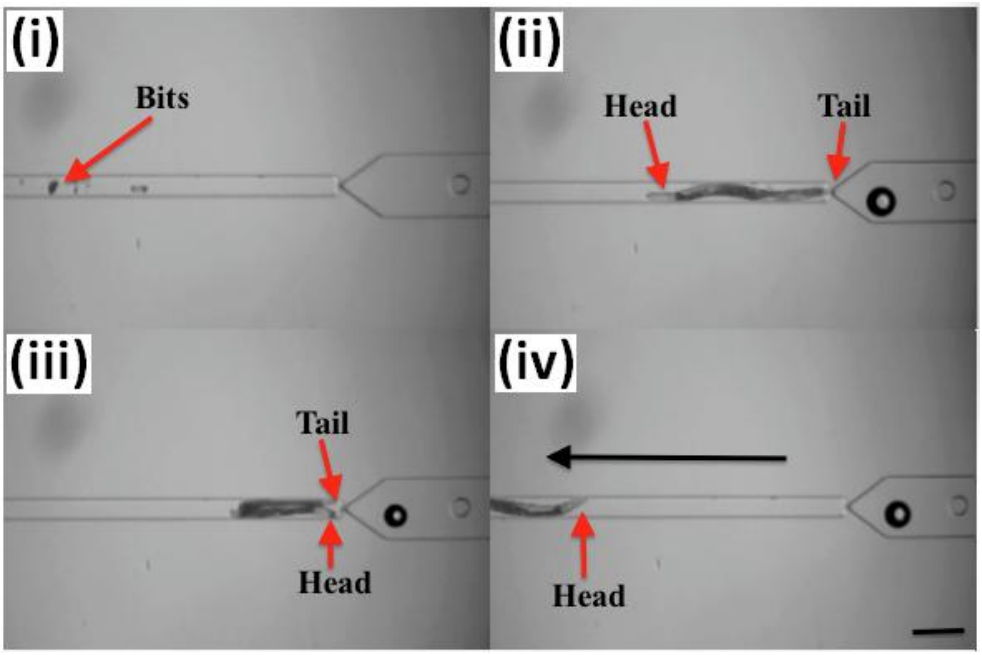

Figure 4.1: Problems encountered in the microfluidic channel. (i) Unexpected bits of material in the inlet channel that block the trap; (ii) Worm enter the trapping channel in the wrong orientation (tail first); (iii) Worms try to escape from the trap by bending; (iv) Worm is being sucked out of the channel through the inlet port. Black arrow indicates the direction of flow. Scale bar: 200 μm.

A good EPG chip requires several desirable properties. First, recording from the worm's head requires correct orientation of the worm in the channel. Secondly reproducible signals from worms of the same genotype, age and in the same experimental conditions require accurate trapping of the worm in the channel so that the seal is made at the same point on the body for each worm. Finally fast and reproducible drug responses of the worms require adequate mechanism for drug delivery. Therefore, improvements need to be made to increase the trapping rate and make it high throughput. Instead of incorporating 8 channels on one single chip, this chapter describes an enhanced microfluidic chip (NeuroChip), which has a trapping channel similar to the shape of a traditional suction tube, a pneumatic valve system for fluid control, and a software based control system.

4.1 Improvement on design of NeuroChip

Four generations have been developed based on the microfluidic channel (Figure 4.2), from which EPG signals have been successfully obtained.

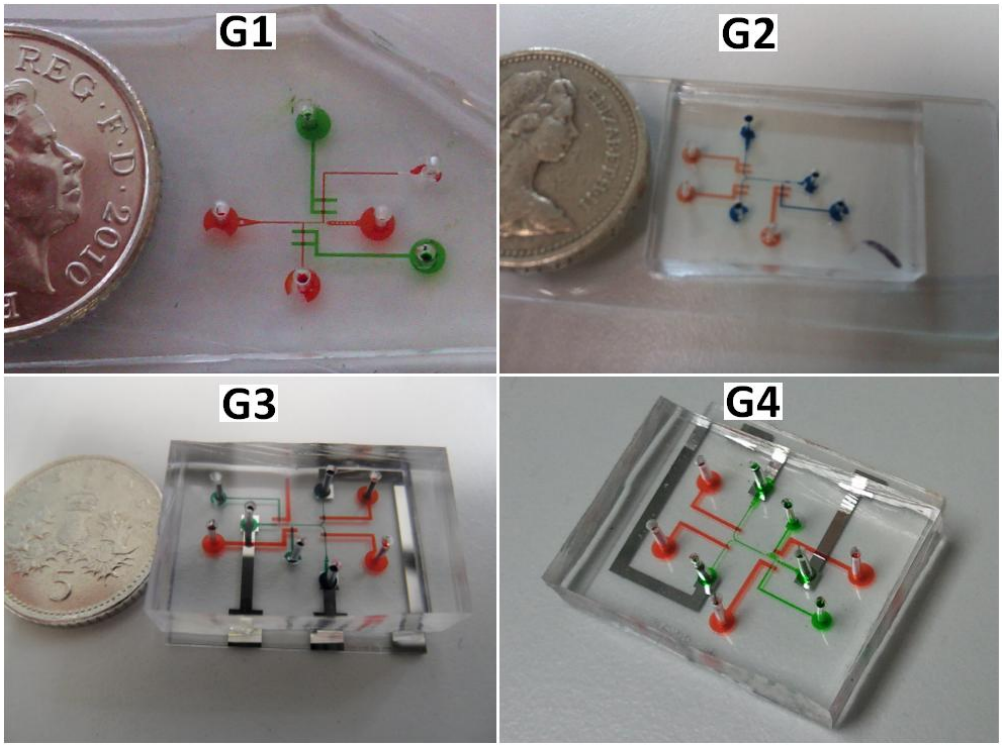

Figure 4.2: Evolution of the improved microfluidic chip. Four generations have been developed. G4 is the NeuroChip.

All four generations were fabricated from two layers of PDMS (Figure 4.2). The first two generations have two additional flow channels for loading and unloading the nematode and drug, while the last two also use integrated electrodes. The fourth generation is the final device - called the NeuroChip.

The NeuroChip was designed to use two layers of PDMS. The top layer is the microfluidic layer, which consists of the trapping channel and several bypass channels (blue in Figure 4.3). The bottom layer contains the microfluidic valve control layer (white in Figure 4.3) with four pneumatic micro-valves [61, 99, 100]. The bypass channels are 50 μm wider than the dimension of young adult (L4+1 day) *C. elegans* and are used to transport worms and drugs. The device is designed so that worms can be loaded into the channel in solution individually (via a pipette tip inserted into the PDMS) or from a reservoir

attached to the chip. Individual worms enter the channel from the inlet marked 'worm port' (Figure 4.3). In initial experiments it was found that the worm enters the channel in a random orientation and was only in the correct orientation (i.e. head first) 42% of the time. It has previously been reported that worms preferentially adopt a head orientation if small pillars are fabricated within such entry channels [26]. These pillars act as obstacles to the worm's movement towards the trap. When a constant hydrostatic pressure is applied to the inlet port, worms escape through this micro-pillar array in the appropriate (head-to-tail) orientation. Thus micro-pillars (50 μm in diameter) were incorporated into the design of the EPG chip (Figure 4.3) and this increased the percentage of worms that entered the channel head first to 71% (of 55 worms tested). The selection of correctly oriented worms was made using valve 3 (Figure 4.3). If a worm enters tail-first, it can be flushed away through the collection outlet by opening this valve.

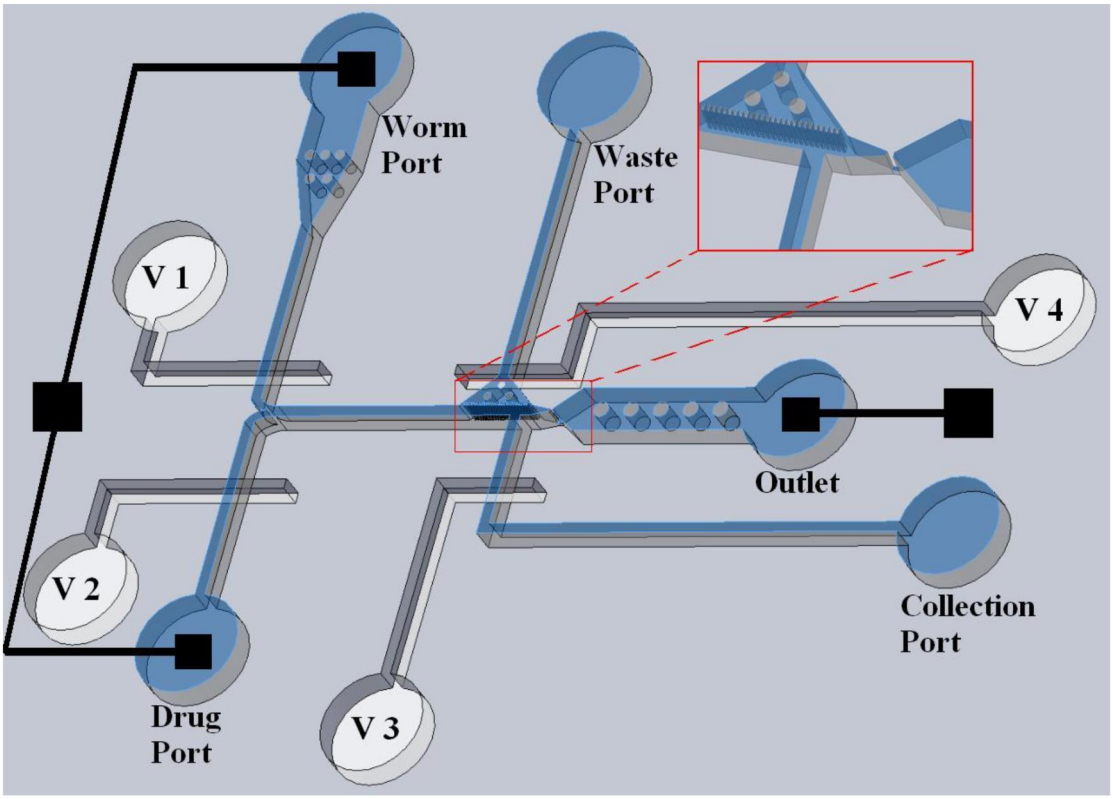

Figure 4.3: Diagram of the NeuroChip. It is a two-layer structure: the blue layer is the microfluidic region that processes worms and delivers drugs. Trapping region is shown in zoomed insert, which also shows the perforated chamber. The micro-pillar region, which is near the

worm port facilitates correct orientation of the worm. The white layer is the pneumatic control layer (V1, V2, V3 and V4 indicate Valve 1, 2, 3 and 4 respectively). The black squares are the electrodes.

The device also allows drugs, compounds or chemicals to be washed on and off the worm while it is trapped in the recording channel. This was achieved by an additional drug port (Figure 4.3), used to deliver drugs to the worm. This was developed in the second generation chip (G2 in Figure 4.2). In order to improve drug delivery to the worm in the trapping channel, the chamber was modified to allow access of the drug along the entire length of the worm's body at once. This was done by adding a wide chamber along one side of the trapping channel as shown in the picture inset in Figure 4.3. This chamber was separated from the main body of the worm by a perforated partition punctuated with a row of 10 μm holes. This improved design is implemented in the third generation (G3 in Figure 4.2), and allows drugs to rapidly access the length of the worm. The device was also designed to incorporate integrated electrodes. Thus it circumvents the need for a separate electrode and allows for direct connection to the recording amplifier.

Four significant improvements (orientation structure, micro-valve system, side perforated wide chamber, and embedded electrode) are implemented in the NeuroChip. These will be discussed further in the following section. The mask design is shown in Appendix 5.

4.1.1 Orientation structure

As previously introduced in chapter 2, most *C. elegans* electrophysiology so far has been done on the pharynx [12]. In the conventional method, the suction tube is controlled by a manipulator which can be moved in three dimensions to trace the head of the nematode (Figure 2.2A). With the microfluidic device, it is not possible to adjust the chip to capture the worm's head, but to play with the swimming direction of the nematode. The challenge is how to direct the nematode towards the trapping channel in a head-to-tail orientation. EPG signals can also be detected from the tail when the worm's tail is trapped in the trapping channel (Figure 4.4A), but the quality of the signal is poor and inferior to that obtained from the head (Figure 4.4B). The possible reason for

that is that the signal could be generated from the movement of the gut, but not from the pharynx.

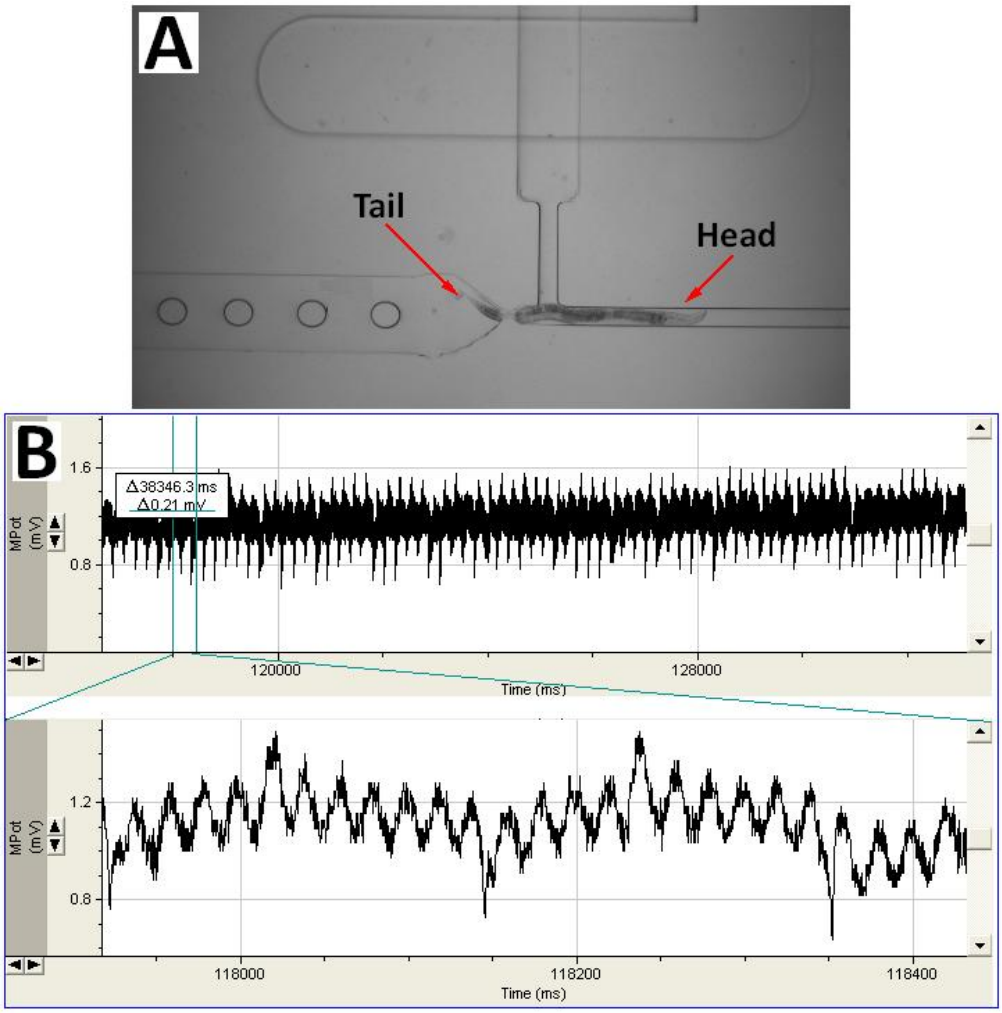

Figure 4.4: Worm is captured by the tail in a microfluidic chip and the EPG signals. (A) A young adult *C. elegans* is trapped on the tail in a microfluidic channel. (B) An EPG trace captured from the tail trapped in the microfluidic chip shown in A. The E and R spikes can be identified from the recording while P spikes are missing. This trace has average amplitude of around 0.4 mV which is slightly higher than the background noise (0.2 mV). P spikes may have been hidden in the noise.

It was recently discovered that electric fields could be used as a stimulus to control the movement of *C. elegans* in a microfluidic environment [32, 73, 101], and its response (termed electrotaxis) is directional. In the presence of

low-voltage direct current electric fields (below 13V cm^{-1}), worms moved towards the negative pole. Razei et al [32] provided evidence that the electric field has no discernible effect on the ability of animals to survive and reproduce. However, its influence on the pharyngeal muscle is still unknown.

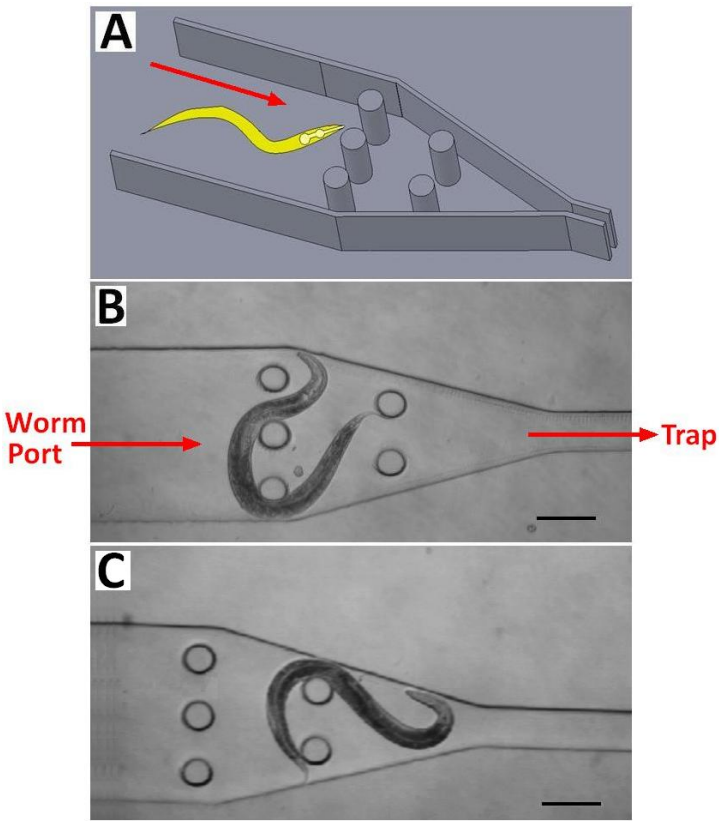

Figure 4.5: Micro-pillars adjacent to the worm port control worm orientation. (A) Schematic of the orientation structure. Five posts in two arrays were added to the right of the worm port, acting as obstacles to the worm's passage towards the trap. In the presence of these posts, the worm is redirected so that it enters the trap with head-to-tail orientation. (B, C) Micrographs of a nematode swimming through the micro-pillars. Red arrows indicate the direction of liquid flow. Scale bar: 100 μm.

Since the effects of electric fields have not been fully identified, a physical method of controlling the worm's orientation [26] was adopted. The structure for the orientation control is quite simple (Figure 4.5). It consists of a chamber with several posts located adjacent to the worm port. These micro-pillars act as obstacles to the worm's passage towards the trap. Chokshi et al [15] showed

that in the presence of constant pressure at the worm port, the worms tend to escape through the micro-pillar array with the appropriate (head-to-tail) orientation.

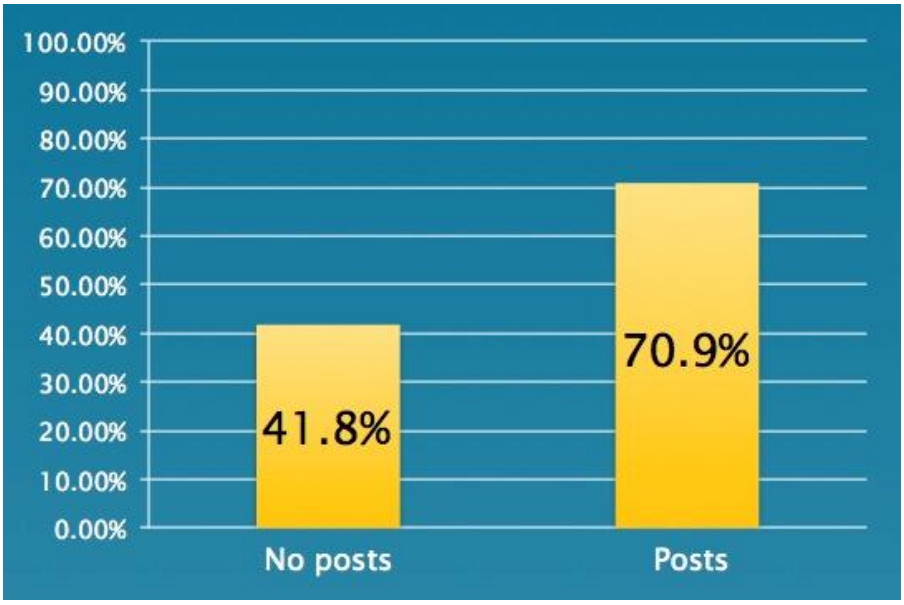

Figure 4.6: Probability of worms entering the trapping channel with head-to-tail orientation in the absence and presence of post structure (n=55).

The performance of the post structure in the microfluidic device was examined by two experiments undertaken on chips with and without the posts. 55 worms were loaded and captured in each chip sequentially. Result shows that with the posts, about 71% (39 in 55) of the nematodes entered the inlet channel with head to tail orientation, compared to around 42% (23 in 55) in the absence of posts (Figure 4.6). Although 100% head-in-first orientation was not achieved, this represents a big improvement. This can be further improved by using the unloading channel that leads to the collection port (Figure 4.3). Any worm that enters the trap in the wrong orientation (tail first) is flushed away directly through the collection port.

4.1.2 Micro-valve system

Several bypass flow channels were added into the microfluidic system to create a microenvironment for more precise and easier manipulation of worms and

drugs. To control the on/off state of these flow channels individually, microfluidic valves were used. Two micro-valve geometries have been demonstrated in previous microfluidic systems [100]. These are Push-down valve and Push-up valve geometries (Figure 4.7). The basic principle of these two kinds of valve is the same that is a deformable thin PDMS membrane closes off a fluid channel. Figure 4.7A illustrates the geometry of a push-down micro-valve, in which the thin membrane separating two channels is pressed down under a positive pressure to seal off the lower channel, which is the flow channel. This geometry has been proven useful in a number of applications and has the advantage that the lower fluid channel can be sealed against any substrate of interest [100]. The geometry of a push-up micro-valve is shown in Figure 4.5B. It is opposite to the push-down valve. In this geometry, the uniform membrane is pressurized upwards to close the upper fluidic channel. The uniform membrane thickness simplifies the dependence of the actuation pressure on the depth of the fluid channel [100].

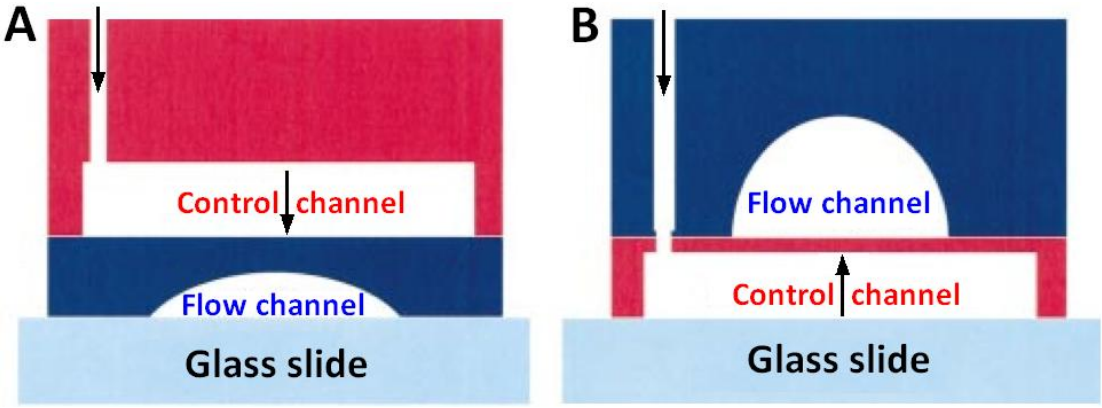

Figure 4.7: Schematic diagram of two micro-valve geometries: push-down and push-up. (A) Schematic of a push-down valve geometry, in which a curved membrane of variable thickness is deflected to seal off a fluidic channel when positive pressure is applied to the control channel. This type of geometry requires a large aspect ratio in the dimensions of the fluid channel. (B) Schematic of a push-up valve geometry, in which a membrane with uniform thickness is deflected to close a fluidic channel when the control channel is pressurized. This geometry allows extra design flexibility because the thickness of the membrane is decoupled from the dimensions of the fluidic channel. Pictures are adopted from [100].

In the NeuroChip, the push-up microfluidic valve was utilized to control the on/off state of the flow channels separately, because the young adult *C. elegans* has a body diameter of ~50 μm, which is beyond the dimension limitation for the flow channel in the push-down valve design. Multilayer soft lithography was used to make the pneumatic control system [61]. Multilayer structures were constructed by bonding layers of elastomer (PDMS), each of which is separately cast from a SU8 mold (Figure 4.8 A, B). Figure 4.8C shows the cross-section of the push-up valve system. The flow and control channel are filled with blue and red colour. When the control channel is pressurised (~30 PSI), the thin PDMS membrane is pushed up and seals off the flow channel. If the pressure is released, the worm and drug can flow through the channel again. By controlling these microfluidic valves separately, worm loading, drug delivery, and worm unloading can be done sequentially.

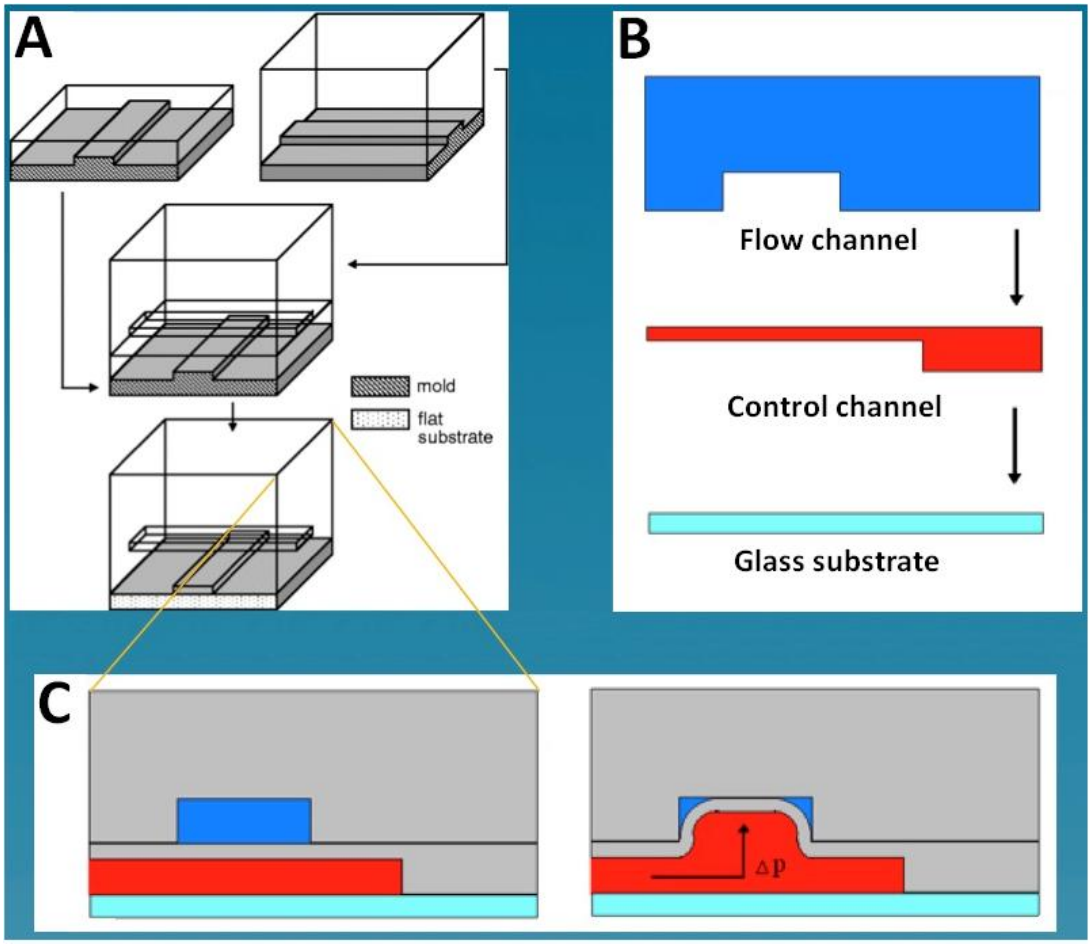

Figure 4.8: Schematic of fabrication procedures for making a multi-layer pneumatic control system. (A) Control and flow layer cast from PDMS (10:1). The flow layer is thick to ensure mechanical stability, and

the control layer is thin, forming an elastic membrane. After baking at 80 ˚C for 1 hour, the flow layer is peeled off and then bonded to the control layer. They are then bonded to the glass substrate with the same process. (B) Cross-section of the system. (C) Cross-section of a bonded chip with push-up valve geometry. Left cartoon shows a chip with blue flow channel and red control channel. Right illustrates the working principle of the push-up valve system. A positive pressure of ~ 30 PSI is applied to pressurize the thin PDMS membrane to seal the flow channel. Picture A is adopted from [61].

Studer et al [100] mapped the actuation pressure of the push-up valve structure as a function of the three parameters that characterize the membrane: width, length, and thickness. Larger dimensions and thinner membranes require smaller actuation pressure (Figure 4.9). When the width of the actuation channel becomes wider than an optimum value (~ 550 μm), the actuation pressure stays steady (~ 2 PSI).

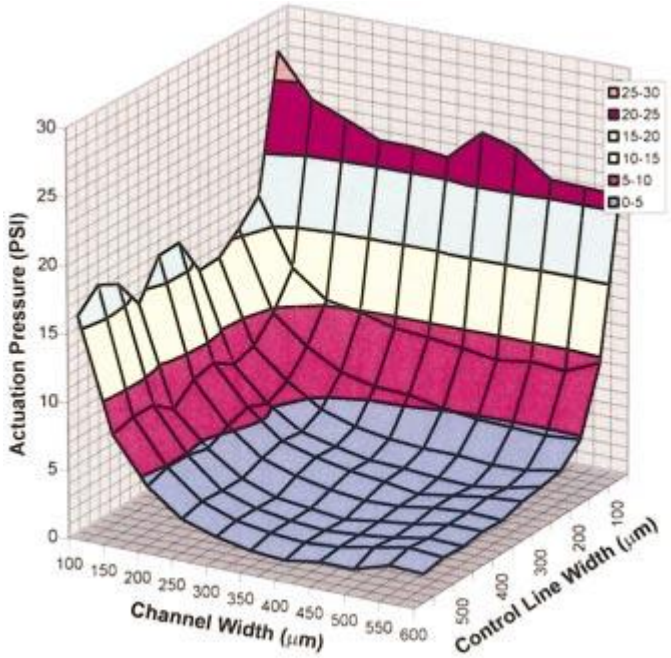

Figure 4.9: Actuation pressure is symmetric with width of both flow and control channels. Picture is copied from [100].

The flow channel in the device has small dimensions (100 μm wide), and is designed to restrain the movement of *C. elegans.* From figure 4.9, it is clear that a 100 μm wide channel requires a high actuation pressure to drive the valve, regardless of how wide the control channel is. To optimize the sealing performance but not increase the width of the whole flow channel, only the dimension of cross over area was increased (Figure 4.10A). The stationary and incompressible flow can be characterized by a single dimentionless number: the Reynolds number (Re) [102]. It is a value that measures the ratio of inertial forces to viscous forces and describes the degree of laminar or turbulent flow [103]. The Reynolds number can be expressed as:

$$Re = \frac{Ul}{v}$$

where U is the characteristic velocity of the fluidic, l is the scale and v is its kinematic viscosity. U is proportional to the scale, thus the Reynolds number (Re) is proportional to the square of the scale (l^2) [102]. This is the reason of low Reynolds number (generally below 0.1) observed in microfluidic systems. If the number is less than about 2000 then flow is defined as laminar, if greater than 4000 then turbulent and in between these then in the transition zone. The Reynolds number in my system is far less than 2000 so that only laminar flow is generated. According to simulation performed in Comsol (Comsol Multiphysics 4.0a), since the Reynolds number is very small, this is not a situation of boundary-layer separation, only a few vortices appeared in the cavity but the streamline of the flow is barely affected by the increased cross-over area (Figure 4.10B). Consequently the flow of the worm along the channel will not be affected by this geometry.

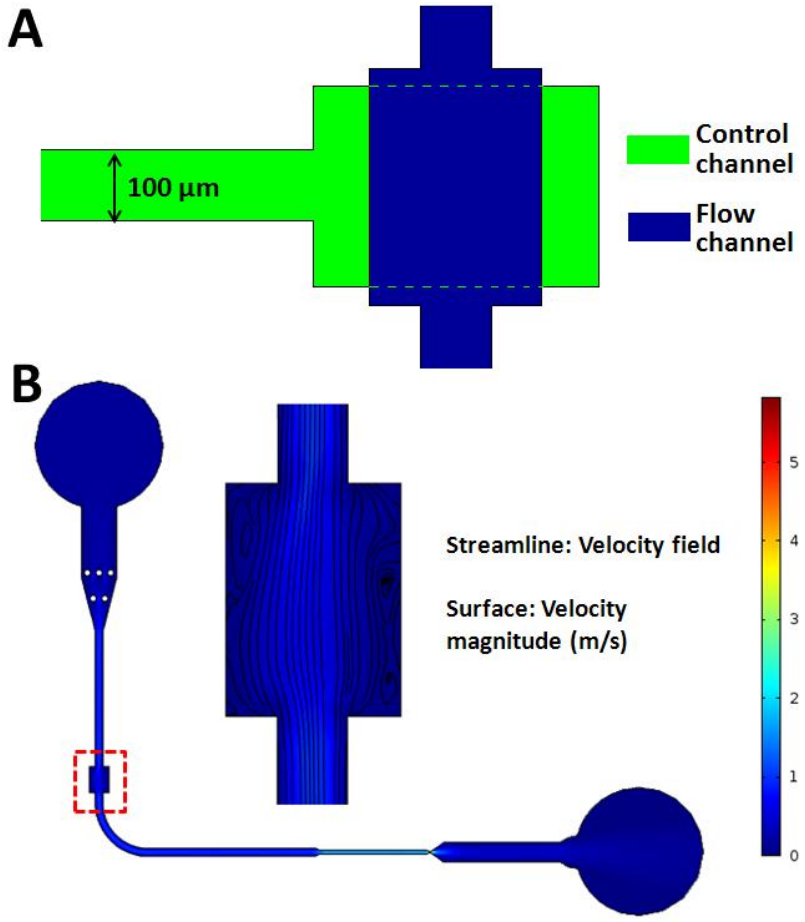

Figure 4.10: Cross-over area is enlarged to optimize the performance of the push-up microfluidic valve. (A) Schematic of the cross over area. Flow channel is on the top (in blue) and control channel is underneath (in green). The side of the cross-over area is lengthened from 100 µm to 250 µm to increase the contact area with the control channel, and therefore to improve the seal. (B) Comsol simulation of the active flow channel. Inset is the enlarged cross-over area which is marked with red square. A pressure of 0.3 Bar was set on the inlet. Since the Reynolds number is small, this is not a situation of boundary-layer separation [102]. The main flow direction did not affected much but only a few vortices appeared in the cavity.

4.1.3 Side perforated chamber

In the first three generations, only straight channels were added to direct the flow of drugs (Figure 4.11A). If the worm is captured in the trapping channel, it

blocks the flow of the solution or drug. This was solved by adding a wide chamber along one side of the trapping channel as shown in Figure 4.11B. This chamber was separated from the main body of the worm by a perforated partition punctuated with a row of 10 µm holes, which allows the drug to interact with the entire worm; it also keeps the nematode in position.

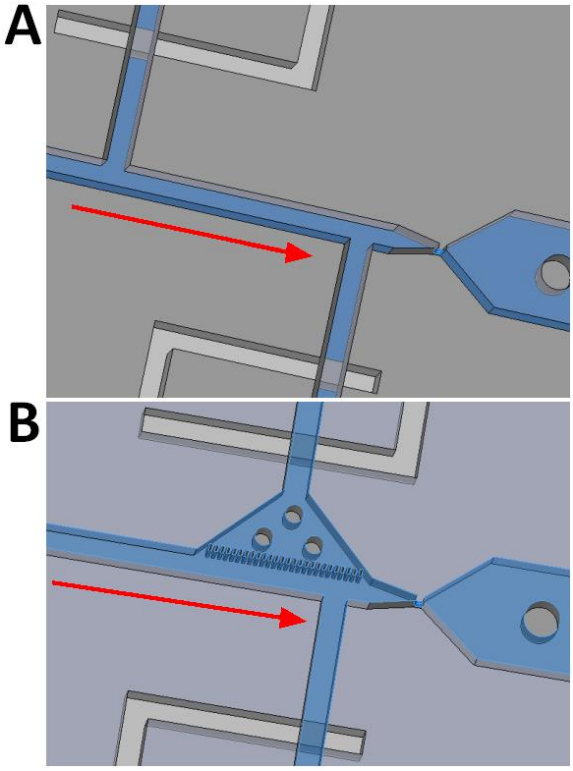

Figure 4.11: Schematic showing the straight channel with a side perforated wide chamber (Flow channel in blue and control in white). (A) Straight flow channel on the left top is used to flow drugs directly to the tail of the trapped worm in a short time. (B) Perforated wide chamber is placed by the side of the trapping channel to provide a improved drug perfusion. Red arrow indicates the direction of the flow.

A Comsol simulation was done to examine the performance of the perforated wide chamber as shown in Figure 4.12. A positive pressure of 0.3 mBar was set on the inlet port in both designs. In the design with a straight channel (Figure 4.12A), liquid flows faster in the bypass flow channel on the left top than the straight main flow channel, which is usually blocked by the worm's body. The perforated wide chamber (Figure 4.12B) has better performance. The velocities

are high on both side of the flow channel even when it is fully blocked by the nematode. 10 μm holes along the side of the main flow channel provide accesses for the drug to surround the entire worm and also keep the nematode in position. Two transport phenomena may occur here: advection and diffusion. Advection [103] is a transport mechanism of a substance or conserved property by a fluid due to the fluid's bulk motion. Drugs were delivered by the laminar flow in the microfluidic system. Unlike advection, diffusion is a physical phenomenon of mixing or mass transport without requiring bulk motion. *Fick's law* [104] governs the diffusion of the solutes, dilute mixtures or solutions. When the trapping channel is occupied by the worm, there is no bulk motion in the 10 μm side holes. However, according to *Fick's law* that the flux goes from regions of high concentration to regions of low concentration, therefore the drug can still get access to the worm through diffusion with a magnitude that is proportional to the concentration gradient.

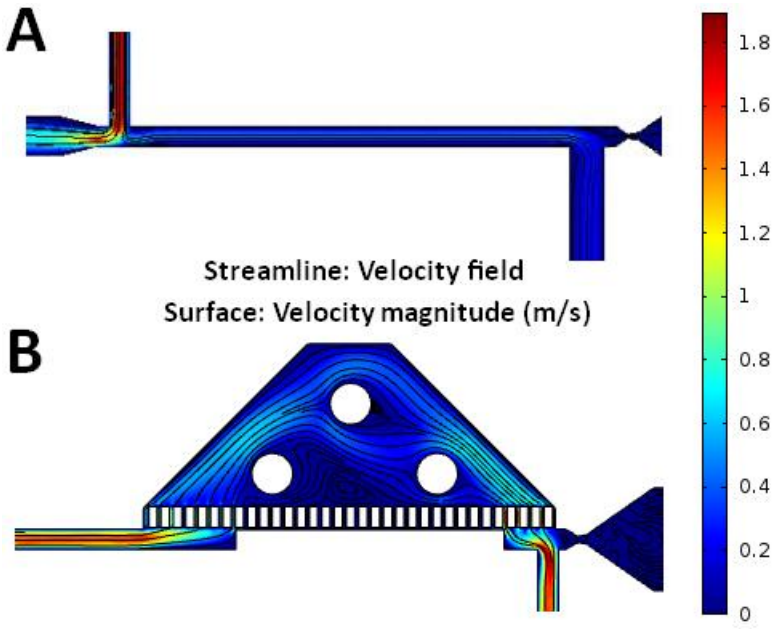

Figure 4.12: Flow velocity simulations for the straight channel and a side perforated wide chamber (0.3 mBar positive pressure is applied on the inlet port in both designs). (A) Simulation of the straight channel design. The flow velocity is much higher in the bypass flow channel on the top left than the straight channel. (B) Simulation of the design of a side perforated wide chamber. The perforated wide chamber is placed by the side of the trapping channel to provide

improved drug perfusion. The velocities are high on both sides of the flow channel even when it is fully blocked by the nematode.

Dye experiments were done using both designs (Figure 4.13). These showed that the drug goes over the nematode quicker with a side perforated wide chamber than just a straight bypass channel. In the experiment, a coloured food dye was flowed from the drug port. Figure 4.13 shows screenshots of both designs with a trapped *C. elegans* 30 seconds after flowing in the dye. In the first design, the dye has just approached the tail of the trapped worm (Figure 4.13A), while it has surrounded the intact nematode in the second design (Figure 4.13B). It normally takes 2 minutes to achieve the same result with the straight bypass channel design.

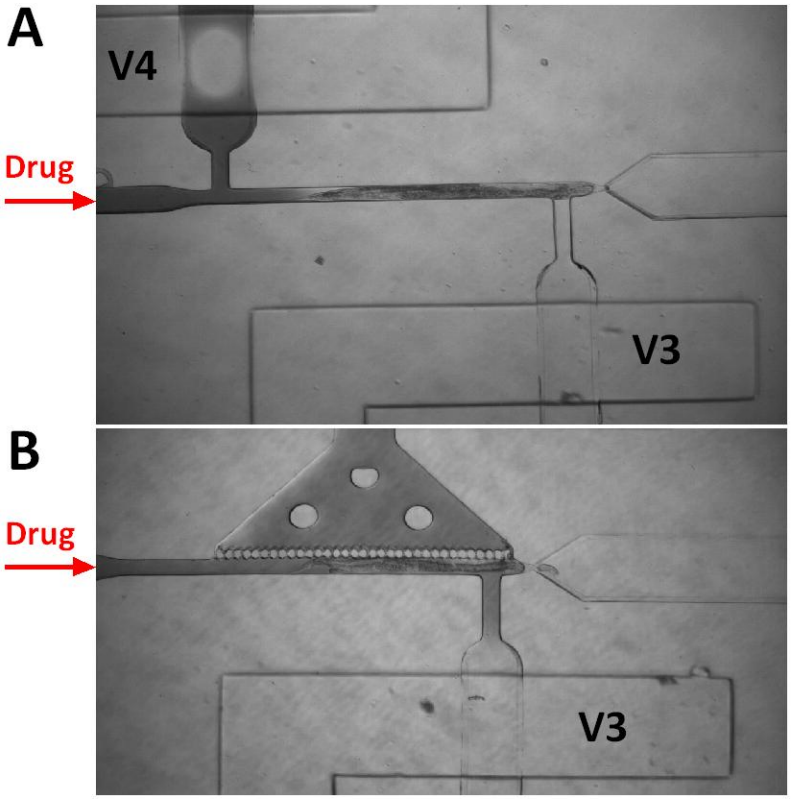

Figure 4.13: Food dye in both designs (with trapped nematodes) showing that the side perforated wide chamber provides a better access for drugs. Images were taken 30 seconds after injecting dye from the drug port. (A) Design with a bypass channel on the left top, dye has just approached the tail of the trapped worm. (B) The

nematode is surrounded by the food dye in the design with a perforated wide chamber.

4.1.4 Integrated electrode

The device was designed to incorporate integrated electrodes, which circumvents the need for a separate externalelectrode and allows for direct connection to the recording amplifier.

In conventional EPG experiments, a silver/silver chloride (Ag/AgCl) electrode is used. As a reliable, non-polarizable electrode, Ag/AgCl electrode is almost exclusively used for recording DC (Direct current) and low-frequency potentials [105]. However, in terms of embedded electrodes, Ag/AgCl electrodes are not easy to either fabricate or maintain. Instead, by sacrificing the signal strength, polarizable platinum electrodes were used. I/V characteristics of polarizable and non-polarizable electrodes are shown in Figure 4.14 A, B. In the case of a polarizable electrode, the I/V characteristic is not exactly horizontal because a small current can traverse the electrode surface due to Faradaic reactions at higher voltage [105]. Thus, a polarizable electrode can be represented as a parallel combination of a double-layer capacitance C_{dl} (Figure 4.15) and a relatively high charge transfer resistance R_{ct} (Figure 4.14 C). A non- polarizable electrode conducts current but without a fixed electrode potential [105]. Its equivalent circuit consists of a voltage source (the electrode potential) in series with a relatively low resistance R_{ct} (Figure 4.14 D). This type of electrode is therefore preferred for DC measurements.

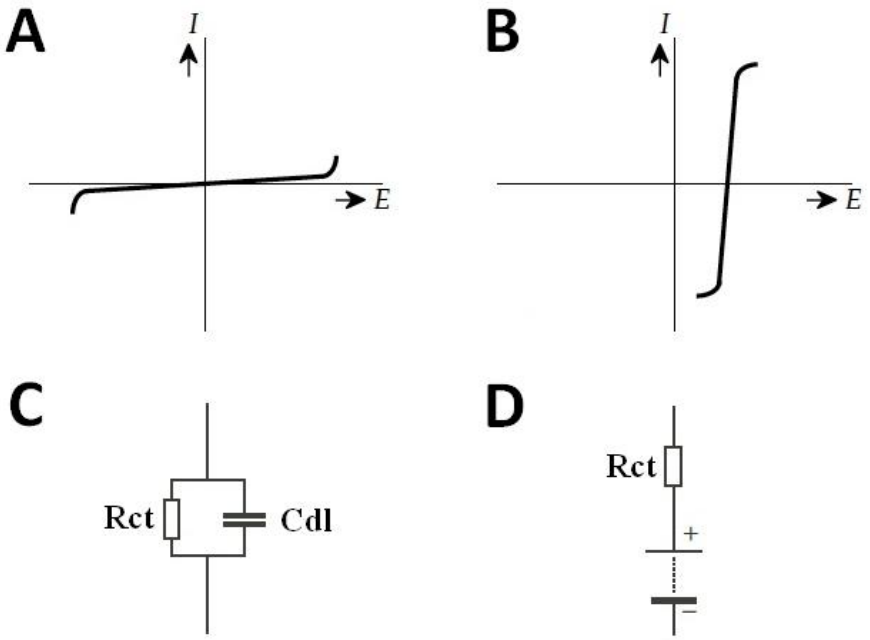

Figure 4.14: I/V characteristic of a polarized and non-polarized electrode and the correlated equivalent circuit. (A) I/V characteristic of a polarized electrode. (B) I/V characteristic of a non-polarized electrode. (C) Equivalent circuit of the polarized electrode. (D) Equivalent circuit of the non-polarized electrode. Pictures are taken from [105].

As introduced in chapter 2, current flow across the seal between the suction tube and the cuticle of the worm produces a voltage drop, which is recorded as the EPG signal. If a platinum electrode is used, the double-layer capacitance C_{dl} (Figure 4.14C; Figure 4.15) prevents a DC current from flowing between the electrodes. In order to increase the signal strength of the EPG recording, the current need to be enhanced. As illustrated in Figure 4.14C, the equivalent circuit of the polarized electrode consists of one resistor and one double-layer capacitor in parallel. The impedance of the polarized electrode Z_P is proportional to the resistance R_{ct} and impedance of the double-layer Z_{Cdl} (Equation 4.1). Reducing either of them leads to an increase in current. As the resistance R_{ct} is constant, Z_P can be reduced by decreasing Z_{Cdl} which is inversely proportional to the double-layer capacitance C_{dl} (Equation 4.2). Capacitance is proportional to the area of overlap and inversely proportional to the separation between conducting sheets (Equation 4.3). Consequently, the

signal strength of the EPG recording can be enhanced by increasing the surface area of the electrode.

$$\frac{1}{Z_P} = \frac{1}{R_{ct}} + \frac{1}{Z_{Cdl}} \tag{4.1}$$

where Z_P is the impedance of the polarized electrode (Figure 4.14C), R_{ct} is the resistance of the electrode, and Z_{Cdl} is the impedance of the double layer.

$$Z_C = \frac{1}{j\omega C} \tag{4.2}$$

$$C = \varepsilon_r \varepsilon_0 \frac{A}{d} \tag{4.3}$$

where C is the capacitance, ε_r is the dielectric constant of the material between the plates, ε_0 is the electric constant, A is the area of overlap of the two plates, d is the separation between the plates, Z_c is the impedance of capacitor, j is the imaginary unit, and ω is the voltage frequency.

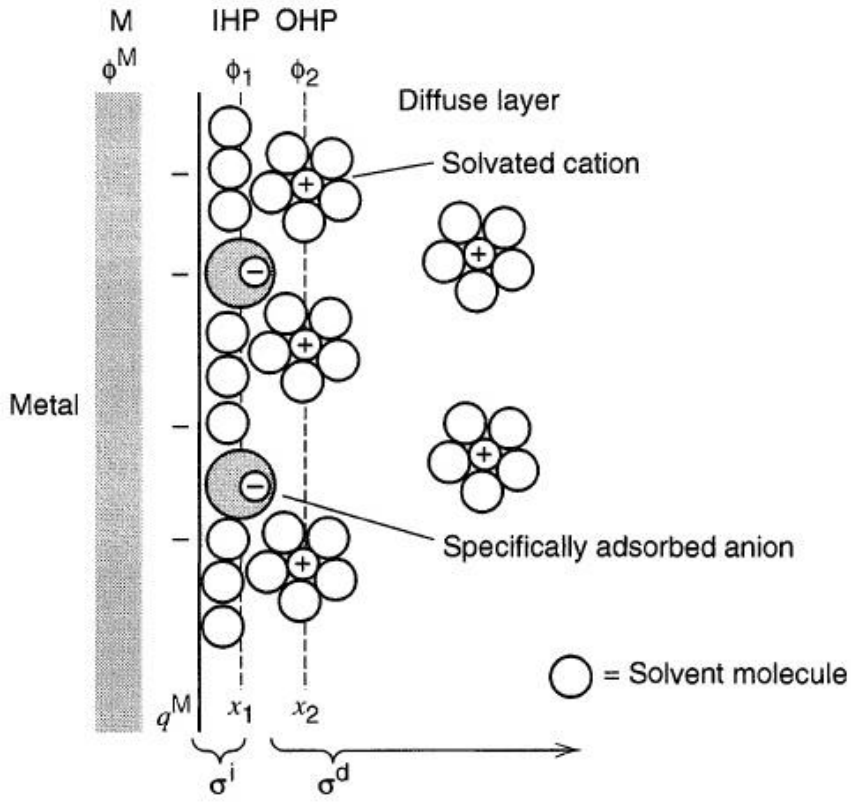

Figure 4.15: Model of an electrical double-layer. The electrode-solution interface is characterized by a double-layer capacitance, C_{dl}, typically in the range of 10 to 40 μF/cm^2 [106]. IHP (Inner Helmholtz plane) indicates the inner layer and OHP (Outer Helmholtz plane) the outer layer. Picture is adopted from [106].

In the NeuroChip, the platinum electrode pads had a size of 1.5mm×1.5mm and are placed underneath the worm, drug and outlet ports (Figure 4.2; Figure 4.3). The worm and drug ports never operate at the same time, thus the two electrode pads underneath them are connected together to the ground. The outlet electrode is connected to the recording amplifier.

4.2 Device fabrication

Devices were fabricated using standard lithography using a two-step process as introduced in last chapter. Acetate masks (Micro Lithography Services Ltd, Essex, UK) were used to define large scale features. As shown in Figure 4.16A, masters for casting PDMS were made from SU8. To make the device a thin layer of SU8-5 was spin-coated on a wafer to make the trapping channel (10 μm thick). Positive resist (AZ40XT, MicroChemicals GmbH, Germany) was used to form the flow channel, which is 60 μm high. After exposure of the resist, the flow layer master was baked at 130°C for 30 seconds to reflow the resist to form semi-cylindrical flow channels. SU8-50 was spin-coated on another wafer to provide the pneumatic control layer of 80 μm thick (Figure 4.16B). Images of the masters for the flow layer and control layer are shown in Appendix 6.

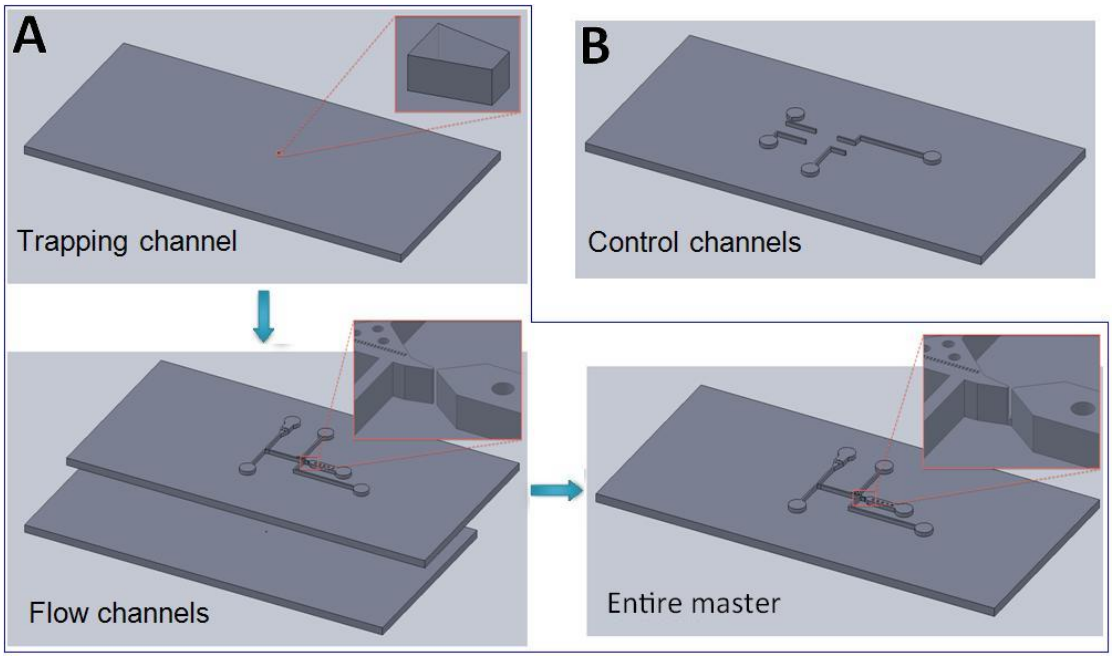

Figure 4.16: Procedures for fabricating masters for casting PDMS channels. (A) Procedure for producing the flow layer. A thin layer of SU8-5 was spin-coated on a silicon wafer to make the trapping channel. Positive resist AZ40XT was then used to build the flow channels. The wafer was at last baked at 130°C for 30 seconds to reflow the resist to form semi-cylindrical flow channels. (B) SU8-50 was spin-coated on another wafer to provide the pneumatic control layer.

Before moulding, the PDMS surfaces were treated with trichloro (1H, 1H, 2H, 2H-perfluorooctyl) silane 97% vapour (Sigma-Aldrich). The procedure for bonding the PDMS channels to the final NeuroChip is shown in Figure 4.17. The channel was made from PDMS (10 part A: 1 part B) with an overall thickness of ~ 5 mm. The control layer was created by spin-coating PDMS onto the control layer master at 900 rpm for 30 seconds, yielding a thickness of 100 µm. After degassing for 30 minutes and curing at 100°C for 1 hour, the PDMS replicas were peeled off the masters. Holes for different ports were punched and cleaned before bonding. After treatment with oxygen plasma (50W, 30s), the PDMS flow layer was bonded onto control layer using hand alignment. The same process was used to bond this onto a glass cover slide, which acted as the base. Finally, sections of polythene tubing were attached to the chip ports. Four solenoid valves (Clippard minimatic, 3-way normally-closed

valve) were used to for external valve control. The inlet is connected to an air compressor and the outlet connected to the NeuroChip. When an excitation voltage of 6 volts is applied to the solenoid valve, the solenoid pulls the valve into the open state and the compressed air pressurizes the micro valve on chip. An I/O board (Phidgets USB Interface 0/16/16) is connected between the power supply and solenoid valves, playing the role of physical switches, to control the on/off states of the valves automatically. The micro-valves in the bottom layer are driven by software and provide a semi-automatic means of loading a single worm, recording an EPG signal, drug delivery and worm unloading.

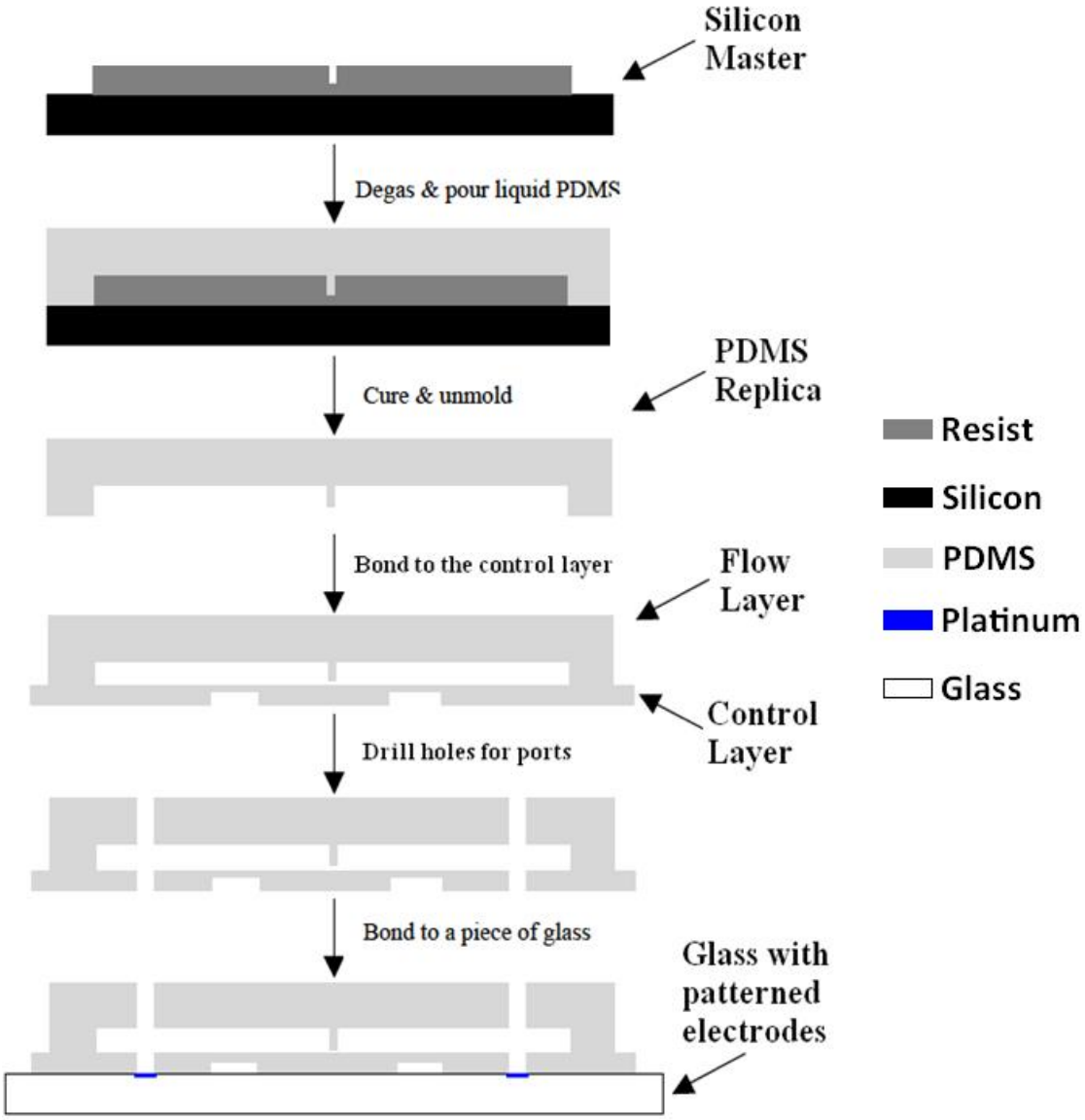

Figure 4.17: The procedure for combining the PDMS channels to the NeuroChip: (i) Silanize the surface of SU-8 master with trichloro silane.

(ii) Degas the liquid PDMS and pour over the flow layer master. Degas again and cast overnight at 50 ˚C. (iii) Peel off the PDMS replica from the master after curing. (iv) Spin-coat the PDMS mixture onto the control layer master at 900 rpm for 30 seconds, yielding a thickness of 100 μm. (v) Bond the flow layer replica onto the control layer using oxygen plasma (50w, 30s). (vi) Peel off from the control layer master. (vii) Drill holes in the replica for ports and wash thoroughly. (viii) Bond onto a piece of glass with patterned platinum electrodes, and bake at 100 ˚C overnight. Valve channels are placed vertically to the direction of the flow channels to form a crossed working region.

Three platinum electrodes were fabricated on the glass substrate, at the entrance of the three fluid ports (Figure 4.3). Three steps were used to make the electrode. First a glass slide was coated with platinum by evaporation to give a thickness of around 300 nm. The platinum wafer was then patterned using standard photolithography. The last step is to etch out the required structure by ion beam milling. Holes were drilled through the two PDMS layers to expose the electrodes to the solution. These integrated electrodes simplify worm handling and markedly improve the signal to noise ratio (SNR). The EPG signals recorded from this chip have a SNR larger than 8, providing a capability for fine resolution of features in the EPG waveform. All electrodes are connected to a conventional high-input impedance amplifier. The electrodes under the worm port and drug port are connected together to the recording electrode, whilst the electrode in the outlet port is grounded. The NeuroChip is placed in a Faraday cage.

4.2.1 Method for improving the valves' performance

As introduced previously, the width of the flow channel is a key parameter in the design of microfluidic valves. The shape of the channel also plays a very important role in the performance of the valve. In the first three generations, the negative photoresist SU-8 was used to make the master for moulding the flow layer. SU-8 products are very resistant to solvents, acids and bases and have excellent thermal and mechanical stability, making them an ideal material

for master fabrication. Because of these unique properties, the PDMS channels made from SU-8 master have sharp edges (Figure 4.18).

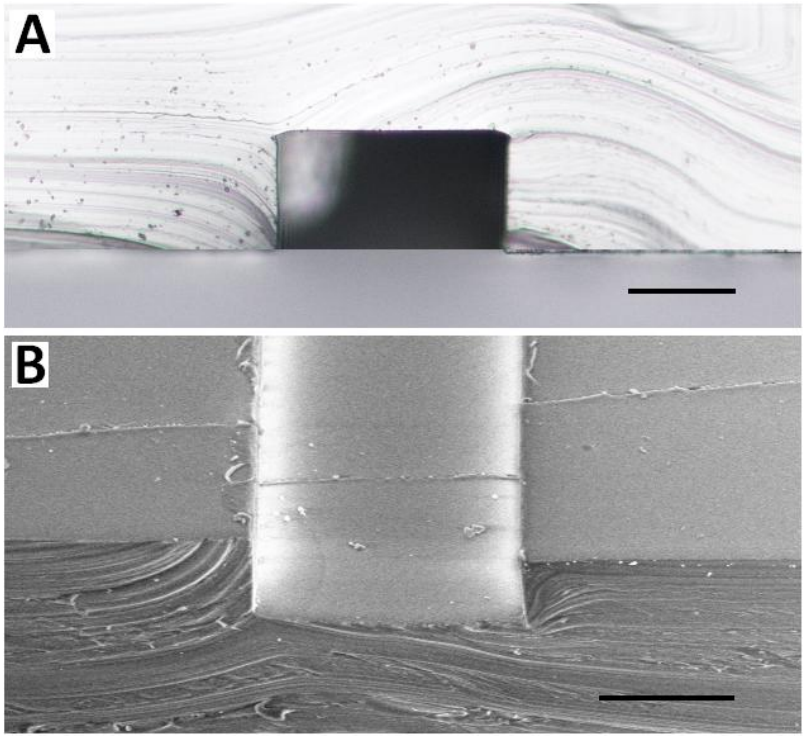

Figure 4.18: The flow channel with a square shape. (A) Micrograph of the cross-section of a PDMS flow channel. (B) Bottom view of a section of PDMS flow channel under Scanning Electron Microscope (SEM). Scale bar: 100 μm.

Nevertheless, regular and square are not ideal for valve seats. They lead to leakage since membranes do not seal to the square flow channel properly when the control channel is actuated (Figure 4.19A). Even if a high positive pressure (~ 30 PSI) is applied, the liquid can still flow along the edges of the channel (Figure 4.19B). In Figure 4.19B, red dye is introduced into the flow layer with green in the control layer. Once the control channel is actuated, the crossover regions turns colour from entirely red to green in the centre, indicating red dye is still flowing along the edges through the valves.

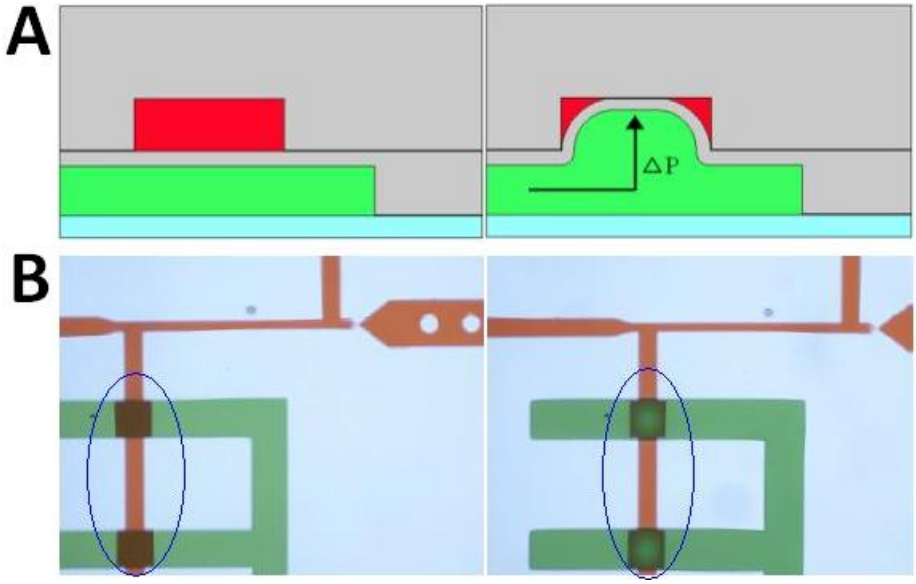

Figure 4.19: Flow channel with a square shape. (A) Two cartoons show the cross-section of the valve system with square flow channel. (B) Two micrographs taken from the top of the chip. Left column illustrates how it looks when the micro valve is switched off and right is the view when the valve is actuated. The flow channel is filled with red food dye and the control channel with green. The crossover area is completely red when the valve is off. Once the valve is pressurized, the colour in the middle area turns green while the edges are still red. Red dye can flow through past the bypass channel even when the valve is on due to the square profile. Blue circles indicate the crossover regions.

Young adult *C. elegans* and dust are blocked by this microfluidic valve (Figure 4.20), but the seal is not tight enough for control of fluid, such as drug application.

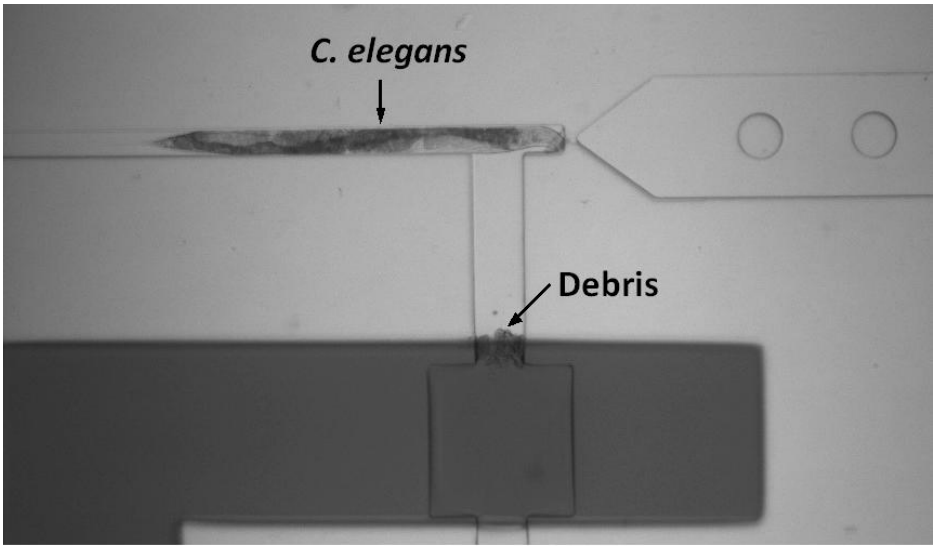

Figure 4.20: A young adult *C. elegans* in the square flow channel. Neither the nematode nor the debris passes through the bypass channel, but the fluidic flow does. The valve does not completely seal.

A complete seal with a square flow channel can only achieved when the flow channel is thin (such as 20 μm). In this device, the flow channel has a height of 60 μm, making it difficult to achieve good sealing. In order to remove the leakage from the edges of the crossover area, a round flow channel is required.

The negative photoresist SU-8 is very stable after exposed to the UV light making it impossible to change the shape of a SU-8 feature/channel by reflow or etching. While most negative photoresists cross-link, all common positive photoresists do not cross-link. Common positive photoresists are based on a mixture of diazonaphthoquinone (DNQ) sensitizer, novolak resin (a phenol formaldehyde resin) and organic solvent. DNQ inhibits the dissolution of the novolak resin, but upon exposure to light, the dissolution rate increases even beyond that of pure novolak [107].

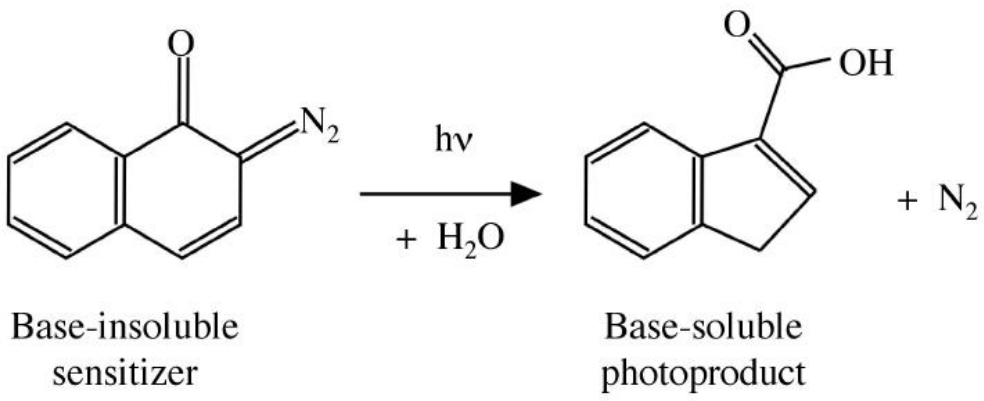

Figure 4.21: Reaction of sensitizer when a positive photoresist is exposed by the UV light. Picture is adopted form [91].

As shown in Figure 4.21, upon absorption of a photon, the DNQ decomposes and produces gaseous nitrogen as a by-product. In the presence of water, the decomposition product forms an indene carboxylic acid, which is base-soluble. However, the formation of acid may not be the reason for increased solubility; the release of nitrogen gas produces a porous structure through which the developer may readily diffuse, resulting in increased solubility [91].

After the photoresist has been developed, it starts to soften at approximately 100 -130˚C [108]. This process is called reflow or roundening. Therefore, the negative photoresist (SU-8) was replaced with a positive one (AZ40XT). The fabrication procedure is the same as making a SU-8 master. The only difference is the exposed area on the positive resist is washed off after developing, while this remains when using a negative resist. The change in shape during reflow (Figure 4.22) can be found in the photoresist datasheet [108]; the exact baking temperature and time are different for different designs.

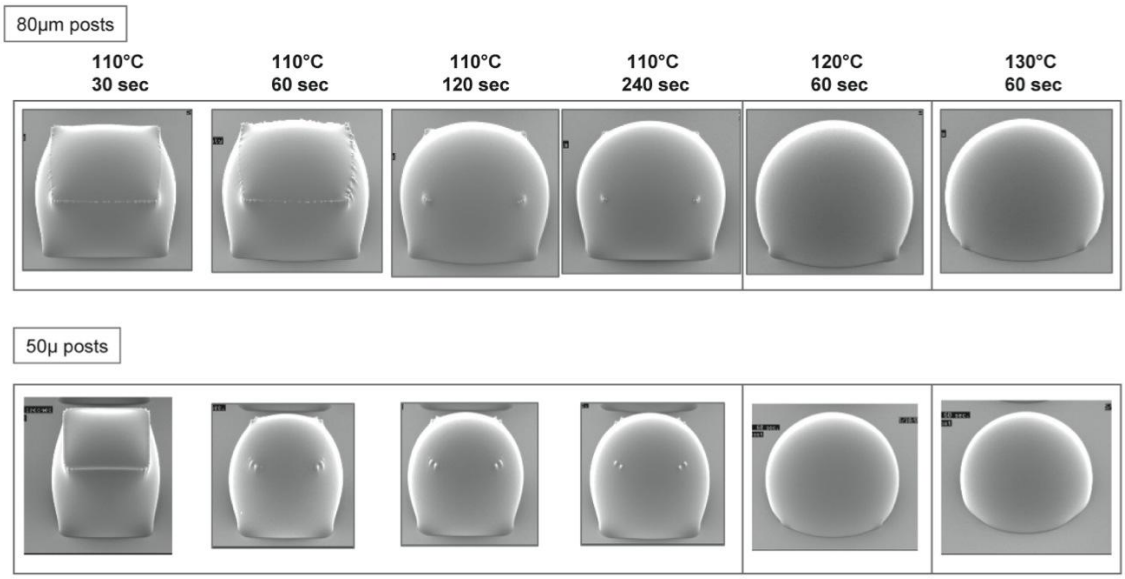

Figure 4.22: Shape change during reflow of resist at different baking temperature and for different times. Images are of 50-µm thick positive photoresist AZ40XT posts. First image is of posts with width of 80 µm while second is 50 µm. Picture is adopted from [108].

After several attempts (Figure 4.23), it was found that 130 ˚C and 30 seconds are the best combination of reflow temperature and time. Figure 4.24 shows the change of the trapping channel region made of positive photoresist AZ40XT before and after the reflow. Obviously, after reflow, the edges of the channel melt, forming a geometry with higher (brighter) centre and lower (darker) edges (Figure 4.24B).

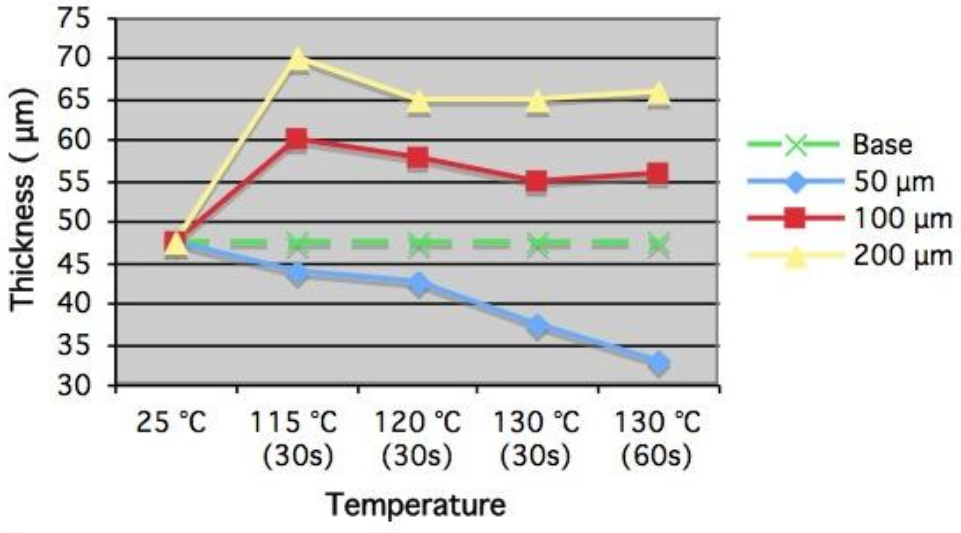

Figure 4.23: Attempts were made to find the best baking temperature and time for different width channels. The AZ40XT master has a thickness of about 47.5 μm at the beginning. With different widths, the shape change is different depending on the baking temperature and time. The depth of a 50 μm wide channel decreases with increasing temperature. For 100 μm and 200 μm width, the depth increases at 115 ˚C for 30 seconds, but keeps dropping when the temperature is increased to 130 ˚C for one minute. In terms of micro valves performance, the depth of the flow channel should be as small as possible for the best seal. But there should be enough space for young adult worms to pass through. The optimum temperature is 130 ˚C and 30 seconds.

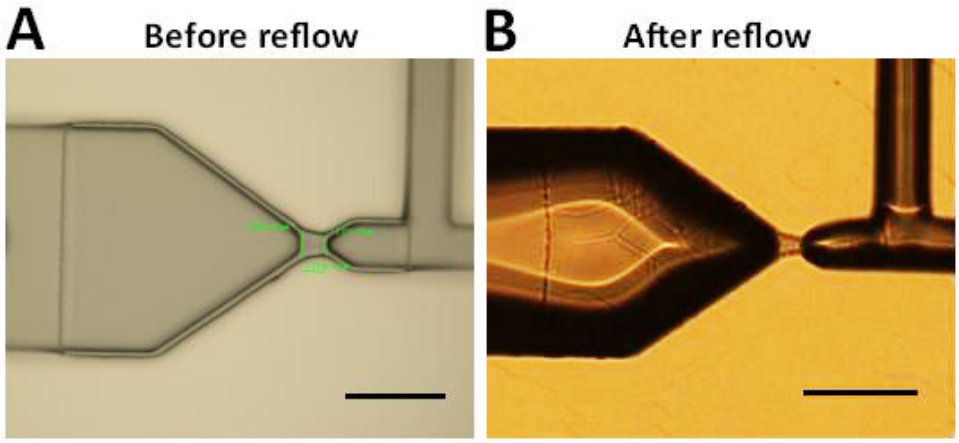

Figure 4.24: Comparison of the trapping channel before and after reflow at 130 ˚C for 30 seconds. 50-μm thick positive photoresist AZ40XT was used. (A) Micrograph of the trapping channel region made from AZ40XT before reflow. (B) Micrograph of the trapping channel region after reflow. Bright area is higher than the dark area. Scale bar: 100 μm.

To examine the reflow result with the positive photoresist AZ40XT, the PDMS channel moulded from reflowed AZ40XT master (130 ˚C and 30 seconds) was cut in the middle. The bottom view and cross-section of the channel was

imaged with microscope. The reflow result is excellent since very regular semi-circular shape channels were observed (Figure 4.25).

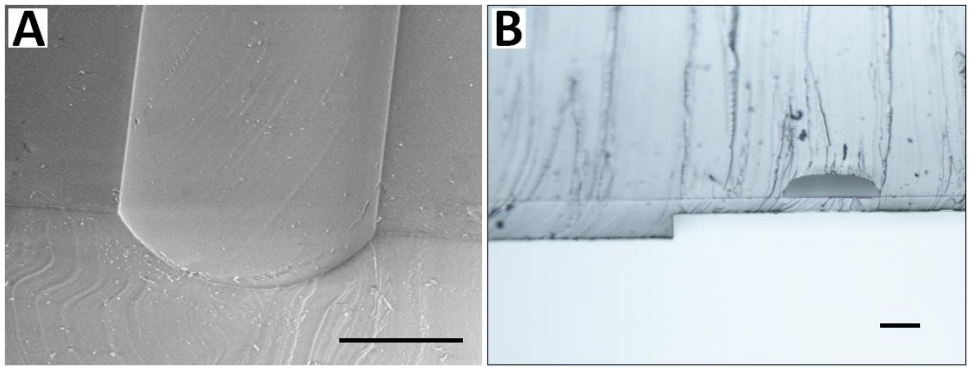

Figure 4.25: Images of flow channel with semi-circular shape moulded from a reflowed AZ40XT master. (A) SEM image taken from the bottom of a PDMS flow channel. Near-regular semi-circular shape is observed. (B) Micrograph of the cross-section of a microfluidic valve with a round flow channel. Scale bar: 100 μm.

As expected, the sealing performance of these microfluidic valves was improved when using a flow channel with semi-circular shape (Figure 4.26). There is no leakage when the valve is pressurized, even if the flow channel has a small amount of positive pressure. With such good sealing, the manipulation of worms in the flow channel is easier and more precise. Further applications, such as drug application and worm sorting, can be undertaken in this device in a high-throughput fashion. With the pneumatic valve system, worms with the correct orientation can be kept (head-to-tail), whilst others are simply flushed away.

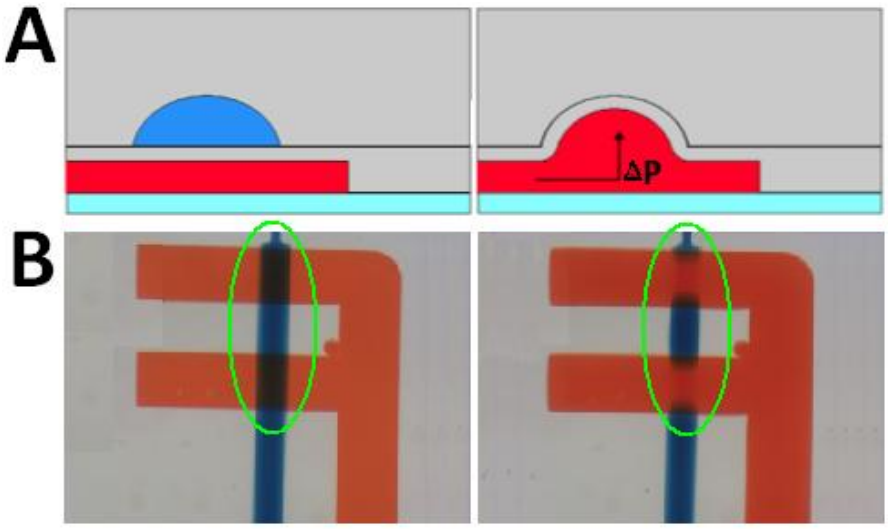

Figure 4.26: Flow channel with semi-circular shape. (A) Two cartoons show the cross-section of the crossover region with round flow channel. (B) Two micrographs taken from the top of the crossover area, marked with green circles. Left column illustrates the chip when the microfluidic valve is off, while right column is on. The flow channel is filled with blue food dye and the control channel with red. Blue colour is seen in the crossover area when the valve is off. Once the valve is pressurized, the colour of the middle area turns red immediately. The flow of blue dye is totally blocked by the valve.

4.2.2 Bonding PDMS onto glass with platinum electrode

Surface treatment with oxygen plasma (50W, 30s) was used to bond the PDMS replica onto a glass substrate base. Strong bonding requires that the surfaces to be bonded are smooth, particle-free, and have surface H_2O/OH groups [109]. The PDMS and glass surface are both hydrophobic [110]. A hydrophilic oxide surface for wafer bonding can be prepared by oxygen plasma treatment. After baking at 100°C for at least 2 hours, methoxysilanes form (Figure 4.27). The high density of methoxysilanes ensures high avidity, thus ensuring high bond strength [111].

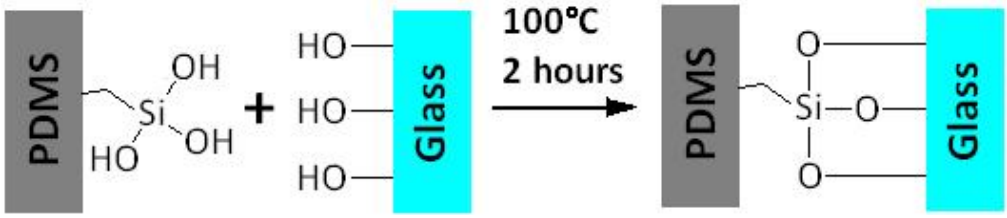

Figure 4.27: After surface treatment with oxygen plasma, hydrophilic oxide surfaces with H_2O/OH groups are produced on both PDMS and glass. Methoxysilanes formed after baking at 100 ºC for at least 2 hours.

In the NeuroChip, the PDMS channels are bonded onto a glass substrate with patterned platinum electrodes, produced by ion beam milling (IBM) [112, 113]. Surface treatment of the Pt with oxygen plasma barely changes the surface property of the metal PDMS thus preventing bonding. Figure 4.28 shows a NeuroChip that was not bonded properly on the electrode region.

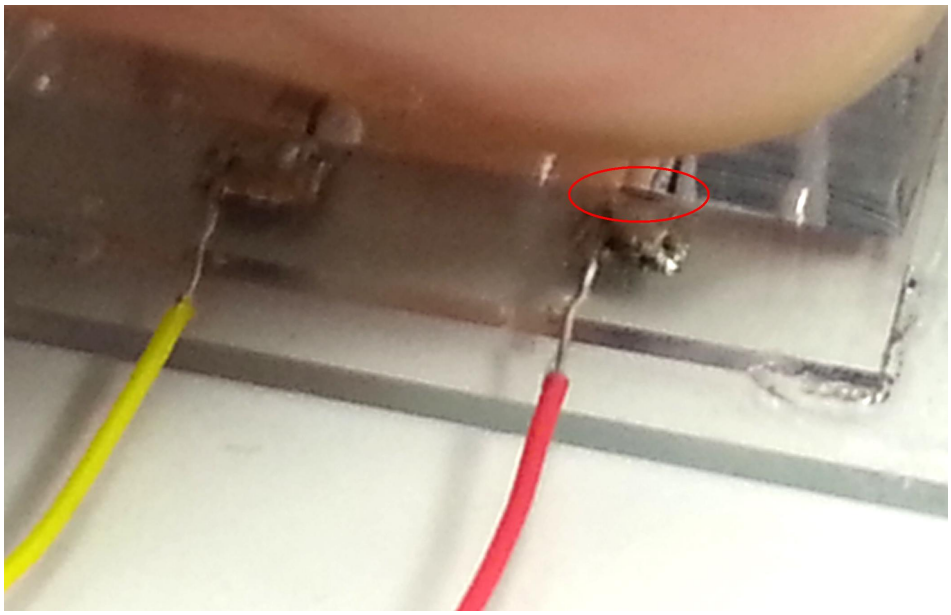

Figure 4.28: A NeuroChip that was not bonded properly over the electrode region. Red circle indicates the gap between the PDMS channel and platinum electrode.

The bonding strength was improved by using a combination of APTES (3-aminopropyltrimethoxysilane) and GPTMS (3-glycidoxypropyltrimethoxysilane).

Figure 4.29 shows the basic concept of chemical bonding with APTES and GPTMS. First, the surfaces of the PDMS replica and the glass substrate with patterned platinum electrodes were treated with oxygen (O_2) plasma (50 W) for 30 seconds (Figure 4.29A). After generating hydroxyl groups on the surfaces of both substrates, 5% (v/v) aqueous solutions of APTES and GPTMS were poured onto the PDMS and glass substrate respectively. The solution was left to react at 60 ºC in an oven for 1 hour to generate surface amine and epoxy functionalities (Figure 4.29B). After thorough ethanol washing and nitrogen gas drying, the solution-treated surfaces were bonded at 100 ºC for 1 hour (Figure 4.29C) to form a strong amine-epoxy bond [114]. The layer thickness of GPTMS is less than 1 nm [115], the charge can easily transport through the chemical film to the electrode [116].

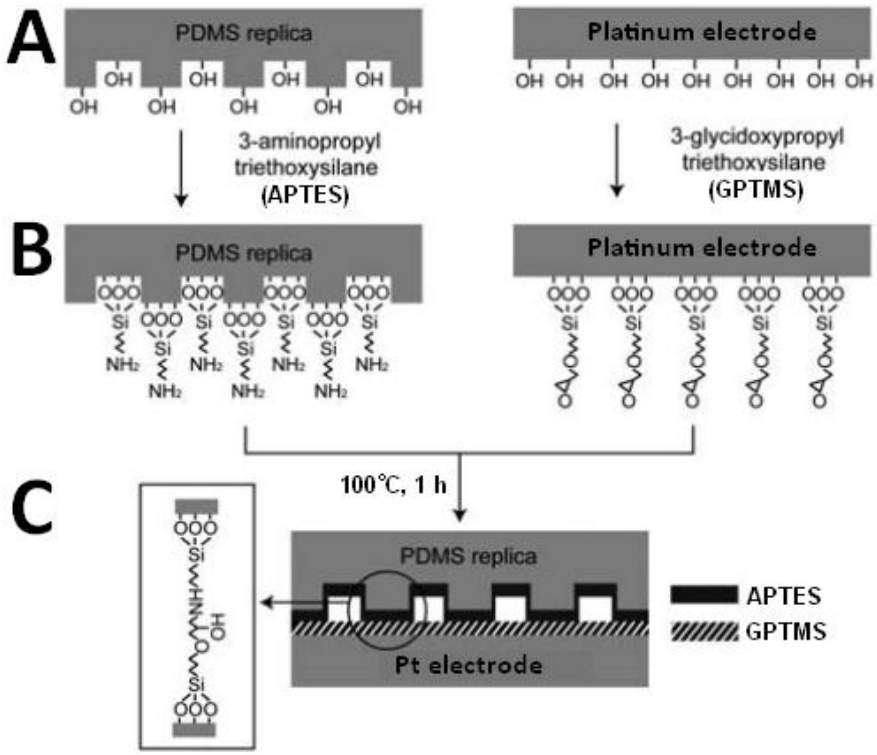

Figure 4.29: Chemical bonding of PDMS to platinum electrodes with APTES and GPTMS. (A) Surface hydroxylation of PDMS and platinum electrode by oxygen plasma treatment at 50 W for 0.5 minute. (B) APTES and GPTMS anchoring on the O2 plasma-treated PDMS and platinum electrode to generate surface amine and epoxy functionalities respectively. (C) The treated surfaces were bonded at 100 ºC for 1 hour to form a strong amine-epoxy bond. Pictures are modified from [114].

4.3 Device Operation

Four microfluidic valves were used to direct the flow in the device; more valves may be added as required. Manual control of the valves is time-consuming. For high-throughput purpose, an external control system (Appendix 7) is used to automate the manipulation process.

4.3.1 External control system

The external control system consists of a power supply, an I/O board (Phidgets USB Interface 0/16/16), a manual switch, a LEDn, a resistor, a comb-style pneumatic manifold, four solenoid electronic valves (Clippard minimatic, 3-way normally-closed valve), and several sections of lead and tubing for connections (Appendix 7). Figure 4.30 shows the electrical circuit diagram of the external control system. Four solenoid valves are connected to four output ports of an I/O board in parallel to control the individual microfluidic valves. They are connected in parallel to a red LED used for visual indication. A power supply controlled by a manual switch provides 6 volts excitation voltage for the solenoid valves.

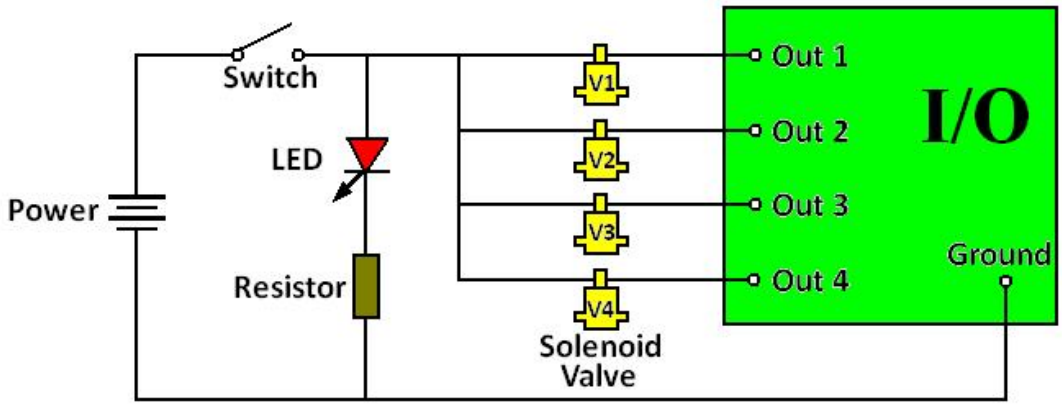

Figure 4.30: Electrical circuit diagram of the external control system.

The key component of this system is the solenoid valve (Clippard minimatic, 3-way normally-closed valve). Figure 4.31A shows the cross-sectional view of the valve. The inlet is connected to an air compressor through a pneumatic manifold and the outlet is connected to the microfluidic valve on the

NeuroChip (Figure 4.31B). This electronic valve is normally closed. When an excitation voltage of 6 volts is applied to the solenoid valve, the solenoid pulls the valve into the open state and the compressed air pressurizes the microfluidic valve on the device.

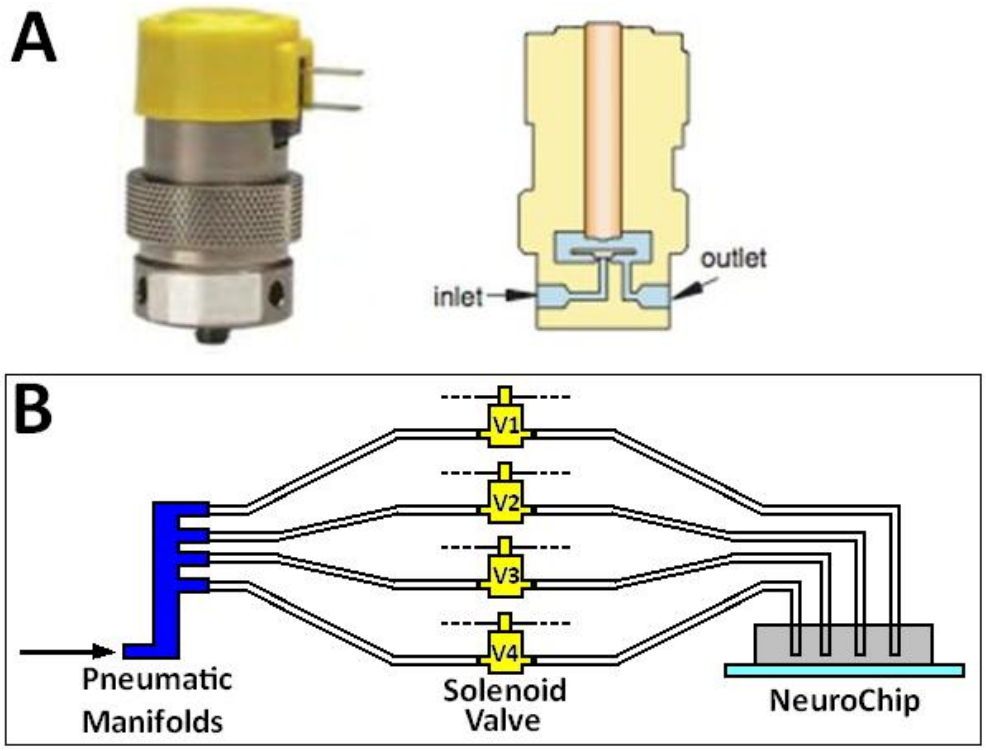

Figure 4.31: Diagram of the solenoid valve and schematic of the pneumatic connections. (A) Two pins on the cap are connected to the power supply; two holes on the bottom are the inlet and outlet for the air. (B) Schematic of the pneumatic connections. The inlets of four solenoid valves (marked in yellow with numbers V1, V2, V3, and V4 on them) are connected to a comb-style pneumatic manifold (marked in blue) for supplying compressed air separately. Four outlets are connected to the NeuroChip, guiding the compressed air to individual microfluidic valves under the control of I/O board.

To control the on/off states of these four solenoid valves, an excitation voltage is applied to each valve separately. The I/O board has 16 digital inlet ports and 16 digital outlet ports, and can be connected directly to a USB port. A custom-designed computer program written in Java (Appendix 8) was used to control each digital output port, to apply the excitation voltage to each valve as

required. The user-friendly interface is shown in Figure 4.32. The microfluidic valves can be actuated by either clicking the individual valve numbers on the right top of the panel, or selecting the shortcut keys (‘Worm in’, ’Drug in’, and ’Worm out’), which can control several valves at a time.

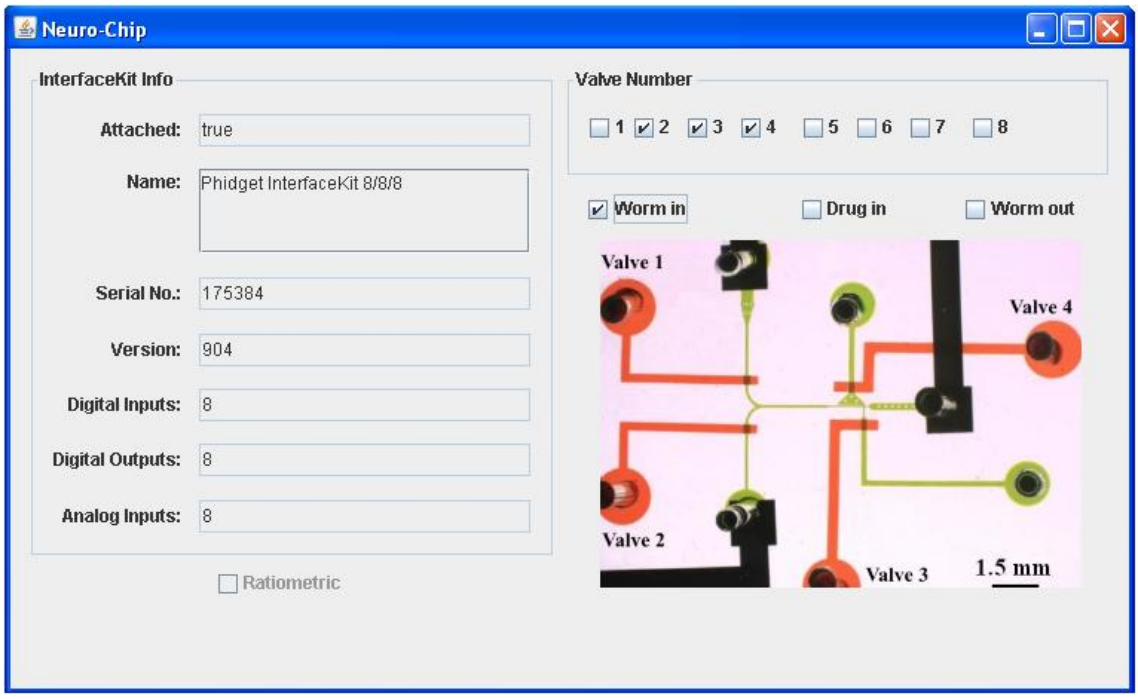

Figure 4.32: Interface of the custom-made computer program written in Java, to control each port of the NeuroChip. Valve numbers on the right top are correlated to the fours valves shown below. Click once to actuate and twice to cancel. Three shortcut keys (‘Worm in’, ’Drug in’, and ’Worm out’) are integrated to further simplify the operation. If ‘Worm in’ is selected, Valve 2, 3, and 4 are actuated to close the correlated bypass channels.

4.3.2 Operation of NeuroChip

The entire microfluidic platform is presented in Appendix 9. The operating procedure is as follows: Valves 2, 3 and 4 (V2, V3, and V4 in Figure 4.33) actuated to close the bypass channels. The worm is pumped by positive pressure (0.3 mBar) into the chip from the worm port by compressed air controlled by the computer. All other ports set to atmospheric pressure. At this small constant positive pressure, the worm is pushed into the trapping region.

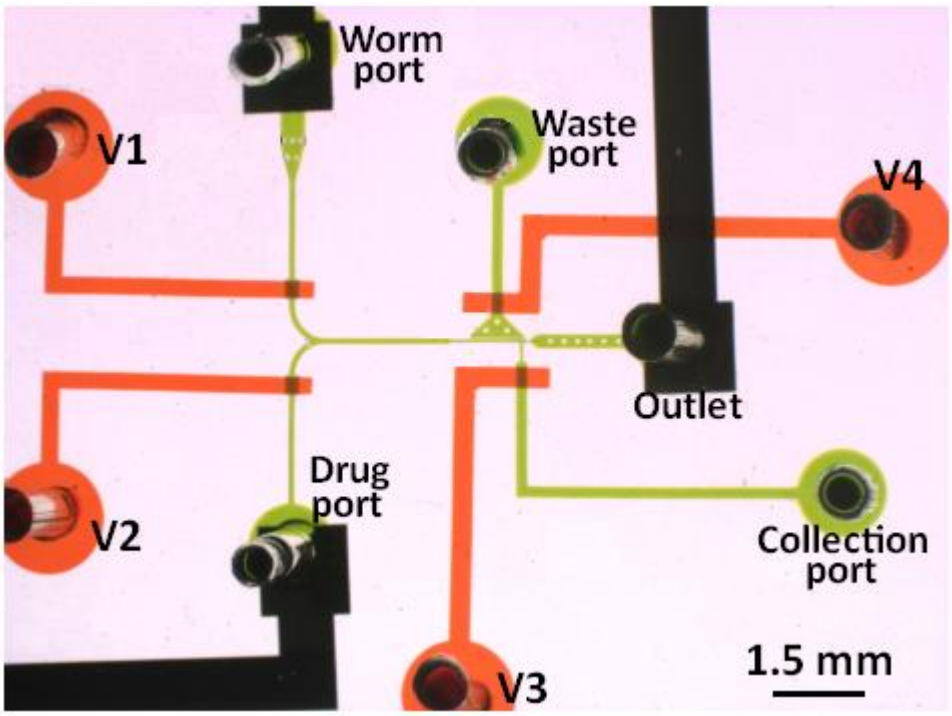

Figure 4.33: Micrograph of the NeuroChip. The flow channel is filled with green food dye and control channel with red. V1, V2, V3 and V4 correspond to the four microfluidic valves for controlling the bypass channels respectively. The black squares are the platinum electrodes.

Electrophysiological signals were then captured and either observed in real time or recorded for *post hoc* analysis. If the worm was in the correct orientation for EPG recording i.e. nose first, then the experiment was continued. If not, the worm was rapidly unloaded from the chip (by closing valve 2 and opening valve 1 and 3). Drugs were applied by closing valve 1 (V1 in Figure 4.33), and opening valve 2 and 4, thus delivering drugs from the drug port. To facilitate access of the drug to the worm, valve 4 (the waste channel) was closed and the drug was allowed to flow into the waste port around the worm. The EPG was then recorded in the presence of the drug. Drugs can be washed off the worm by closing valve 2 and opening valve 1. Finally valve 2 and 4 was closed and valve 1 and 3 opened to unload the worm from the device. This worm could be collected after EPG recording e.g. for genotyping by PCR, and the device was then ready to receive the next worm.

4.4 Conclusions

In this chapter, an integrated microfluidic platform has been designed and built. The device is called a NeuroChip. Compared to the microfluidic channel introduced in last chapter, the NeuroChip has additional bypass flow channels, enabling transportation of worm and drugs under precise control. Another layer of control channel was designed to actuate individual pneumatic microfluidic valves to open and close these bypass flow channels. A micro-pillar structure was placed near the worm port to direct the orientation of the nematode, so that the animal goes into the trap with head-to-tail orientation. Platinum electrodes were included in the chip, replacing the external silver/silver chloride electrodes, making this device an integrated microfluidic platform for electrophysiological analysis on *C. elegans*.

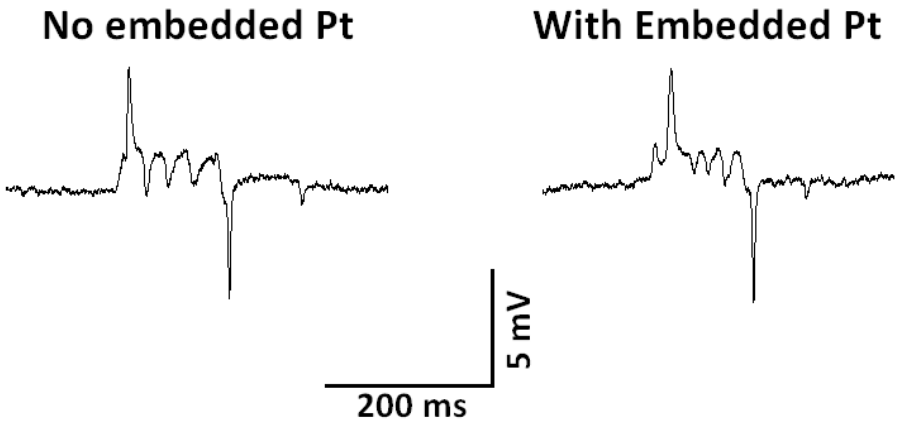

Figure 4.34: Comparison of the examples of single EPG traces obtained from the microfluidic device with external Ag/AgCl and with the integrated platinum electrodes. No obvious difference was seen in either the waveform or amplitude, indicating the platinum electrode does not affect the EPG recording.

Serotonin has been applied to the worm through the microfluidic channel. The EPG recording traces seems to be as good as a conventional assay. To demonstrate the functionality of the NeuroChip, 10 mM 5-HT was pre-loaded to increase the pharyngeal pumping rate. NeuroChips with and without embedded platinum electrodes were tested. High quality EPG signals were

obtained, regardless of whether the electrode is made of external Ag/AgCl or embedded platinum (Figure 4.34). Compared to the EPG signal taken with conventional method, no obvious difference was observed in either the waveform or amplitude, although Pt and Ag/AgCl are two distinct electrodes. As the solution contains Cl^-, redox reaction ($AgCl + e^- \rightleftharpoons Ag + Cl^-$) processes on the Ag/AgCl electrode, and forms a non-polarisable electrode capable of passing current with less polarisation. When the pharyngeal is pumping, the current is directly exchanged between the metal and the solution and to be recorded by the amplifier. In terms of polarisable electrode Pt, no redox process occurs on the electrode surface due to the double layer capacitance. The electrons can not be exchanged on the metal/liquid interface, but a current-induced change of charge distribution near the electrode surface may result in a changed potential function and consequently a changed half-cell potential [117]. In physiological environment, the platinum electrode is very suitable for dc potential reading applications under zero dc current conditions [117]. The polarisation impedance can be reduced by increasing the effective metal surface area. Therefore, the embedded platinum electrode is capable of producing the EPG recording, regardless of its electrical property.

Chapter 5: Experiments with NeuroChip for Genetic and Chemical Biology Screening of *C. elegans*

Subsequent to the good performance exhibited by the NeuroChip, experiments for genetic and chemical biology screening of *C. elegans* by electrophysiological means were undertaken. These encompass detection of effects on synaptic cholinergic signalling, rapid application of compounds and simultaneous electrophysiological recording, detection of effects on inhibitory neurotransmission and mutant sorting, and interrogating neural network properties with optogenetics.

5.1 Preparation

5.1.1 Worm culture and sample preparation

Wild-type *C. elegans* (N2, Bristol) and *eat-4* mutants (strain MT6308, *eat-4(ky5)*III and strain MT6318, *eat-4(n2474)*III) were cultured according to standard protocols [118]. Experiments were performed on age-synchronized worms. Dent's saline compound (composition in mM; D-glucose 10, HEPES 10, NaCl 140, KCl 6, CaCl2 3, MgCl2 1, pH 7.4 with NaOH) was injected into the chip to provide a liquid environment. The *peat-4::ChR2;mRFP* integrated line was crossed into *eat-4 (ky5)* to generate a strain carrying a visual marker, red fluorescent protein, for the *eat-4 mutant*, as shown in Appendix 10 (This work was done by colleagues from Professor Lindy Holden-Dye's group).

5.1.2 Data acquisition and signal analysis setup

The NeuroChip was connected to an AxoClamp 2A amplifier using a x1 headstage (Axon Instruments, USA). Recordings were acquired using a Digidata 1320 interface and Axoscope software (Axon Instruments, USA). Axoscope recordings were made for 5 minutes for comparison of EPG parameters between conventional and chip recordings, and for 2 minutes for the screening experiments. They were analysed either manually or using AutoEPG [15], as indicated. The EPG parameters that were measured were i) peak to peak

amplitude (manually) ii) average frequency (AutoEPG) iii) the duration of a single EPG waveform or 'pump' measured as the peak E to peak R time interval (AutoEPG) iv) the interval between consecutive individual pumps measured as the R to E interval (AutoEPG) v) the average number of 'P' waves per pump (AutoEPG) vi) the average amplitude of 'e' (manually by measuring the perpendicular distance of the peak of the waveform from the baseline of the EPG) vii) the ratio of the amplitude of 'R' to 'E', as an overall measure of EPG shape (AutoEPG). Low frequency drift could be removed by Clampfit 9.0 (Axon Instruments) with a Highpass Bessel filter and 0.5 Hz -30 dB cut-off frequency.

5.2 Validation of the performance of NeuroChip

In order to validate the utility of the microfluidic device in comparison to conventional recordings, in particular with respect to resolving discrete neural components of the waveform, parallel experiments were performed using both methods on wild-type worms without 5-HT (Figure 5.1) and with 5-HT (Figure 5.2; Table 2), and *eat-4 (n2474)* mutant worms without 5-HT (Figure 5.3; Table 3). Each recording was collected for at least 5 minutes and analyzed either manually or using AutoEPG [15], as indicated. As described previously in chapter 2, 5-HT is a neurotransmitter, which has the ability to regulate repolarisation of the *C.elegans* pharyngeal muscle so as to facilitate the pharyngeal pumping and reduce the movement of worm.

C. elegans is a fast-moving nematode in the absence of 5-HT, therefore it is not easy to collect recordings from the intact nematode with the conventional approach. First, it is hard to trap the worm's head when it is swimming and foraging. Second, once the worm is trapped, more suction is required to keep it in position and the increased resistance of the seal decreases the signal to noise ratio; thus the waveform may require filtering (Figure 5.1A(i)), or may be abnormal (Figure 5.1A(ii)). The trapping chamber successfully restrains the worm to provide stability of recording and recordings can consequently be made in the absence of 5-HT (Figure 5.1B).

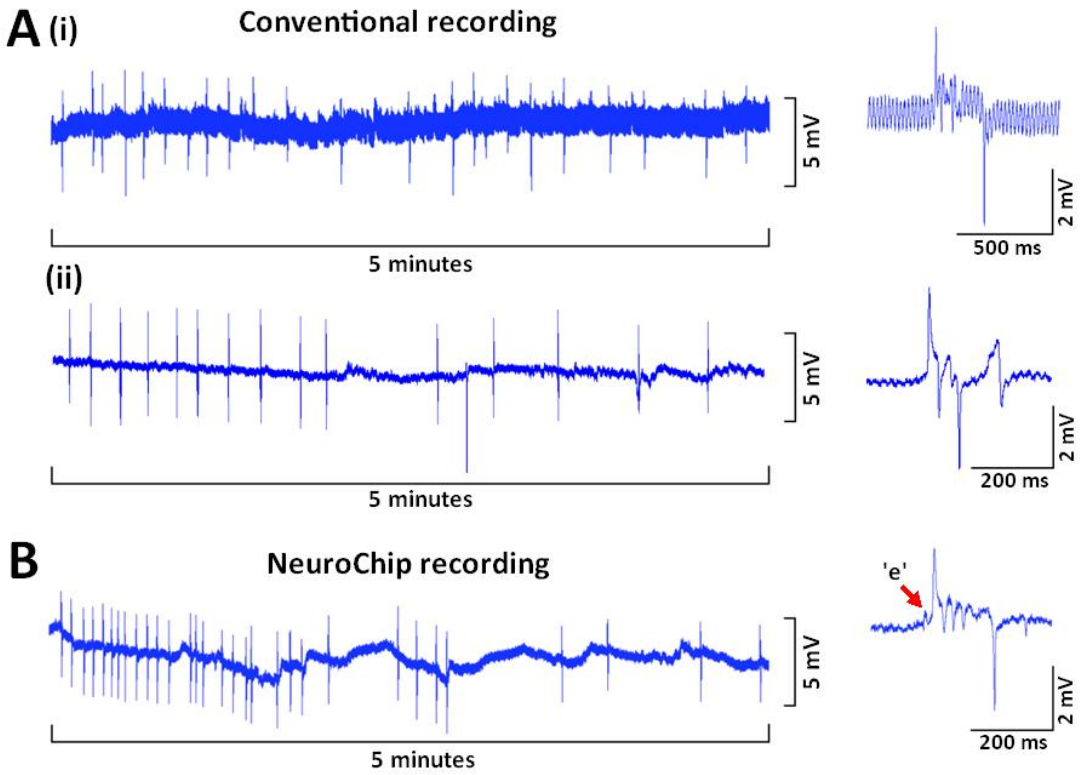

Figure 5.1: A comparison of basal EPG recordings with conventional method and the microfluidic device. Recordings were made from wild-type worms in the absence of 5-HT and therefore the frequency of the EPGs is low (around 0.1 Hz). (A) 5 minutes of conventional recordings from intact worm and correlated single EPG waveforms. To secure the freely moving worm on the suction tube, greater suction has to be exerted, leading to an increased noise background (i) and distorted waveform (ii). (B) 5 minutes of recording and an example of a single EPG waveform using the NeuroChip. Drift in the baseline is probably likely due to residual movement of the worm in the chamber and stable EPG waveforms can be captured for extended periods of time. Note the much improved signal to noise ratio in the NeuroChip compared with a conventional recording.

5-HT (10mM) stimulates pharyngeal pumping [82, 119, 120] and this was observed for both conventional and NeuroChip recordings (Figure 5.2). However, in the presence of 5-HT, the pump rate was greater and the pump duration was less for the NeuroChip than for conventional recordings (Figure 5.2; Table 2). An explanation for this is provided by a recent paper showing

that the pharyngeal pumping rate of worms moving in liquid is inhibited [121]: Worms in the conventional recording configuration are still able to move their bodies vigorously, unlike worms trapped in the NeuroChip thus these latter worms might be expected to pump at a higher rate. As pharyngeal pumping frequency increases the pump duration typically decreases [82]. This also provides an explanation for the slightly lower pump duration observed with the device. An alternative possibility is that the pressure exerted to hold the worm in the trapping chamber may affect pharyngeal pumping in the NeuroChip device.

Previous studies have shown that 5-HT increases signalling from the cholinergic pacemaker neurone MC [13, 82, 122] and this therefore predicts that 5-HT should increase the amplitude of 'e'. NeuroChip is able to directly resolve this effect at least as reliably as conventional recordings (Table 2; compare Figure 5.1B with Figure 5.2B) and therefore is capable of defining effects on excitatory cholinergic synaptic transmission. A caveat to this is that the amplitude of 'e' may be affected by the interval between 'e' and the larger 'E' spike. If this interval becomes briefer then 'e' may become superimposed on the 'E' spike which would contribute to an increase in amplitude as measured with the current approach. Future analyses could be optimised to resolve this e.g. by extracting the 'e' waveform from the 'E' spike.

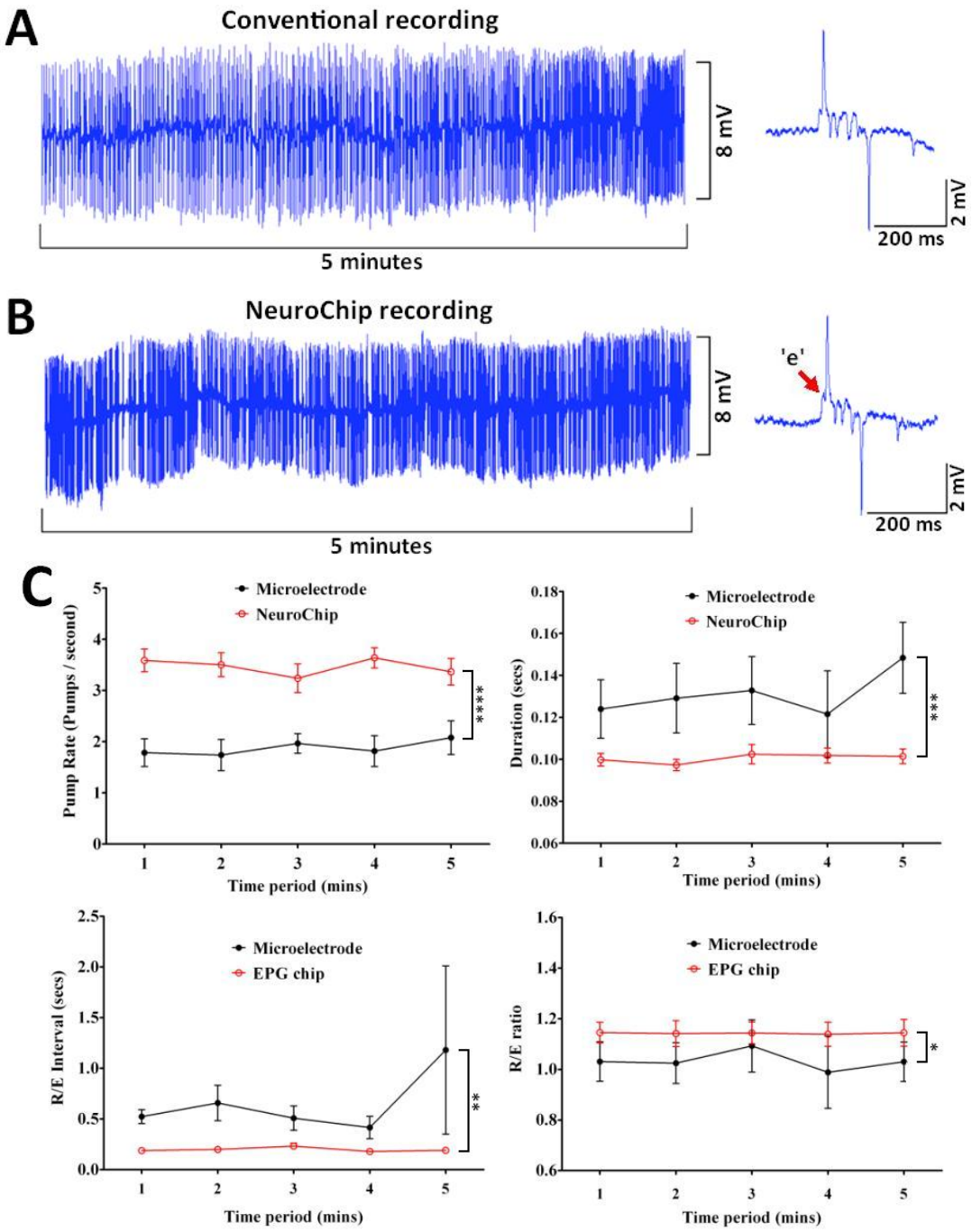

Figure 5.2: 5-HT (serotonin) stimulated worms: comparison of conventional method and the microfluidic device. Wild-type worms were incubated in 10 mM 5-HT for at least 10 minutes before, and throughout the entire experiment. (A) 5 minute trace and example of a single EPG waveform recorded using a conventional suction tube. (B) 5 minute trace and example of a single EPG waveform recorded using the NeuroChip. (C) Time courses of the EPG frequency, duration, R-E interval and R/E ratio, comparing the stability of recording with

conventional method and the NeuroChip. Data are the mean ± SEM. A higher frequency and shorter pump duration is observed with NeuroChip compared to conventional recordings, (n=10). Note that conventional recordings from intact worms have an improved signal to noise ratio in the presence of 5-HT compared to without 5-HT (Fig. 5.1A(i)). 5-HT reduces motility [123, 124] and so less suction has to be applied to hold the worms in the recording electrode. Reduced seal resistance is predicted to reduce the noise [125].

Table 2: A summary of EPG parameters compared for NeuroChip and conventional recordings. These recordings were made from the same populations of wild-type N2 worms. Data are the mean ± s.e.mean of recordings from 'n' worms. Each parameter was derived from either AutoEPG analysis of all the EPGs captured in a recording of 5 minutes or, for manual analysis, from 60 EPGs for 'n' worms. Comparisons made by unpaired Student's t-test to the same parameter for [1]conventional wild-type N2 recording without 5-HT (P=0.001); [2]conventional wild-type N2 recording with 5-HT (P<0.0001); [3]conventional wild-type N2 recording with 5-HT (P=0.0002); [4]conventional wild-type N2 recording without 5-HT (P<0.0001); [5]NeuroChip recording without 5-HT (P<0.0001).

	Conventional recording	NeuroChip
Wild-type (N2) (n=5)		
EPG amplitude (mV)	4.780 ±1.006	4.410 ±0.051
EPG frequency (s^{-1})	0.060 ±0.016	0.075 ±0.019
EPG duration (s)	0.112 ±0.015	0.116 ±0.006
Average number of P waves ($pump^{-1}$)	0.590 ±0.143	1.788 ±0.225 ***[1]
'e' amplitude (mV)	0.203 ±0.039	0.257 ±0.037
R-E interval (s)	28.973 ±6.863	24.658 ±5.407
R-E ratio	1.006 ±0.097	1.222 ±0.085
Wild-type with 5-HT (10mM) (n=10)		
EPG amplitude (mV)	7.580 ±0.769	8.370 ±0.835
EPG frequency (s^{-1})	1.878 ±0.120	3.467±0.104 ****[2]
EPG duration (s)	0.135 ±0.007	0.101 ±0.002 ***[3]
Average number of P waves ($pump^{-1}$)	0.201 ±0.087	0.126 ±0.035
'e' amplitude (mV)	1.080 ±0.062 ****[4]	1.753±0.079 ****[5]
R-E interval (s)	0.550 ±0.170	0.198 ±0.009
R-E ratio	1.046 ±0.043	1.143±0.020

The microfluidic device was tested for capability to detect changes in inhibitory neurotransmission. The *eat-4* mutant was chosen for this study as it harbours a loss of function mutation in a vesicular glutamate transporter and is deficient in inhibitory glutamatergic signalling [13]. In the pharyngeal system this leads to loss of signalling through the inhibitory glutamatergic motorneurone M3 with a concomitant and distinctive loss of the EPG 'P' waves, which result from M3 activity, and a characteristic lengthening of pump duration [13]. Similar to the comparison made for wild-type worms (Table 2), for eat-4 the pump frequency was higher and duration shorter in NeuroChip compared to conventional recordings (Figure 5.3), again perhaps reflecting the impact of constraining worm movement in the microfluidic chamber on pumping rate [121]. The number of 'P' waves per pump and the R/E ratio was different between conventional and NeuroChip recordings for *eat-4* (Figure 5.3C; Table 3) but the significance of these differences are unclear. Importantly, a comparison of the data obtained from the mutant *eat-4 (n2474)* (Table 3) with that of wild-type (Table 2) confirmed the capability of NeuroChip to detect changes in inhibitory neural transmission. As with conventional recordings, and consistent with published data [13] eat-4 was shown to have a reduced number of 'P' waves and increased pump duration (Table 2; Table 3).

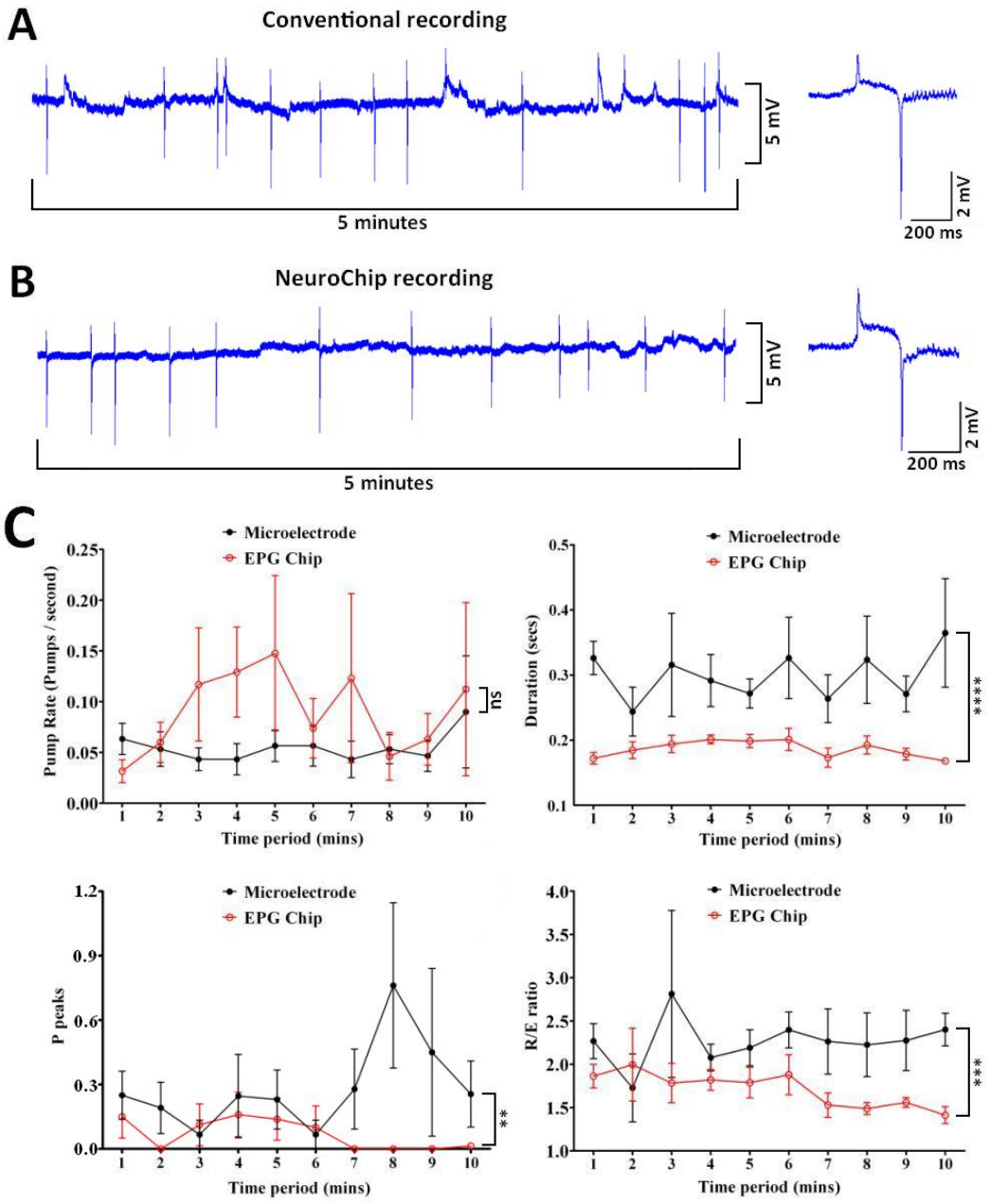

Figure 5.3: A comparison of basal EPG recordings with conventional method and the microfluidic device. Recordings were made from *eat-4 (n2474)* mutant worms in the absence of 5-HT. (A) 5 minute trace and example of a single EPG waveform recorded using a conventional suction tube. (B) 5 minute trace and example of a single EPG waveform recorded using the NeuroChip. (C) Time courses of the EPG frequency, duration, R-E interval and R/E ratio, comparing the stability of recording with conventional method and the NeuroChip. Data are the mean ± SEM. A shorter pump duration and lower R/E ratio is observed with NeuroChip compared to conventional recordings, (n=5).

Table 3: *eat-4* mutants recorded with NeuroChip or conventional recordings have the same phenotype. Data are the mean ± s.e.mean of recordings from 'n' worms. Each parameter was derived from AutoEPG analysis of all the EPGs captured in a recording of 5 minutes or, for manual analysis, from 60 EPGs. Eat-4 had increased pump duration and decreased number of 'P' waves compared to wild-type. Comparisons made by unpaired Student's t-test to the respective parameters for [1,2] conventional wild-type N2 recording without 5-HT, P<0.0001 and P=0.0208, respectively; or [3,4] to wild-type N2 NeuroChip recording without 5-HT, P<0.0001. Wild-type data are provided in Table 2.

	Conventional recording	NeuroChip
eat-4(n2474) **(n=5)**		
EPG frequency (s^{-1})	0.055 ±0.007	0.090 ±0.015
EPG duration (s)	0.287 ±0.014 ****[1]	0.172 ±0.009 ****[3]
Average number of P waves	0.280 ±0.065 *[2]	0.103 ±0.022 ****[4]
'e' amplitude (mV)	0.368 ±0.030	0.376 ±0.034
R-E interval (s)	26.513 ±3.078	22.288 ±3.867
R-E ratio	2.170 ±0.117	1.491 ±0.085

5.3 Rapid application of compounds

For drug screening and chemical biology it is advantageous to have the capability to rapidly apply and remove drugs or chemicals whilst simultaneously capturing the EPG waveform to monitor the effect on the activity of the neural circuit. In conventional drug screening assays, chemicals are applied via the perfusate or by aspiration of the bathing solution in the recording chamber [11, 74]. It is hard to control the flow rate and wastes a large amount of chemical or drug.

The microfluidic device provides a means for consistent drug injection and small amount of chemical usage. Three different designs (Figure 5.4A) were adopted in this experiment. The first one has a bypass channel near the tail of the trapped worm. The flow channel was narrowed to immobilize the worm more tightly, which in return dramatically slows down the drug diffusion time. This bypass channel was added to reduce the time for drug transportation.

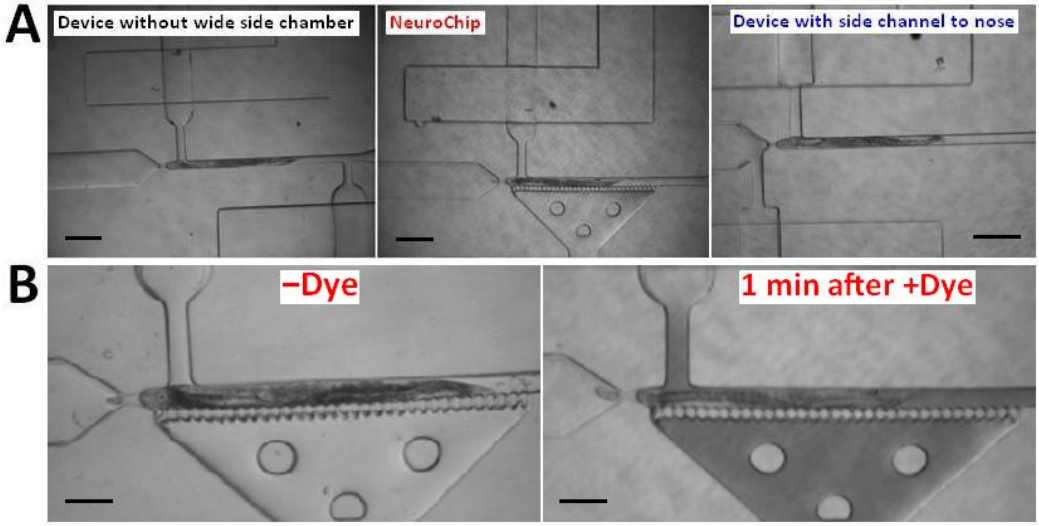

Figure 5.4: Three different designs of microfluidic chips for rapid application of compounds. Dye labelling of the perfusate was used to track the time-course of application. (A) Three different designs of microfluidic chips. The first one has a bypass channel near the tail of the trapped worm, reducing the time for drug diffusion and flow. In the middle is the NeuroChip. It has a wide perforated chamber alongside the trapped nematode, providing a path for drug flowing around the worm. The last design provides an access for directly applying drugs to the nose of the captured *C. elegans*. Scale bar: 250 μm. (B) Dye experiment with the NeuroChip. The immobilized worm was completely surrounded by the food dye just one minute after actuating the drug port. Scale bar: 100 μm.

Another one is the NeuroChip. The wide perforated chamber alongside the trapped nematode provides a path for drug going round the worm. Instead of adding a bypass channel near the tail of the nematode, the last design has a side channel close to the head of the trapped *C. elegans* for directly applying drugs to the nose of the worm. Dye experiments were undertaken to examine the time for drug transportation from the drug port to the collection channel (Figure 5.4B). The result indicates that drug access to the channel of NeuroChip is very rapid (Figure 5.4B). Without the perforated side chamber the access time was 46 ± 5.4 sec, n=5 ± s.d., whilst with the perforations the dye access occurred within seconds. Furthermore, this design reduced the time required to wash out the drug.

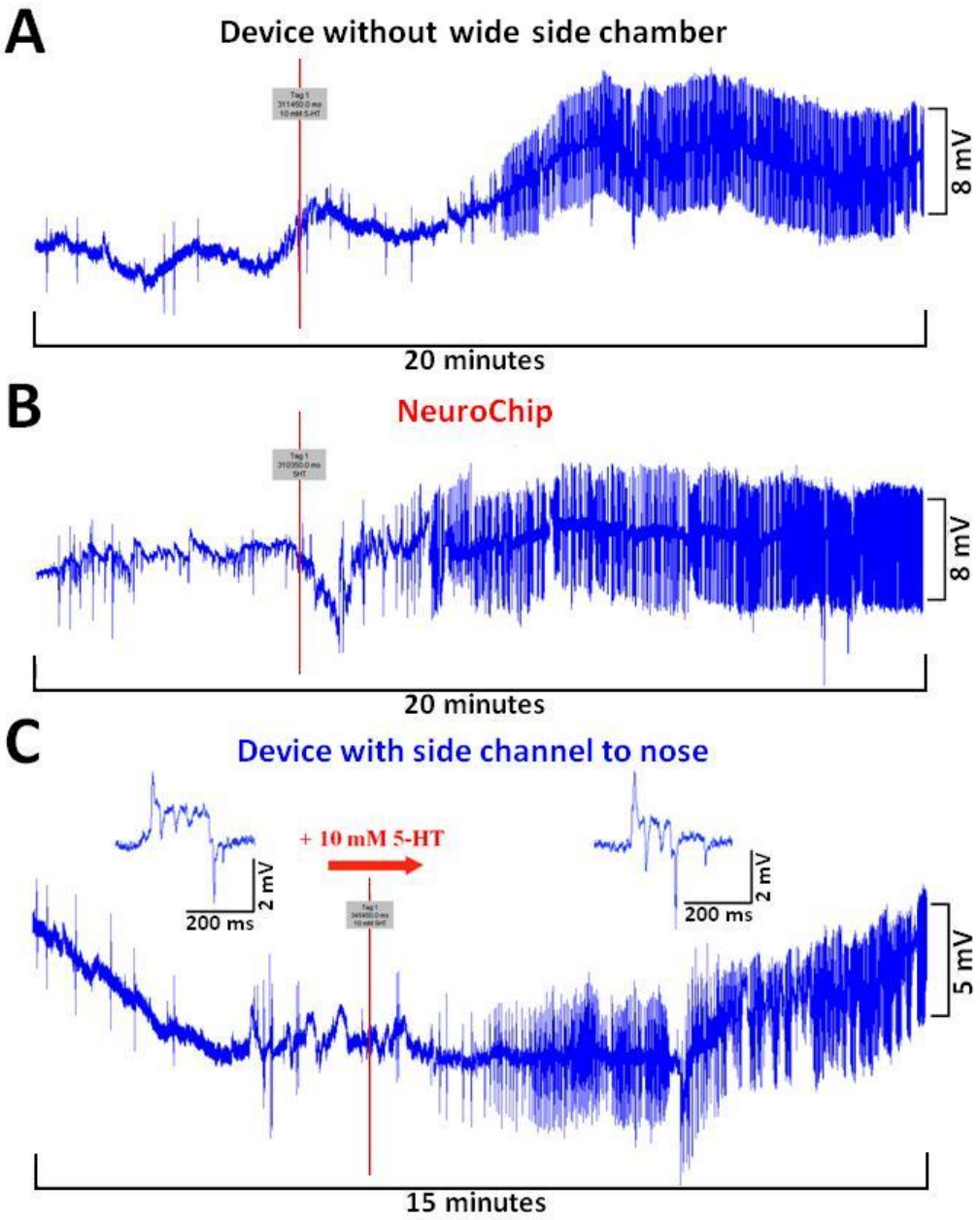

Figure 5.5: EPG recordings taken from three different designs of microfluidic chips for rapid application of compounds. They were made from wild-type worms whilst 5-HT (10 mM) was added via the drug port or outlet channel after taking 5 minutes basal recordings. The red vertical line indicates when the 5-HT was added to the drug port or outlet channel under a positive pressure. (A) EPG recording made using the device without the wide side chamber. (B) EPG recording made using the NeuroChip. (C) EPG recording made using the device with side channel to the nose of the trapped worm.

10 mM 5-HT was chosen for this experiment as it rapidly stimulates the pharyngeal pumping. Using the design without wide side chamber, responses to 5-HT were observed that had a latency of 5 min and achieved the maximal effect (i.e. same pump rate as worms that were pre-exposed to 5-HT before addition to the chamber) after around 12 minutes, whilst using NeuroChip responses to 5-HT were observed that had a latency of 2 min and achieved maximal effect after 12 minutes (Figures 5.5, 5.6). The time taken for the full response to 5-HT to develop likely reflects the time taken for 5-HT to gain access to its site of action inside the worm. It was considered that this might be improved if the device was configured to allow drug to flow across the mouth of the worm. However, when 5-HT was applied directly to the mouth of the worm there was no significant overall effect on the time-course of the response (Figures 5.5, 5.6). The maximum pump rate following 5-HT application to NeuroChip closely matched that observed in worms that were pre-incubated in 5-HT prior to addition to the device (Figure 5.6; Table 2) suggesting full equilibration of the drug with the worm. The experiments in which the 5-HT was added to the nose via the outlet port had to be terminated after 15 minutes as the increased pressure in the channel made it difficult to maintain the worm in the trap. However, 2 minutes after addition of 5-HT there was a significantly greater increase in frequency when 5-HT was applied to the nose compared to addition via the drug port (Figure 5.6) (n=5 worms for each design $P=0.0013$, one-way ANOVA) suggesting that the onset of response might be slightly faster following this route of application.

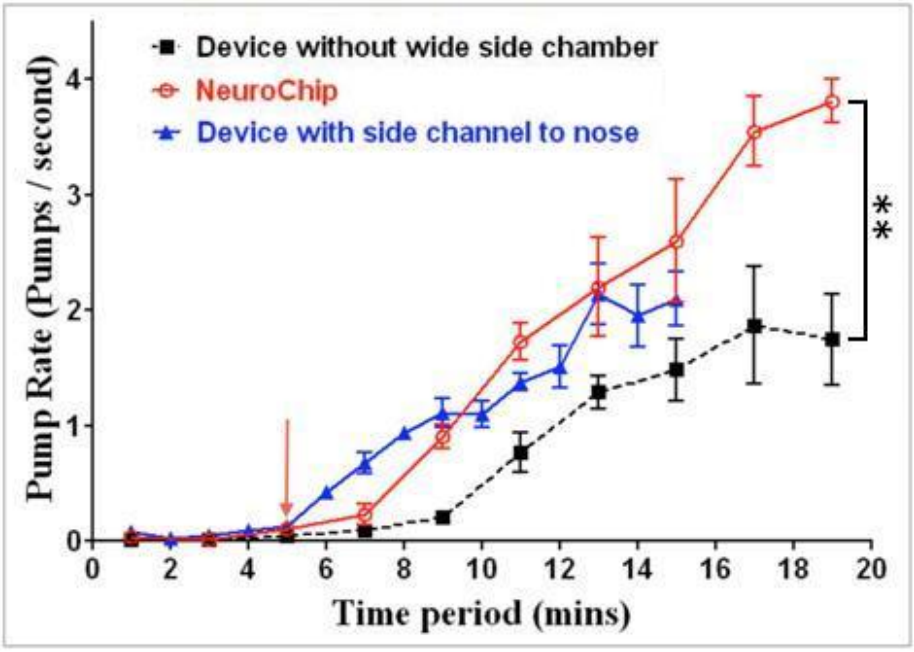

Figure 5.6: Response time to 5-HT for three different designs. The red arrow indicates when 5-HT was applied either via the drug port or via the outlet port as indicated. The dotted black line indicates the response time for the device without the wide side chamber. The red line indicates the response time for the NeuroChip. The blue line indicates the response time for the device with 5-HT added directly to the nose via the outlet port. The response to 5-HT in NeuroChip was significantly greater than the response that was recorded compared to the device without the side chamber (n=5 worms for each design; data are mean ± SEM; ** P=0.0089, Student's t-test for the last time point).

The response time to compounds for which there is evidence that the cuticle does not present a barrier i.e. ethanol [83] and for which the rate-limiting factor in the response time would be the time taken for the drug to get access to the recording chamber was tested. For these experiments the response time was very rapid, t1/2 < 2 min, (Figure 5.7) supporting the contention that the cuticle does not present a significant diffusion barrier to ethanol [83]. Ethanol (400 mM) had a modulatory effect on 5-HT (10mM) stimulated pharyngeal pumping causing a decrease in frequency, an increase in pump duration, a decrease in the number of P waves per pump and a relative reduction in the amplitude of the E spike (Figure 5.7).

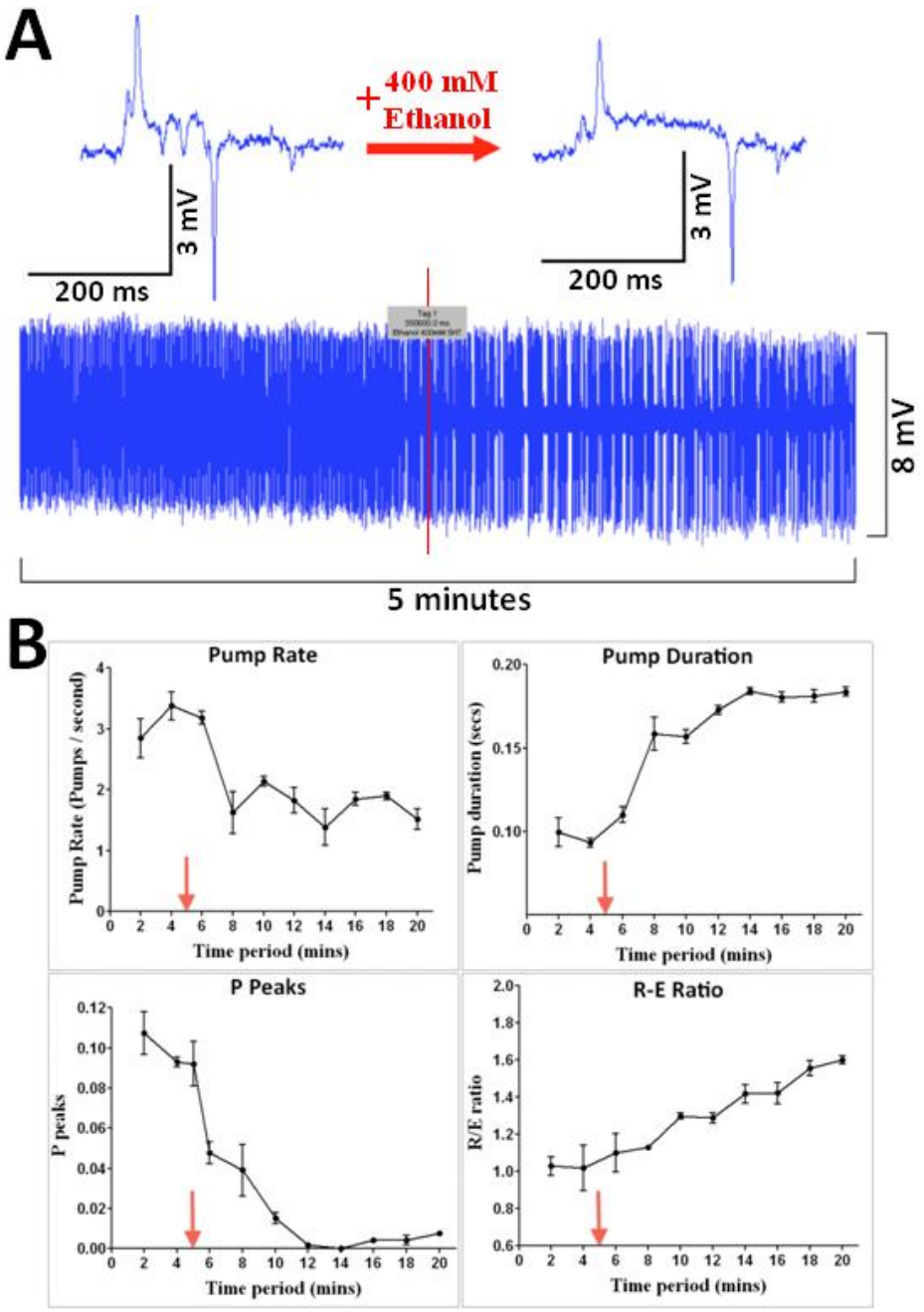

Figure 5.7: Detecting modulatory drug effects with NeuroChip. Wild-type worms in the presence of 10mM 5-HT were used. Ethanol was applied through the drug port of NeuroChip. (A) An example of the change in the EPG waveform with 400 mM ethanol and (below) a 5 minute recording showing the time-course of the ethanol effect. The red line indicates the point at which ethanol was added to the drug port. Note the rapid reduction in EPG frequency. (B) Ethanol modulates four parameters of the EPG (red arrows indicate the time of addition of

ethanol via the drug port); n=3 worms for each graph; data are mean ± SEM.

5.4 Mutant sorting

Genetic screens of *C. elegans* pharyngeal phenotypes by visually scoring the activity of the pharynx in intact worms has been of great utility in identifying novel mutants and providing insight into gene function [96]. Therefore the ability of NeuroChip to resolve mutant from wild-type pharyngeal function was tested. For this mutant *eat-4* worms were sorted from wild-type on the basis of electrophysiological signature. A wild-type population of worms was spiked with mutant worms, *eat-4(ky5)*, and a sample was analysed on NeuroChip. EPG signals were collected from worms loaded from a reservoir and analysed in real time (5 minutes recording per worm). The difference of the EPG signals from these two types of worms was clear enough to be easily distinguished by just observation. Two groups of worms were selected by prediction from the NeuroChip and the result was then validated by single worm PCR or fluorescent mark. Similar to the comparison made for wild-type worms (Table 2), for *eat-4* the pump frequency was higher and duration shorter in NeuroChip compared to conventional recordings, again perhaps reflecting the impact of constraining worm movement in the microfluidic chamber on pumping rate [121]. The number of 'P' waves per pump and the R/E ratio was different between conventional and NeuroChip recordings for *eat-4* (Table 3) but the significance of these differences are unclear. Importantly, a comparison of the data obtained from the mutant *eat-4 (n2474)* (Table 3) with that of wild-type (Table 2) confirmed the capability of NeuroChip to detect changes in inhibitory neural transmission. As with conventional recordings, and consistent with published data [13] *eat-4* was shown to have a reduced number of 'P' waves and increased pump duration (Figure 5.8A, B; Table 2; Table 3).

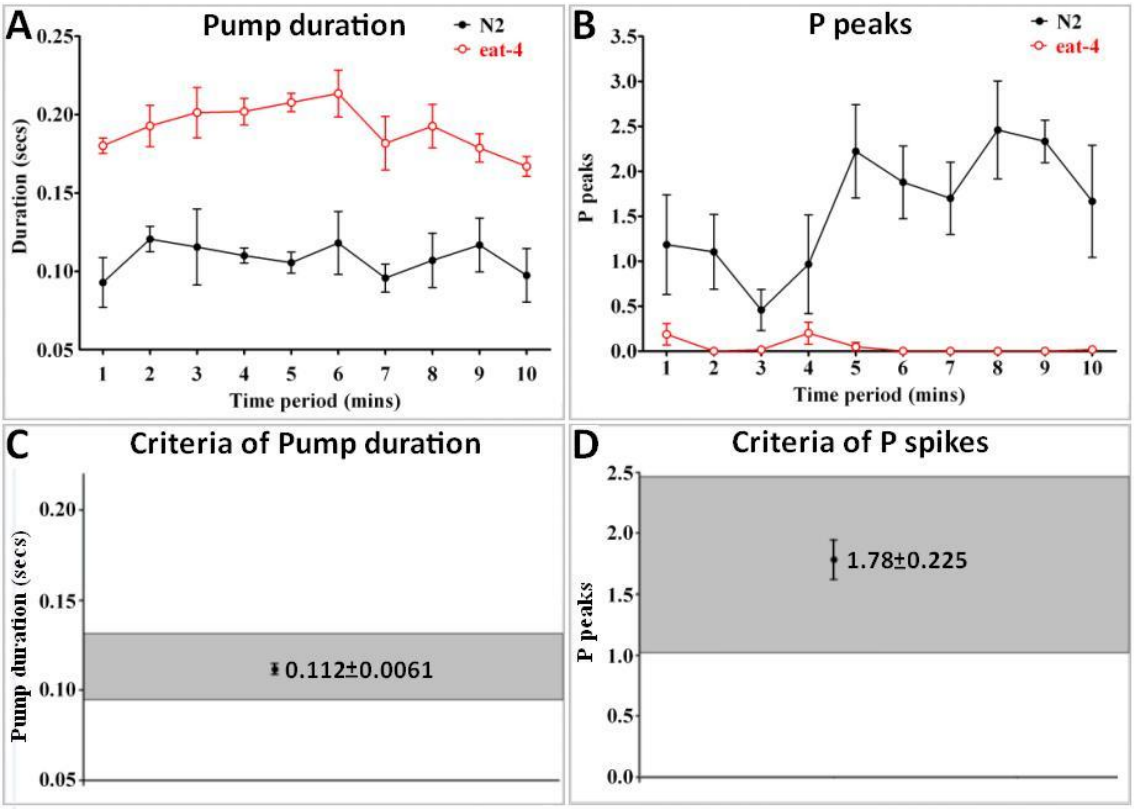

Figure 5.8: Criteria of NeuroChip detection and selection of *C. elegans* mutants. Two distinguishable parameters for detecting *eat-4* mutants: (A) Time courses of the EPG pump duration and (B) 'P' peaks. Data are the mean ± SEM. A longer pump duration and less P peaks is observed from *eat-4* mutants, (n=5). (C) Criteria of EPG pump duration and (D) number of 'P' waves per pump that were used for the selection of mutant from wild-type worms. The boundaries of the wild-type phenotype were defined as three times the standard deviation of the mean for wild-type recordings. Any worm with a mean value lying outside this boundary was identified as a mutant.

For a worm to be identified as 'wild-type' it had to fulfil the criteria of having a pump duration and number of P waves per pump within three times the standard deviation of the mean established for wild-type recordings in the validation experiment (Figure 5.8C and D). Thus any worm that had average pump duration greater than 0.1445 s and number of P waves less than 0.169 was identified as a mutant i.e. *eat-4* (Figure 5.9A and B). On these criteria three worms were identified as *eat-4*. Subsequent genotyping by single worm PCR

(thanks to James Dillon for helping me with single worm PCR) confirmed that all three worms that were identified as *eat-4* by NeuroChip carried the *eat-4* mutation i.e. there were no false positives (Figure 5.9C). Thus, NeuroChip is capable of mutant sorting from wild-type worms based on the electrophysiological signature. To test whether or not there were false negatives in a NeuroChip mutant screen, a further analysis was carried out using a strain carrying both the *eat-4 (ky5)* mutation and red fluorescent protein, *eat-4(ky5);peat-4::ChR2;mRFP*. This permitted robust discrimination of wild-type worms from *eat-4* worms after mutant selection and screening on the basis of the absence of red fluorescence. For this experiment 18 wild-type and 13 *eat-4* mutants were mixed together and then 20 were randomly transferred to the loading chamber. 17 worms were recorded head-first in the correct orientation for EPG and of these 8 were identified as wild-type, 4 as *eat-4* on the basis of EPG signal and 5 could not be distinguished due to weak or noisy signals. Subsequent visual inspection (independent observer, single blind trial) confirmed this identification as correct. Thus this screen generated no false negatives. However, a caveat to this is that the current device cannot phenotype worms that enter the device tail first. A solution to this would be to carry out an iterative approach in which worms that entered tail first were collected and re-applied to the device.

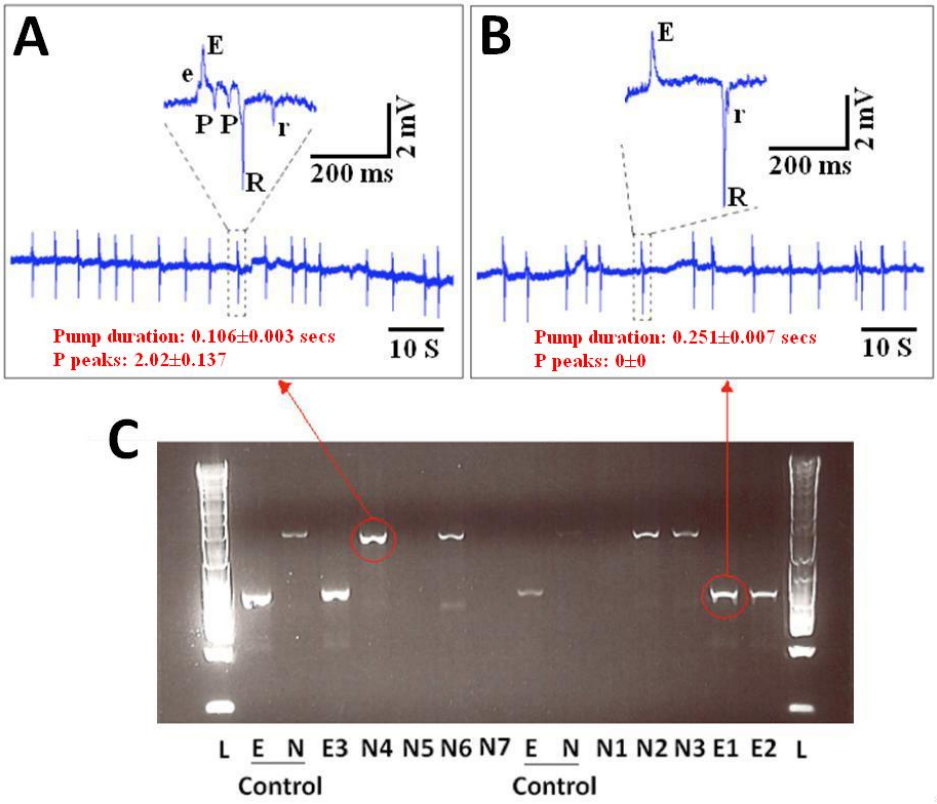

Figure 5.9: A population of wild-type worms was spiked the mutant *eat-4* (7 N2 wild-type plus 3 *eat-4*) and subjected to NeuroChip analysis to select the mutant worms. (A) Example of an EPG recording obtained from wild-type worm and (B) from the mutant eat-4(ky5). Note the longer pump duration and absence of P waves. (C) Matching the NeuroChip phenotype to the worm genotype by PCR. Genotyping was by PCR to amplify the *eat-4* locus and confirmed whether or not the worm carried the genomic deletion. 'E' and 'N' are the reference lanes for eat-4 and wild type, respectively. N1 – N7 are worms that were sorted as wild-type and E1-E3 are worms that were sorted as mutants from the NeuroChip, phenotyped as *eat-4*. In three of the samples identified as wild-type the PCR reaction failed (N1, N5 and N7), but in the remaining samples the PCR result confirms the phenotype assigned by the NeuroChip analysis. There were no false positive or false negative results. The red arrows indicate the corresponding PCR result for the two EPG traces shown in A and B.

When conducting the genetic screen described above the throughput was timed. In 1 hour 2 min, 15 worms were recorded (total time taken, from loading reservoir and adding first worm to the channel to release of the last worm). Of these, three were tail first and discarded; thus 12 EPGs were recorded in this time period. The rate-limiting step is the time required to record enough EPG waveforms in order to delineate a wild-type or mutant signature, up to 5 minutes depending on the pumping frequency. This experiment demonstrates an initial capability of a throughput of 12 worms per hour. This is a significant improvement on the conventional recording approach which is slower because of the need to make the suction tube, fill it, position it and manually capture the motile worm. A skilled operator employing the conventional approach would have a throughput maximum of about 2 to 4 recordings per hour.

5.5 Interrogating neural network properties with optogenetics

Optogenetics is a powerful approach for interrogating the function of neural networks. It deploys genetically encoded light sensitive ion channels to provide a means of remotely activating specific neural pathways by light [126] and has previously been used to activate neural pathways in *C. elegans* [127] including in the pharyngeal nervous system [128]. Whether NeuroChip could resolve optogenetic modulation of the neural network mediated via glutamatergic neurone activation was tested.

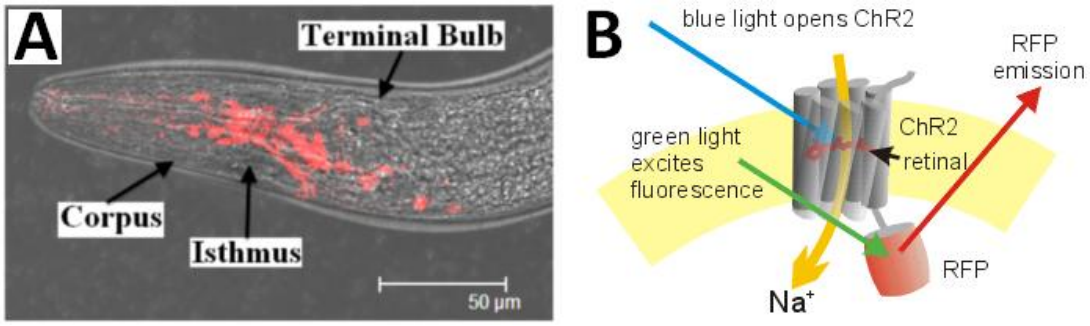

Figure 5.10: (A) Confocal image of an adult worm (L4 + 1 day; *peat-4::ChR-2;mRFP*). Red fluorescence reports the expression pattern of the light-activated channel ChR2 and shows expression in glutamate

neurones of the nervous system. *C. elegans* strain expressing the blue-light activated ion channel (470 nm) ChR2 in glutamate neurones was used (*peat-4::ChR2;mRFP*). (B) Scheme of ChR2-RFP fusion construct. The blue-light (470 nm) activates ChR2 that has been treated with retinal, the cofactor for ChR2 activation, allowing cations to enter through the ion channel. The green light excites the red fluorescence protein (RFP), leading to a RFP emission which is necessary for the visual inspection.

For this a transgenic strain of *C. elegans* stably expressing Channelrhodopsin2 (ChR2) exclusively in glutamate neurones (*peat-4::ChR2;mRFP*) was used (Figure 5.10A). The method (Appendix 11) is based on that previously described for expression of ChR2 in cholinergic neurones [128] (This work was done by colleagues from Professor Lindy Holden-Dye's group). A single integrated transgenic line expressing *peat-4::ChR2;mRFP* was used in the microfluidic experiments. ChR2 requires the cofactor retinal for light activation, thus prior to the experiment L4 worms were incubated overnight either off (control) or on retinal feeding plates as previously described [128].

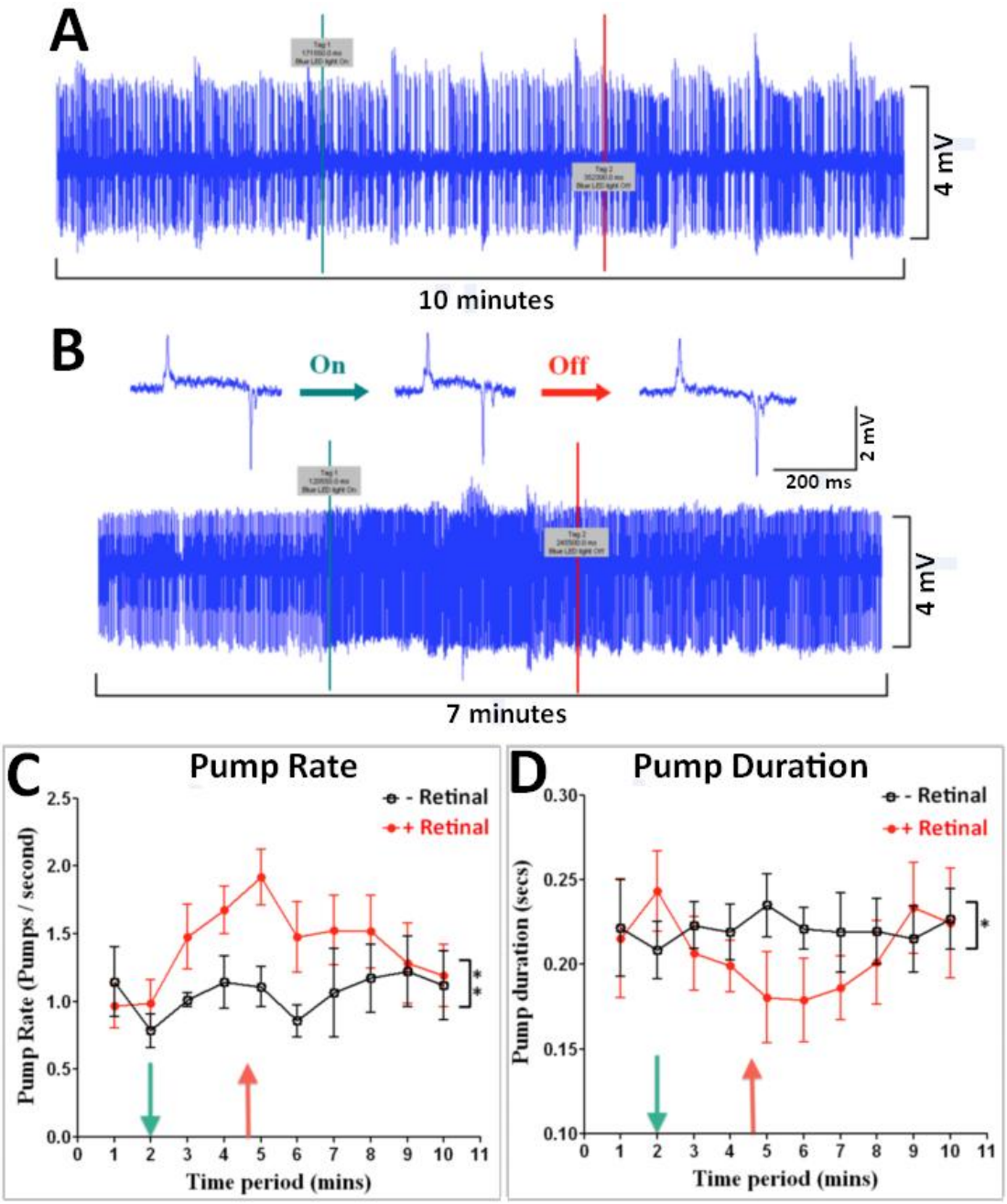

Figure 5.11: Interrogation of neural network properties with optogenetics. A *C. elegans* strain expressing the blue-light activated ion channel (470 nm) ChR2 in glutamate neurones was used (*peat-4::ChR2;mRFP*). NeuroChip recordings were made from these worms in the presence of 2 mM 5-HT. (A) Illumination (470nm) of worms that had not been treated with retinal, the cofactor for ChR2 activation had no effect on EPG recordings. Light on at 3 min (green line) and off at 6 min (red line). (B) EPG recording obtained from a retinal treated worm. Light on at 2 min (green line) and off at 4.5 min (red line). LED illumination increased the pump rate and decreased the pump

duration, which can be observed from single EPG traces (shown above). (C) Pump rate and (D) Pump duration in response to light activation with (red curve) and without (black curve) retinal. Data are the mean ± SEM; n= 4. Pump rate was significantly increased following light activation in the retinal treatment group ($P<0.001$; paired Student's t-test, 2 min compared to 6 min) and overall pump rate was higher in the retinal treatment group compared to control during light activation (two way ANOVA; $F=8.03$ $P=0.0298$ for the retinal treated group compared to control during light activation). Light activation significantly decreased pump duration in the retinal treatment group ($P<0.01$ paired Student's t-test, 2 min compared to 6 min) whilst there was no change in the control group ($P=0.2261$ paired Student's t-test, 2 min compared to 6 min).

Worms were subjected to light (470nm) illumination which was achieved using a narrow bandwidth ultra bright blue (470nM) LED (Maplin Electronics) as previously described [128] whilst capturing EPG signals. The LED was placed on the top of the trapping channel in contact with the chip. Individual worms were loaded into the microfluidic chamber with 2mM 5-HT to stimulate pharyngeal pumping. EPG signals were captured 2 minutes before, 2 minutes during and 2 minutes after LED illumination of the chamber. Control experiments were conducted in parallel in which the worms were not treated with retinal, the co-factor for ChR2 activation (Figure 5.10B). A selective light-dependent decrease in pump duration was observed in retinal treated worms but not in controls (Figure 5.11). This recapitulates an earlier study which used a photolysable 'caged' glutamate compound and observed a light-dependent decrease in pump duration [14]. The optogenetic approach in combination with the NeuroChip permitted capture of EPG signals over a long time course and thus also resolved a concomitant and sustained increase in pharyngeal frequency following light activation of *peat-4;ChR2;mRFP* (Fig. 9D). A neurobiological explanation of this observation is provided by previous studies which have demonstrated a key role for glutamate signalling in shortening the duration of the pharyngeal contraction-relaxation cycle in the presence of 5-HT [82]. This suggests that optogenetic activation of glutamate signalling in the presence of 5-HT may act to shorten the contraction-relaxation cycle thus permitting the

pharynx to pump at a faster rate. An alternative or additional explanation is that glutamate may be directly excitatory to the pharynx and this is supported by observations of glutamate-dependent depolarisation of pharyngeal muscle from intracellular recordings [129].

5.6 Comparison with another 'EPG chip'

A microfluidic device for whole-animal chemical screens using non-invasive electrophysiological readouts of neuromuscular function in the *C. elegans* has been developed recently in 2012 [125]. It has a one layer structure, containing eight recording modules (Figure 5.12A) for taking EPG signals from multiple worms at the same time. A tree-like architecture provides equal flow distribution into each of the recording modules. A population of nematodes were injected into the device with the flow of Dent's saline. Open channels had continuous flow through until they were occupied by a worm. Worms were captured by a gradual narrowing channel (Figure 5.12B, C), just big enough to fit the worm's head. Once the worm is trapped, the flow is diverted into the side-arm channel which is also used to flow the drug. Stainless steel tubes were inserted into the worm electrode ports and the inlet/reference port, acting as the working electrodes for electrical recordings. They were connected to eight differential amplifiers, enabling eight EPG recordings to be acquired from eight different nematodes simultaneously. EPG signals, associated with the pharyngeal pumping, were observed (Figure 5.12D). They have clear 'E' and 'R' spikes, which is similar to the waveforms collected from conventional method.

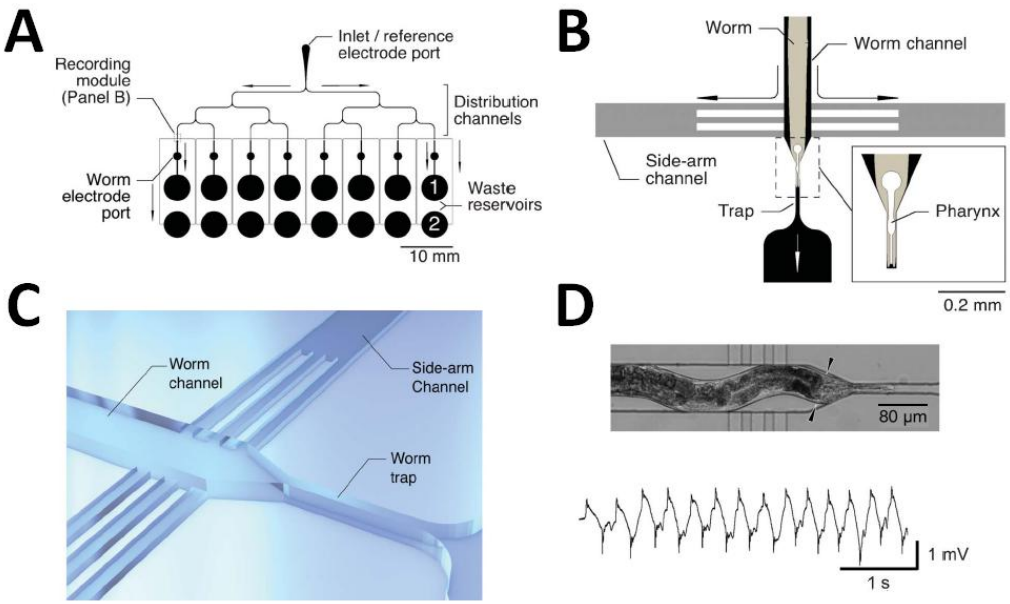

Figure 5.12: Shawn Lockery's microfluidic design for recording EPGs. (A) Overall design of the microfluidic device. Eight recording modules are placed in parallel to trap worms from one inlet port at the same time. (B) Top view of a single recording module. The inset shows the funnel-shaped entrance to the worm trap and position of the head of the worm in the trap under headfirst recording conditions. Colour indicates feature height (black, 50 mm; grey, 10 mm). (C) Three dimensional rendering of the recording module. (D) Micrograph of the recording module and the associated EPG recording with the syringe pump turned on, forcing the worm's head into the trap. Pictures are adopted from [125].

The anthelmintic ivermectin was used to demonstrate drug perfusion in the microfluidic device. Ivermectin inhibits pharyngeal muscles and extra-pharyngeal neurons by activating a class of glutamate-gated chloride ion channels [130]. 3 µM ivermectin rapidly blocked EPG activity in wild type worms (Figure 5.13A), regardless of the orientation of the worm heading into the trap. The tree-like distribution allows 6 single drug diffusion experiments to be performed at the same time, giving comparable results (Figure 5.13A). If the concentration of the drug increased to 10 µM, changes in EPG waveform and pump frequency are easy to be observed from the recordings within 50 minutes (Figure 5.13B).

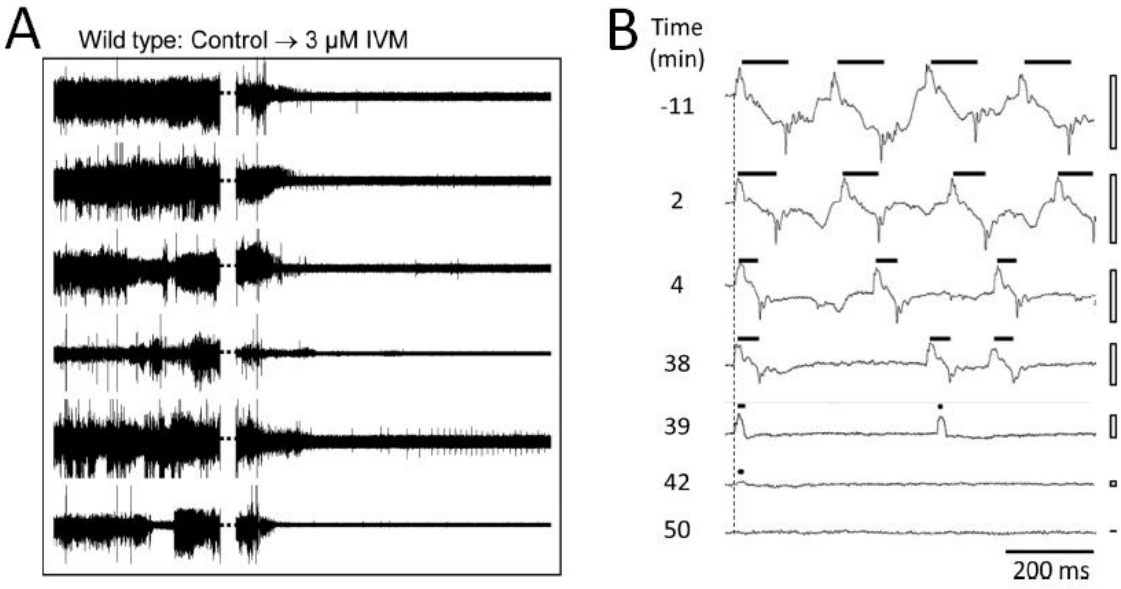

Figure 5.13: Ivermectin (IVM) effects on wild-type *C. elegans* and changes in EPG waveform and frequency. (A) 3 μM ivermectin blocked the EPG activities rapidly in wild-type worms. Six recordings were collected from a single microfluidic device. (B) Changes in EPG waveform and frequency. After applying 10 μM ivermectin, the pump frequency and pump duration kept dropping, and at 50 minute, they were gone. Pictures are adopted from [125].

Parallelization gives this device medium throughput for drug screening tests, providing a means to examine gross drug effects on the rate of pharyngeal pumping. However, this device lacks the detail of the EPG recorded from the head, thus it cannot be used to resolve the activity of different neural components of the pharyngeal circuit. The differences between the two microfluidic designs for electrophysiological analysis of *C. elegans* are listed in Table 4.

Table 4: Differences between Shawn Lockery's device and the NeuroChip.

	S. Lockery's Device	**NeuroChip**
Layout	Single layer (Figure 5.12)	Double layers (Figure 4.3)
Throughput	8 channels in parallel. 8 individual worms are pushed into the trap at a time.	Single channel with several bypass channels, enabling analyzing worms one after another under control of microfluidic valves.
Electrode	Stainless steel tubes insert into the channel.	Embedded Platinum electrode.
Waveform of EPG Signal (Within 10 mM 5HT)	Amplitude is small and cannot detect P spikes. Signal is filtered with a low-pass cutoff of 1Hz and a high-pass cutoff of 1 kHz, and further conditioned by a 60 Hz notch filter.	Amplitude is as big as that obtained from conventional approach, and the waveform is similar with all functional spikes. No filtering is required.
Real-time Observation	Worm head is squeezed into the trap. It is hard to observe the real time pharyngeal pumping under the microscope.	The pharynx can be clearly seen even it is in the trap, so that the correlation between the pharyngeal pumping and the EPG signal can be observed.
N2 Basal recording	n/a	High quality and similar to that collected with conventional method.

Released Worm	n/a	Worm is healthy and producing as usual.
Drug delivery	Need to unplug basal syringe and then put in drug syringe to apply the drug.	Drug flow is precisely controlled by the micro-valves through the drug port.
Mutant Sorting	n/a	Easy to distinguish the difference of waveform between N2 and eat-4. Also suitable for other mutants.
Reuse the chip	Did not mention how to unload worm. Not sure if it is reusable.	Worm can be unloaded and the chip is reusable.
Smaller nematode	n/a	Easy to be modified for smaller animals.

5.7 Conclusions

This chapter describes an important development in the experimental approach as it opens the way for a precise definition of neuroactive compounds and mutations with synaptic phenotypes. The properties of the EPG waveform recorded during basal activity with either the conventional method or with NeuroChip were very similar with the exception that the device resolved more 'P' waves per pharyngeal contraction-relaxation cycle, or 'pump' (Table 2). Recordings were also highly reproducible between worms conferring advantage for the detection of discrete electrophysiological phenotypes. The activity of the pharyngeal circuit is regulated by a plethora of neurotransmitter receptors and channels which represent major targets for human medicines and anthelmintic drugs and through which toxic drug side effects may also occur [131]. Thus NeuroChip has applications in chemical biology and toxicology screens. The principle that NeuroChip can be used for selecting mutant worms from a wild-type population on the basis of the electrophysiological signature has been demonstrated. Furthermore viable

worms can be recovered following recordings, both of which are important properties if this platform is to be utilised for mutagenesis screens. Also, a feature which permits very rapid drug application has been designed which optimises the device for chemical screens. Currently the throughput is 12 worms per hour. However as Lockery et al demonstrate [125] it is possible to incorporate at least 8 channels on a single chip and thus the throughput could readily be increased to ~100 worms per hour. NeuroChip also has application in pharmacokinetic studies as it provides the opportunity to precisely capture the time-course of drug response and the ability to make comparisons on different genetic backgrounds which have modified susceptibility to drugs or chemicals e.g. drug transporter mutants. Such insight is useful particularly with respect to the emergence of drug resistance in parasitic nematodes the mechanisms of which may involve mutations affecting drug transport [132].

Chapter 6: Modified NeuroChip for Smaller Nematodes

Microfluidic devices for electrophysiological analysis of adult *C. elegans* have been successfully developed [2, 125]. These devices measure the activity of a neural microcircuit in the worm that drives pharyngeal muscle contraction and thus feeding behaviour. They have many advantages over conventional methods: easier manipulation, less drug usage, and higher throughput, providing a new tool for research on gene function, drug screening, and mutant sorting. So far, no microfluidic chip has been published for electrophysiological studies on smaller species of nematodes but this would be of great utility in analysis of feeding in this economically and medically important phylum and furthermore have potential applications in antiparasitic drug discovery. In this chapter, microfluidic platforms for electrophysiological analysis of larva 2 (L2) stage *C. elegans*, and plant parasitic nematode *Globodera pallida (G. pallida)* will be demonstrated.

6.1 EPGs from second stage larvae (L2) *C. elegans*

Size is the key for this microfluidic chip design. Without an optimized trapping channel size for capturing the worm's head, the electrophysiological recordings are of poor quality and cannot deliver key information about neural function or drug effects. Compared to young adult *C. elegans*, the L2 stage worm has a much smaller body size (~400 μm in length, ~20 μm in diameter) (Figure 6.1), making it more difficult to manipulate it in a conventional way. L2 stage worms were obtained by putting some adults in the culture plate 29 hours before the experiment.

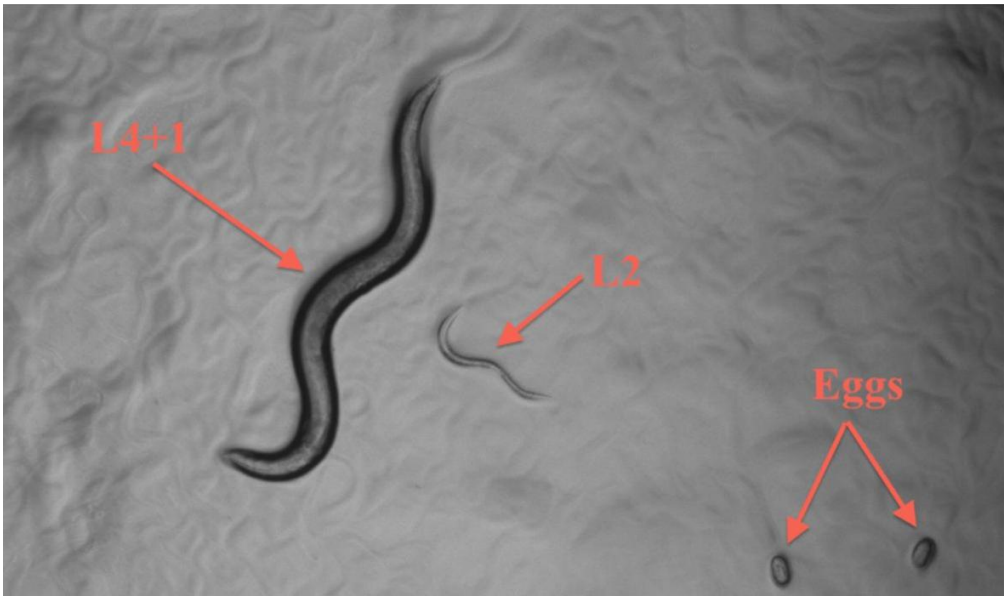

Figure 6.1: Comparison of the size between the young adult (L4+1) and L2 stage *C. elegans*. Adult worms are between 1110-1150 μm whilst L2 are 360-380 μm in length [133].

6.1.1 Two-photon polymerization

Based on the design of NeuroChip, the aperture of the trapping channel was decreased to accommodate L2 larva stage *C. elegans*. Ordinarily, a quartz mask is used to make small geometries, less than 20 μm, and high quality features can be fabricated by using this kind of mask. But a quartz mask is quite expensive (around £500) and usually takes nearly one month from designing to obtaining it. Besides, the best shape for a trap is semi-circular, which could not be easily fabricated by using standard photolithography for such small dimension. Alternatively, a technology called two-photon polymerization [134-136] may be used.

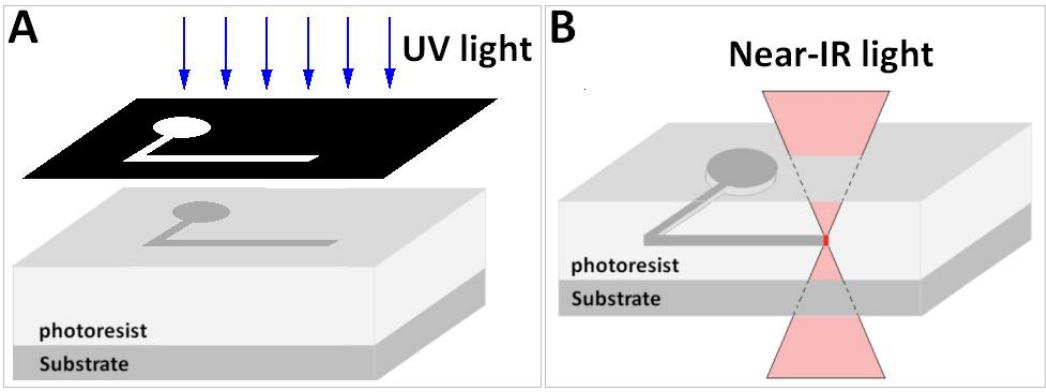

Figure 6.2: Two approaches for polymerization of photoresist. (A) UV lithography. UV light is applied from the top of the photosensitive material, producing pseudo-3D structures through the mask. (B) Two-photon polymerization. 3D structures are directly written inside the photoresist by a pulsed near-IR laser.

Unlike UV lithography (Figure 6.2A) which uses flood UV (365 nm wavelength) exposure through a mask, two-photon polymerization employs a pulsed ultrashort near-infrared (IR) laser with a wavelength of around 780 nm. Based on two-photon absorption [137], when the near-IR light is focused inside the photoresist, the spatial density of the photons is high at the focal point causing the resist to be polymerized. Each initiator, which usually absorbs a UV photon, absorbs two near-IR photons at the same time and becomes a radical when the spatial density of the near-IR photons is high (Figure 6.2B). Because the photoresist is transparent to near-IR light, the structures that are out-of-focus do not attenuate the laser beam [134]. Very precise localization of laser energy in time and space allows fabrication of any computer-generated 3-D structure by direct laser writing into a volume of photosensitive material [136]. With two-photon polymerization, miniaturised structures ranging from hundreds of nanometres to several micrometres of different irregular shapes can be made in one day, from design to product.

6.1.2 Fabrication of modified chip for L2 stage *C. elegans*

6.1.2.1 3D lithography with Nanoscribe

The "Nanoscribe" (Nanoscribe GmbH, Germany) [138] that uses two-photon polymerization was used to fabricate the modified chip for L2 stage *C. elegans*. Figure 6.3 shows the procedure to fabricate a master with 3D structure. A 3 dimensional model of the design is first generated by a Computer-aided design (CAD) application, in Standard Tessellation Language (STL) file format, which contains a triangular surface tessellation of the original 3D solid model. The data from the STL file is then read and sliced into 2D layers by intersecting the 3D solid with a series of parallel planes by software called Nanoslicer. For each plane, Nanoslicer computes the intersection contours of the solid with the plane and subsequently fills each obtained contour with a line hatch. Finally, the computed slicing contours as well as the hatched layers are saved as General Writing Language (GWL) files that are suitable for loading into the working interface NanoWrite [139].

Figure 6.3: The procedure (three steps) for fabricating a 3D structure with Nanoscibe. First, the 3D structure of interest is designed by a Computer-aided design (CAD) application and exported as a Standard Tessellation Language (STL) file format. The Nanoslicer tool then reads the STL files and produces a General Writing Language (GWL) output files which are then loaded into NanoWrite to drive the direct laser writing of the structure. Picture is adopted from [139].

The system consists of a computer with dedicated software, laser controlling interface, fibre laser, inverted microscope, CCD (charge-coupled device)

camera, acousto-optic modulator (AOM), and piezoelectric 3D scanning stage (Figure 6.4).

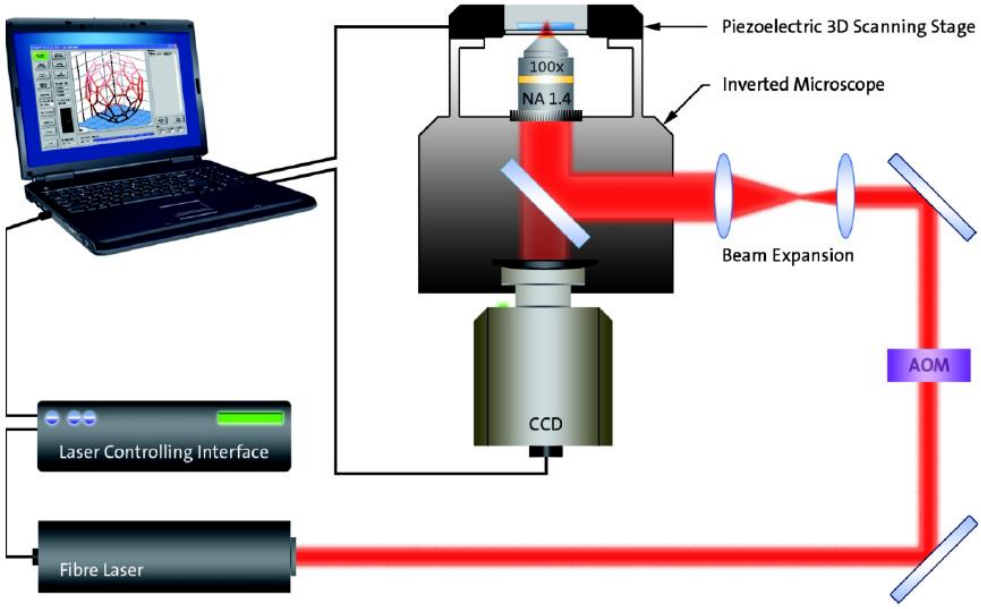

Figure 6.4: Schematic of the two-photon polymerization with Nanoscribe. Picture is adopted from [139].

SolidWorks is used to build the 3D model of the modified trapping channel. A large design like NeuroChip can take days to be built. To save time, only the trapping channel was made with the Nanoscribe, whilst the rest of the device was fabricated in the conventional way (Figure 6.5). The Nanoscribe has the ability to directly write irregular shaped structures in photoresist, giving a trapping channel with semicircular shape (Figure 6.5A), which is the perfect geometry for capturing the worm's head. After measuring the size of the L2 worms and after several attempts at capturing, a trapping channel with size of 12-8×21 μm (left width-right width×length) was made. The height of the trap is 9.5 μm and the depth of the flow channel is 25 μm which is slightly bigger than the diameter of L2 worm's body, allowing the worm to swim in the chip.

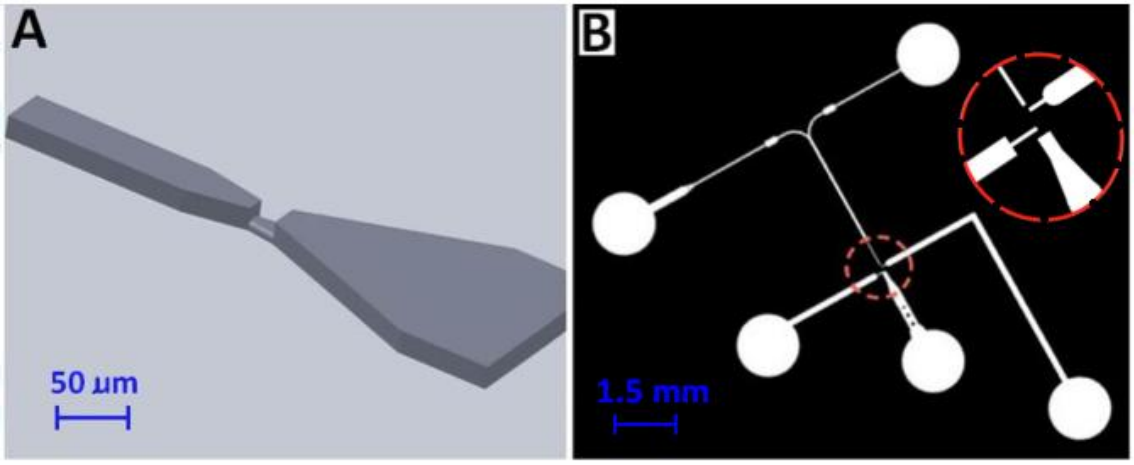

Figure 6.5: Designs a microfluidic device for smaller *C. elegans*. (A) 3D model of the modified trapping channel for L2 stage *C. elegans*. The round shape is designed in the model since it can be directly written by the Nanoscribe, aiming for a better seal for worms. (B) Mask design for the modified NeuroChip without the trapping channel. Standard photolithography is used to fabricate the large channels.

Nanoslicer (Figure 6.6) is the slicing software that comes with the Nanoscribe. It was used to read the STL file and convert it into two GWL files: the Contour file and the Solid file. This conversion process requires the computation of a sequence of laser trajectories that will fill up the complete volume enclosed by the 3D solid object [139]. The Contour file contains all slicing contours, defining only the surface of the 3D structure through a collection of closed curves. Writing this file yields a hollow shell. The Solid file contains all hatch lines from all intersection planes. It fills the bulk volume of the 3D structure with a layer-by-layer arrangement of parallel straight lines. Writing this file yields a fully solidified structure [139]. The slice distance and hatch (line) distance are quite important for the resolution of the final structure. The smaller the slice and hatch distance, the higher the resolution, but the longer the built time.

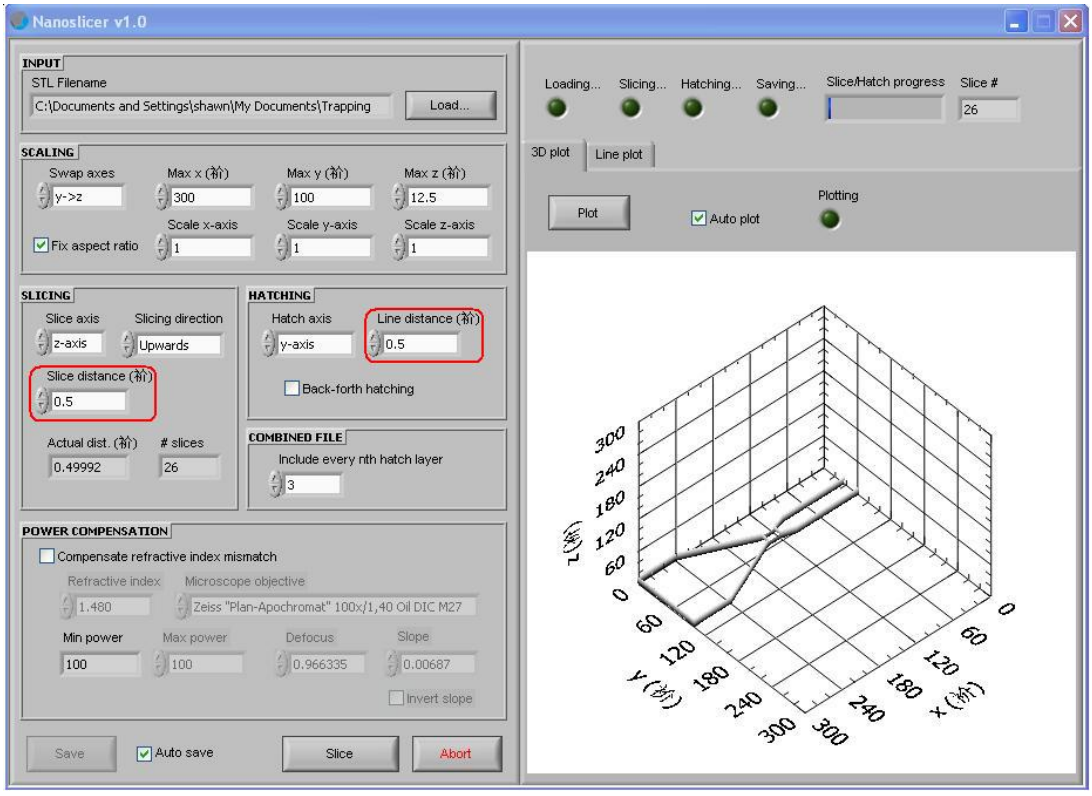

Figure 6.6: Application main window of the Nanoslicer. The Slice distance sets the desired distance between two adjacent intersection planes. The Line distance sets the distance between neighbouring hatch lines in each intersection plane. They are two important parameters for deciding the resolution of the final master.

The custom text editor DeScribe that comes with Nanoscribe was used for authoring GWL files. The code written in DeScribe includes the laser power, the scan speed, the position of structure to be built, and the interface to be focused on et al (Figure 6.7). The parameters defined here are important to the resolution and size of the final structure. The Contour and Solid gwl files converted by the Nanoslicer are also included in the code.

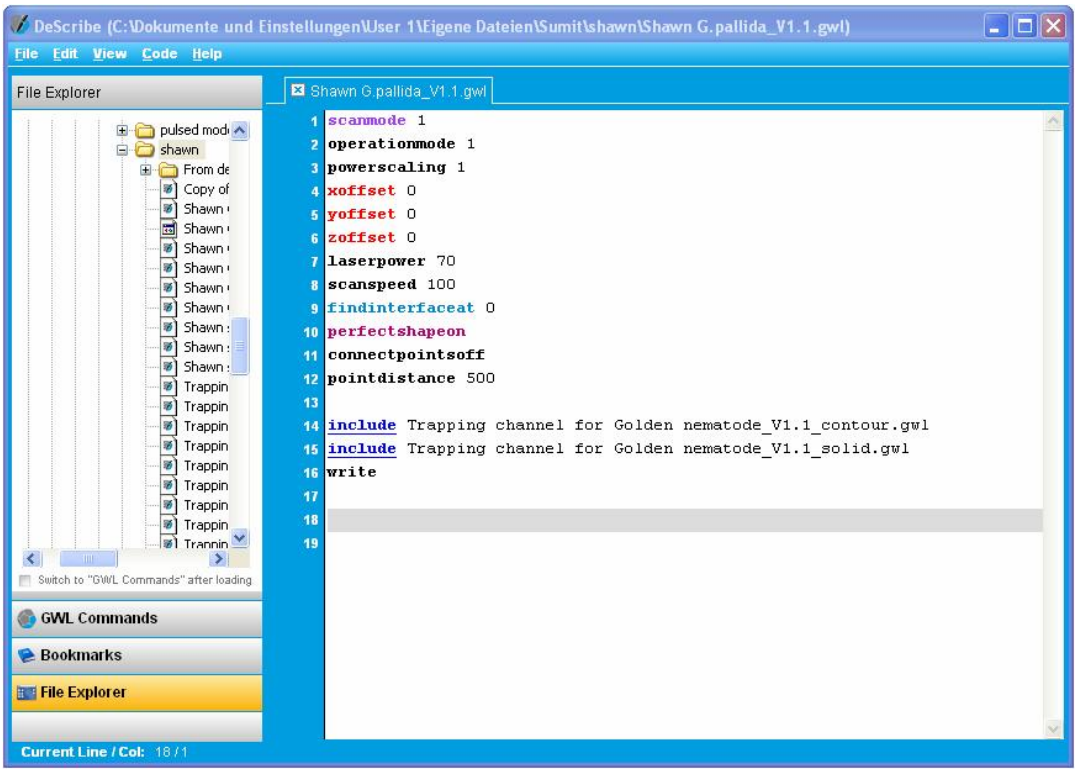

Figure 6.7: Application main window of the DeScribe. The laser power, scan speed, focus position et al. are defined with this software.

The Nanowrite (the user interface) (Figure 6.8) is the last step for 3D writing. In this step, the microscope objective is selected, the interface for writing is found, and the code written in DeScribe is loaded. After loading the final code, the structure is visualized in the graph view of NanoWrite and an estimated writing time for the structure is displayed (Figure 6.8 and 6.9). Start DLW triggers the writing.

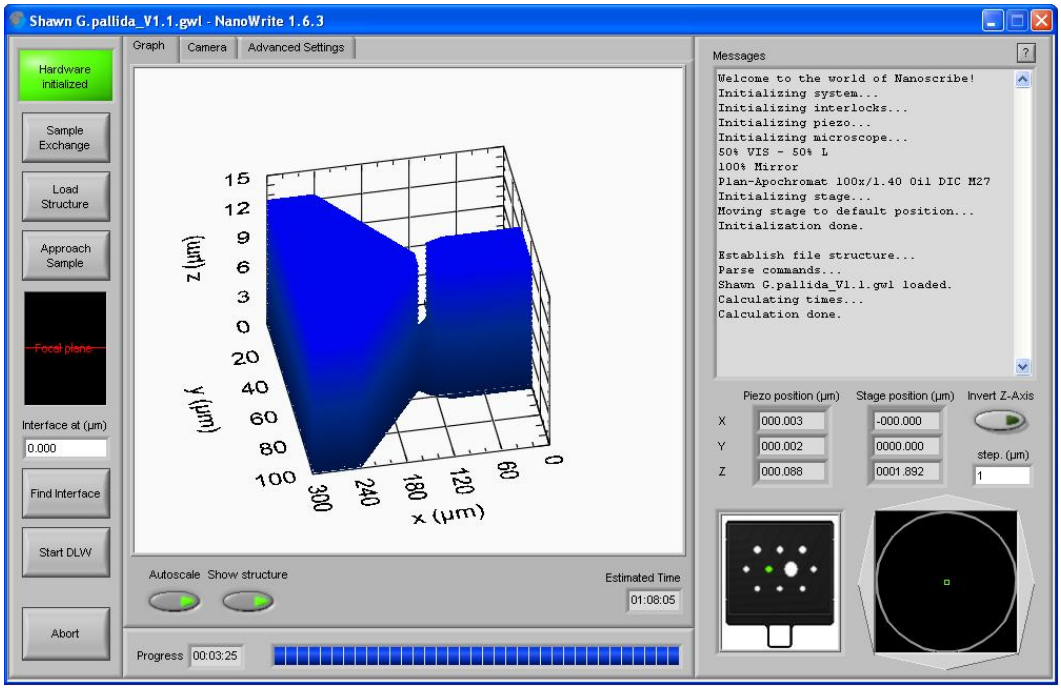

Figure 6.8: Application main window of the Nanowrite with loaded structure for L2 stage *C. elegans*.

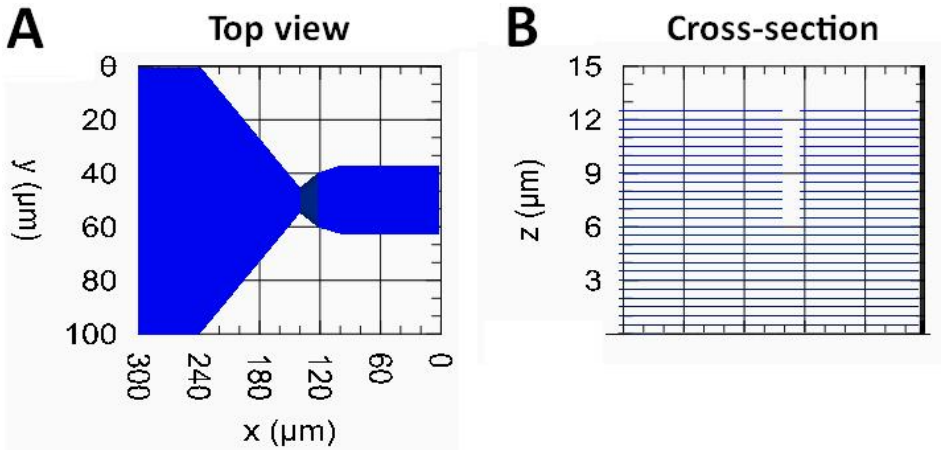

Figure 6.9: The structure visualized in graph view of NanoWrite. (A) Top view of the structure. Dimensions of the structure can be clearly seen in the view. (B) Cross-section of the structure, showing the numbers and distances of the slices as well as the height of the design.

6.1.2.2 Results of 3D lithography

The resolution of two-photon polymerization depends on several factors, which are laser power, scan speed, slice and hash distance, and the numerical aperture (NA) of the objective lens [140].

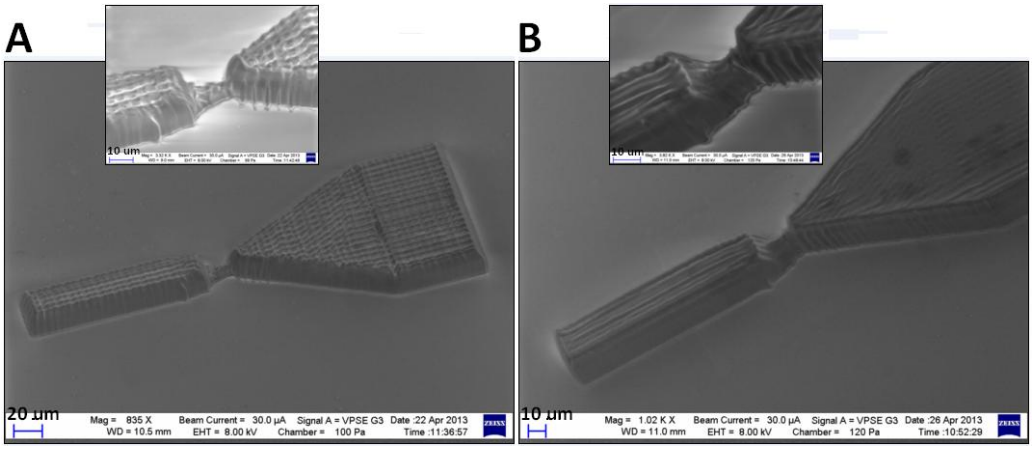

Figure 6.10: Comparison of resolution after reducing the hatch distance by half. (A) SEM image of the SU8 trapping channel for L2 stage C. elegans written with 50% laser power (10 mW), 200 µm/s scan speed, 0.5 µm slice distance, 1 µm hatch distance, and 20× objective in around 1 hour. Zoomed view of the trap is inset. (B) SEM image of the trapping channel written with the same parameters but 0.5 µm hatch distance. Zoomed view of the trap is inset.

The following parameters were used: 50% laser power (10 mW), 200 µm/s scan speed, 0.5 µm slice distance, 1 µm hatch distance, and 20× objective. This took approximately 1 hour to write the structure, but with poor resolution (Figure 6.10A). “Net” patterns can be observed on the surface of the channel, indicating that the hatch distance was bigger than required. The hatch distance was decreased by half to improve the surface roughness. The result therefore is improved (Figure 6.10B) but the process time is increased to 2 hours.

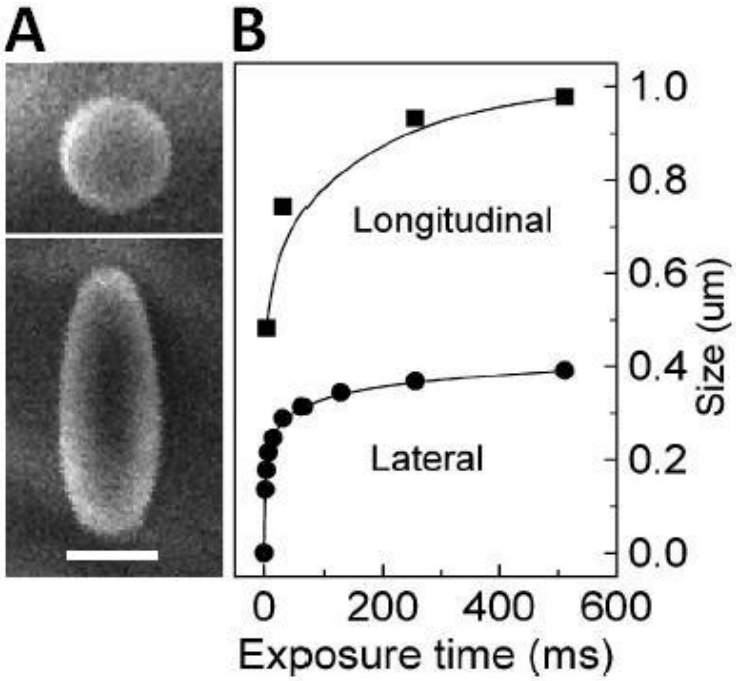

Figure 6.11: Isolated complete voxel, the 3D image of the two photon excitation focal spot. (A) SEM images of the top and lateral of a focal spot. Scale bar: 1 μm. (B) Exposure time-dependent voxel size. Pictures are adapted from [141].

The surface is still not as smooth as that obtained with standard photolithography. The numerical aperture (NA) of the objective lens plays an important role in the quality of the polymerization. High-NA objectives guarantee small focal spots and the best resolution. The 20× objective has a low magnification and NA of 0.5, used for writing very large structures. For small features, the 100× objective with NA of 1.4 gives a better result. In general, the smaller the NA, the larger the working distance and the larger the voxel. Therefore the focal spots which reflect the voxel (photopolymerization of a volume pixel) is essential for the resolution [141]. Instead of a round spot, it resembles a spinning ellipsoid (Figure 6.11). The length-to-width ratio, which is also known as elongation factor [141] of the ellipsoid is quite different between the 20× (more than 10) and 100× (2.4) objectives. The voxels are very elongated resulting in very high polymerized volumes even with one single shot or line [139]. With 100× objective, a high resolution trapping channel was written (Figure 6.12), but it took more than 20 hours.

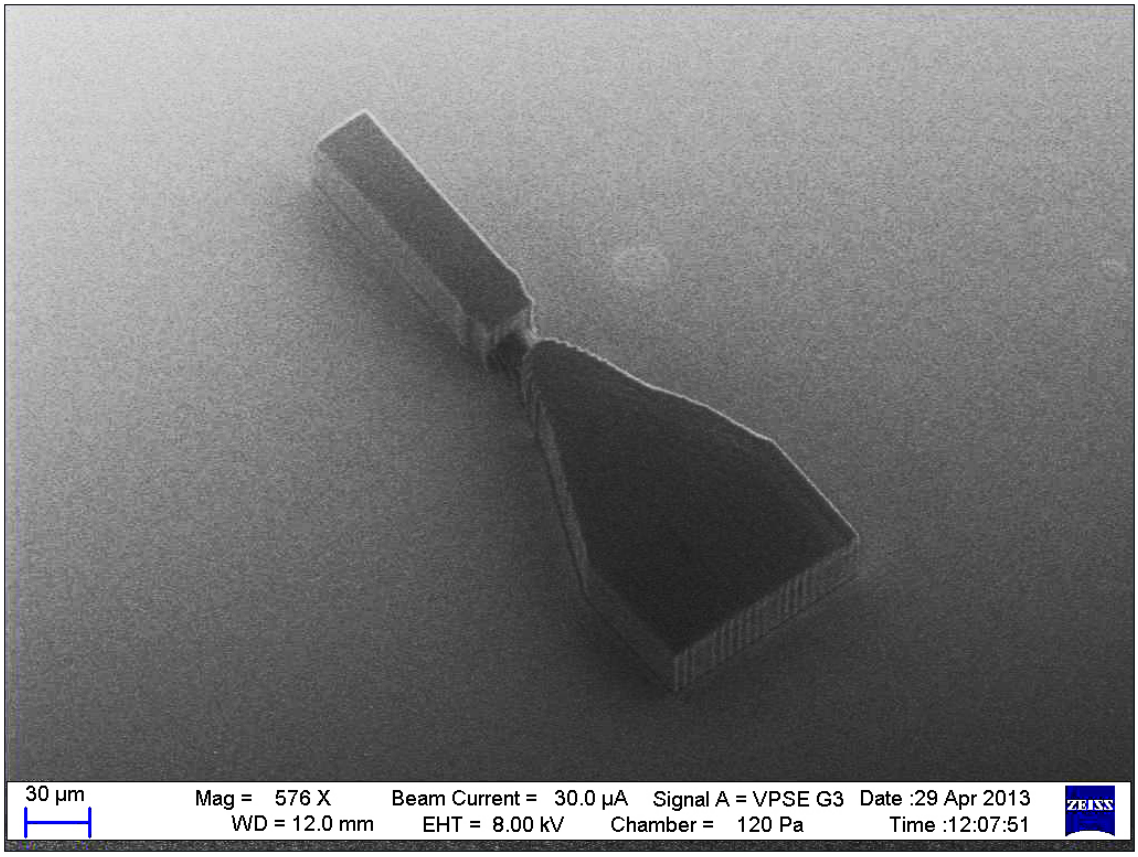

Figure 6.12: SEM image of the trapping channel written with 100× objective.

The elongation factor leads to another issue, which is the thickness written by the laser. Before starting writing in Nanowrite, the interface for focusing had to be found. For pre-spin coated negative photoresist SU8, two interfaces were recognised (Figure 6.13) which are the glass-resist and resist-air interfaces. Nanoscribe uses a bottom-up writing principle, so that the glass-resist interface was focused on initially. The 20× objective has an elongation factor of more than 10 depending on the laser power and exposure time, leading to an unpredictable larger thickness.

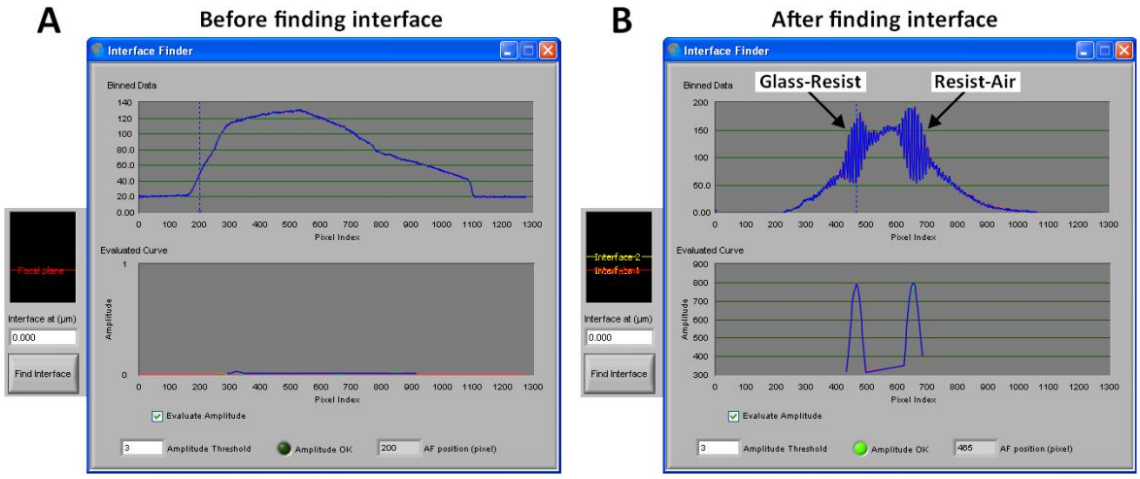

Figure 6.13: The interface for focusing is found before writing. (A) Before finding the interface. (B) After finding the interface. Two interfaces were found for SU8 photoresist. One is the glass to resist interface and the other is the resist to air interface.

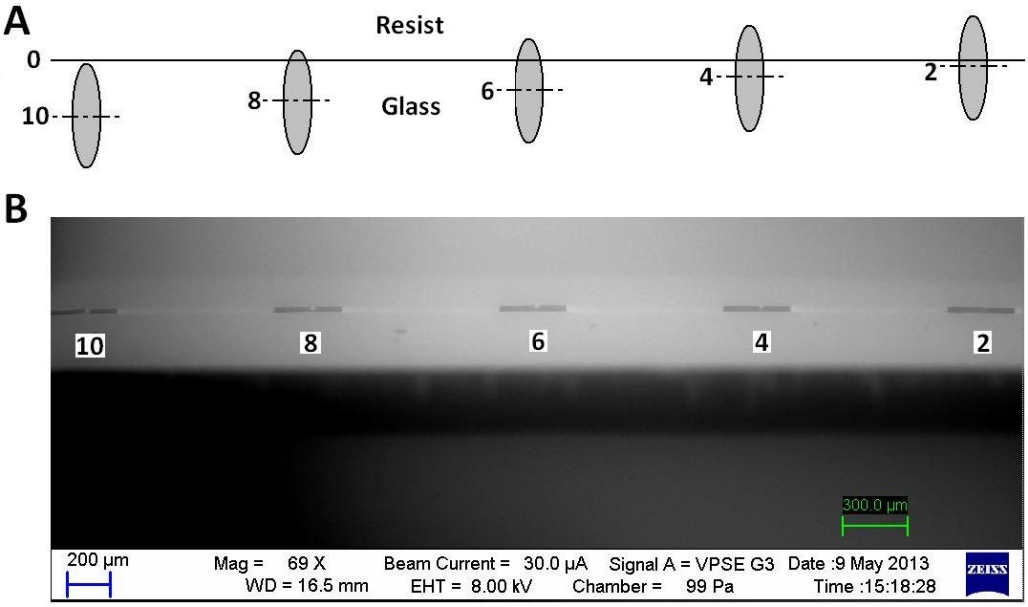

Figure 6.14: Different initial writing interfaces gives different trap thickness. (A) Schematic of the voxel position for different interfaces from 2 to 10. Interface 0 indicates the glass-resist interface. Every increase in numerical 2 stands for 2 µm below the glass-resist interface. (B) SEM images of patterns with different initial writing interfaces that were polymerised on a single chip.

Patterns with different initial writing interfaces were polymerised on a single chip (Figure 6.14) to investigate the best thickness for trapping the L2 stage *C. elegans*. Interface 0 indicates the glass to resist interface, and the larger the number, the lower the focal spot. In total, 6 different interfaces (Figure 6.14A) were investigated, giving 6 different thickness traps (Figure 6.14B).

After several attempts, Interface 8 was considered to be the best interface for L2 stage *C. elegans*, giving a trap thickness of 9.5 µm (Figure 6.15).

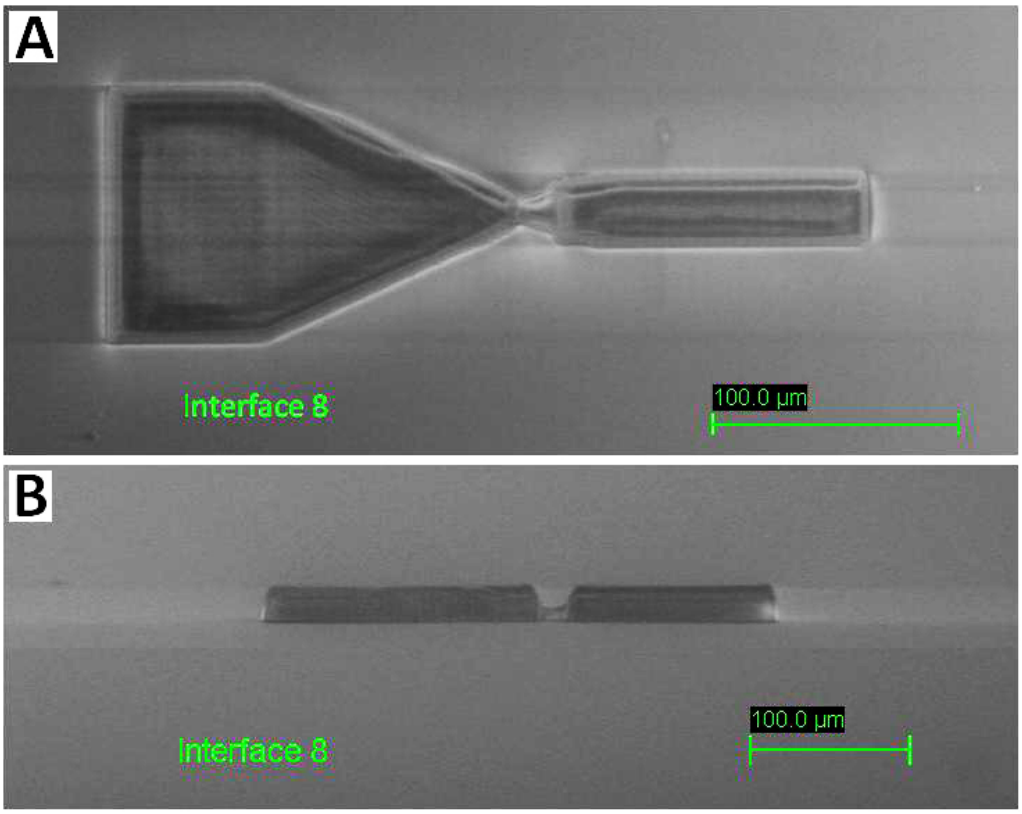

Figure 6.15: SEM images of the trapping channel master with an interface 8 µm below the glass-resist interface. (A) TOP view. (B) Cross-section.

Interestingly, different writing interfaces give different surface roughness. Interface 0 produced the smoothest surface while Interface 10 generated the worst (Figure 6.16). The reason could be that during the writing process with Interface 0, the focal spot moves up to write the structure and finally moves beyond the pre-spin coated photoresist, leaving a smooth surface.

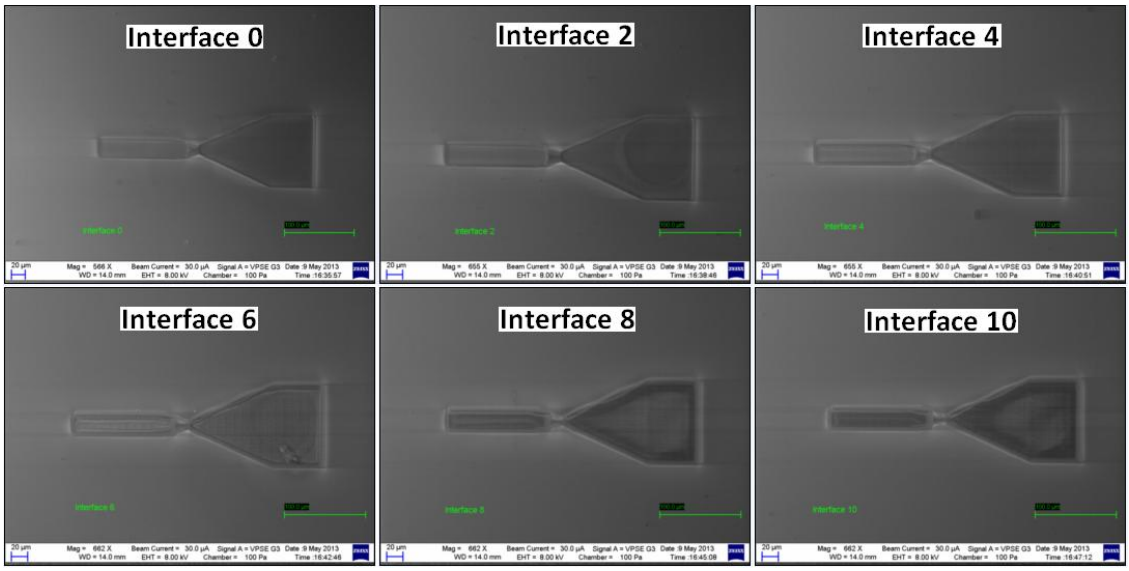

Figure 6.16: Top view of 6 trapping channels written by Nanoscribe with different interfaces, showing that Interface 0 has the best surface roughness while Interface 10 has the worst.

By increasing the thickness of the trapping channel, but maintaining the thickness of the trap, a trapping channel master with the desired thickness, as well as a smooth surface was obtained. The remainder of the flow channels were fabricated (Figure 6.17A) by standard photolithography with an acetate film mask as shown in Figure 6.4B. The procedure is: (1) take the substrate that has been written out of the Nanoscribe; (2) bake it at 65 ºC for 30 seconds to make the trapping channel visible; (3) manually align the acetate film mask onto the substrate under the microscope or do the alignment with mask aligner; (4) bake it at 65 ºC for 1 minute and at 95 ºC for 3 minutes; (5) develop it and N_2 dry. Although the connection area was exposed twice (Figure 6.17B), the pre-spin coated photoresist provides uniform thickness all over the substrate. The microfluidic chip was then fabricated following standard lithography as described in chapter 3.

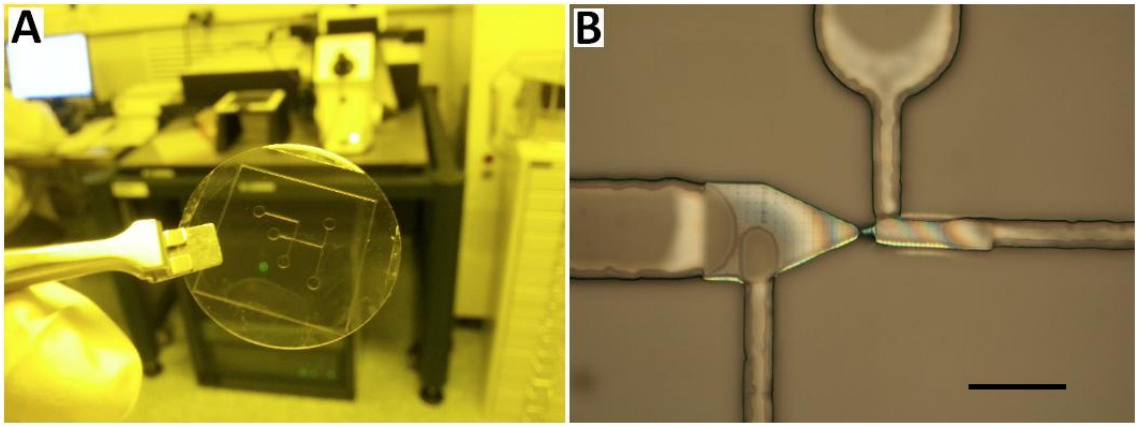

Figure 6.17: SU8 master fabricated by two-photon polymerization combined with standard photolithography. (A) Photogragh of a completed SU8 substrate after adding on the rest flow channels. (B) Close-up view of the trapping channel. Overlapped parts from double exposure of the trapping region and the rest flow channels are visible but have uniform thickness. Scale bar: 100 μm.

6.1.3 EPGs from L2 stage *C. elegans*

The trap with size of 8-12×20 μm (9.5 μm thick) was used in the EPG experiment (Figure 6.18) for *L2 C. elegans*, operated with the same procedure as for L4+1 worm. There is no obvious difference between the waveforms obtained from young adult and L2 worms except the amplitude, which is greater in adult compared to larvae. All functional spikes correlating to muscles and neurons were observed clearly from the EPG waveform (Figure 6.18).

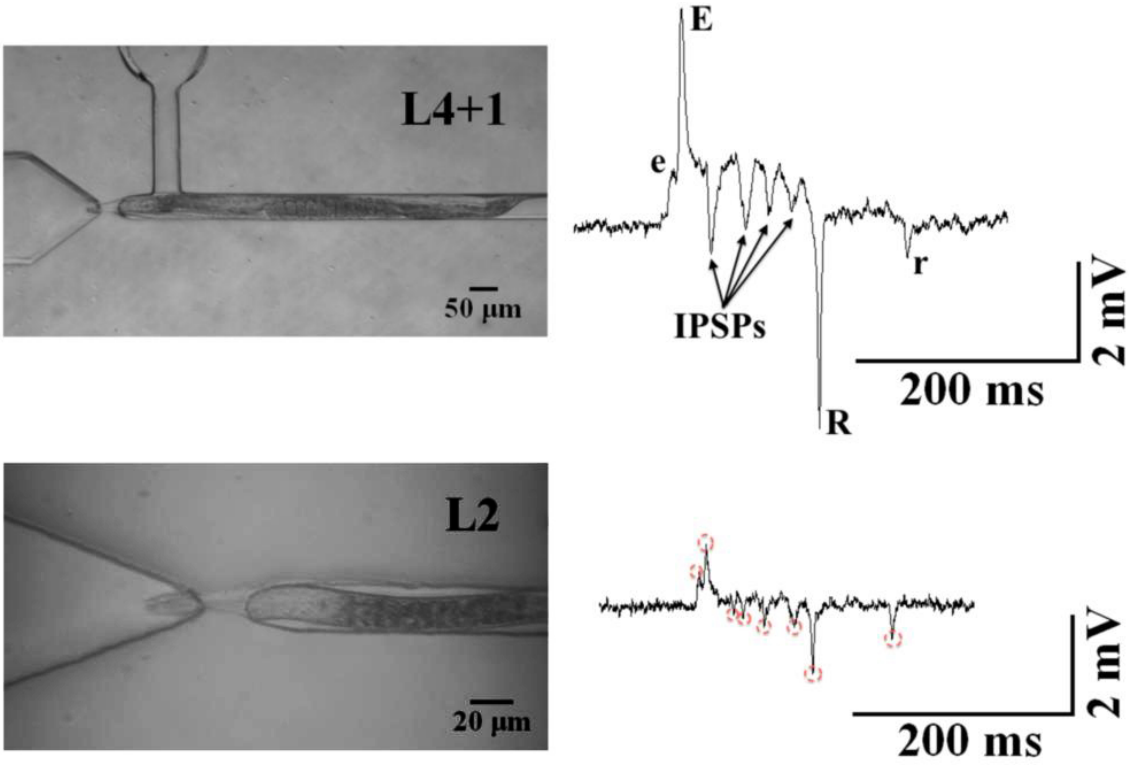

Figure 6.18: Comparison of the trapped images and EPG waveforms collected from young adult (L4+1) and L2 *C. elegans* on-chip. All functional spikes correlated to muscles and neurons were observed clearly from the EPG waveform obtained from the L2 worm.

Videos were taken of both the trapped pumping nematode and ongoing EPG signals synchronously. By analyzing the video on a frame by frame basis, the correlation between the pharyngeal pumping and signal formation was revealed (Figure 6.19). The contraction of pharyngeal muscle triggers a big positive spike and the relaxation leads to a big negative spike.

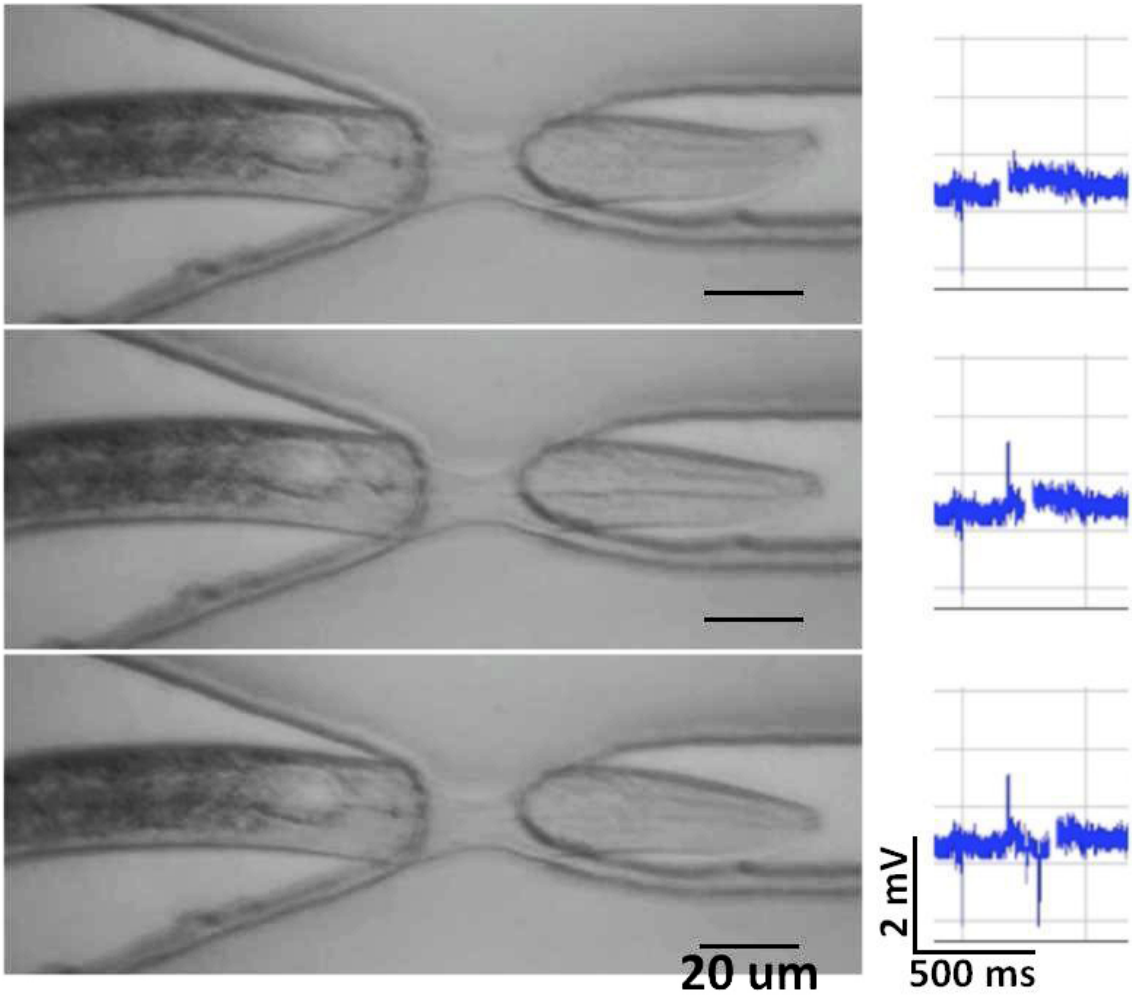

Figure 6.19: Video frames reveal the correlation between the pharyngeal pumping and the EPG waveform. The contraction of pharyngeal muscle triggers a big positive spike and the relaxation leads to a big negative spike. (Scale bar: 20 μm)

5-HT (serotonin) is a known activator of *C. elegans* feeding behaviour [122]. Our analysis reveals that the pump frequency of L4+1 *C. elegans* exposed to 10 mM 5-HT was the same as that of the L2 stage worm exposed to concentration of 2 mM 5-HT (Figure 6.20) suggesting that the larvae may be more sensitive to this neurohormonal stimulus. Further pharmacological studies are required to investigate this.

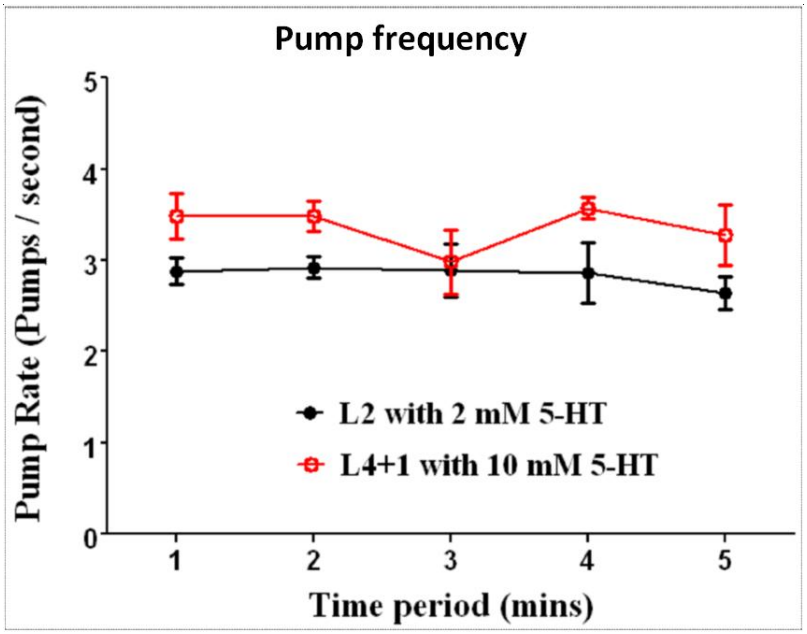

Figure 6.20: Comparison of the pump frequency collected from L4+1(3.43±0.15) and L2 (2.84±0.05) *C. elegans* on-chip. (Mean±s.e.m; n=5)

As demonstrated for L2 stage *C. elegans*, the design can readily be modified to accommodate other developmental stages of *C. elegans*, and opens the way for a discrete analysis of age-dependent pharyngeal function. This illustrates that the chamber could also be modified to trap parasitic species of nematode which are otherwise too small to study easily with conventional approaches, and permit a higher throughput analysis of these species.

6.2 EPGs from plant parasitic nematode *Globodera pallida*

EPGs have been successfully collected from L2 stage *C. elegans* with the modified microfluidic chip. Subsequently, this device was modified to record from the plant parasitic nematode *Globodera pallida* (*G. pallida*), the second-stage juveniles (J2), which has a similar size to L2 *C. elegans* (Figure 6.21).

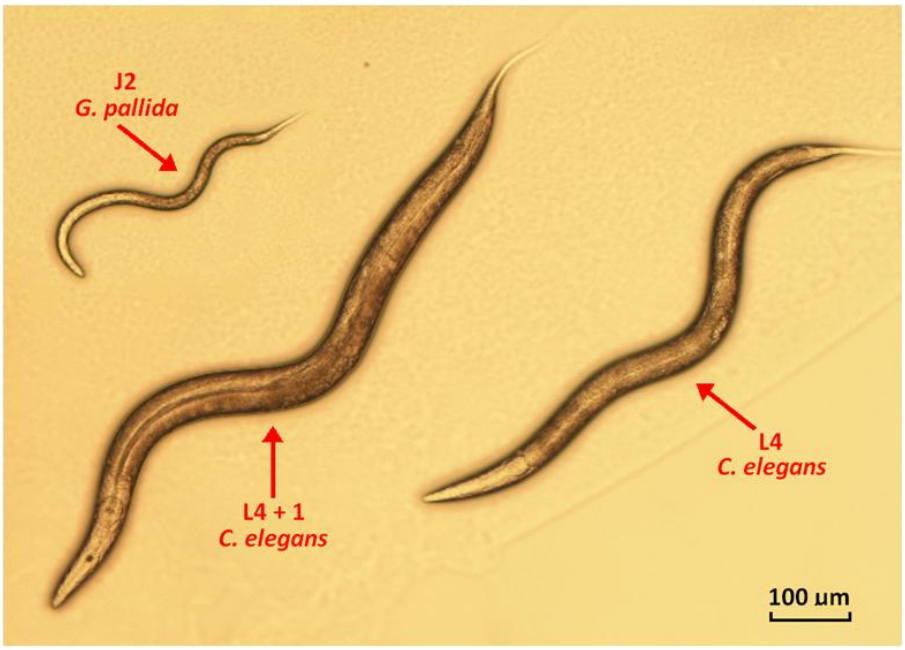

Figure 6.21: Micrographic image shows the difference of the dimensions of the young adult *C. elegans*, L4 *C. elegans* and J2 *G. pallida*.

6.2.1 The plant parasitic nematode *Globodera pallida*

Globodera pallida, commonly known as white potato cyst nematode, is a plant pathogenic nematode. It is a pest of plants in the family solanaceae, primarily infesting potatoes and tomatoes, as well as a variety of other root crops [142].

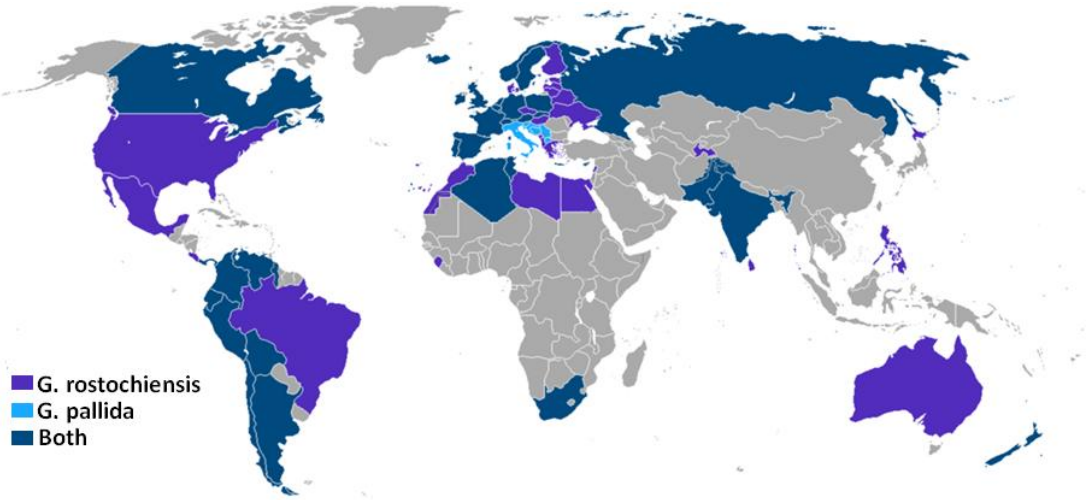

Figure 6.22: Geographical Distribution of the Potato Cyst Nematodes (PCN) distribute over the globe. Picture is adapted from [143].

Together with its close relative *Globodera rostochiensis (G. rostochiensis)*, the Potato Cyst Nematodes (PCN) is distributed over the globe from temperature zones down to sea level to the tropics at high altitudes (Figure 6.22).

Second-stage juveniles hatch, under stimulus from host root exudates, from eggs within cysts in the soil, and invade the roots (Figure 6.23). Each individual nematode feeds on a group of cells in the pericycle, cortex or endodermis, transforming them into a syncytium or transfer cell [142]. After another two stage juveniles, the nematode is mature, and the females die when they are fully mature, turning their skins to cysts to protect the eggs within. Cysts can remain infective for many years in the absence of solanaceous hosts [144-146]. In fact, 65% of U.K. potato land is infected by the *G. rostochiensis* and *G. pallida* and the latter is present at 92% of these sites [147].

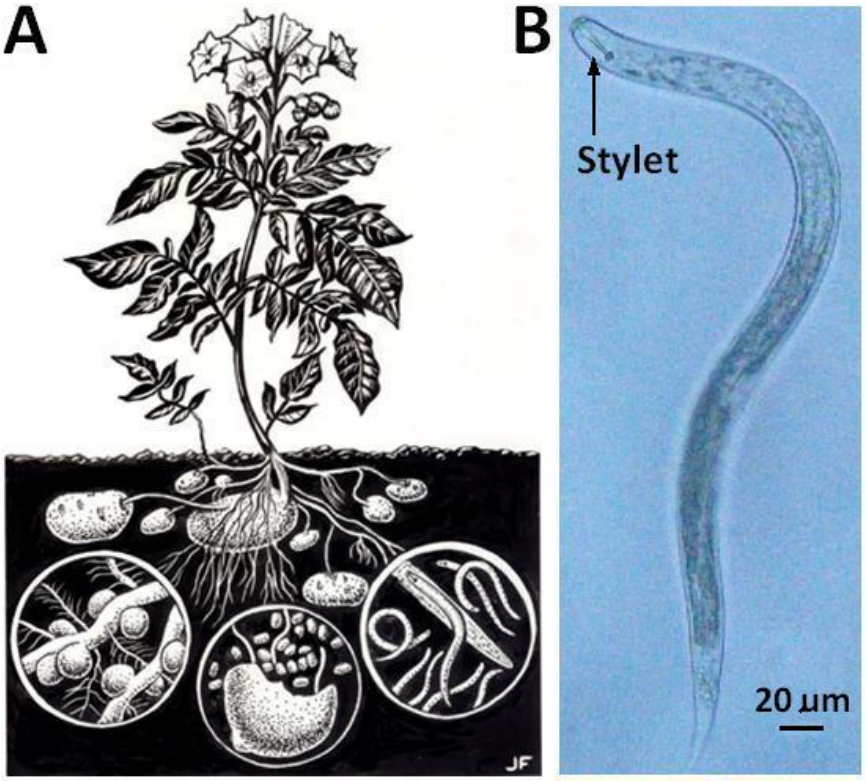

Figure 6.23: The process of J2 *G. pallida* invading the potato root. (A) Illustration of J2 *G. pallida* invading the potato root. (B) Micrographic image of a J2 *G. pallida*. Thrusting movement of the stylet helps the nematode to pierce into the root. Picture A is adopted from [17].

PCN impose an annual cost in excess of £50 million on the United Kingdom. Effective control of *G. pallida* is an essential requirement to maintain the competitiveness of U.K. potato production. Natural parasites and biological control are being studied in order to identify natural agents for potato cyst nematode control, without needing to use the toxic chemicals currently in use. But at present, no solution can be used to control the infection efficiently [142].

6.2.2 Electrophysiological recordings from the nematode *G. pallida*

Recordings from the pharyngeal-stylet system of PCN may provide a route to understand how they invade the host plant and to screen chemicals that interrupt this process.

6.2.2.1 Reported EPGs research on *Globodera*

In 2001, Rolfe and Perry [148] published their research on EPG analysis of stylet protractor muscle activity of J2 *Globodera rostochiensis* (Figure 6.24A), in response to different concentrations of the neurotransmitter serotonin (5-HT). They correlated the EPG with stylet protrusion and retraction using video analysis (Figure 6.24B). This is the first and only published article that describes EPG recordings obtained from the potato cyst nematode with conventional EPG method.

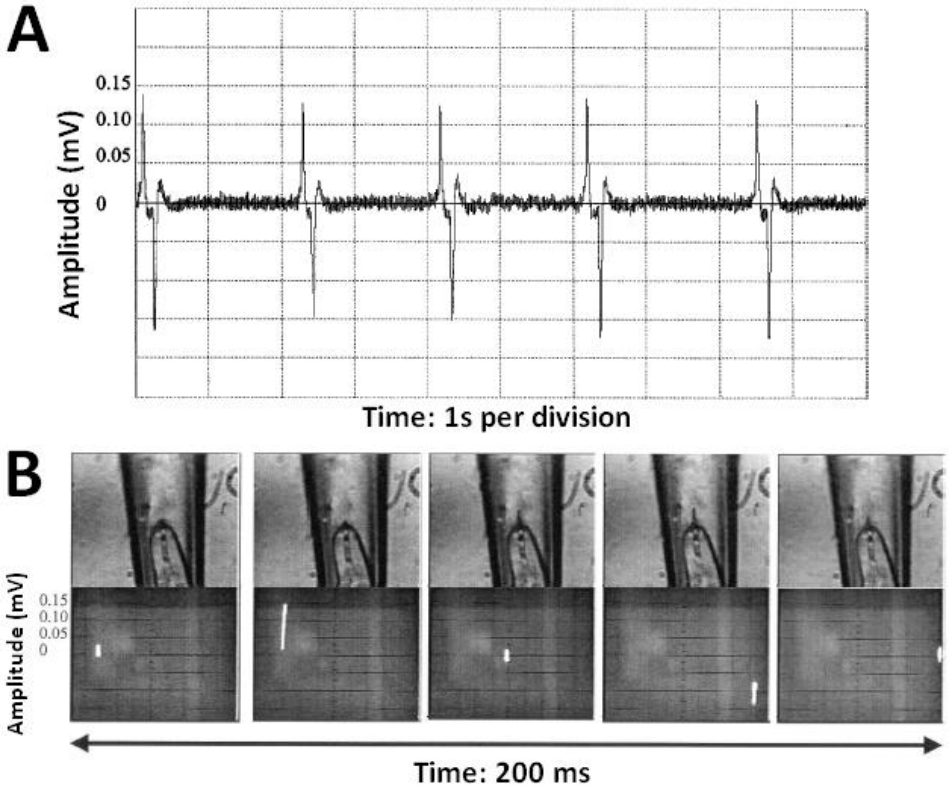

Figure 6.24: Previously reported EPG recording obtained with conventional method. (A) Electropharyngeograms showing five successive contractions and relaxations of stylet protractor muscles of J2 *G. rostochiensis* in response to 10 mg/ml serotonin. (B) Five frames (rate 25 frames per second) showing one wave of protractor muscle electrical activity (a positive spike, a period at resting potential and a negative spike) and associated stylet activity of a J2 *G. rostochiensis* stimulated with 10 mg/ml serotonin. The positive spike (frame 2) indicates protractor muscle contraction with the stylet being extended 20-40 ms afterwards (frame 3). The negative spike (frame 4) indicates relaxation of the protractor muscle with stylet retraction following (frame 5). Picture is adopted from [148].

For EPG recording, individual J2 *G. rostochiensis* was transferred to a recording petri dish, and then the anterior of the nematode was sucked into the suction tube. Under a consistent suction, the nematode was kept in the trap and EPG signals obtained. Control experiments were done by putting only artificial tap water (ATW), indicating that ATW alone did not cause stylet thrusting of J2 *G. rostochiensis*. The electrical activity in response to serotonin is classical as

observed in *C. elegans*. It consists of three components, a positive spike, followed by a period at resting potential, and finally a negative spike (Figure 6.24A) [148]. In order to better understand the correlation between muscular activity and the EPG signal, a two-camera system [148] was used. The stylet activity and electrical activity were filmed individually at the same time. The signals recorded from the two cameras were combined together, showing that the EPG signals were correlated with stylet motions (Figure 6.24B). Therefore, EPG is a good means to determine stylet thrustings.

6.2.2.2 EPGs collected from *G. pallida* with modified NeuroChip

A trap with size of 8-12×20 μm (9.5 μm thick) was used for the EPG experiment (Figure 6.18) for the J2 *G. pallida,* since it has a similar size to the L2 *C. elegans*. However, the J2 *G. pallida* could not even squeeze into a trap of this size. As shown in Figure 6.25A, unlike the tapering shape of the *C. elegans* head, the plant nematode has a round head. Although these two species have similar body dimensions, the J2 *G. pallida* has a bigger head than the L2 *C. elegans*. After several attempts, it was found that a trap with size 10-15×20 μm (11 μm thick) can capture the plant nematode. Also because of its round head, only half the head was captured in the trap (first picture in Figure 6.25B) and no EPG signal was detected. To find the best geometry for capturing the round head of J2 *G. pallida*, three different shape designs were used (Figure 6.25B). The design with a bigger front than back (second picture in Figure 6.25B) was chosen for best performance, with a size of 15-10×20 μm (11 μm thick).

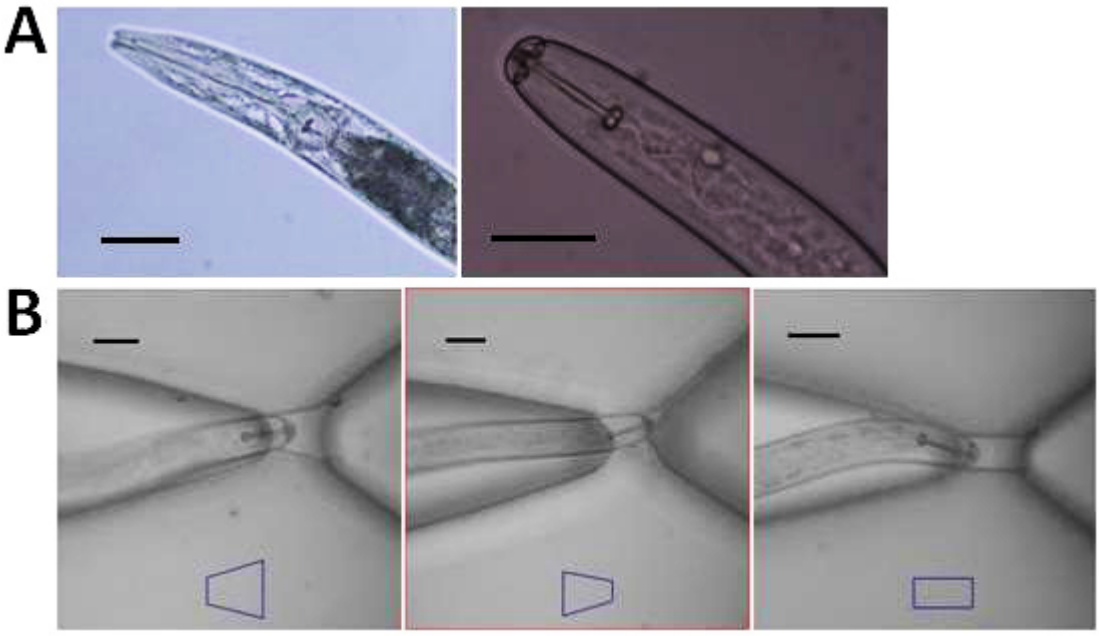

Figure 6.25: Several trap shapes were tested to find the best shape for capturing the anterior of J2 *G. pallida*. (A) Anterior of the L2 *C. elegans* and J2 *G. pallida* imaged with Differential Interference Contrast (DIC) microscopy. Unlike the tapering shape of *C. elegans*, the plant nematode has a round head, making it difficult to capture in the trap. Scale bar: 20 μm. (B) Three different shaped designs for the trapping channel. The one with best performance for trapping the nematode is in the middle marked with red square. Scale bar: 20 μm.

Following the experimental procedure of collecting EPG signals from L2 *C. elegans*, the electrical activity correlating to the stylet thrusting was obtained (Figure 6.26). The J2 *G. pallida* was trapped by its head (Figure 6.26A) at the beginning. 2 mM 5-HT was applied to stimulate stylet thrusting. The electrical activity was detected and correlated to stylet motion, but with very small amplitude (Figure 6.26A). Interestingly, when the nematode was trapped on the body, large EPG signals were obtained (Figure 6.26B). One possible explanation is that when the worm's head is captured in the trapping channel, the movement of stylet thrusting might be restricted due to the tight seal. Experiments were undertaken by trapping the nematode at different body positions, giving similar signal waveforms and amplitudes (~ 1 mV).

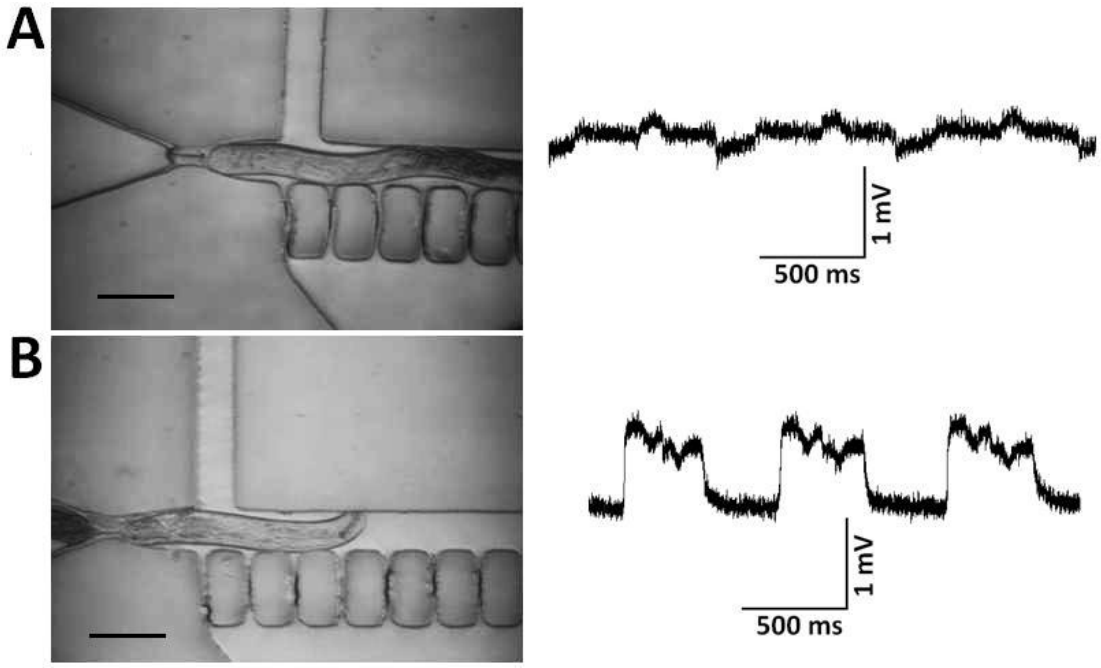

Figure 6.26: Different trapping position of J2 *G. pallida* generate EPG signal with different amplitude (in the presence of 2 mM 5-HT). (A) A plant nematode that was captured by its head in the modified NeuroChip, and the correlated electrical activity. (B) A plant nematode that was captured by its body in the modified NeuroChip, and the correlated electrical activity. The amplitude of EPG signal obtained from the trapped body is much larger than that from the trapped head. Scale bar: 50 μm.

Control experiments were done using only Dent's saline, showing that Dent's saline alone did not cause stylet thrusting as deduced by Rolfe and Perry [148] In 2001. Unexpectedly, the EPG signal collected from the trapped J2 *G. pallida* with the modified NeuroChip in the presence of 2 mM 5-HT did not contain negative spikes (Figure 6.27C). Figure 6.27 shows a comparison of the EPG signal waveforms adopted from L4+1 *C. elegans* with NeuroChip, J2 *G. rostochiensis* measured with the conventional method [148], and J2 *G. pallida* with the modified NeuroChip. The EPGs obtained from *G. rostochiensis* has similar waveform to *C. elegans*, containing one positive spike, several spikes at rest potential, and one negative spike (Figure 6.27A, B). However the feeding system of the two species is totally different. *C. elegans* mainly depends on pharyngeal muscle contraction and relaxation, and excitation of a pharyngeal

muscle causes a pulse flow out of the mouth resulting a positive spike in the EPG; relaxation of the muscle leads to a negative spike. *G. pallida* relays on stylet thrusting controlled by the stylet protractor muscles. These muscles control the stylet protrusion so as ingestion of food through the stylet. The relaxation of the protractor muscle leads to tension in the alimentary tube, resulting in retraction of the stylet [148]. *G. rostochiensis* and *G. pallida* are close relatives, which means their EPG waveforms are expected to be similar. However, the waveform taken from the *G. pallida* on chip consists only of one positive spike with several peaks (Figure 6.27C).

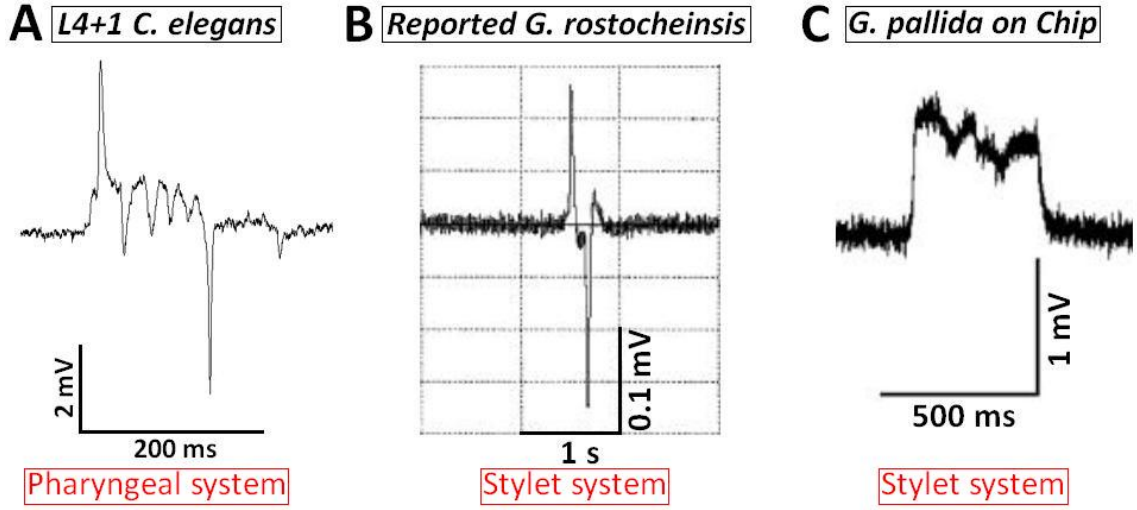

Figure 6.27: Comparison of EPG waveforms from L4+1 *C. elegans*, J2 *G. rostochiensis* [148], and J2 *G. pallida* on chip. (A) A typical single EPG waveform obtained from a trapped L4+1 *C. elegans* on NeuroChip. (B) A single EPG waveform taken from a trapped J2 *G. rostochiensis* with the conventional method [148]. (C) A single EPG waveform collected from a trapped J2 *G. pallida* on modified NeuroChip. No negative spikes were observed.

Although *G. rostochiensis* and *G. pallida* are two different species, their stylet system and feeding behaviour are basically the same. The difference between the published EPG waveforms of *G. rostochiensis* and the electrical signals of *G. pallida* obtained from the modified NeuroChip makes it difficult to understand the correlation between electrical activity and stylet motion. Besides the missing negative spike, there is a further difference between the published EPG signals and the modified NeuroChip, namely the amplitude. Rolfe and Perry

demonstrated an EPG trace with peak-to-peak amplitude of ~ 0.3 mV, while the EPG signal obtained by the modified NeuroChip has ~ 1 mV amplitude and 0.2 to 0.3 mV background noise (Figure 6.27B, C). Their EPG traces might have been optimised by filtering to remove the background noise, which may have altered the waveform. The microfluidic chip itself could be the reason for the difference, as the plant nematode might not behave normally in the chip. Therefore conventional EPG recordings were obtained to investigate this. Figure 6.28A shows an EPG trace obtained with conventional method in the presence of 2 mM 5-HT. This is similar to that collected from the modified NeuroChip (Figure 6.28B), indicating that the microfluidic chip did not affect the EPG signal waveform.

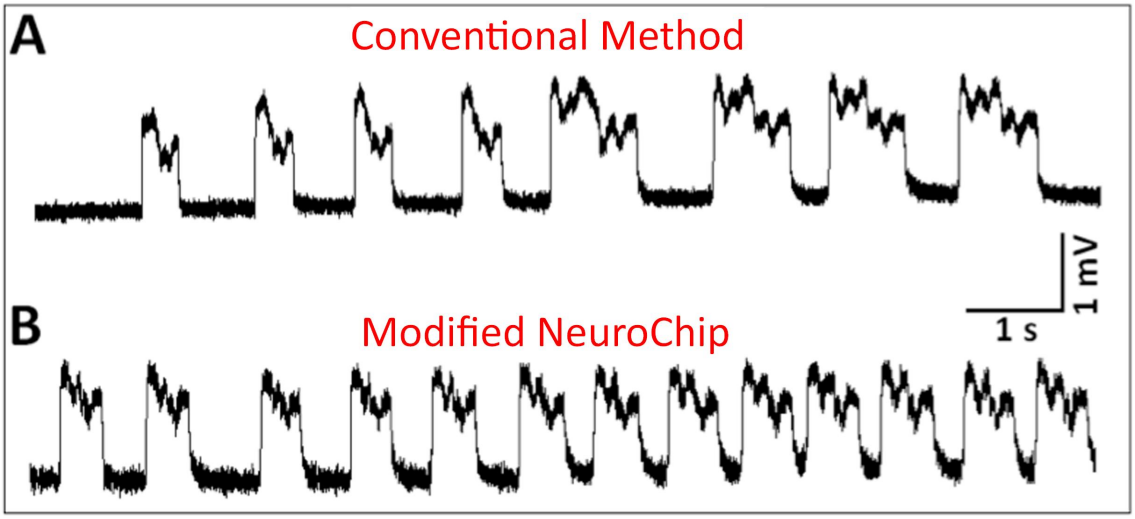

Figure 6.28: Comparison of EPG signals from J2 *G. pallida*, taken with the conventional method and the modified NeuroChip. (A) An EPG trace obtained from trapped J2 *G. pallida* with the conventional method. (B) An EPG trace obtained from trapped J2 *G. pallida* with the modified NeuroChip. Both traces have similar waveform shapes with the absence of negative spikes, and have amplitudes of ~ 1 mV.

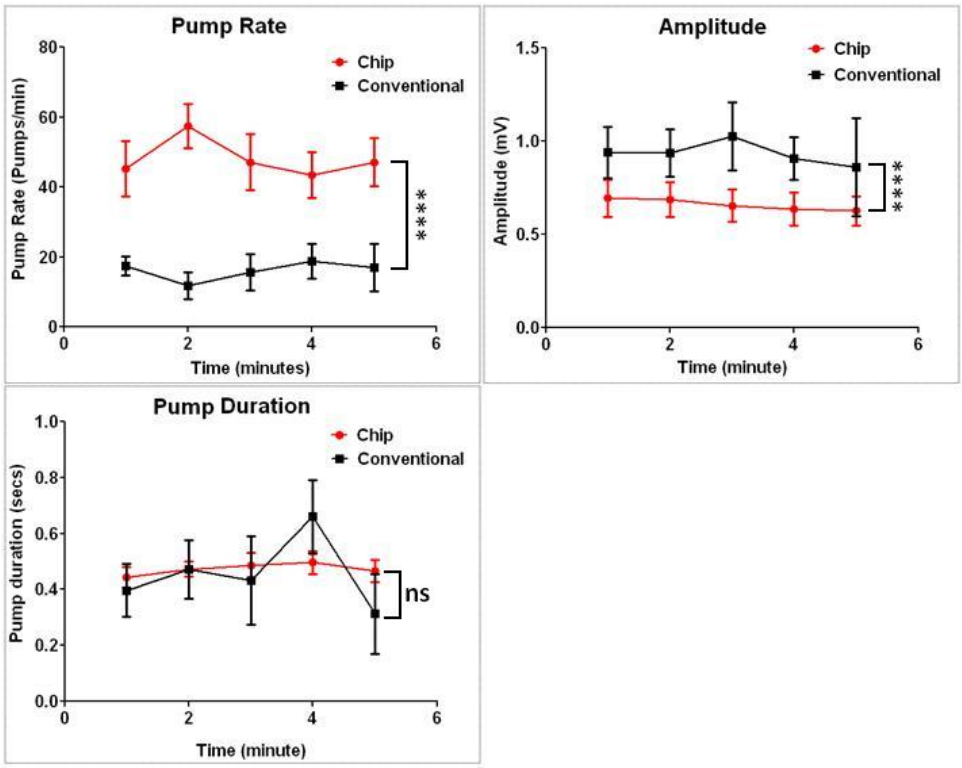

Figure 6.29: Time courses of EPG pump frequency, pump duration, and amplitude, comparing the stability of recording with conventional method (n=5) and the NeuroChip (n=9). Data are the mean ± S.E.M. A higher pump rate and shorter pump duration is observed with NeuroChip compared to conventional recordings.

In the presence of 2 mM 5-HT, the pump rate was greater and the pump duration less for the NeuroChip than for conventional recordings (Figure 6.29; Table 5), as already observed with *C. elegans* (Figure 5.2). Nematodes in the conventional recording configuration are still able to move their bodies vigorously, unlike nematodes trapped in the NeuroChip, thus these latter worms might be expected to pump at a higher rate. As pharyngeal pumping frequency increases, the pump duration typically decreases [82]. This also provides an explanation for the slightly lower pump duration observed with the device.

Table 5: J2 *G. pallida* recorded with the modified NeuroChip or conventional recordings have the same phenotype. Data are the mean ± s.e.mean of recordings from 'n' worms. Each parameter was derived from AutoEPG analysis of all the EPGs captured for a recording of 5 minutes or for manual analysis from 50 EPGs. Comparisons made by unpaired Student's t-test on the respective parameters for [1,2,3] conventional recording with 2 mM 5-HT are: P<0.0001, P=0.7656 and P<0.0001 respectively.

	Modified NeuroChip	Conventional method
J2 G. pallida	**(n=9)**	**(n=5)**
EPG pump frequency (m^{-1})	48.04 ± 2.42 ****[1]	16.13 ± 1.19
EPG pump duration (ms)	487.9 ± 6.1 ns[2]	455.0 ± 57.6
Amplitude (mV)	0.66 ± 0.013 ****[3]	0.93 ±0.027

The stylet activity of J2 *G. pallida* was viewed at ×40 magnification on a Zeiss Axiovert 200 inverted microscope (Carl Zeiss, Cambridge, UK) and recorded by an ImagingSource DMK 31BU03 USB 2.0 monochrome camera (ALRAD Instrument, Newbury, UK) attached. The electropharyngeogram signal was amplified by AXOClamp-2A (Axon Instruments, Inverurie, UK), collected by a Digidata 1320A 16-BIT DATA acquisition system (Axon Instruments, Inverurie, UK) and displayed by Axon AxoScope 9.0 (Axon Instruments, Inverurie, UK). The correlation between the stylet motion and EPG activity was then recorded by screen capturing software called Screen video Specialist (PingLu Software Studio, ZheJiang, China). By breaking the video on a frame-to-frame basis, the correlation was revealed (Figure 6.30). Thrusting of stylet triggers a positive spike, followed by several peaks when the stylet is kept extended, and finally the back motion of the stylet returns the spike back to the baseline.

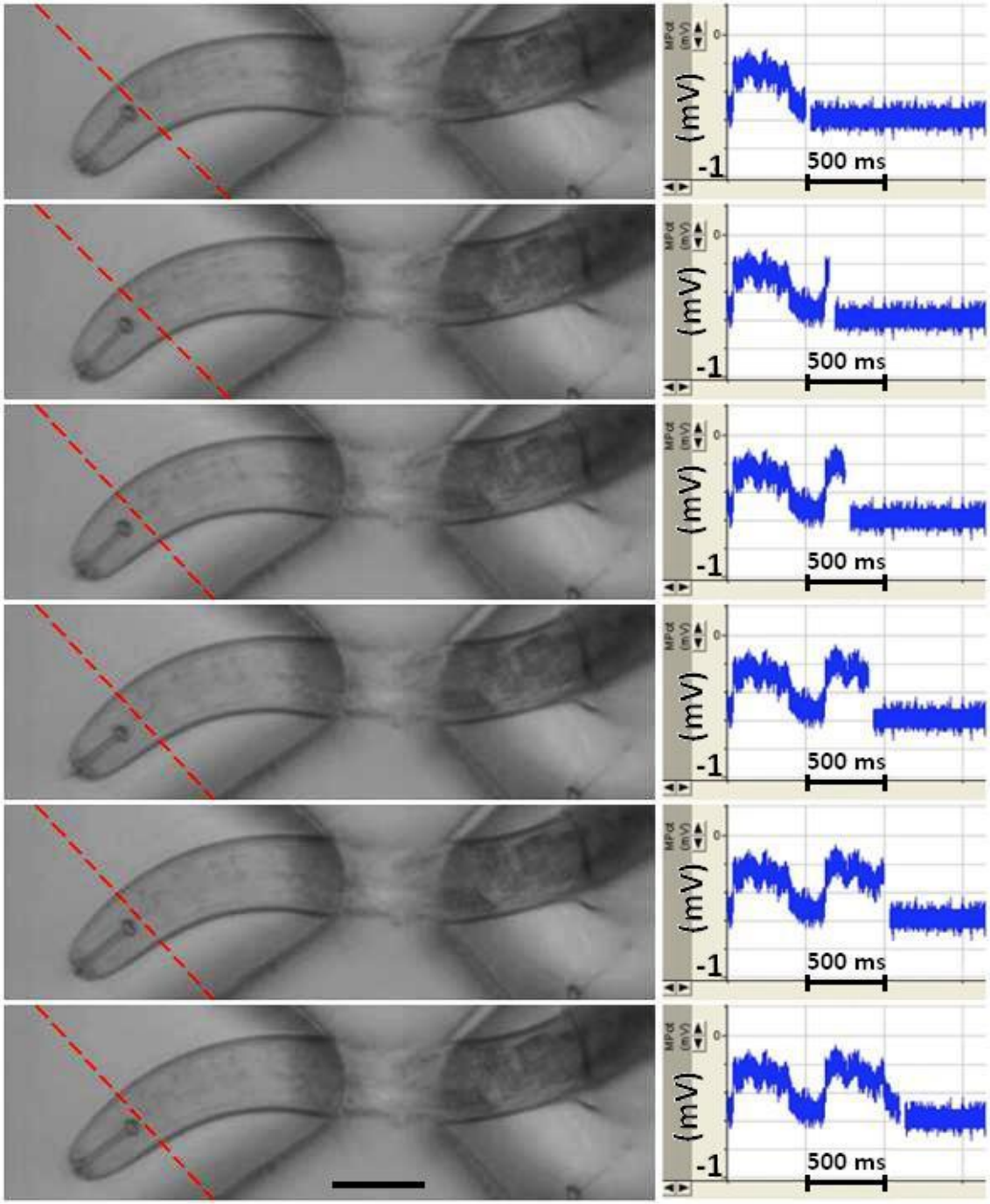

Figure 6.30: Video frames (80ms per frame) reveal the correlation between the stylet motion of J2 *G. pallida* and the EPG waveform. The thrusting of stylet triggers a big positive spike and the back motion returns the spike back to the baseline. Dashed red line indicates the original position of the stylet. Scale bar: 25 μm.

Three different kinds of EPG waveforms were observed in both conventional experiment and with the modified NeuroChip (Figure 6.31). The first kind (Figure 6.31A) has only two peaks in one single pump with pump duration of ~ 300 ms named Short Pump (SP). The second one (Figure 6.31B) which is also the most frequent one is Normal Pump (NP). 3 to 5 peaks are usually generated in one single pump with a longer pump duration of ~ 500 ms. The last kind of EPG waveform has a very long pump duration as several single pumps might merge together inside when the stylet of the nematode is kept extended. It is called Rapid Pump (RP). Although all three kinds of waveforms have been measured, the neurobiological basis is not known. Further experiments are required to resolve this, and the device provides an extremely useful tool for this.

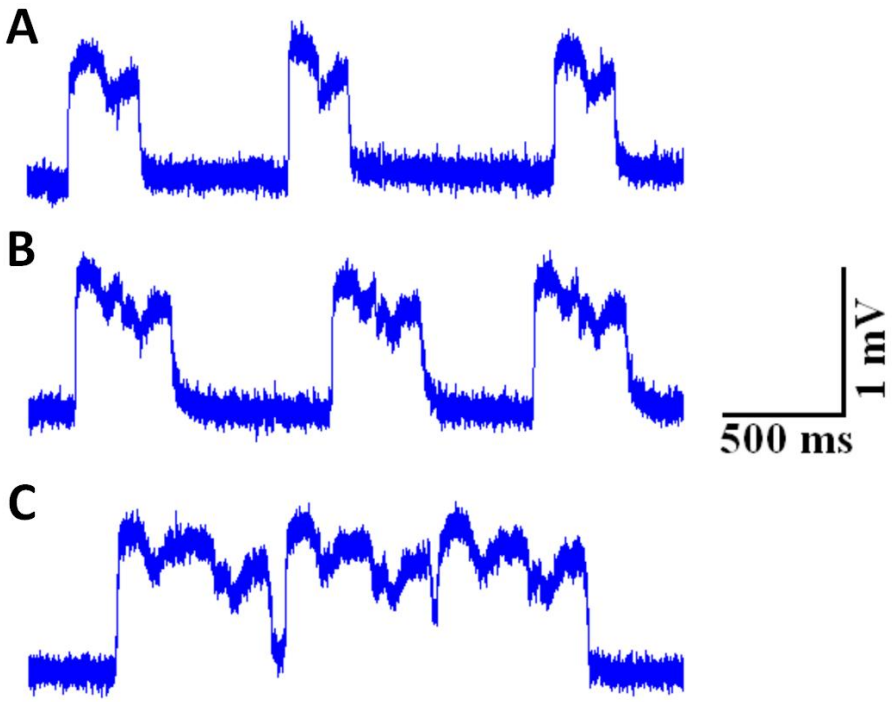

Figure 6.31: Three different EPG waveforms observed during recording with the modified NeuroChip on J2 *G. pallida*. (A) Short Pump (SP): only two peaks generated during one single pump with pump duration of ~ 300 ms. (B) Normal Pump (NP): three to five peaks generated during one single pump with pump duration of ~500 ms. Normal pump occurs in most occasions. (C) Rapid Pump (RP): several single pumps merge together to form one long pump when the stylet remains extended for a while.

Drug diffusion experiment was undertaken to validate the performance of the modified NeuroChip on J2 *G. pallida.* Following the same procedure described in the last chapter, J2 G. *pallida* was firstly suspended in Dent's saline and transported into the modified NeuroChip; Under a consistent positive pressure, the plant nematode was kept in the trap and EPG signals recorded; 2 mM 5-HT was then injected from the drug port and EPG signals recorded; the nematode was flushed away and a new one inserted for a repeat of the procedure.

Capturing the nematode by the head did not give good EPG signals (Figure 6.26A), so that the worm was trapped on the body by pushing it into the trap with its tail first (Figure 6.32A), making it easy to expose the nematode to the drug. Control experiments were done using only Dent's saline, indicating that Dent's saline alone did not cause stylet thrusting of J2 *G. pallida*. After two minutes basal recording, 2 mM 5-HT was applied. The reaction of the plant nematode to this concentration was quick and 2 minutes later electrical signals were observed (Figure 6.32B). The pump frequency reached its plateau after another three minutes (Figure 6.32C), which is similar to the data from experiments with pre-loaded 2 mM 5-HT (Table 5).

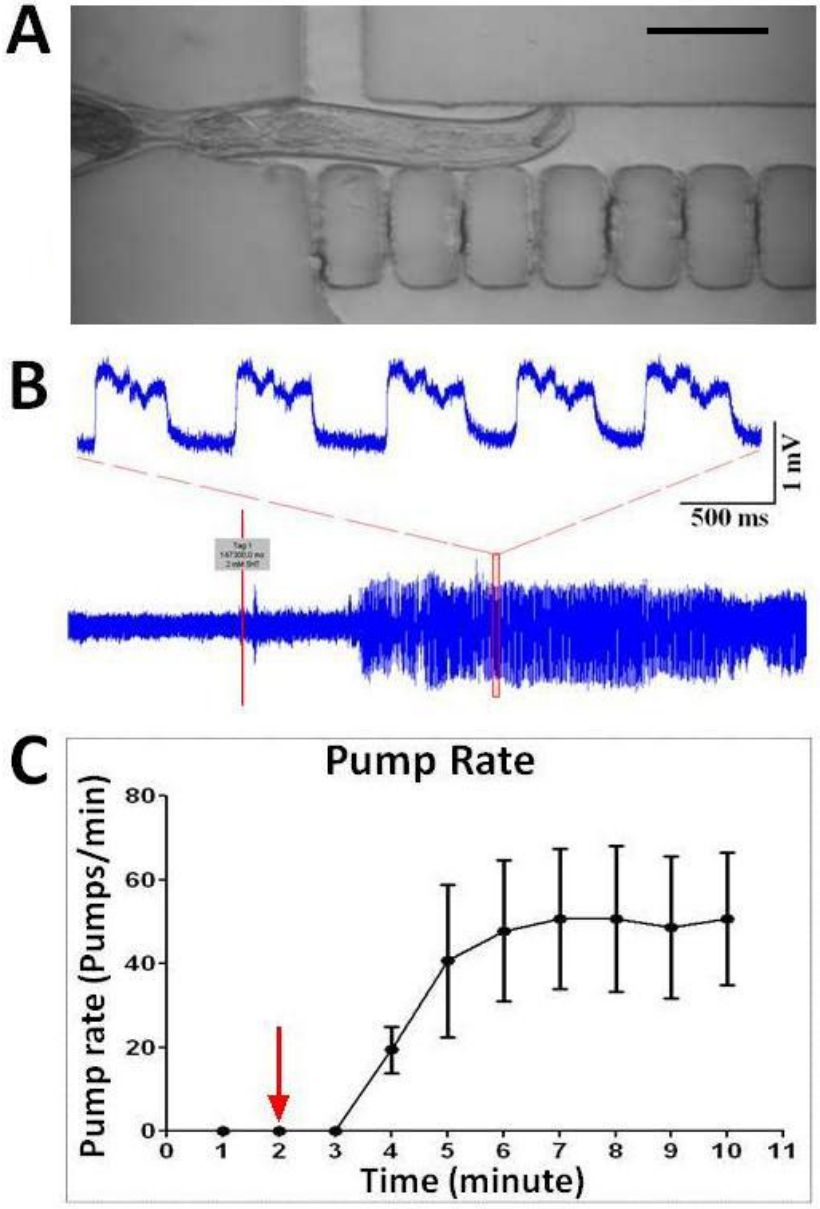

Figure 6.32: Drug diffusion experiment to validate the performance of the modified NeuroChip on J2 *G. pallida*. (A) Micrograph of a trapped J2 *G. pallida* in the modified NeuroChip. Nematode was put in tail first and trapped on the middle of the body, so that the drug has direct access to the worm's head. Scale bar: 50 μm. (B) A sample of an EPG trace obtained from the drug diffusion assay. 2 mM 5-HT was applied at 2 minutes and 5 single EPG signals (red squared area) are shown. Low frequency drift was removed by Clampfit 9.0 (Axon Instruments) with a Highpass Bessel filter and 0.5 Hz -30dB cut-off frequency. (C) Response time to 5-HT for a drug diffusion assay. The red arrow indicates the time of drug addition. Data are the mean ± s.e.mean of recordings from 5 worms.

6.3 Conclusions

EPG signals were obtained that corresponded to the pharyngeal pumping activities of both second stage larvae (L2) *C. elegans* and second stage juveniles (J2) *G. pallida* with the modified NeuroChip.

As demonstrated for L2 stage *C. elegans*, the design can readily be modified to accommodate other developmental stages of *C. elegans* and opens the way for discrete analysis of age-dependent pharyngeal function.

The reduced mobility of the plant nematode *G. pallida* in liquid reduces the difficulty in capturing the animal's head in a conventional method. However, the size of the worm is still a challenge for getting EPG signals. The conventional EPG method has the ability to obtain EPG signals from the L2 *G. pallida*, but it is time consuming and difficult. The modified NeuroChip provides a robust platform for investigating factors involved in activation and perturbation of stylet protrusion.

This microfluidic device could also be modified to trap other parasitic species of nematode which are otherwise too small to study easily with conventional approaches, and permit a higher throughput analysis of these species which are of great relevance to human and animal disease.

Chapter 7: Conclusion and Future Work

The work documented in this thesis investigated the development of microfluidic electrophysiological device for genetic and chemical biology screening of nematodes. Specifically the aims of the work were to demonstrate a system that allowed transportation of worms and drugs in its design, had a specific structure to capture the nematode, was capable of automatic processes with microfluidic valves, and was able to record eletropharyngeal pumping signals of the nematode with integrated electrodes.

At the start of this project, electrophysiological recording from the neural circuits of *C. elegans* was obtained by applying suction from extracellular electrodes. It has the advantage that it can capture a waveform that reports on the activity of a number of neural components in any given circuit encompassing excitatory, inhibitory and modulatory signals [11, 74, 149-151] and thus provides a route to defining the effect of drugs or mutations on neural function. Extracellular recordings from the *C. elegans* pharyngeal network have been useful in this regard [77] but *C. elegans* is a fast-moving nematode and therefore it is not easy to collect EPG recordings from the whole nematode with the conventional suction electrode approach [11]. Cut head preparations may be used to overcome this problem but this is more time-consuming and not amenable to a high throughput approach. The emergence of microfluidic technology opened a way for manipulating the small nematode. Thus approaches have been developed to circumvent this by the design of a microfluidic chamber - NeuroChip for intact worm EPG recordings that completely replaces the need for micromanipulation and a conventional extracellular suction tube.

To meet the aim of allowing transportation of worms in the microfluidic chip and having specific structure to capture the head of *C. elegans*, a single microfluidic channel was fabricated by standard soft lithography (chapter 3). It has an inlet port for introducing the *C. elegans*, an outlet port for disposing of liquids, and a trapping channel for capturing the worm's head. Young adult *C. elegans* was successfully immobilised inside the channel with the head trapped using optimal trap and inlet channel size. High quality EPG recordings were collected from the trapped worm, correlated with the pharyngeal pumping. By changing the shape of the aperture from a square aperture to an opening that

moulds to the shape of the worm's head, more closely mimicking the way the worm is held in conventional suction tube recording, a detailed waveform was obtained that can reliably detect components of the EPG.

Designing an integrated microfluidic platform that can trap *C. elegans* and capture EPG activity in a system that has the capability to apply drugs sequentially in a high-throughput fashion is one important aim of this project (chapter 4). Based on the design of the microfluidic channel, another three flow channels were added for introducing drugs, facilitating drug flow, and worm collection. To meet the aim of automating processes, microfluidic valves were used to control the flow channels individually. To achieve the best control performance, semi-circular flow channels were fabricated by reflowing the master made of photoresist. In addition, platinum electrodes were placed under the PDMS channel to increase the integration of the microfluidic system.

Parallel experiments were performed using both conventional methods and the NeuroChip on wild type and *eat-4 (n2474)* mutant worms to validate the utility of the microfluidic device in comparison to conventional recordings. High quality EPG signals were obtained that could resolve discrete neural components of the waveform. Subsequent experiments were undertaken for genetic and chemical biology screening of *C. elegans* by electrophysiological means with NeuroChip (chapter 5). It was shown that NeuroChip has the capability to rapidly apply and remove 5HT whilst simultaneously capturing the EPG waveform, monitoring the effect on the activity of the neural circuit. It was also able to resolve mutant from wild-type pharyngeal function, which is used as genetic screens of *C. elegans* pharyngeal phenotypes by visually scoring the activity of the pharynx in intact worms. It has great potential for identifying novel mutants and providing insight into gene function. In addition, NeuroChip was used to resolve optogenetic modulation of the neural network mediated via glutamatergic neurone activation. For this a transgenic strain of *C. elegans* stably encoding light sensitive ion channels (Channelrhodopsin2) exclusively in glutamate neurones (*peat-4::ChR2;mRFP*) was adopted. When subjected to light (470nm) illumination, a selective light-dependent decrease in pump duration and increase in pump frequency were observed in retinal treated worms. NeuroChip makes it possible to screen *C. elegans* on the basis of electrophysiological phenotype and thus has the potential to provide new insight into gene function in the nervous system. In this regard the integration

of NeuroChip with a platform for optogenetics adds a capability to stimulate and record responses due to activation of discrete components of the neural network and further extends its capability for neurogenetic investigation.

Also demonstrated in this work is a modified NeuroChip which is capable of recording electrophysiological signals from smaller nematodes (chapter 6). The size of the trapping channel and its opening dictates the size of the worm that can be captured and recorded. Larvae 2 stage *C. elegans* were selected for testing owing to its small body size (~400 µm in length, ~20 µm in diameter) which makes it difficult to manipulate using conventional methods. Two-photon polymerization was used to fabricate the trapping channels to capture the small nematode head. Very small structures of arbitrary geometry can be directly written with this method, making it easy to make a small trapping channel of semi-circular shape in a short time. No difference was observed between the waveforms obtained from young adult and L2 *C. elegans* except the amplitude, which is greater in adults compared to larvae. The plant parasitic nematode *G. pallida* was tested with the modified NeuroChip; the second-stage juvenile has a similar size as L2 *C. elegans*. Unlike *C. elegans*, the EPG waveform taken from the stylet thrusting of J2 *G. pallida* included only one square positive spike with several peaks on the plateau. This was subsequently validated by conventional experiment. Drug diffusion experiments were repeated on the plant nematode using the modified NeuroChip. This chip provides a robust platform for investigating factors involved in activation and perturbation of stylet protrusion.

In conclusion, compared to the conventional method, the NeuroChip has several advantages: consistent trap geometry for capturing individual worms in the same position; minimised operational environment, reducing usage of chemicals; integrated functions leading to a simple manipulation; small size of chip, portable and compatible with a conventional electrophysiological setup; automated operation making it high-throughput; better immobilization of the worm, broadening the application with one single device.

There is scope to improve the throughput and further reduce the need for manual operation by including automated data capture and online extraction of EPG parameters so that automated sorting may be performed in real time. This will include automated detection of worms that enter the channel tail first

so that these can be rapidly discarded without the need for visual inspection. As we demonstrated for L2 *C. elegans*, the design can be modified to accommodate other developmental stages or ages of *C. elegans* and opens the way for a discrete analysis of age-dependent pharyngeal function. The NeuroChip has the ability to be modified for other organisms with different sizes, which are difficult to analyze in the conventional way. It has the potential to be utilized in different research areas, such as gene function, drug screening, behavioural observation, and real-time imaging.

Appendices

Appendix 1: Mask for microfluidic channel

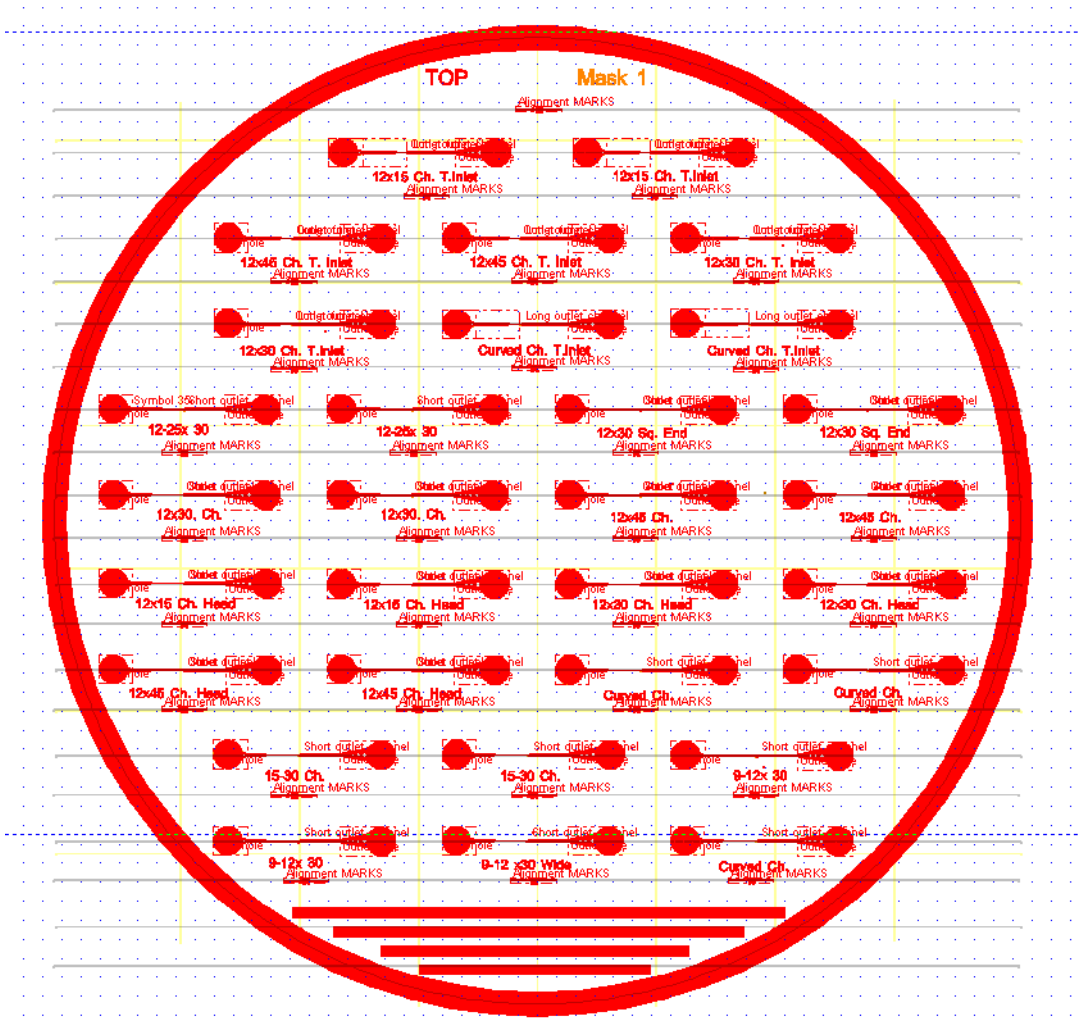

In total, 15 different geometries for the trapping channel have been designed.

Appendix 2: SU-8 5 recipe (12 µm)

1) Spin Ti-Prime, and the spinner setup should be:

	Speed	Accelerate	Time
1.	500	5000	5.0
2.	3000	5000	30.0
3.	500	5000	5.0

2) Bake 120°C for 2 minutes on Sawtech

3) Spin SU8-5, and the spinner setup should be:

	Speed	Accelerate	Time
1.	500	100	5.0
2.	1100	300	30.0
3.	500	100	5.0

4) Soft Bake

Pre-bake 65°C for 2 minutes, and soft bake 95°C for 5 minutes

5) Release for a few minutes to cool down

6) Exposure (EVG620TB)

Time=(216mJ)/(12mJ/s)=18s

7) Post-exposure Bake (PEB)

PBE1 65°C for 1 minute, and PEB2 95°C for 1.5 minute

8) Release for a few minutes to cool down

9) Develop

Dip in EC Solvent for 3 minutes and use IPA to rinse for 30s

10) Nitrogen to dry out.

Appendix 3: SU-8 50 recipe (60 µm)

1) Get the first layer with SU-8 5 master prepared

2) Spin SU8-50, and the spinner setup should be:

	Speed	Accelerate	Time
1.	500	100	10.0
2.	2000	300	60.0
3.	500	100	10.0

3) Soft Bake

Pre-bake 65°C for 6 minutes, and soft bake 95°C for 21 minutes

4) Release for a few minutes to cool down

5) Exposure (EVG620TB)

Time=(312mJ)/(12mJ/s)=26s

6) Post-exposure Bake (PEB)

PBE1 65°C for 1 minute, and PEB2 95°C for 5 minute

7) Release for a few minutes to cool down

8) Develop

Dip in EC Solvent for 5 minutes and use IPA to rinse for 30s

9) Nitrogen to dry out.

Appendix 4: SU-8 master for microfluidic channel

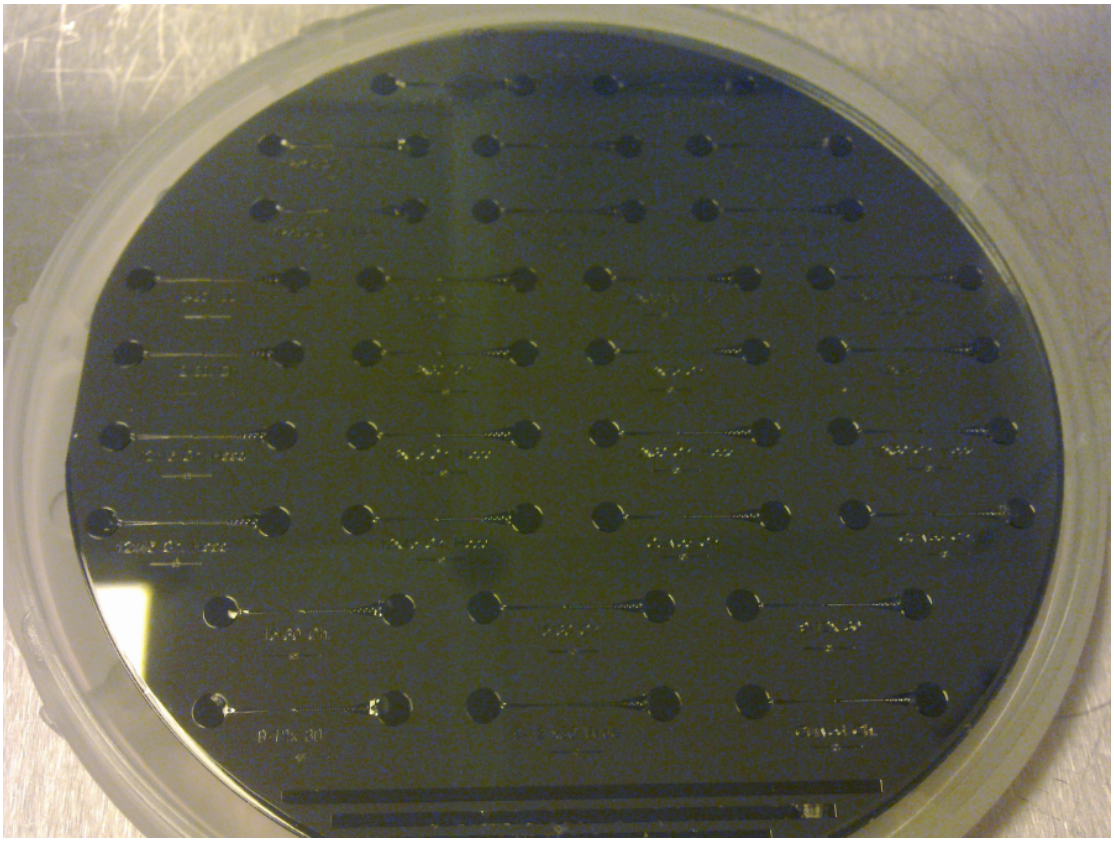

4 inch silicon wafer is used as the substrate.

Appendix 5: Mask for NeuroChip

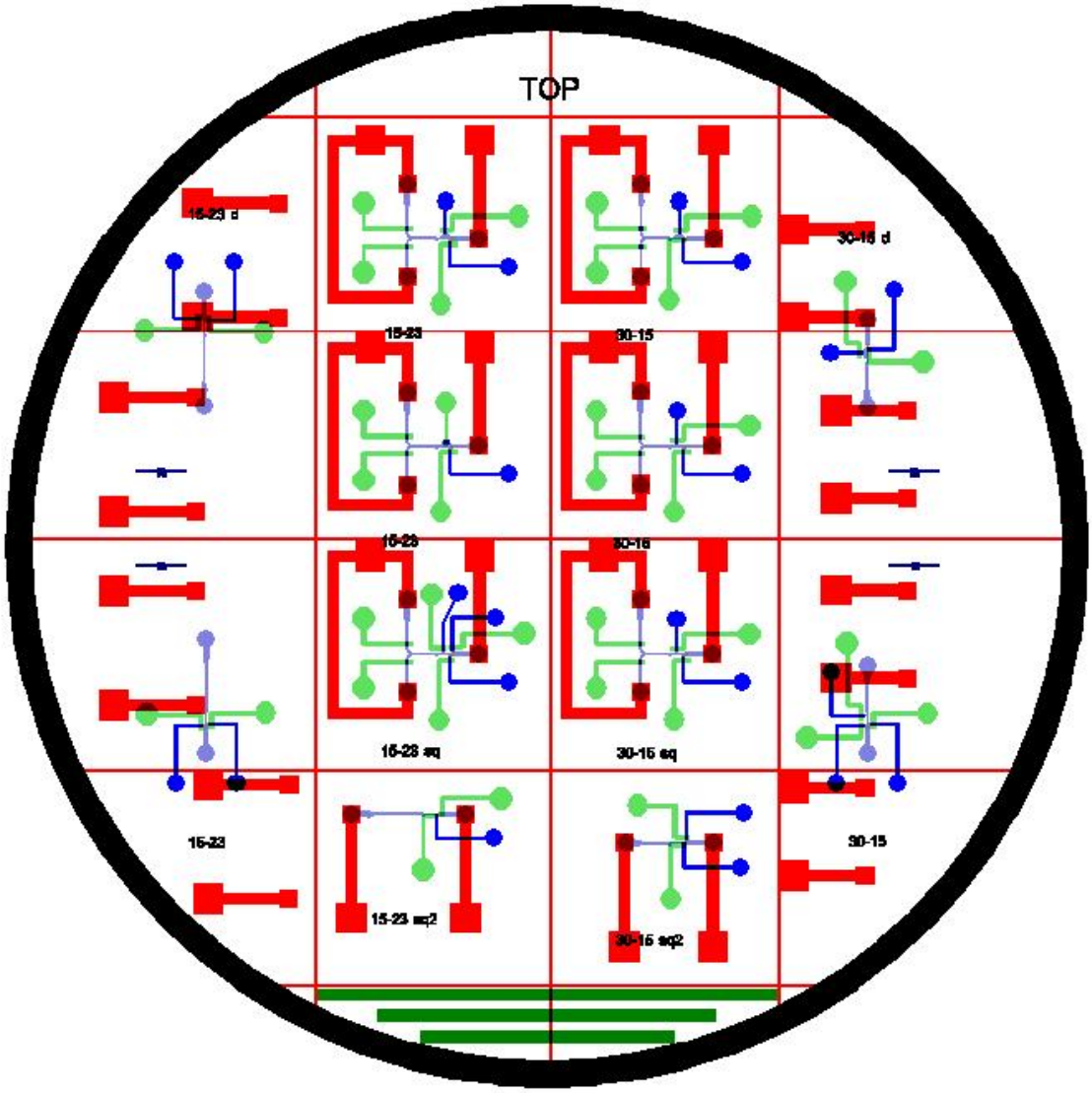

The flow layer is drawn in blue; the control layer is drawn in green; the electrode layer is drawn in red.

Appendix 6: Masters for NeuroChip

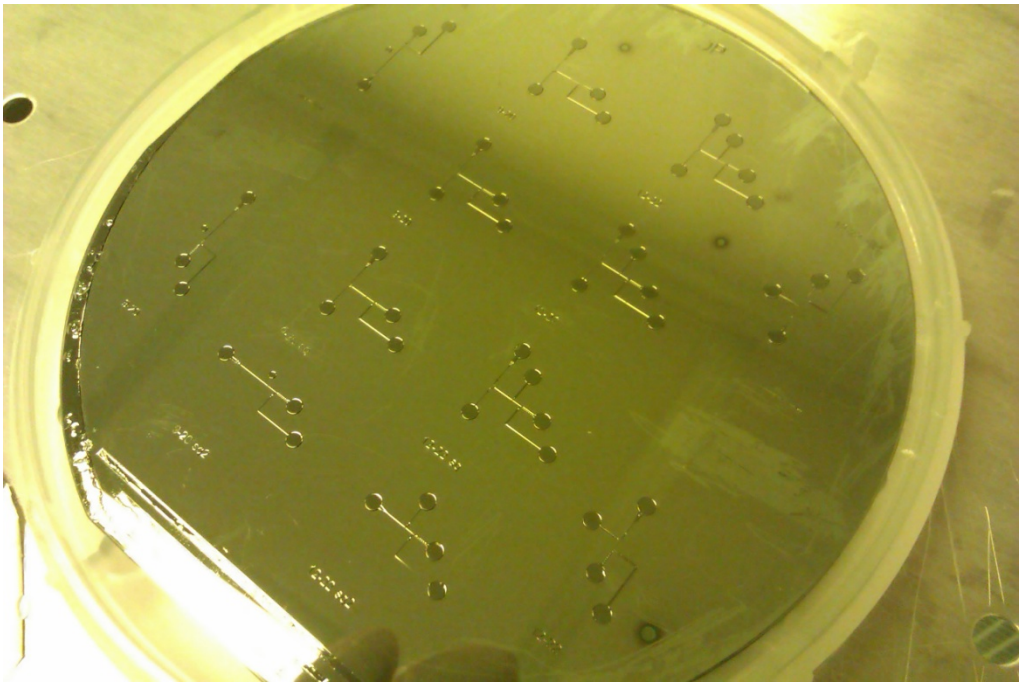

Master for the flow layer

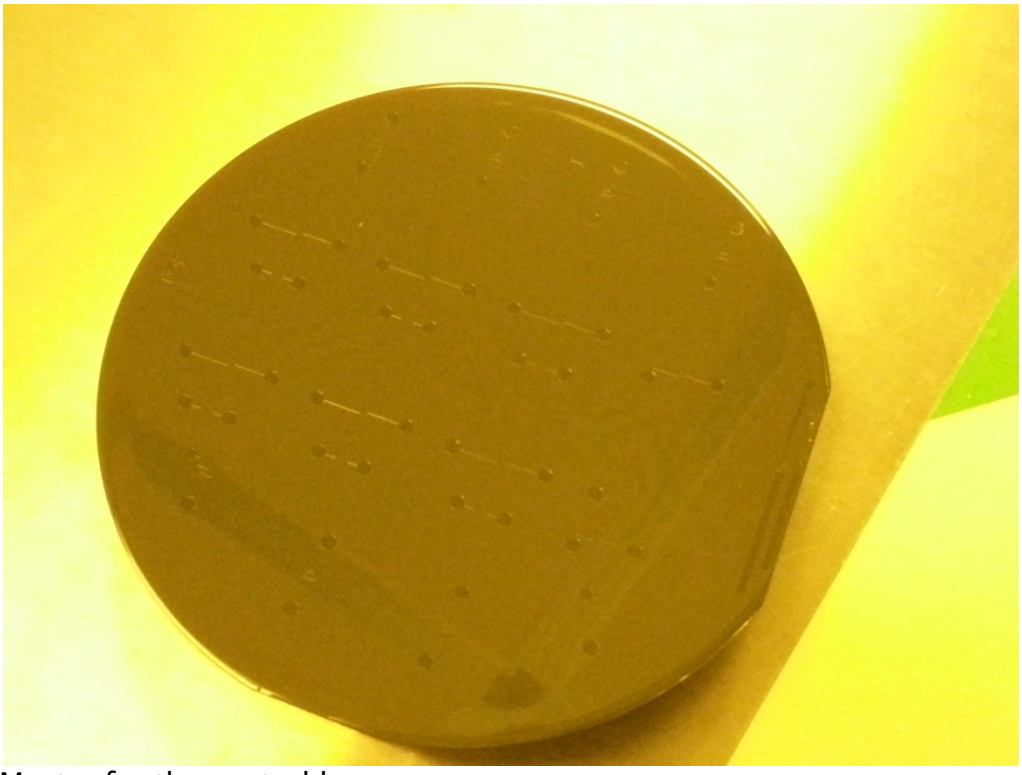

Master for the control layer

Appendix 7: External Control System

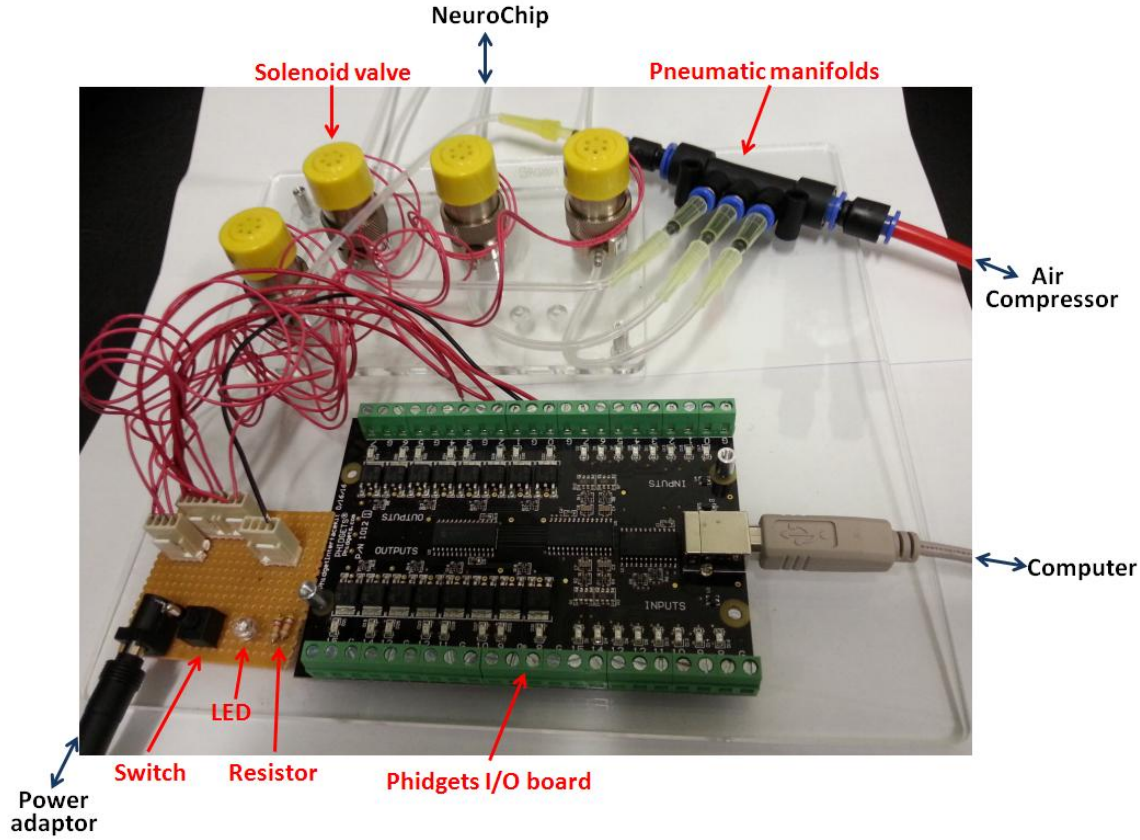

Appendix 8: Java programme for controlling the microfluidic valves

```
package InterfaceKit;

import com.phidgets.InterfaceKitPhidget;
import com.phidgets.PhidgetException;

import javax.swing.JCheckBox;
import javax.swing.JOptionPane;
import javax.swing.JTextField;

import listeners.*;

public class InterfaceKit extends javax.swing.JFrame {

    private static String runArgs[];
    private InterfaceKitPhidget ifk;
    private JCheckBox digiInArray[];
    private JCheckBox digiOutArray[];
    private JTextField sensorInArray[];
    private IFKitAttachListener attach_listener;
    private IFKitDetachListener detach_listener;
    private IFKitErrorListener error_listener;
    private IFKitInputChangeListener input_listener;
    private IFKitOutputChangeListener output_listener;
   private IFKitSensorChangeListener sensor_listener;

   public InterfaceKit() {
         initComponents();
      }

   private void formWindowOpened(java.awt.event.WindowEvent evt) {

         makeDigiInArray();
         makeDigiOutArray();
         /*makeSensorInArray();*/

         this.ratioChk.setEnabled(false);
         this.ratioChk.setSelected(false);

         this.jLabel8.setVisible(false);
         this.sensitivityTxt.setText("");
         this.sensitivityTxt.setVisible(false);
         this.sensitivityScrl.setEnabled(false);
         this.sensitivityScrl.setVisible(false);

         try {
            ifk = new InterfaceKitPhidget();

            attach_listener = new IFKitAttachListener(this, this.attachedTxt,
this.nameTxt,
```

```
                this.serialTxt, this.versionTxt, this.numDigiInTxt,
this.numDigiOutTxt,
                this.numSensorTxt, this.digiInArray, this.digiOutArray,
this.sensorInArray,
                this.ratioChk, this.jLabel8, this.sensitivityTxt,
this.sensitivityScrl);

            detach_listener = new IFKitDetachListener(this, this.attachedTxt,
this.nameTxt,
                this.serialTxt, this.versionTxt, this.numDigiInTxt,
this.numDigiOutTxt,
                this.numSensorTxt, this.digiInArray, this.digiOutArray,
this.sensorInArray,
                this.ratioChk, this.jLabel8, this.sensitivityTxt,
this.sensitivityScrl);

            error_listener = new IFKitErrorListener(this);

            input_listener = new IFKitInputChangeListener(this, this.digiInArray);

            output_listener = new IFKitOutputChangeListener(this,
this.digiOutArray);

            ifk.addAttachListener(attach_listener);
            ifk.addDetachListener(detach_listener);
            ifk.addErrorListener(error_listener);

            ifk.addInputChangeListener(input_listener);
            ifk.addOutputChangeListener(output_listener);

            if((runArgs.length > 1) && (runArgs[1].equals("remote")))
            {
                ifk.open(Integer.parseInt(runArgs[0]), null);
            }
            else if(runArgs.length > 0)
            {
                ifk.open(Integer.parseInt(runArgs[0]));
            }
            else
            {
                ifk.openAny();
            }

        } catch (PhidgetException ex) {
            JOptionPane.showMessageDialog(this, ex.getDescription(), "Phidget
Error" + ex.getErrorNumber(),
JOptionPane.ERROR_MESSAGE);
        }
    }

  private void ratioChkActionPerformed(java.awt.event.ActionEvent evt) {
        if(ratioChk.isEnabled())
        {
```

```
            try
            {
                ifk.setRatiometric(ratioChk.isSelected());
            }
            catch (PhidgetException ex)
            {
                JOptionPane.showMessageDialog(this, ex.getDescription(), "Phidget
Error" + ex.getErrorNumber(), JOptionPane.ERROR_MESSAGE);
            }
        }
    }

    private void formWindowClosed(java.awt.event.WindowEvent evt) {
        try
        {
            //unhook the event listeners
            ifk.removeSensorChangeListener(sensor_listener);
            ifk.removeOutputChangeListener(output_listener);
            ifk.removeInputChangeListener(input_listener);

            ifk.removeErrorListener(error_listener);
            ifk.removeDetachListener(detach_listener);
            ifk.removeAttachListener(attach_listener);

            //close the phidget
            ifk.close();

            ifk = null;

            dispose();
            System.exit(0);
        }
        catch(PhidgetException ex)
        {
            JOptionPane.showMessageDialog(this,   ex.getDescription(),   "Phidget
Error" + ex.getErrorNumber(), JOptionPane.ERROR_MESSAGE);
            dispose();
            System.exit(0);
        }
    }

    private void DrugInActionPerformed(java.awt.event.ActionEvent evt) {
        // TODO add your handling code here:
         if(DrugIn.isSelected()) {
            jCheckBox17.setSelected(true);
            jCheckBox19.setSelected(true);
            jCheckBox20.setSelected(true);
        }
        else {
            jCheckBox17.setSelected(false);
            jCheckBox19.setSelected(false);
            jCheckBox20.setSelected(false);
        }
```

```
    }

    private void WormInActionPerformed(java.awt.event.ActionEvent evt) {
        // TODO add your handling code here:
         if(WormIn.isSelected()){
            jCheckBox18.setSelected(true);
            jCheckBox19.setSelected(true);
            jCheckBox20.setSelected(true);
        }
        else{
            jCheckBox18.setSelected(false);
            jCheckBox19.setSelected(false);
            jCheckBox20.setSelected(false);
        }
    }

    private void WormOutActionPerformed(java.awt.event.ActionEvent evt) {
        // TODO add your handling code here:
        if(WormOut.isSelected()){
            jCheckBox18.setSelected(true);
            jCheckBox20.setSelected(true);
        }
        else{
            jCheckBox18.setSelected(false);
            jCheckBox20.setSelected(false);
}
    }

private void makeDigiInArray()
    {
     digiInArray = new JCheckBox[16];

     digiInArray[0] = jCheckBox1;
     digiInArray[1] = jCheckBox2;
     digiInArray[2] = jCheckBox3;
     digiInArray[3] = jCheckBox4;
     digiInArray[4] = jCheckBox5;
     digiInArray[5] = jCheckBox6;
     digiInArray[6] = jCheckBox7;
     digiInArray[7] = jCheckBox8;
     digiInArray[8] = jCheckBox9;
     digiInArray[9] = jCheckBox10;
     digiInArray[10] = jCheckBox11;
     digiInArray[11] = jCheckBox12;
     digiInArray[12] = jCheckBox13;
     digiInArray[13] = jCheckBox14;
     digiInArray[14] = jCheckBox15;
     digiInArray[15] = jCheckBox16;

      for(int i = 0; i < 16; i++)
      {
      digiInArray[i].setVisible(false);
```

```
        digiInArray[i].setEnabled(false);
        }
        }

    private void makeDigiOutArray()
      {
         digiOutArray = new JCheckBox[16];

         digiOutArray[0] = jCheckBox17;
         digiOutArray[1] = jCheckBox18;
         digiOutArray[2] = jCheckBox19;
         digiOutArray[3] = jCheckBox20;
         digiOutArray[4] = jCheckBox21;
         digiOutArray[5] = jCheckBox22;
         digiOutArray[6] = jCheckBox23;
         digiOutArray[7] = jCheckBox24;
         digiOutArray[8] = jCheckBox25;
         digiOutArray[9] = jCheckBox26;
         digiOutArray[10] = jCheckBox27;
         digiOutArray[11] = jCheckBox28;
         digiOutArray[12] = jCheckBox29;
         digiOutArray[13] = jCheckBox30;
         digiOutArray[14] = jCheckBox31;
         digiOutArray[15] = jCheckBox32;

         for(int i = 0; i < 16; i++)
         {
            digiOutArray[i].setVisible(false);
         }
      }

    public static void main(String args[]) {
         runArgs = args;
         java.awt.EventQueue.invokeLater(new Runnable() {
            public void run() {
               new InterfaceKit().setVisible(true);
            }
         });
      }

    private javax.swing.JCheckBox DrugIn;
      private javax.swing.JCheckBox WormIn;
      private javax.swing.JCheckBox WormOut;
      private javax.swing.JTextField attachedTxt;
      private javax.swing.JCheckBox jCheckBox1;
      private javax.swing.JCheckBox jCheckBox10;
      private javax.swing.JCheckBox jCheckBox11;
      private javax.swing.JCheckBox jCheckBox12;
      private javax.swing.JCheckBox jCheckBox13;
      private javax.swing.JCheckBox jCheckBox14;
      private javax.swing.JCheckBox jCheckBox15;
      private javax.swing.JCheckBox jCheckBox16;
      private javax.swing.JCheckBox jCheckBox17;
```

```
    private javax.swing.JCheckBox jCheckBox18;
    private javax.swing.JCheckBox jCheckBox19;
    private javax.swing.JCheckBox jCheckBox2;
    private javax.swing.JCheckBox jCheckBox20;
    private javax.swing.JCheckBox jCheckBox21;
    private javax.swing.JCheckBox jCheckBox22;
    private javax.swing.JCheckBox jCheckBox23;
    private javax.swing.JCheckBox jCheckBox24;
    private javax.swing.JCheckBox jCheckBox25;
    private javax.swing.JCheckBox jCheckBox26;
    private javax.swing.JCheckBox jCheckBox27;
    private javax.swing.JCheckBox jCheckBox28;
    private javax.swing.JCheckBox jCheckBox29;
    private javax.swing.JCheckBox jCheckBox3;
    private javax.swing.JCheckBox jCheckBox30;
    private javax.swing.JCheckBox jCheckBox31;
    private javax.swing.JCheckBox jCheckBox32;
    private javax.swing.JCheckBox jCheckBox4;
    private javax.swing.JCheckBox jCheckBox5;
    private javax.swing.JCheckBox jCheckBox6;
    private javax.swing.JCheckBox jCheckBox7;
    private javax.swing.JCheckBox jCheckBox8;
    private javax.swing.JCheckBox jCheckBox9;
    private javax.swing.JLabel jLabel1;
    private javax.swing.JLabel jLabel2;
    private javax.swing.JLabel jLabel3;
    private javax.swing.JLabel jLabel4;
    private javax.swing.JLabel jLabel5;
    private javax.swing.JLabel jLabel6;
    private javax.swing.JLabel jLabel7;
    private javax.swing.JLabel jLabel8;
    private javax.swing.JLabel jLabel9;
    private javax.swing.JPanel jPanel1;
    private javax.swing.JPanel jPanel2;
    private javax.swing.JPanel jPanel3;
    private javax.swing.JScrollPane jScrollPane1;
    private javax.swing.JTextArea nameTxt;
    private javax.swing.JTextField numDigiInTxt;
    private javax.swing.JTextField numDigiOutTxt;
    private javax.swing.JTextField numSensorTxt;
    private javax.swing.JCheckBox ratioChk;
    private javax.swing.JSlider sensitivityScrl;
    private javax.swing.JTextField sensitivityTxt;
    private javax.swing.JTextField serialTxt;
    private javax.swing.JTextField versionTxt;

}
```

Appendix 9: Microfluidic platform for NeuroChip

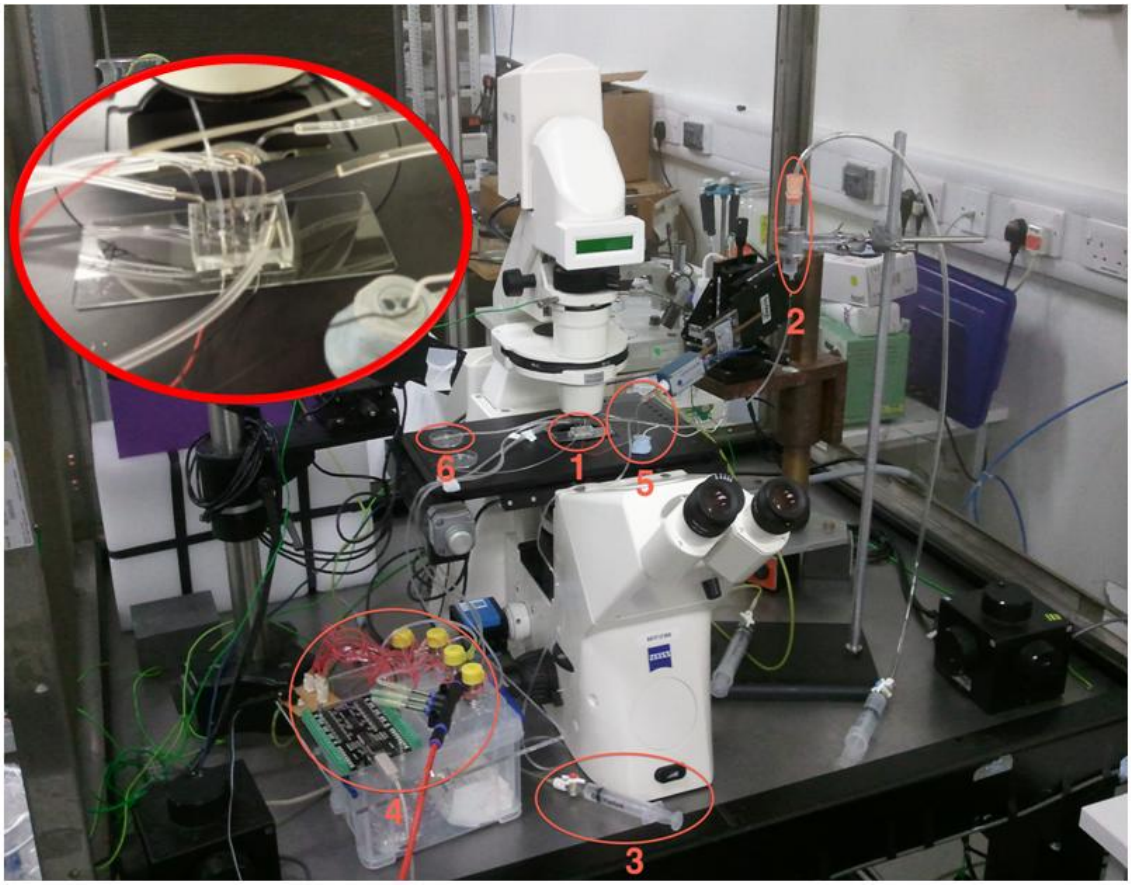

1: The NeuroChip

2: Reservoir for loading large amount of *C. elegans*

3: Syringe for applying drugs

4: In/Out board and solenoid valves for controlling the microvalves separately by computer

5: Leads to connect the NeuroChip and amplifier

6: Petri dish to collect the tested worm for further use

Appendix 10: *peat-4::ChR2;mRFP* integration for *eat-4* mutant

Males carrying the integrated transgene were produced by heat-shocking L4 hermaphrodites at 30 °C for 6 hours. A population of males was maintained by crossing with L4 hermaphrodites from the same line. Young males carrying the integrated transgene were mated with L4 *eat-4(ky5)* hermaphrodites. In the F1 generation, L4 hermaphrodites expressing mRFP were picked to individual plates and allowed to self. In the F2 generation, L4 hermaphrodites expressing mRFP were picked to individual plates and allowed to self. Their progeny, the F3 generation, were screened for plates where all F3 animals expressed mRFP, i.e., the F2 hermaphrodite was homozygous for the transgene. This screening was carried out before the first F3 progeny reached the adult stage, allowing the F2 animal from such plates to be identified and removed for single worm lysis and genotyping of the *eat-4(ky5)* allele. Genotyping of the *eat-4(ky5)*, a 613bp deletion, was carried out by Polymerase Chain Reaction (PCR) which was performed according to established protocols [152] using optimised cycling parameters and Taq polymerase (Qiagen). Primers used to amplify over the *eat-4(ky5)* genomic breakpoints were 5'-GCTTGTCAGAAGACAAGTGC-3' and 5'-CATATGATCCTGTGAATGC-3'.

Appendix 11: Method for expression of ChR2 in cholinergic neurones

For expression in glutamatergic neurones, ChR2 was amplified from the plasmid *pmyo-3::ChR2(gf)::yfp* (provided by Alexander Gottschalk). ChR2 was amplified using primers that introduce restriction sites flanking the coding sequence: (from 5'-3'): ChR2-SpeI-F: CTAGAGACTAGTATGGATTATGGAGGCGCCCTG; and ChR2-KpnI-R: ATGGGGTACCttaGGGcACCGCGCCAGCCTCGGCCTC. The R primer was designed to introduce a stop codon at the end of the *ChR2* coding sequence and a synonymous substitution that disrupts the KpnI site in the 3' end of the *ChR2* coding sequence, shown in lowercase in the primer sequence. *mRFP* was amplified with the following primers: (from 5'-3'): mRFP-AgeI-F CTA GAA CCG GTC AAT GGC CTC CTC CGA GGA CG and mRFP-EcoRI-R GCA CTG AAT TCT TAG GCG CCG GTG GAG TGG C. PCR was carried out according to standard procedures and purified PCR products were subcloned into pCR-BluntII-TOPO (Invitrogen). The fidelity of the DNA amplification was verified by sequencing (MWG). *ChR2* and *mRFP* were cut out of the TOPO constructs with SpeI/KpnI and AgeI/EcoRI respectively and sequentially ligated into a Gateway pENTR backbone. XL-10 Gold cells (Stratagene) were transformed with the ligation product according to the manufacturer's instructions. The entry clone *pENTR::ChR2;mRFP* was recombined with a Gateway destination vector containing the promoter region of *eat-4, pDESTpeat-4* (*pDESTpeat-4* contains the *eat-4* promoter region from nucleotide position -6022 to -1), in an LR recombination reaction according to the manufacturer's instructions (Invitrogen) to produce *peat-4::ChR2;mRFP*. To generate transgenic lines, an injection mix containing 1x injection buffer (final concentration 2% polyethylene glycol, molecular weight 6000-8000, 20mM potassium phosphate, pH 7.5, 3mM potassium citrate, pH 7.5), and *peat-4;ChR2;mRFP* (50ng/µl) was injected into the gonads of wild-type (N2) day old adult *C. elegans*. Each injected worm was transferred to a new plate and incubated at 20oC. F1 animals expressing mRFP were picked to new plates. Lines were established from plates where expression of mRFP persisted in the F2 generation. The extrachromosomal array was integrated into the genome by UV irradiation. 25-30 L4 hermaphrodites carrying the extrachromosomal array, as determined by visual confirmation of mRFP expression, were transferred to

three unseeded NGM plates. These plates, with lids removed, were subjected to a UV dose of 300J/mz in a Stratagene UV crosslinker. UV irradiated worms (P0) were transferred to NGM plates seeded with OP50 approximately 5 worms per plate, and were incubated at 20oC. 24 hours after exposure, P0 animals were transferred to fresh seeded plates to ensure that the first progeny of irradiated animals were not used. On the third and fourth day after UV exposure, 250 L4 animals from the F1 generation were picked to individual seeded plates, giving 500 F1 animals. On the seventh and eighth day after UV exposure, two F2 L4s from each F1 plate were transferred to individual plates, giving a total of 1000 F2s. The progeny of these F2 animals were screened for 100% transmission of the transgene, determined by expression of mRFP in the pharyngeal neurons. Following confirmation of ChR2 activity, integrated lines were backcrossed into N2 six times to remove background mutations.

Bibliography

Reference List

[1] C. Hu, *et al.*, "An integrated microfluidic device for high-throughput electrophysiological analysis of C. elegans," in *MicroTAS 2012*, Okinawa, Japan, 2012.

[2] C. Hu, *et al.*, "NeuroChip: A Microfluidic Electrophysiological Device for Genetic and Chemical Biology Screening of Caenorhabditis elegans Adult and Larvae," *PLoS One,* vol. 8, p. e64297, 2013.

[3] R. Waterston and J. E. Sulston, "The Human Genome Project: reaching the finish line," *Science,* vol. 282, pp. 53-4, Oct 2 1998.

[4] W. B. Wood, *The Nematode Caenorhabditis elegans*. Cold Spring Harbor, N.Y.: Cold Spring Harbor Laboratory, 1988.

[5] C. I. Bargmann, "Neurobiology of the Caenorhabditis elegans genome," *Science,* vol. 282, pp. 2028-33, Dec 11 1998.

[6] H. Tabara, *et al.*, "RNAi in C. elegans: soaking in the genome sequence," *Science,* vol. 282, pp. 430-1, Oct 16 1998.

[7] K. Shen and C. I. Bargmann, "The immunoglobulin superfamily protein SYG-1 determines the location of specific synapses in C. elegans," *Cell,* vol. 112, pp. 619-30, Mar 7 2003.

[8] D. Sieburth, *et al.*, "Systematic analysis of genes required for synapse structure and function," *Nature,* vol. 436, pp. 510-7, Jul 28 2005.

[9] L. Chen, *et al.*, "Axon regeneration pathways identified by systematic genetic screening in C. elegans," *Neuron,* vol. 71, pp. 1043-57, Sep 22 2011.

[10] M. Jensen, *et al.*, "Wnt signaling regulates acetylcholine receptor translocation and synaptic plasticity in the adult nervous system," *Cell,* vol. 149, pp. 173-87, Mar 30 2012.

[11] L. Avery, *et al.*, "Electrophysiological methods," *Methods Cell Biol,* vol. 48, pp. 251-69, 1995.

[12] D. M. Raizen and L. Avery, "Electrical activity and behavior in the pharynx of Caenorhabditis elegans," *Neuron,* vol. 12, pp. 483-95, Mar 1994.

[13] R. Y. Lee, *et al.*, "EAT-4, a homolog of a mammalian sodium-dependent inorganic phosphate cotransporter, is necessary for glutamatergic neurotransmission in caenorhabditis elegans," *J Neurosci,* vol. 19, pp. 159-67, Jan 1 1999.

[14] H. Li, *et al.*, "Identification of chemical synapses in the pharynx of Caenorhabditis elegans," *Proc Natl Acad Sci U S A,* vol. 94, pp. 5912-6, May 27 1997.

[15] J. Dillon, *et al.*, "AutoEPG: software for the analysis of electrical activity in the microcircuit underpinning feeding behaviour of Caenorhabditis elegans," *PLoS One,* vol. 4, p. e8482, 2009.

[16] A. Ben-Yakar, *et al.*, "Microfluidics for the analysis of behavior, nerve regeneration, and neural cell biology in C. elegans," *Curr Opin Neurobiol,* vol. 19, pp. 561-7, Oct 2009.

[17] J. Floyd. *Pale Cyst Nematode, Globodera pallida, on potato*. Available: http://joelfloydillustration.com/pathogens.html

[18] V. M. Williamson and C. A. Gleason, "Plant-nematode interactions," *Curr Opin Plant Biol,* vol. 6, pp. 327-33, Aug 2003.

[19] U. WYSS and U. ZUNKE, "Observations on the behaviour of second stage juveniles of Hetero inside host roots," *Revue Nematol,* vol. 9, pp. 153-165, 1986.
[20] T. V. Chokshi*, et al.*, "CO2 and compressive immobilization of C. elegans on-chip," *Lab Chip,* vol. 9, pp. 151-7, Jan 7 2009.
[21] S. E. Hulme*, et al.*, "A microfabricated array of clamps for immobilizing and imaging C. elegans," *Lab Chip,* vol. 7, pp. 1515-23, Nov 2007.
[22] F. Zeng*, et al.*, "Sub-cellular precision on-chip small-animal immobilization, multi-photon imaging and femtosecond-laser manipulation," *Lab Chip,* vol. 8, pp. 653-6, May 2008.
[23] J. Krajniak and H. Lu, "Long-term high-resolution imaging and culture of C. elegans in chip-gel hybrid microfluidic device for developmental studies," *Lab Chip,* vol. 10, pp. 1862-8, Jul 21 2010.
[24] X. Cui*, et al.*, "Lensless high-resolution on-chip optofluidic microscopes for Caenorhabditis elegans and cell imaging," *Proc Natl Acad Sci U S A,* vol. 105, pp. 10670-5, Aug 5 2008.
[25] N. Chronis*, et al.*, "Microfluidics for in vivo imaging of neuronal and behavioral activity in Caenorhabditis elegans," *Nat Methods,* vol. 4, pp. 727-31, Sep 2007.
[26] T. V. Chokshi*, et al.*, "An automated microfluidic platform for calcium imaging of chemosensory neurons in Caenorhabditis elegans," *Lab Chip,* vol. 10, pp. 2758-63, Oct 21 2010.
[27] S. H. Chalasani*, et al.*, "Dissecting a circuit for olfactory behaviour in Caenorhabditis elegans," *Nature,* vol. 450, pp. 63-70, Nov 1 2007.
[28] S. R. Lockery*, et al.*, "Artificial dirt: microfluidic substrates for nematode neurobiology and behavior," *J Neurophysiol,* vol. 99, pp. 3136-43, Jun 2008.
[29] J. Qin and A. R. Wheeler, "Maze exploration and learning in C. elegans," *Lab Chip,* vol. 7, pp. 186-92, Feb 2007.
[30] S. Park*, et al.*, "Enhanced Caenorhabditis elegans locomotion in a structured microfluidic environment," *PLoS One,* vol. 3, p. e2550, 2008.
[31] W. Shi*, et al.*, "Droplet-based microfluidic system for individual Caenorhabditis elegans assay," *Lab Chip,* vol. 8, pp. 1432-5, Sep 2008.
[32] P. Rezai*, et al.*, "Electrotaxis of Caenorhabditis elegans in a microfluidic environment," *Lab Chip,* vol. 10, pp. 220-6, Jan 21 2010.
[33] S. E. Hulme*, et al.*, "Lifespan-on-a-chip: microfluidic chambers for performing lifelong observation of C. elegans," *Lab Chip,* vol. 10, pp. 589-97, Mar 7 2010.
[34] R. Sznitman*, et al.*, "Multi-environment model estimation for motility analysis of Caenorhabditis elegans," *PLoS One,* vol. 5, p. e11631, 2010.
[35] M. Zimmer*, et al.*, "Neurons detect increases and decreases in oxygen levels using distinct guanylate cyclases," *Neuron,* vol. 61, pp. 865-79, Mar 26 2009.
[36] C. B. Rohde*, et al.*, "Microfluidic system for on-chip high-throughput whole-animal sorting and screening at subcellular resolution," *Proc Natl Acad Sci U S A,* vol. 104, pp. 13891-5, Aug 28 2007.
[37] M. M. Crane*, et al.*, "Computer-enhanced high-throughput genetic screens of C. elegans in a microfluidic system," *Lab Chip,* vol. 9, pp. 38-40, Jan 7 2009.
[38] J. N. Stirman*, et al.*, "High-throughput study of synaptic transmission at the neuromuscular junction enabled by optogenetics and microfluidics," *J Neurosci Methods,* vol. 191, pp. 90-3, Aug 15 2010.

[39] X. C. i Solvas, *et al.*, "High-throughput age synchronisation of Caenorhabditis elegans," *Chemical Communications,* vol. 47, pp. 9801-9803, 2011.
[40] S. Johari, *et al.*, "High-Throughput Microfluidic Sorting of C. elegans for Automated Force Pattern Measurement," in *Materials Science Forum*, 2012, pp. 182-187.
[41] M. M. Crane, *et al.*, "Autonomous screening of C. elegans identifies genes implicated in synaptogenesis," *Nat Methods,* vol. 9, pp. 977-80, Oct 2012.
[42] M. D. Levenson, *et al.*, "Improving resolution in photolithography with a phase-shifting mask," *Electron Devices, IEEE Transactions on,* vol. 29, pp. 1828-1836, 1982.
[43] Y. Xia and G. M. Whitesides, "Soft lithography," *Annual review of materials science,* vol. 28, pp. 153-184, 1998.
[44] Rutgers. *C. elegans as a Model System.* Available: http://avery.rutgers.edu/WSSP/StudentScholars/project/introduction/worms.html
[45] R. Kosinski and M. Zaremba, "Dynamics of the model of the caenorhabditis elegans neural network," *ACTA PHYSICA POLONICA SERIES B,* vol. 38, p. 2201, 2007.
[46] R. Kerr, *et al.*, "Optical imaging of calcium transients in neurons and pharyngeal muscle of C. elegans," *Neuron,* vol. 26, pp. 583-94, Jun 2000.
[47] M. B. Goodman, *et al.*, "Active currents regulate sensitivity and dynamic range in C. elegans neurons," *Neuron,* vol. 20, pp. 763-72, Apr 1998.
[48] J. A. Lewis, *et al.*, "The genetics of levamisole resistance in the nematode Caenorhabditis elegans," *Genetics,* vol. 95, pp. 905-28, Aug 1980.
[49] S. X. Guo, *et al.*, "Femtosecond laser nanoaxotomy lab-on-a-chip for in vivo nerve regeneration studies," *Nat Methods,* vol. 5, pp. 531-3, Jun 2008.
[50] K. Chung, *et al.*, "Automated on-chip rapid microscopy, phenotyping and sorting of C. elegans," *Nat Methods,* vol. 5, pp. 637-43, Jul 2008.
[51] G. M. Whitesides, *et al.*, "Soft lithography in biology and biochemistry," *Annu Rev Biomed Eng,* vol. 3, pp. 335-73, 2001.
[52] K. Chung, *et al.*, "Microfluidic chamber arrays for whole-organism behavior-based chemical screening," *Lab Chip,* vol. 11, pp. 3689-97, Nov 7 2011.
[53] J. Krajniak and H. Lu, "CLIP–CONTINUOUS LIVE IMAGING PLATFORM FOR C. elegans AT PHYSIOLOGICAL CONDITIONS."
[54] G. Nagel, *et al.*, "Channelrhodopsin-1: a light-gated proton channel in green algae," *Science,* vol. 296, pp. 2395-8, Jun 28 2002.
[55] G. Nagel, *et al.*, "Channelrhodopsin-2, a directly light-gated cation-selective membrane channel," *Proc Natl Acad Sci U S A,* vol. 100, pp. 13940-5, Nov 25 2003.
[56] H. Suzuki, *et al.*, "In vivo imaging of C. elegans mechanosensory neurons demonstrates a specific role for the MEC-4 channel in the process of gentle touch sensation," *Neuron,* vol. 39, pp. 1005-17, Sep 11 2003.
[57] M. Mank, *et al.*, "A FRET-based calcium biosensor with fast signal kinetics and high fluorescence change," *Biophys J,* vol. 90, pp. 1790-6, Mar 1 2006.

[58] M. Mank, *et al.*, "A genetically encoded calcium indicator for chronic in vivo two-photon imaging," *Nat Methods,* vol. 5, pp. 805-11, Sep 2008.
[59] R. S. Kamath, *et al.*, "Systematic functional analysis of the Caenorhabditis elegans genome using RNAi," *Nature,* vol. 421, pp. 231-7, Jan 16 2003.
[60] D. C. Duffy, *et al.*, "Rapid Prototyping of Microfluidic Systems in Poly(dimethylsiloxane)," *Anal Chem,* vol. 70, pp. 4974-84, Dec 1 1998.
[61] M. A. Unger, *et al.*, "Monolithic microfabricated valves and pumps by multilayer soft lithography," *Science,* vol. 288, pp. 113-6, Apr 7 2000.
[62] T. Kaletta and M. O. Hengartner, "Finding function in novel targets: C. elegans as a model organism," *Nat Rev Drug Discov,* vol. 5, pp. 387-98, May 2006.
[63] J. Melin and S. R. Quake, "Microfluidic large-scale integration: the evolution of design rules for biological automation," *Annu Rev Biophys Biomol Struct,* vol. 36, pp. 213-31, 2007.
[64] J. Yang, *et al.*, "A microfluidic device for rapid screening of chemotaxis-defective Caenorhabditis elegans mutants," *Biomedical microdevices,* pp. 1-10, 2012.
[65] F. Bourgeois and A. Ben-Yakar, "Femtosecond laser nanoaxotomy properties and their effect on axonal recovery in C. elegans," *Opt. Express,* vol. 15, pp. 8521-8531, 2007.
[66] A. Ben-Yakar and F. Bourgeois, "Ultrafast laser nanosurgery in microfluidics for genome-wide screenings," *Current opinion in biotechnology,* vol. 20, pp. 100-105, 2009.
[67] P. B. Allen, *et al.*, "Single-synapse ablation and long-term imaging in live C. elegans," *J Neurosci Methods,* vol. 173, pp. 20-6, Aug 15 2008.
[68] S. Y. Teh, *et al.*, "Droplet microfluidics," *Lab Chip,* vol. 8, pp. 198-220, Feb 2008.
[69] W. Shi, *et al.*, "Droplet microfluidics for characterizing the neurotoxin-induced responses in individual Caenorhabditis elegans," *Lab Chip,* vol. 10, pp. 2855-63, Nov 7 2010.
[70] B. Chen, *et al.*, "Microfluidic bioassay to characterize parasitic nematode phenotype and anthelmintic resistance," *Parasitology,* vol. 138, pp. 80-8, Jan 2011.
[71] J. M. Schwenkenbecher, *et al.*, "Characterization of beta-tubulin genes in hookworms and investigation of resistance-associated mutations using real-time PCR," *Mol Biochem Parasitol,* vol. 156, pp. 167-74, Dec 2007.
[72] R. J. Martin, *et al.*, "Methyridine (2-[2-methoxyethyl]-pyridine]) and levamisole activate different ACh receptor subtypes in nematode parasites: a new lead for levamisole-resistance," *Br J Pharmacol,* vol. 140, pp. 1068-76, Nov 2003.
[73] J. A. Carr, *et al.*, "A microfluidic platform for high-sensitivity, real-time drug screening on C. elegans and parasitic nematodes," *Lab Chip,* vol. 11, pp. 2385-96, Jul 21 2011.
[74] A. Cook, *et al.*, "Electrophysiological recordings from the pharynx," *WormBook,* 2006.
[75] J. T. Chiang, *et al.*, "Evolution of pharyngeal behaviors and neuronal functions in free-living soil nematodes," *J Exp Biol,* vol. 209, pp. 1859-73, May 2006.
[76] L. Avery and H. R. Horvitz, "Pharyngeal pumping continues after laser killing of the pharyngeal nervous system of C. elegans," *Neuron,* vol. 3, pp. 473-85, Oct 1989.

[77] C. J. Franks, *et al.*, "Anatomy, physiology and pharmacology of Caenorhabditis elegans pharynx: a model to define gene function in a simple neural system," *Invertebrate Neuroscience,* vol. 6, pp. 105-122, 2006.
[78] D. G. Albertson and J. N. Thomson, "The pharynx of Caenorhabditis elegans," *Philos Trans R Soc Lond B Biol Sci,* vol. 275, pp. 299-325, Aug 10 1976.
[79] D. M. Raizen, *et al.*, "Interacting genes required for pharyngeal excitation by motor neuron MC in Caenorhabditis elegans," *Genetics,* vol. 141, pp. 1365-82, Dec 1995.
[80] L. Avery, "Motor neuron M3 controls pharyngeal muscle relaxation timing in Caenorhabditis elegans," *J Exp Biol,* vol. 175, pp. 283-97, Feb 1993.
[81] J. A. Dent, *et al.*, "avr-15 encodes a chloride channel subunit that mediates inhibitory glutamatergic neurotransmission and ivermectin sensitivity in Caenorhabditis elegans," *EMBO J,* vol. 16, pp. 5867-79, Oct 1 1997.
[82] T. Niacaris and L. Avery, "Serotonin regulates repolarization of the C. elegans pharyngeal muscle," *J Exp Biol,* vol. 206, pp. 223-31, Jan 2003.
[83] P. H. Mitchell, *et al.*, "The concentration-dependent effects of ethanol on Caenorhabditis elegans behaviour," *Pharmacogenomics J,* vol. 7, pp. 411-7, Dec 2007.
[84] R. G. Eckenhoff and B. J. Yang, "Absence of pressure antagonism of ethanol narcosis in C. elegans," *Neuroreport,* vol. 6, pp. 77-80, Dec 30 1994.
[85] P. G. Morgan and M. M. Sedensky, "Mutations affecting sensitivity to ethanol in the nematode, Caenorhabditis elegans," *Alcohol Clin Exp Res,* vol. 19, pp. 1423-9, Dec 1995.
[86] R. Dhawan, *et al.*, "Comparison of lethality, reproduction, and behavior as toxicological endpoints in the nematode Caenorhabditis elegans," *J Toxicol Environ Health A,* vol. 58, pp. 451-62, Dec 10 1999.
[87] J. B. Rand and C. D. Johnson, "Genetic pharmacology: interactions between drugs and gene products in Caenorhabditis elegans," *Methods Cell Biol,* vol. 48, pp. 187-204, 1995.
[88] A. G. Davies and S. L. McIntire, "Using C. elegans to screen for targets of ethanol and behavior-altering drugs," *Biol Proced Online,* vol. 6, pp. 113-119, 2004.
[89] J. P. McKay, *et al.*, "eat-2 and eat-18 are required for nicotinic neurotransmission in the Caenorhabditis elegans pharynx," *Genetics,* vol. 166, pp. 161-9, Jan 2004.
[90] R. C. Jaeger, "Lithography," *Introduction to Microelectronic Fabrication,* 2002.
[91] A. Barron, "Composition and Photochemical Mechanisms of Photoresists," ed, 2009.
[92] MICROCHEM. *SU-8 Negative Epoxy Series Resists*. Available: http://microchem.com/Prod-SU8_KMPR.htm
[93] D. M. Altpeter. (2005). *Description of SU-8*. Available: http://www.mesacrl.utwente.nl/mis/generalinfo/downloads/equipment/Delta%2020%20SU-8/Description%20of%20SU.pdf
[94] B.-H. Jo, *et al.*, "Three-dimensional micro-channel fabrication in polydimethylsiloxane (PDMS) elastomer," *Microelectromechanical Systems, Journal of,* vol. 9, pp. 76-81, 2000.

[95] S. Bhattacharya, *et al.*, "Studies on surface wettability of poly (dimethyl) siloxane (PDMS) and glass under oxygen-plasma treatment and correlation with bond strength," *Microelectromechanical Systems, Journal of,* vol. 14, pp. 590-597, 2005.
[96] L. Avery, "The genetics of feeding in Caenorhabditis elegans," *Genetics,* vol. 133, pp. 897-917, Apr 1993.
[97] MNX. *Lithography*. Available: https://www.mems-exchange.org/MEMS/processes/lithography.html
[98] C. D. Keating, *et al.*, "Whole-genome analysis of 60 G protein-coupled receptors in Caenorhabditis elegans by gene knockout with RNAi," *Curr Biol,* vol. 13, pp. 1715-20, Sep 30 2003.
[99] T. Thorsen, *et al.*, "Microfluidic large-scale integration," *Science,* vol. 298, pp. 580-4, Oct 18 2002.
[100] V. Studer, *et al.*, "An integrated AC electrokinetic pump in a microfluidic loop for fast and tunable flow control," *Analyst,* vol. 129, pp. 944-9, Oct 2004.
[101] P. Rezai, *et al.*, "Electrical sorting of Caenorhabditis elegans," *Lab Chip,* vol. 12, pp. 1831-40, Apr 24 2012.
[102] P. Tabeling, *Introduction to microfluidics*. Oxford, U.K. ; New York: Oxford University Press, 2005.
[103] B. R. Munson, *et al.*, *Fundamentals of fluid mechanics*: New York, 1990.
[104] A. Fick, "On Liquid Diffusion (Reprinted from the London, Edinburgh, and Dublin Philosophical Magazine and Journal of Science, Vol 10, Pg 30, 1855)," *Journal of Membrane Science,* vol. 100, pp. 33-38, Mar 31 1995.
[105] F. Bretschneider and J. R. De Weille, *Introduction to electrophysiological methods and instrumentation*: Academic Press, 2006.
[106] A. J. Bard and L. R. Faulkner, *Electrochemical methods: fundamentals and applications* vol. 2: Wiley New York, 1980.
[107] Wikipedia. *Photoresist*. Available: https://en.wikipedia.org/wiki/Photoresist
[108] MicroChemicals. (2010). *Reflow of Photoresist*. Available: http://www.microchemicals.com/technical_information/reflow_photoresist.pdf
[109] D. M. Hansen, *et al.*, "Chemical role of oxygen plasma in wafer bonding using borosilicate glasses," *Applied physics letters,* vol. 79, pp. 3413-3415, Nov 19 2001.
[110] A. Ainla. (2008). *Valves for Microfluidic Devices*. Available: http://www.ims.ut.ee/~alar/microtech/Ch1_5/#
[111] C. W. Beh, *et al.*, "OXYGEN PLASMA-FREE MICROFLUIDIC DEVICE SEALING."
[112] A. A. Tseng, "Recent developments in micromilling using focused ion beam technology," *Journal of Micromechanics and Microengineering,* vol. 14, pp. R15-R34, Apr 2004.
[113] S. Reyntjens and R. Puers, "A review of focused ion beam applications in microsystem technology," *Journal of Micromechanics and Microengineering,* vol. 11, pp. 287-300, Jul 2001.
[114] L. Tang and N. Y. Lee, "A facile route for irreversible bonding of plastic-PDMS hybrid microdevices at room temperature," *Lab on a Chip,* vol. 10, pp. 1274-1280, 2010.
[115] J. H. Monserud and D. K. Schwartz, "Effects of molecular size and surface hydrophobicity on oligonucleotide interfacial dynamics," *Biomacromolecules,* vol. 13, pp. 4002-11, Dec 10 2012.

[116] R. W. Murray, *et al.*, "Chemically modified electrodes. Molecular design for electroanalysis," *Anal Chem,* vol. 59, pp. 379A-390A, Mar 1 1987.
[117] S. Grimnes and O. Martinsen, "Bioimpedance and Bioelectricity Basics. 2000," ed: Academic press.
[118] S. Brenner, "The genetics of Caenorhabditis elegans," *Genetics,* vol. 77, pp. 71-94, May 1974.
[119] L. Avery and H. R. Horvitz, "Effects of starvation and neuroactive drugs on feeding in Caenorhabditis elegans," *J Exp Zool,* vol. 253, pp. 263-70, Mar 1990.
[120] C. M. Rogers, *et al.*, "Regulation of the pharynx of Caenorhabditis elegans by 5-HT, octopamine, and FMRFamide-like neuropeptides," *J Neurobiol,* vol. 49, pp. 235-44, Nov 15 2001.
[121] A. G. Vidal-Gadea, *et al.*, "Coordination of behavioral hierarchies during environmental transitions in," *Worm,* vol. 1, pp. 5-11, Jan 2012.
[122] B. M. Song and L. Avery, "Serotonin activates overall feeding by activating two separate neural pathways in Caenorhabditis elegans," *J Neurosci,* vol. 32, pp. 1920-31, Feb 8 2012.
[123] L. Segalat, *et al.*, "Modulation of serotonin-controlled behaviors by Go in Caenorhabditis elegans," *Science,* vol. 267, pp. 1648-51, Mar 17 1995.
[124] H. R. Horvitz, *et al.*, "Serotonin and octopamine in the nematode Caenorhabditis elegans," *Science,* vol. 216, pp. 1012-4, May 28 1982.
[125] S. R. Lockery, *et al.*, "A microfluidic device for whole-animal drug screening using electrophysiological measures in the nematode C. elegans," *Lab Chip,* vol. 12, pp. 2211-20, Jun 21 2012.
[126] F. Zhang, *et al.*, "Multimodal fast optical interrogation of neural circuitry," *Nature,* vol. 446, pp. 633-9, Apr 5 2007.
[127] G. Nagel, *et al.*, "Light activation of channelrhodopsin-2 in excitable cells of Caenorhabditis elegans triggers rapid behavioral responses," *Curr Biol,* vol. 15, pp. 2279-84, Dec 20 2005.
[128] C. J. Franks, *et al.*, "A comparison of electrically evoked and channel rhodopsin-evoked postsynaptic potentials in the pharyngeal system of Caenorhabditis elegans," *Invert Neurosci,* vol. 9, pp. 43-56, Mar 2009.
[129] D. J. Pemberton, *et al.*, "Characterization of glutamate-gated chloride channels in the pharynx of wild-type and mutant Caenorhabditis elegans delineates the role of the subunit GluCl-alpha2 in the function of the native receptor," *Mol Pharmacol,* vol. 59, pp. 1037-43, May 2001.
[130] J. A. Dent, *et al.*, "The genetics of ivermectin resistance in Caenorhabditis elegans," *Proc Natl Acad Sci U S A,* vol. 97, pp. 2674-9, Mar 14 2000.
[131] A. K. Jones, *et al.*, "Chemistry-to-gene screens in Caenorhabditis elegans," *Nat Rev Drug Discov,* vol. 4, pp. 321-30, Apr 2005.
[132] R. Yan, *et al.*, "The role of several ABC transporter genes in ivermectin resistance in Caenorhabditis elegans," *Vet Parasitol,* vol. 190, pp. 519-29, Dec 21 2012.
[133] D. Hall, *et al.*, "Cold Spring Harbor Laboratory Press," *New York,* 2008.
[134] S. Maruo, *et al.*, "Three-dimensional microfabrication with two-photon-absorbed photopolymerization," *Opt Lett,* vol. 22, pp. 132-4, Jan 15 1997.
[135] B. H. Cumpston, *et al.*, "Two-photon polymerization initiators for three-dimensional optical data storage and microfabrication," *Nature,* vol. 398, pp. 51-54, Mar 4 1999.

[136] A. Ostendorf and B. N. Chichkov, "Two-photon polymerization: A new approach to micromachining," *Photonics Spectra,* vol. 40, pp. 72-+, Oct 2006.
[137] W. Denk*, et al.*, "Two-photon laser scanning fluorescence microscopy," *Science,* vol. 248, pp. 73-6, Apr 6 1990.
[138] N. Anscombe, "Direct laser writing," *Nature Photonics,* vol. 4, pp. 22-23, 2010.
[139] G. Nanoscribe GmbH. (2012). *Photonic Professional User Manual*. Available: http://www.nanoscribe.de/
[140] S. Maruo and J. T. Fourkas, "Recent progress in multiphoton microfabrication," *Laser & Photonics Reviews,* vol. 2, pp. 100-111, 2008.
[141] H.-B. Sun*, et al.*, "Three-dimensional focal spots related to two-photon excitation," *Applied physics letters,* vol. 80, pp. 3673-3675, 2002.
[142] EPPO. Data Sheets on Quarantine Pests Globodera rostochiensis and Globodera pallida [Online].
[143] WikiGardener. *Potato cyst nematode*. Available: http://gardener.wikia.com/wiki/Potato_cyst_nematode
[144] H. Stelter, *Der Kartoffelnematode Heterodera rostochiensis Wollenweber*: Akademie-Verlag Berlin, 1971.
[145] A. Stone, "Heterodera Pallida N. Sp.(Nematoda: Heteroderidae), a Second Species of Potato Cyst Nematode 1)," *Nematologica,* vol. 18, pp. 591-606, 1972.
[146] F. G. W. Jones and M. G. Jones, *Pests of field crops*: Edward Arnold, 1984.
[147] P. Urwin, "Biotechnological Control of Plant Parasitic Nematodes," in *Biotechnology and Sustainable Agriculture 2006 and Beyond*, ed: Springer, 2007, pp. 181-190.
[148] R. N. Rolfe and R. N. Perry, "Electropharyngeograms and stylet activity of second stage juveniles of Globodera rostochiensis," *Nematology,* vol. 3, pp. 31-34, 2001.
[149] G. M. Lees and D. I. Wallis, "Hyperpolarization of rabbit superior cervical ganglion cells due to activity of an electrogenic sodium pump," *Br J Pharmacol,* vol. 50, pp. 79-93, Jan 1974.
[150] O. Steward*, et al.*, "Potentiation of excitatory synaptic transmission in the normal and in the reinnervated dentate gyrus of the rat," *Exp Brain Res,* vol. 26, pp. 423-41, Nov 23 1976.
[151] H. G. Heinzel*, et al.*, "The behavioral repertoire of the gastric mill in the crab, Cancer pagurus: an in situ endoscopic and electrophysiological examination," *J Neurosci,* vol. 13, pp. 1793-803, Apr 1993.
[152] B. D. Williams*, et al.*, "A genetic mapping system in Caenorhabditis elegans based on polymorphic sequence-tagged sites," *Genetics,* vol. 131, pp. 609-24, Jul 1992.